



Grant Agreement No.: 226479

# SafeLand

Living with landslide risk in Europe: Assessment,  
effects of global change, and risk management strategies

7<sup>th</sup> Framework Programme  
Cooperation Theme 6 Environment (including climate change)  
Sub-Activity 6.1.3 Natural Hazards

## Deliverable 2.5

D2.5: Physical vulnerability of elements at risk to landslides: Methodology for evaluation, fragility curves and damage states for buildings and lifelines

Work Package 2.2 - Vulnerability to landslides

Deliverable/Work Package Leader: AUTH

Revision: 2 – Final

April, 2011

Rev.	Deliverable Responsible	Controlled by	Date
0	AUTH	AMRA-BRGM	22-03-2011
1	AUTH	AMRA	28-03-2011
2	AUTH	BRGM	02-04-2011

## SUMMARY

This Deliverable is aimed at the proposition and quantification, in a measurable and reproducible way, of efficient methodologies for assessing the physical vulnerability of buildings (or sets of buildings), lifelines and population exposed to different landslide hazards. The applicability of the developed methodologies varies in relation to the landslide type and mechanism, the specified elements at risk and the analysis scale. The vulnerability of the affected elements is estimated using the concept of probabilistic fragility (or vulnerability) functions and appropriate definition of relevant damage states including various sources of uncertainty.

## Note about contributors

The following organisations contributed to the work described in this deliverable:

### **Lead partner responsible for the deliverable:**

[AUTH]

*Deliverable prepared by:*

Kyriazis Pitilakis, Stavroula Fotopoulou, Sotiris Argyroudis, Dimitris Pitilakis, Kostas Senetakis, Kostantinos Treulopoulos, Kaliopi Kakderi, Evi Riga

### **Partner responsible for quality control:**

*Deliverable reviewed by:*

[BRGM]: Evelyne Foerster

[AMRA]: Giulio Zuccaro

### **Other contributors:**

[UPC] : Jordi Corominas, Olga Mavrouli

[UNISA] : Leonardo Cascini, Settimio Ferlisi, Giovanni Pesciotta

[AMRA] : Giulio Zuccaro, Francesco Cacace, Massimiliano Rauci

[TRL] : Mike Winter, Jessica Smith

[BRGM] : Evelyne Foerster, Thomas Ulrich, Maria Stoikidou (from AUTH)

[ETHZ] : Matthias Schubert, Michael H. Faber, Harikrishna Narasimhan

# CONTENTS

<b>1</b>	<b>Physical vulnerability of elements at risk to landslides .....</b>	<b>6</b>
1.1	Introduction.....	6
1.2	Definitions .....	6
1.2.1	Physical vulnerability.....	6
1.2.2	Elements at risk- Taxonomy and typology .....	7
1.3	Quantitative estimation of physical vulnerability .....	12
1.3.1	Fragility curves .....	12
1.3.2	Vulnerability index .....	14
<b>2</b>	<b>Physical vulnerability assessment methodologies with respect to landslide type, element at risk and analysis scale .....</b>	<b>16</b>
2.1	Conceptual Framework of the methods.....	16
2.2	Brief description of the proposed methodologies .....	20
<b>3</b>	<b>Physical vulnerability to rockfalls .....</b>	<b>23</b>
3.1	Introduction (UPC).....	23
3.2	Methodology for buildings at site specific scale (UPC).....	24
3.2.1	Analytical evaluation of the structural response.....	26
3.2.2	Quantification of the vulnerability using a damage index .....	31
3.2.3	Development of fragility curves .....	32
3.3	Vulnerability model for rockfall protection galleries (ETHZ) .....	35
3.3.1	Introduction .....	35
3.3.2	Definition of the exposure for rockfall protection galleries....	36
3.3.3	Resistance modelling for rockfall protection galleries .....	40
3.3.4	Development of vulnerability curves for rockfall protection galleries	40
<b>4</b>	<b>Physical vulnerability to fast moving landslides .....</b>	<b>50</b>
4.1	Introduction.....	50
4.2	Methodology for buildings at large scale (1:5,000) (UNISA).....	50
4.2.1	Introduction .....	50
4.2.2	Analysis and zoning at large scale.....	50
4.3	Impact forces against fixed obstacles (UNISA).....	52
4.4	Methodology for buildings at site specific to local scales (AMRA)...	55
4.4.1	Introduction .....	55
4.4.2	Action on the buildings .....	55
4.4.3	Damage scale.....	56
4.4.4	Building vulnerability .....	57
4.4.5	Mechanisms and critic collapse load .....	61
4.4.6	Numeric elaborations .....	73
4.4.7	Missiles .....	77
4.4.8	Combination of elementary vulnerability .....	80
4.5	Methodology for roads/ debris flow (TRL-AUTH-UPC) .....	86
4.5.1	Introduction .....	86

---

4.5.2	Road Characterization.....	87
4.5.3	Damage States and Definitions .....	87
4.5.4	Description of Probabilities.....	88
4.5.5	Response to the questionnaire .....	89
4.5.6	The basic data .....	91
4.5.7	Experience of the Respondents .....	94
4.5.8	Further Interpretation of the Data.....	97
4.5.9	Completing the Curves.....	97
4.5.10	Geographical Variations.....	100
4.5.11	Variations in Background.....	100
4.5.12	Confidence Ratings.....	102
4.5.13	Frequency of Events .....	104
4.5.14	Qualitative Responses .....	105
4.5.15	Comparison with Real Events .....	107
4.5.16	Conclusions .....	115
<b>5</b>	<b>Physical vulnerability to slow moving landslides.....</b>	<b>116</b>
5.1	Introduction.....	116
5.2	Methodology for buildings at small scale (1:100,000) (UNISA) .....	116
5.2.1	Introduction .....	116
5.2.2	Analysis and zoning at small scale .....	117
5.3	Methodology for buildings at medium scale (1:25,000) (UNISA).....	119
5.3.1	Introduction .....	119
5.3.2	Analysis and zoning at medium scale .....	119
5.4	Methodology for buildings at detailed scale (1:2,000) (UNISA) .....	121
5.4.1	Introduction .....	121
5.4.2	Analysis and zoning at detailed scale .....	121
5.5	Methodology for buildings at site specific scale (AUTH) .....	123
5.5.1	Earthquake triggered landslides.....	123
5.5.2	Methodology.....	123
5.5.3	Application .....	126
5.5.4	Parametric study .....	137
5.6	Site specific Methodology for Vulnerability assessment of RC buildings to slow-moving earth slides (BRGM) .....	147
5.6.1	Introduction .....	147
5.6.2	Methodology.....	147
5.6.3	Parametric study .....	149
5.7	Methodology for roads (AUTH).....	159
<b>6</b>	<b>Physical vulnerability to fast and slow moving landslides ..</b>	<b>164</b>
6.1	Methodology for pipelines (AUTH) .....	164
6.1.1	Analytical approach .....	164
6.1.2	Empirical relationships .....	165
6.1.3	Damage states.....	167
6.2	Physical vulnerability of persons to landslides (AUTH).....	169
6.2.1	Introduction .....	169
6.2.2	Review of quantitative methodologies.....	169

---

- 6.2.3 Conclusive remarks..... 175
- 7 References .....176**
- 8 Appendices .....186**
  - 8.1 Appendix I: Questionnaire and responses for roads and debris flow 186
    - 8.1.1 Questionnaire..... 186
  - 8.2 Appendix II..... 192
    - 8.2.1 R.C. Buildings – vulnerability curves for each combination 192
    - 8.2.2 Masonry buildings – vulnerability curves for each combination 195

# 1 PHYSICAL VULNERABILITY OF ELEMENTS AT RISK TO LANDSLIDES

## 1.1 INTRODUCTION

Stemming from the considerable amount of damage to the built environment in many areas of the world resulting from the occurrence of different landslide hazards, the present deliverable aims at the quantification of risk and losses in terms of physical vulnerability of the exposed assets i.e. environment, buildings of different typology, pipelines, roads, population etc.

In this regard, the main goal of Deliverable 2.5 is to establish efficient methodologies for assessing the physical vulnerability of buildings, infrastructures and persons to different landslide hazards using the concept of probabilistic fragility functions and appropriate definition of relevant damage states.

## 1.2 DEFINITIONS

### 1.2.1 Physical vulnerability

In engineering and natural sciences, physical vulnerability is commonly expressed as the degree of loss (expressed on a scale of 0: no loss to 1: total loss) to a given element or set of elements at risk (i.e. buildings, infrastructures, persons), resulting from the occurrence of a specified hazard of given magnitude. The term of vulnerability [V], closely related to the consequences of natural hazards, is generally enclosed in the definition of risk [R] through the following formulation (Varnes, 1984):

$$[R] = [H] \times [V] \times [E] \quad [1.1]$$

Where [H]: hazard, [E]: exposure (global value or cost of elements at risk in a given territorial system).

Within the context of a landslide risk assessment methodology, physical (technical) vulnerability comprises a key component (Leone et al., 1996; Dai et al., 2002) that still requires significant research. It may be defined as the degree of loss to a given element or set of elements subjected to a landslide event of a given type and intensity. For property, the loss will be the value of the damage relative to the value of the property; for persons, it will be the probability that a particular life (the element at risk) will be lost, given the person(s) is affected by the landslide. Physical vulnerability of structures depends on the structural properties of exposed elements (e.g. typology, construction quality, state of maintenance, use etc), but also on the mechanism and magnitude of the landslide processes. For instance, buildings subject to the same landslide event may experience different vulnerability indices owing to their particular different structural (strength and stiffness) characteristics. Furthermore, buildings having exactly the same typological and structural properties may suffer less or more damage, determined by the landslide mechanism and their location with respect to the sliding zone. Population vulnerability may depend on many factors such as the landslide type, size and intensity, the resistance ability of the individual persons affected by the landslide hazard and their relative position to the exposed area.

Physical vulnerability of the exposed elements to the different landslide hazards may be expressed both in qualitative and quantitative terms. A quantitative risk analysis (QRA) is

usually preferable compared to qualitative whenever possible (Uzielli et al., 2008), as it allows for a more explicit characterization of the causes of damages (in terms of permanent deformation, tension cracks, etc), and offers an improved basis for communication among the research community, local authorities and emergency planners. Several approaches have been proposed to estimate vulnerability of structures and persons subject to different landslide hazards at different scales. An overview of the existing methods including different landslide types and elements at risk can be found in SAFELAND WP2.1-D2.4, § 8.1 “Vulnerability assessment”. However, a unified quantitative methodology that incorporates several possible aspects for assessing physical vulnerability is not yet available (Glade and Crozier, 2005; Li et al., 2010).

### 1.2.2 Elements at risk- Taxonomy and typology

The first step in assessing physical vulnerability is the identification of elements at risk. The physical elements affected by the landslide hazards can be classified into four main categories:

- Buildings of different typologies and categories: RC, unreinforced masonry, steel and timber or other light constructions
- Infrastructures: Bridges, tunnels, embankments
- Lifelines. Transportation systems (including roadways, railways, airport and port facilities) and utility systems (including potable water, waste-water, natural gas, electric power stations and networks and communication systems).
- Population

This classification requires reliable and complete databases containing several levels of information. Data acquisition and archiving at local and regional scales can be based on various already existing thematic maps (topography, geology, geotechnical, building typologies, lifelines, etc). Aerial photographs and different imagery techniques can be also used. Relevant information may also be collected from local authorities, insurance companies, railway and road management companies and local inhabitants (Remondo et al. 2005). Field surveys may be also used in particular to identify the typological characteristics of the exposed elements.

For a landslide of a given type, mechanism and intensity, the typology of the exposed elements is a key data in any quantitative vulnerability assessment methodology. Geometry, material properties, age, code design level, soil conditions, foundation and superstructure details, number of floors etc. are among typical typological parameters that are directly associated with the structural damage. At this point it is necessary to stress the crucial role of the scale of analysis. We identify three levels: regional, local and element specific. From element specific to local and regional scales, it is common to consider aggregated levels in the form of homogeneous units (van Westen 2004). For example this may consist of groups of buildings within the same area, block or district, characterized by a relative homogeneity of building type, construction materials, number of floors and land use distribution. Very few contributions regarding this subject exist in the literature. Maquaire et al. (2004), for instance, propose a semi-automatic procedure, based on GIS technology and statistical analyses, developed at large scale (1:5,000 ÷ 1:10,000).

A significant effort is devoted in SAFELAND to the detection of the proper criteria to identifying the elements at risk at different scales (Figure 1.2.1). In this regard, at small (1:100,000) and at medium (1:25,000) scales, elements at risk are defined in terms of building's (homogeneous) aggregates. At large (1:5,000) and detailed (1:2,000) scales instead, exposed element are considered as coincident with single buildings actually or potentially interacting with the landslide body mass.

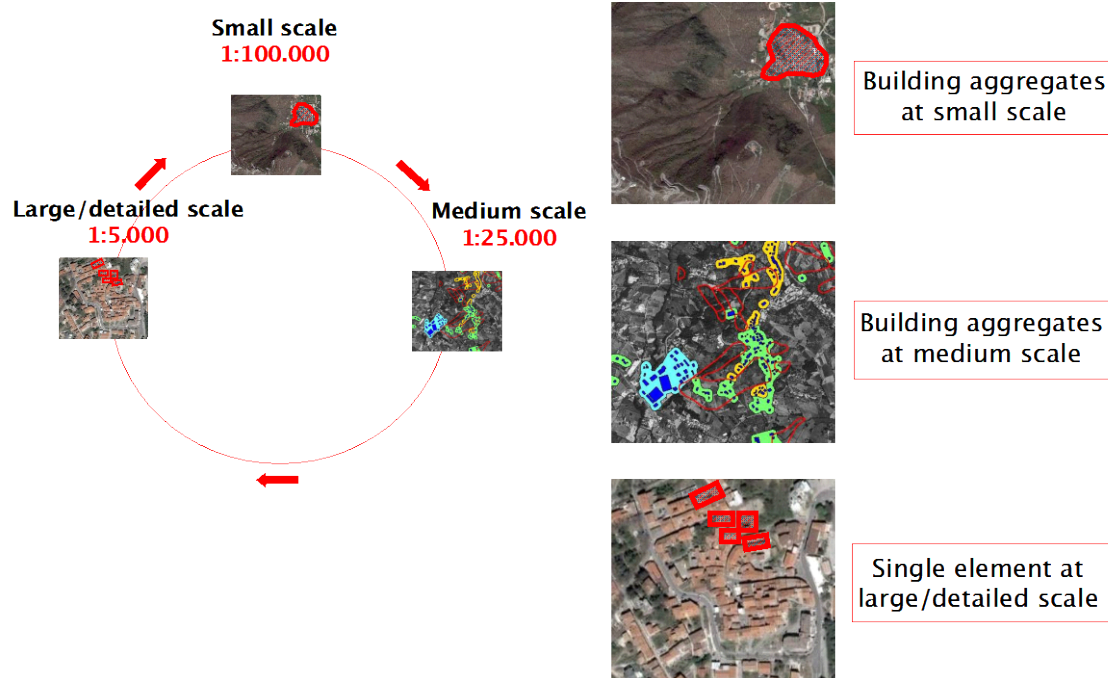


**Figure 1.2.1** Identification of buildings exposed to the landslide risk at different scales (UNISA).

### 1.2.2.1 Building typology

Similar to the classification of the general building stock adopted in many earthquake engineering studies (Milutinovic et al. 2003, Mouroux et al. 2006; FEMA and NIBS 2009b; Kappos et al. 2010), the typology proposed in SAFELAND for RC and unreinforced masonry buildings impacted by earth slides, is illustrated in Table 1.2.1.

**Table 1.2.1 Building Typology Matrix**

Label	Structural system	Foundation system	Building Height	No. of storey
RC1.1L	R/C moment bare frames	Shallow flexible foundation	Low	1–3
RC1.1M			Medium	4–7
RC1.1H			High	8+
RC1.2L		Shallow stiff foundation	Low	1–3
RC1.2M			Medium	4–7
RC1.2H			High	8+
RC1.3L		Deep foundation	Low	1–3
RC1.3M			Medium	4–7
RC1.3H			High	8+
RC4.1L	R/C dual systems (R/C frames and walls)	Shallow flexible foundation	Low	1–3
RC4.1M			Medium	4–7
RC4.1H			High	8+
RC4.2L		Shallow stiff foundation	Low	1–3
RC4.2M			Medium	4–7
RC4.2H			High	8+
RC4.3L		Deep foundation	Low	1–3
RC4.3M			Medium	4–7
RC4.3H			High	8+
MSt1	Unreinforced (brick and stone) Masonry	Shallow continuous foundation	Low	1
MSt2-3			Medium	2-3
MBr1			Low	1
MBr2-3			Medium	2-3

The nomenclature used for R/C buildings is of the type RCixyz where i indicates the structural system, x the foundation system, y the height and z the code level (not presented in table 1.2.1). Regarding the structural system, both frames and dual (frame + shear wall) systems are addressed. Each of the above RC buildings is assumed to have three different foundation configurations:

- Shallow flexible foundation (e.g. isolated footings),
- Shallow stiff foundations (e.g. grade beam footings) and
- Deep foundations (e.g. piles).

For unreinforced (brick and stone) masonry buildings, a shallow continuous foundation is considered in all cases. No specific categories are identified as in RC structures. Similar matrices may be adopted for different landslide types (e.g. debris flows, rockfalls).

Regarding the code design level, two subclasses are defined, as follows:

- *Low code*: poorly designed or constructed (usually old, bare frame) R/C buildings with low confinement level.
- *High code*: well -designed and constructed (usually new, bare or dual frame) R/C buildings with adequate confined members founded on shallow stiff or deep foundations.

Acquiring all this building information in local and regional scales is in general a difficult and time-consuming task. Expert judgment is usually applied to this effect. In this regard, as already discussed above, at small (1:100,000) and medium (1:25,000) scales, a definition of elements at risk in terms of building's (homogeneous) aggregates is commonly accepted (Fig. 1.2.1).

#### 1.2.2.2 Infrastructure and Lifeline typology

The infrastructures considered in this work are related to the road network. They are classified into three categories:

- Bridges
- Tunnels
- Slopes and embankments possibly including earth retaining structures

Damages on these elements may affect seriously the serviceability of a road network. For the typology it is proposed to follow the methodology of HAZUS.

### **Road classification**

Vulnerability of roads due to different landslide impacts may be attributed both to the partial or complete blockage of the road, as well as to the structural damage to surfacing and it is associated to the serviceability level of the road.

The main typological distinction is between *high speed* and *local roads*. Their main characteristics finally adopted in SAFELAND are briefly summarized below:

#### High speed

- 80-110km/h speed limit
- At least one lane running in each direction, most likely in conjunction with a hard strip

#### Local

- Speed limit typically <50km/h
- One lane running in each direction or single-track
- Paved (bituminous, unreinforced or reinforced concrete) or unpaved

The road width as well as the traffic volume may also be considered as important parameters to assess the vulnerability of transportation infrastructure (FEMA and NIBS 2009b).

## Pipeline classification

Buried pipelines are commonly used to transport water, sewage, fuels and natural gas. They can be classified as either continuous or segmented.

Pipelines cover large areas and consequently are subjected to a variety of geotectonic hazards. Landslide hazards, generally defined in terms of permanent ground displacement, are usual at regional scale and their potential for damage is very high since they impose large deformation on pipelines. Among the most important factors that influence the performance of pipelines subject to landslides (ALA 2001a and b; Pitilakis et al., 2006a and b; FEMA and NIBS 2009b), we can mention:

- Construction material (e.g. ductile or fragile),
- Length and thickness
- Orientation with respect to the landslide,
- Stiffness in relation to the surrounding soil,
- Type of joints,
- Burial depth,
- Age and corrosion,
- Appurtenances and branches,
- Connection points (e.g. tanks),
- Valves or SCADA equipments, etc.

The basic failure mode of a pipe crossing a landslides perpendicular to the direction of sliding is bending; otherwise pipe is subjected to tension and compression (fig. 1.2.2).

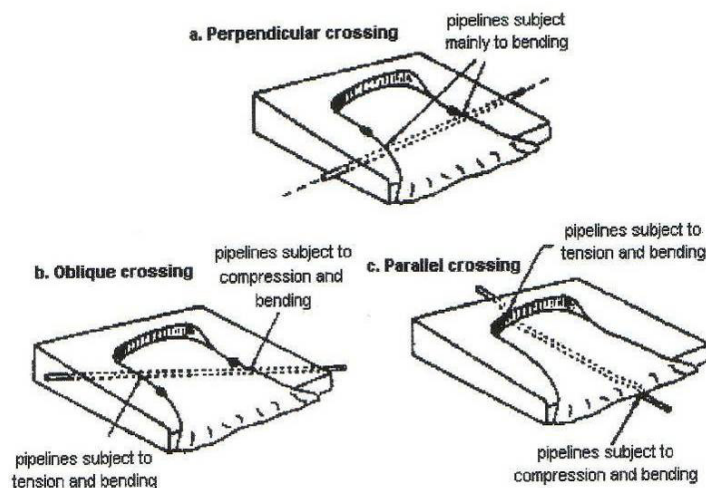


**Figure 1.2.2** Failure modes for pipes as a result of landslides (O'Rourke et al., 1998).

### 1.2.2.3 Population

The resistance of the person to landslides is a function of the intellectual maturity (e.g. perception about risk) and physical ability (e.g. age) (Uzielli et al. 2008). The population density and the annual income of the affected persons are also important contributing factors. The capacity of the population to withstand the landslide hazard varies for persons in open space, vehicles and inside buildings.

## **1.3 QUANTITATIVE ESTIMATION OF PHYSICAL VULNERABILITY**

### **1.3.1 Fragility curves**

The physical vulnerability of elements at risk to landslides will be described through **fragility functions**. Fragility relationships are essential components of quantitative risk assessment (QRA) studies as they allow for the estimation of risk within a performance or consequence-based framework. They are expressed for every element at risk (i.e. building, road, pipeline), in terms of relating landslide intensity with damage probabilities. Fragility curves provide for every element at risk, the conditional probability for the element to be in or exceed a certain damage state, under a landslide event of given type and intensity. Figure 1.3.1 illustrates a generalized vulnerability function. The determination of an appropriate statistical distribution (usually normal or lognormal) is of major importance to account for the various sources of uncertainty.

The methods used to estimate fragility curves can be classified into four categories – empirical, engineering judgmental, analytical, and hybrid – based on the scale of the study area, the availability and quality of input data and the local technology in construction practice.

Damage observation from previous landslide events are the main source of information for *empirical* curves that are generally more realistic compared to the other categories as they fit real-event data. The most common problem when applying a purely empirical approach is the unavailability of (sufficient and reliable) statistical data for several landslide types and intensities. *Engineering judgmental* fragility relationships resort to expert opinion (ATC-13, 1985). The reliability of judgment-based curves is questionable due to their dependence on the individual experience of the experts consulted.

*Analytical* fragility curves are essentially based on numerical modeling (e.g. Pitilakis et al., 2006a and b; Fotopoulou et al., 2011; Mavrouli and Corominas, 2010a; Negulescu & Foerster, 2010; etc). Analytical fragility relations offer a higher level of detail compared to the previous ones. With the expansion of computational power and the development of reliable analysis tools, the limitations in the analytical derivation of vulnerability curves are decreasing.

*Hybrid* relationships attempt to compensate for the scarcity of observational data, subjectivity of judgmental data and modeling deficiencies of analytical procedures by combining observed data and analytical estimations (Kappos et al., 2006).

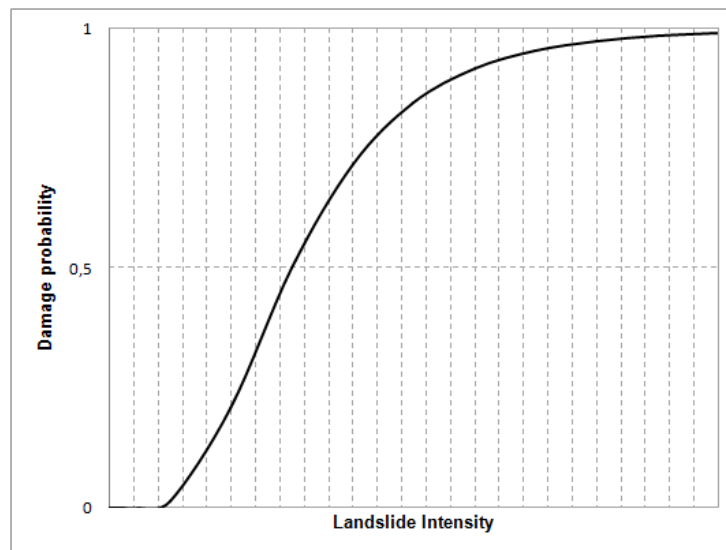


**Figure 1.3.1** Generalized vulnerability function

Intensity (demand) of a given landslide event can be expressed in different ways depending on the landslide type (slow moving or rapid slide, rockfall, etc.) and the relative position of the exposed element (e.g. uphill, downhill or inside the potential unstable slope) to the landslide. Commonly used intensity measures are defined in terms of the absolute or differential displacement, velocity, kinetic energy, volume of the landslide deposit, impact force, etc.

In order to identify the structure's performance (damage) state and to construct the corresponding fragility curves, a damage index (DI) is introduced based on global and local parameters of the structure and a relationship between the damage index and the landslide intensity parameter is established. The damage states often describe different fragility curves for *slight, moderate, extensive and complete damage (collapse)*. Typically multiple damage (or performance) criteria need to be satisfied. The number of damage states is normally between two and six, depending on the element at risk and the available data. They are defined by a threshold value of the damage index that could be a limit value of a component strain, joint displacement, inter-story drift, or other fragility criteria (Pitilakis et al. 2006a and b). The threshold value for each damage state and element at risk is defined based on engineering judgment and damage observations. Figure 1.3.2 presents the form of HAZUS (FEMA and NIBS 2009a) fragility curves to estimate seismic vulnerability of buildings for different damage states as well as the expected building performance for each damage state. The intensity in this work may be the absolute or differential permanent movement at the foundation level due to landslides. Figure 1.3.3 depicts a very draft sketch of the form of fragility functions for two different building typologies (masonry and RC) illustrating the higher vulnerability of masonry structures compared to RC structures.

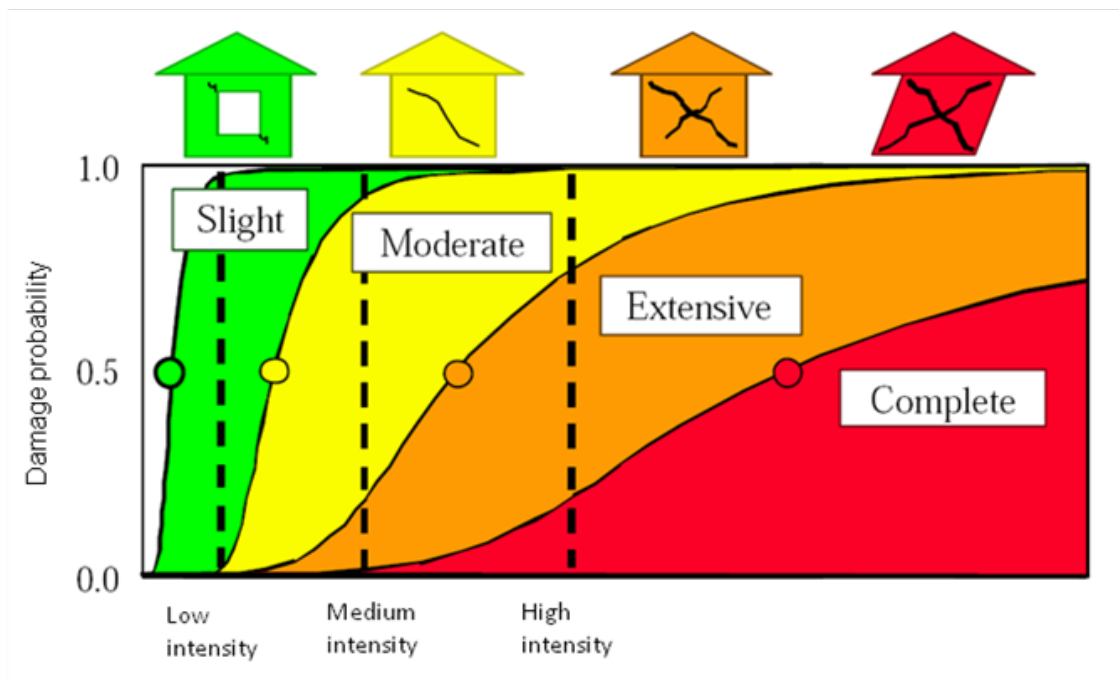


*Figure 1.3.2 HAZUS fragility curves derived for buildings for different damage states (FEMA and NIBS 2009a)*

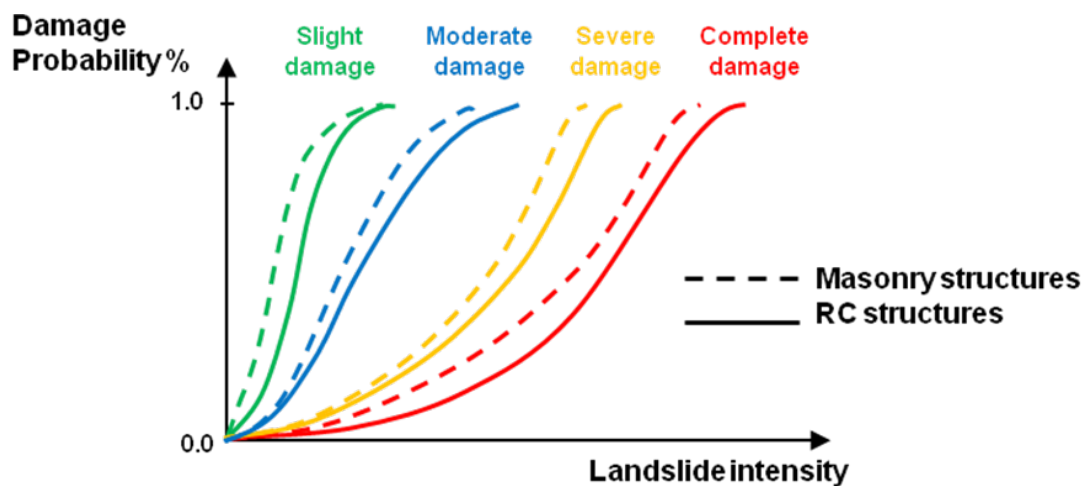


*Figure 1.3.3 Fragility curves for different building typologies*

### 1.3.2 Vulnerability index

The damage (or vulnerability) index is an alternative way, compared to fragility curves, to express vulnerability (Pitilakis et al., 2006b). Approaches using damage indices intend to assess vulnerability of different components without complex calculations, based on the definition of indicators resulting in most cases from empirical expressions that combine the

main factors affecting the behavior of the element at risk and for the given landslide type and size (Leone et al., 1996; Amatruda et al., 2004; Liu 2006 etc.). A rating system is usually used to assign a score in each attribute of the selected factors. The scaling factors may be defined based on an extended and in-depth literature review, expert judgment and the experience of past landslide events. The expression may include weighting factors in order to account for the relative influence of each attribute to the total vulnerability of the component. The total vulnerability can finally be determined using a decision tree analysis. An example of this procedure is proposed in SAFELAND, WP2.2-D2.6 to assess the expected socio-economic impact of a landslide event in terms of vulnerability.

## **2 PHYSICAL VULNERABILITY ASSESSMENT METHODOLOGIES WITH RESPECT TO LANDSLIDE TYPE, ELEMENT AT RISK AND ANALYSIS SCALE**

### **2.1 CONCEPTUAL FRAMEWORK OF THE METHODS**

In the following, an attempt to distinguish between different types of landslides and affected assets (building and infrastructure) is presented. The applicability of the developed methodologies varies in relation to the landslide type, specified elements at risk and the analysis scale. The main landslide movement types considered herein are:

- Rockfalls
- Debris and earth flows
- Slow moving landslides

Four different analysis scales are considered: small (1:100,000), medium (1:25,000), large (1:5,000) and detailed/site specific (1:2000) scales, requiring different criteria to identify the elements at risk.

The landslides considered are either rainfall triggered or earthquake triggered considering different intensity criteria in each case. A synthesis of the methods, proposed by different research groups in WP2.2-D2.5, in relation to the landslide type, the elements at risk and the analysis scale is presented in Table 2.1.1.

The derived approaches in regard to the input intensity parameter as well as to the methodological framework used to estimate vulnerability (empirical, engineering judgemental, analytical and hybrid) are summarized in Tables 2.1.2 and 2.1.3 respectively.

**Table 2.1.1** Synthesis of methodologies proposed by different research groups to estimate physical vulnerability to landslides

Methodology to Assess Physical Vulnerability to Landslides						
			Scale of Analysis	Landslide Classification		
				Rockfalls	Fast movements	Slow movements
Elements at risk	Buildings	RC	small			UNISA
			medium			UNISA
			large		AMRA, UNISA	
			detailed-site specific	UPC, ETHZ	AMRA, UNISA	AUTH, BRGM, UNISA
		Masonry	small			UNISA
			medium			UNISA
			large		AMRA, UNISA	
			detailed-site specific		AMRA, UNISA	UNISA
	Roads	small				
		medium				
		large		TRL- AUTH- UPC	AUTH	
		detailed-site specific				
	Pipelines	small				
		medium				
		large		AUTH		
		detailed-site specific				
	Persons	small		AUTH		
		medium				
		large				
		detailed-site specific				

**Table 2.1.2 Proposed methodologies with respect to the input intensity parameter**

<b>Methodology to Assess Physical Vulnerability to Landslides –input intensity parameter</b>						
			<b>Scale of Analysis</b>	<b>Landslide Classification</b>		
				Rockfalls	Fast movements	Slow movements
<b>Elements at risk</b>	<b>Buildings</b>	<b>RC</b>	Small (building aggregates)			Vulnerable area
			Medium (building aggregates)			Vulnerable area
			Large (single building)	Impact velocity, mass of the falling stone	Landslide velocity	
			detailed-site specific (single building)	Kinetic energy, Impact velocity	Speed of flow, Impact force	Differential displacement
		<b>Masonry</b>	Small (building aggregates)			Vulnerable area
			Medium (building aggregates)			Vulnerable area
			Large (single building)		Landslide velocity	
			detailed-site specific (single building)		Speed of flow, Impact force	Differential displacement
	<b>Roads</b>	small				
		medium				
		large		Volume of the landslide deposit insert into the road	Permanent displacement	
		detailed-site specific				
	<b>Pipelines</b>	small				
		medium				
		large		Permanent displacement, strains		
		detailed-site specific				
	<b>Persons</b>	small		Landslide velocity, landslide magnitude		
		medium				
		large				
		detailed-site specific				

**Table 2.1.3 Proposed methods in relation to the methodological framework (empirical, engineering judgemental, analytical or hybrid)**

<b>Methodology to Assess Physical Vulnerability to Landslides -outputs</b>						
			<b>Scale of Analysis</b>	<b>Landslide Classification</b>		
				Rockfalls	Fast movements	Slow movements
<b>Elements at risk</b>	<b>Buildings</b>	<b>RC</b>	Small (building aggregates)			Empirical and expert judgment
			Medium (building aggregates)			Empirical and expert judgment
			Large (single building)		Analytical, Empirical and expert judgment	
			detailed-site specific (single building)	Analytical	Analytical, Hybrid	Analytical
		<b>Masonry</b>	Small (building aggregates)			Empirical and expert judgment
			Medium (building aggregates)			Empirical and expert judgment
			Large (single building)		Analytical, Empirical and expert judgment	
			detailed-site specific (single building)		Analytical, Hybrid	Analytical
	<b>Roads</b>	small				
		medium				
		large				
		detailed-site specific		Expert judgment	Empirical and expert judgment	
	<b>Pipelines</b>	small				
		medium				
		large		Analytical, Empirical		
		detailed-site specific				
	<b>Persons</b>	small		Empirical and expert judgment		
		medium				
		large				
		detailed-site specific				

## 2.2 BRIEF DESCRIPTION OF THE PROPOSED METHODOLOGIES

The methodologies proposed by different research groups within the framework of Deliverable D2.5 are briefly summarized in the following paragraphs:

- UPC research group has developed an analytical methodology to assess physical vulnerability of RC buildings impacted by single fragmented rocks at their base in function of the velocity and the volume of the rock boulder. It includes: (a) the analytical evaluation of the structural response of RC buildings to rockfalls, (b) the quantification of vulnerability using a vulnerability index for rockfalls and (c) the development of fragility curves for RC buildings impacted by rockfalls. The methodology is applied at site specific scale for the case of a prototype two-storey reinforced concrete building.
- A generic vulnerability model which can be used for a large portfolio of rockfall protection galleries is proposed by ETHZ. The methodology includes three main steps: (a) definition of the exposure for rockfall protection galleries, (b) resistance modelling for rockfall protection galleries and (c) development of vulnerability curves for rockfall protection galleries; each of these involves various sub-steps. Different sources of uncertainty can be included in the analysis in a quantitative cost-effective manner.
- UNISA research group has developed a methodology to estimate physical vulnerability of building aggregates due to fast moving landslides at large scale (1:5000) based on expert judgment and empirical data. The proposed approach is articulated into the following steps: (a) detection of buildings at risk, (b) definition of buildings' occupancy (residential, commercial, industrial, etc.) and typology (masonry, reinforced concrete, etc.), (c) collection of information on past damages and losses, (d) estimation of landslide intensity (i.e. the mean velocity of the impacting front) via results of numerical modelling of flow-slides' propagation stage, (e) estimation of the physical vulnerability of the buildings impacted by fast-moving landslides. Vulnerability indices for a single building are defined as a function of its occupancy type, its typology, the theoretical velocity of the flow material and the probability of structural collapse.

Moreover, UNISA explore the applicability of different methods to adequately predict the value of the force acting at the impact of the fast-moving landslide against a fixed obstacle by implementing a Distinct Element Method that simulates the debris evolution. The value of this force can be used within procedures aimed to estimate the vulnerability of (RC and masonry) buildings to fast-moving landslide at detailed scale (1:5000).

- AMRA research group has developed an analytical methodology to assess physical vulnerability of RC and masonry buildings to fast moving landslides. Vulnerability classes for prominent structural and non-structural elements of the building are defined, and the limit load for each of these is computed by limit state analysis related with experimental tests. The weight of each vulnerable class and their possible

combinations is investigated to estimate the global vulnerability and define buildings typological classes.

- TRL research team, in collaboration with AUTH and UPC, has developed a methodology to estimate physical vulnerability of roads to debris-earth flows, based on engineering judgment. An appropriate questionnaire has been prepared and widely distributed to experts on debris flows and road vulnerability. Fragility curves were constructed as a function of the volume of the landslide deposit for each road type (high speed, local) and damage state (limited, serious, destroyed). The final tool (in terms of fragility curves) is based on the statistical exploitation of the results of the questionnaire. In order to assess the validity of the curves, a comparison with real debris flow events from both Scotland in the UK and the Republic of Korea was carried out.
- UNISA research team has developed a method to assess physical vulnerability of building aggregates due to slow movements at small (1:100,000) scale based on expert opinion and empirical data. Physical vulnerability is defined as “the ratio between the whole damageable vulnerable areas and the whole vulnerable areas of a given municipality”. The procedure involves four main steps: (a) analysis of landslide – affected area distribution, (b) identification of the vulnerable areas in terms of building aggregation, (c) identification of the homogeneous areas in which damage to facilities occurs, and (d) physical vulnerability estimation. Appropriate vulnerability thresholds ( $V_{min}$  and  $V_{max}$ ) were established, for each of the considered homogeneous areas in order to construct fragility curves.
- UNISA research group has developed a heuristic –empirical methodology to estimate physical vulnerability of building aggregates due to slow moving landslides (at medium (1:25,000) scale. Physical vulnerability was defined as “*the expected degree of damage to an aggregate, constituted by a given number of buildings, falling within an area affected by slow-moving landslides of a given intensity*”. The procedure involves five sequential steps: (a) analysis of landslide proneness, (b) identification of the building aggregates, (c) analysis of the landslide induced damage, (d) probability of aggregate recovering and damageability, (e) vulnerability curves.
- UNISA research group has also contributed to the development of a methodology to estimate physical vulnerability of RC and masonry buildings due to rainfall triggered slow moving slides at site specific scale. The methodological approach includes two main steps. The first one deals with the development of numerical analyses devoted to: i) the simulation of the groundwater regime during rainfall event of given intensity and duration; ii) the detection of the mean values of the shear strength parameters mobilized along the shear zones; iii) FEM stress-strain analyses. The second step consists in the interpretation of the output data of the stress-strain analyses via damageability criteria. The obtained results can be profitably used to validate the fragility curves derived via parametric numerical analyses.
- AUTH research group has developed a methodology for assessing physical vulnerability of RC buildings due to earthquake triggered slow moving slides at site specific scale based on numerical formulations and expert judgment. A two-step uncoupled analysis is proposed: (a) the differential permanent displacements at the

building's foundation level are estimated using an adequate finite difference dynamic slope model; (b) the calculated differential displacements are statically imposed to building's model at the foundation level to assess the building's response for different ground landslide displacements induced by the earthquake. The computed permanent displacements at the foundation level were validated through comparison with simplified Newmark-type displacement methods. Limit states are defined in terms of a threshold value of building's material strain. An application of the proposed framework to an idealized case study is presented. The fragility curves were derived via an extensive sensitivity analysis to account for various sources of uncertainty and to determine the most influential parameters in the structure's performance. The methodology can be applied for other sources of landslide-triggered mechanisms.

- BRGM research team has contributed to the development of an analytical/numerical methodology to estimate physical vulnerability of RC buildings subjected to slow moving slides at site specific scale assuming various triggering mechanisms. A parametric study is performed to allow for the identification of parameters which mostly affect the building's vulnerability. This product is directly related to the previous one proposed by AUTH. Both are contributing on the same target that is the generation of fragility curves via numerical parametric analysis in case of relative slow moving earth slides.
- AUTH research group has proposed a semi-empirical methodology to assess physical vulnerability of roads subjected to earthquake induced landslides. Fragility curves for roads in case of earthquake triggered slides are obtained as a function of peak ground acceleration (PGA) considering the characteristics of the slope (i.e. yield coefficient,  $k_y$ ). In this respect, the existing HAZUS curves are modified using the Bray and Travararou (2007) model for the Newmark rigid sliding block case ( $T_s=0$ ).
- AUTH has also contributed to the vulnerability assessment of pipelines to different landslide hazards by providing a review of the most widely acceptable analytical and empirical approaches proposed in the literature.
- Finally, AUTH provided a literature review on existing models for the quantification of physical vulnerability of persons exposed to different landslide hazards. The most important factors concerning the different aspects of physical vulnerability of persons to landslides were discussed.

### 3 PHYSICAL VULNERABILITY TO ROCKFALLS

#### 3.1 INTRODUCTION (UPC)

As observed from historical rockfalls and damage caused to buildings, the damage extent due to rockfalls presents a large dispersion from slight non-structural damage to total collapse, according to the building characteristics, the rock's size and velocity. Here some selected cases of rock impacts to buildings that cover a full range of types and levels of damage are presented.

Non-structural damage, i.e. destruction of infill walls, doors and windows is often reported as in the case of rockfalls in BÍldudalur, Iceland (Bell and Glade, 2004). Corominas et al. (2005) have reported several rockfall events in Andorra, among which one in 1997 when a block of 25 m<sup>3</sup> volume penetrated the slabs of a residence building, ending down to its basement. The building stood without further extensive damage. Serious structural damage occurred at the event of Segovia, Spain, in 2004, when boulders fell on the roof of the Fuencisla Sanctuary (Romana, 2009). Very interesting observations of damage could be carried out at the Fiumelatte rockfall of 2004 in Italy (Agliardi et al. 2009). In this event a large number of blocks were released from a cliff above the village causing a variety of damage to buildings, ranging from slight damage to total loss. For instance, roof damage was caused by a block of 8 m<sup>3</sup> impacting on the corner of a building while extensive damage was observed in two multiple storey buildings by a block of 96 m<sup>3</sup>. Recent devastating rockfall events resulting in utterly flattened houses were reported by the media for the rockfalls of Yemen in 2005 and Cairo in 2008 involving massive failure of rock blocks fragments of several hundreds of cubic meters. Additionally, serious damages have been registered for various events at Hong Kong (Chau et al., 2002), Canada (Evans and Hungr, 1993) and United States (Wieczorek and Snyder, 2004 and Castleton, 2009).

The amount of damage in the afore-mentioned cases depends on the impact location and the importance of the impacted members on the stability of the building. For RC buildings situated at the foot of rocky slopes, four major impact locations can be distinguished: impact and penetration of the roof; impact and damage of columns and/or beams; penetration of slabs; and impact and damage of infill walls and openings (including doors, windows, etc.). Considering the importance of the impacted members, loss can be classified, depending on the type of the affected elements, as damage of: (i) primary structural elements (i.e. columns and beams for RC); (ii) secondary structural elements (i.e. slabs); (iii) primary non-structural elements (i.e. infill walls and ceilings); and (iv) furniture and electrical/mechanical equipment.

The only impact location that might lead to instability of the whole structure is that affecting columns and/or beams. Instead, impacts on secondary structural elements are not crucial for the stability of the load-bearing system; however their damage could have side effects like the blow of debris resulting in further damage and injuries. The same applies to primary non-structural elements while damage of electrical/mechanical equipment though repairable, may be costly as well.

Taking this into account, in the approach proposed here, the response of the primary structural elements will define the vulnerability of the building. The damage that is initially produced to the affected columns is localized at the vicinity of the impact. Depending on the rock motion

parameters and the column's resistance, the latter may lose its load-bearing ability. This change to the boundary conditions of the structure may initiate a progressive collapse leading to high damage disproportionate to the original cause.

The presented method proposes a tool for the quantification of the vulnerability of reinforced concrete buildings, which are impacted at their base by a single fragmented rock.

For the simulation of the phenomenon, a spherical rock block diameter is considered to be moving against an exposed building's façade and impacting directly on it. The intensity parameter is the kinetic energy of the rock block, that is given by Eq. (3.1). The vulnerability, as it will be explained in the following, depends on the magnitude (volume) of the rock block and its velocity that determines the probability of encounter with a structural or non-structural element of the reinforced concrete building and the damage potential of the rock block. Given that the amount of the rotational energy in most cases does not represent but a small fraction of its total kinetic energy (Chau et al. 2002), only the translational motion parameters of the block are considered. The investigated phenomenon is shown in Figure 3.1.1.

$$E_k = \frac{1}{2}mv^2 \quad [3.1]$$

where,

m: rock mass

v: rock velocity

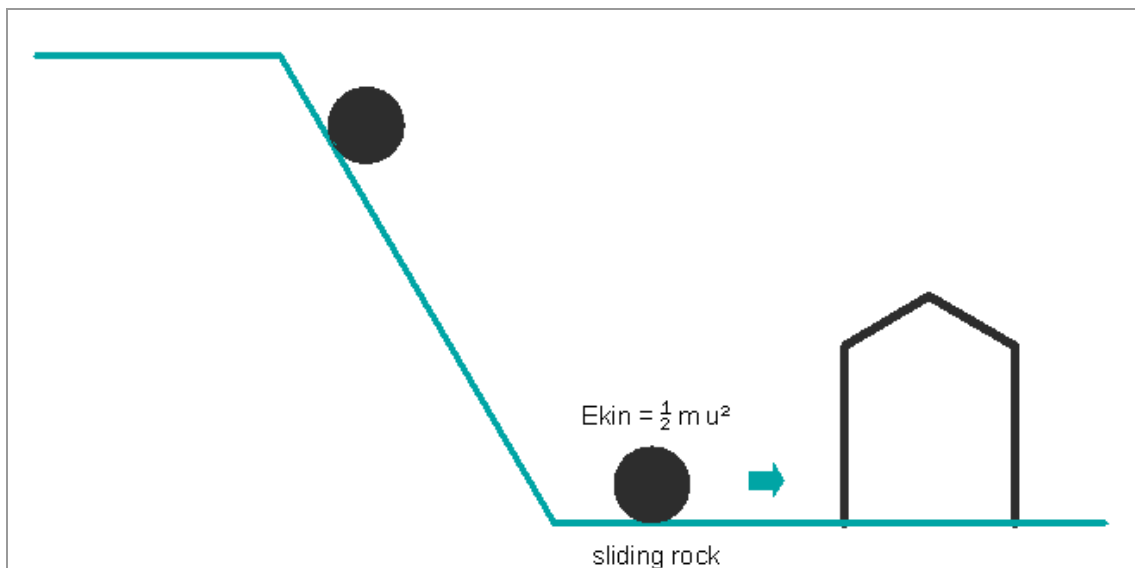


**Figure 3.1.1** Direct impact of a rock on the façade of a building at the bottom of the slope

### 3.2 METHODOLOGY FOR BUILDINGS AT SITE SPECIFIC SCALE (UPC)

The proposed methodology can be applied for the evaluation of reinforced concrete RC buildings. The methodology is explained through an example where the consequences of the impact of a single block are analyzed. Block impact intensities used in the example

correspond to velocities ranging from 0.5 to 8 m/sec and block diameters  $d$  from 0.20 to 4.6 m. The maximum  $E_k$  reached by the block is 4075 kJ ( $d = 4.60$  m,  $v = 8$  m/sec).

The vulnerability index is calculated for the case of a simple RC building (Fig. 3.2.1). It has a basement and two floors with 2 bays at x-direction and 3 at y-direction. The two-story building was designed using Eurocode 2 (BS EN 1992), so as to withstand its dead and live loads. Columns have a section of 35 x 35 cm and beams 25 x 60 cm. Columns have longitudinal reinforcement 1.46 % (Fig. 3.2.2) and beam 1.04 %. The shear reinforcement is 0.16 % and 0.13 % respectively. The typical storey height is 3 m. The materials are for concrete C20 (compressive strength 20 MPa) and for steel S500s (tensile strength 500 MPa).

The façade x is exposed to the impact of a single rock block that is assumed to move perpendicularly to the face of 11.05 m length. The soil structure interaction is not considered at the foundation level.

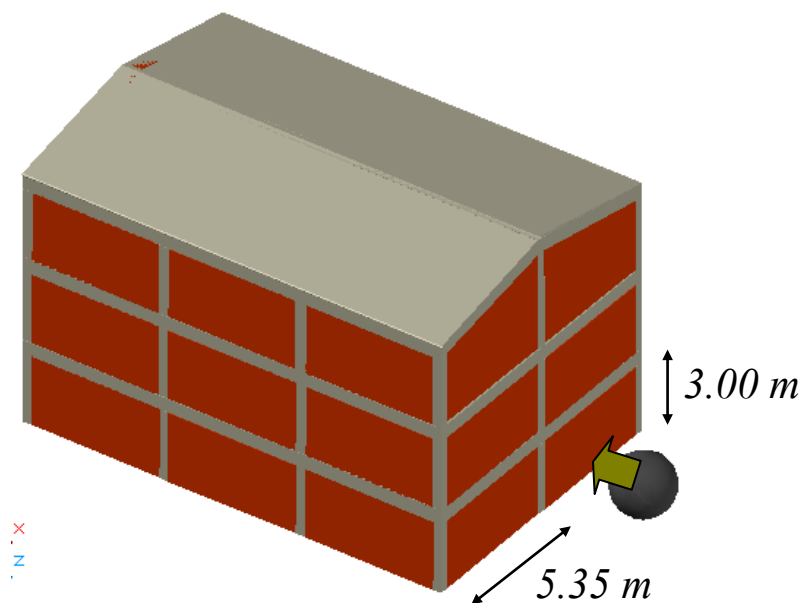


**Figure 3.2.1** The building geometry (dimensions in m)

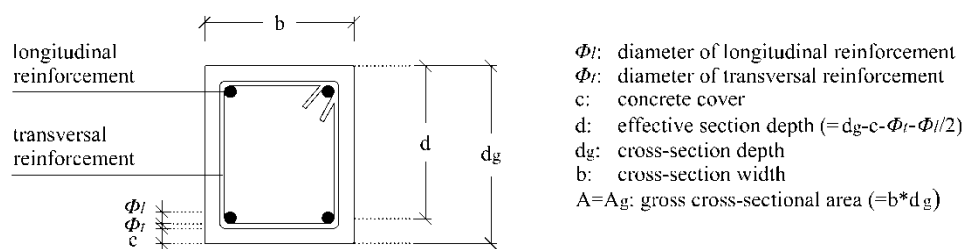


**Figure 3.2.2** Cross section of the column

The proposed methodology applies to reinforced concrete structures RC which are impacted by single fragmented rocks at their base, according to Mavrouli and Corominas (2010a and 2010b). It is analytical and it includes:

- analytical evaluation of the structural response of RC buildings to rockfalls,
- the quantification of the vulnerability using a vulnerability index for rockfalls,
- the development of fragility curves for RC buildings impacted by rockfalls.

### 3.2.1 Analytical evaluation of the structural response

The analytical evaluation of the structural response of RC buildings to rockfalls includes the following steps:

- Evaluation of whether the impacted element(s) is/are destroyed:
  - Calculation of the energy capacity of the impacted element(s):

A review of the existing experimental work on the ultimate impact resistance of reinforced concrete linear elements, such as columns, has indicated a predominant shear failure mode, instead of a flexural one (Remennikov and Kaewunruen 2006). This is, mainly, attributed to the high strain rate of the loading. Given this, the piecewise linear lateral load-shear displacement model developed by Sezen (2008) is used to predict the column's response. The model is presented in Fig. 3.2.3. The critical points identified in the proposed model include: Point A (lateral load:  $V_{cr}$ , displacement:  $\Delta_{cr}$ ) which represents the conditions under which the first diagonal cracking in concrete due to shear occurs. After the formation of the first crack the stiffness of the column is lower than the initial one, up to point B (lateral load:  $V_n$ , displacement:  $\Delta_n$ ), where the stress resistance is reached. Under the maximum shear stress the column is deformed up to point C (lateral load:  $V_n$ , displacement:  $\Delta_u$ ), where from the shear strength degrades (due to extensive cracking). During this phase, the column experiences additional shear deformations. The ultimate shear deformation is represented by Point D (lateral load=0, displacement:  $\Delta_{af}$ ) where the axial-load carrying capacity of the column is lost.

The high strain-rate effect enhances the strength and ductility of reinforced concrete and to take the associated dynamic effect into account, resistance should be multiplied with a Dynamic Increase Factor DIF of the order of 1.3 (Tsang and Lam 2008; and CEB 1990).

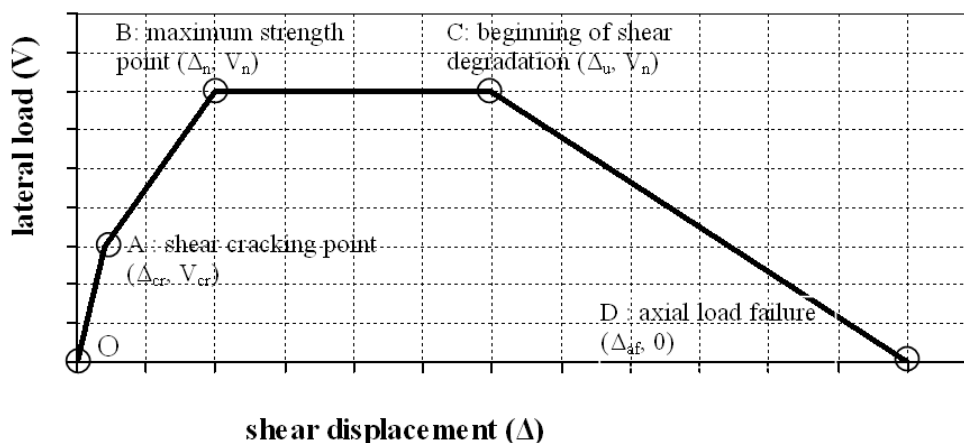


**Figure 3.2.3** Sezen's monotonic lateral load-shear displacement relationship

The critical points are calculated using Equations (3.2) to (3.7).

Point A: Shear cracking initiation (lateral load:  $V_{cr}$ , displacement:  $\Delta_{cr}$ )

$$V_{cr} = \left( \frac{P}{2 * f'_c * A_g} + 0.10 \right) \frac{G * A}{L} \quad [3.2]$$

$$\Delta_{cr} = \frac{V_{cr} * L}{G * A_g} \quad [3.3]$$

Point B: Maximum strength point (lateral load:  $V_n$ , displacement:  $\Delta_n$ )

$$V_n = V_s + V_c = k \frac{A_v * f_{yv} * d}{s} + k * \left( \frac{0.5 * \sqrt{f'_c}}{a/d} \sqrt{1 + \frac{P}{0.5 * \sqrt{f'_c} * A_g}} \right) * 0.8 * A_g \quad [3.4]$$

$$\Delta_n = \left( \frac{1}{25000} * \frac{(a/d) * f_{yt} * \rho_v}{\sqrt{\frac{P}{A_g * f'_c}}} - 0.0011 \right) * L \quad [3.5]$$

Point C: Beginning of shear degradation (lateral load:  $V_n$ , displacement:  $\Delta_u$ )

$$\Delta_u = \left( 4 - 12 \frac{V_n}{f'_c} \right) * \gamma_n * L \quad [3.6]$$

Point D: Ultimate shear deformation until the lost of the axial-load capacity (lateral load=0, displacement:  $\Delta_{af}$ )

$$\Delta_{af} = L * \frac{4}{100} * \frac{1 + \tan^2 \theta}{\tan \theta + P * \left( \frac{s}{A_v * f_{yv} * d_c * \tan \theta} \right)} \quad [3.7]$$

where P: axial load,  $f'_c$ : concrete compressive strength, A: gross cross-sectional area (Fig. 5), L: column length, G: shear modulus,  $A_g$ : gross cross-sectional area,  $A_v$ : cross sectional area of transverse reinforcement oriented parallel to the applied shear, s: longitudinal spacing between transverse reinforcement, k: constant varying according to displacement ductility (1.00 for ductility less than 2),  $f_{yv}$ : transverse steel yield strength, a: shear span, d: effective section depth,  $f_{yt}$ : longitudinal steel yield strength,  $\rho_v$ : transverse steel reinforcement ratio,  $v_n = V_n / (b * d)$ , b: width of the cross section,  $\theta$ : angle of the shear crack and  $d_c$ : depth of the core concrete, measured to the centerlines of the transverse reinforcement.

Using this model, the energy capacity of one column of the investigated building is 14 kJ.

- Consideration of the column destruction when the energy capacity is exceeded during the impact:

From the safety side, elastic collision and full transmission of the kinetic energy of the block to the impacted element is considered. When the kinetic energy of the rock block is higher than the energy capacity of the columns, destruction of the latter is considered.

- Evaluation of the potential of the structure for progressive collapse:
  - Selection of the alternative scenarios:

Alternative scenarios must be chosen with respect to the rock block kinetic energy at the moment of the impact, the location of the initial impact and the affected columns after the initial impact. For each kinetic energy level, at least the most unfavourable scenarios for each kinetic energy level should be considered concerning the number of the impacted columns.

For the evaluation of the potential structural damage, four levels of  $E_k$  and three impact locations are considered. The selected  $E_k$  levels are those capable to cause the destruction of one, two, three or four columns. For this particular building the  $E_k$  thresholds are 14, 28, 42, 56 kJ respectively. The three impact locations for this building are: a lateral column, a central column or an infill wall. Under these assumptions, for the damage of 1, 2, 3, or 4 central or lateral columns, the possible consequence scenarios are nine (Fig. 3.2.4). Each scenario will result in a specific DI.

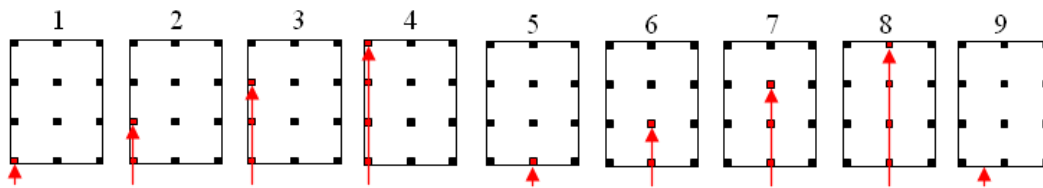


**Figure 3.2.4** The 9 considered scenarios (columns in the path of the red arrows have failed)

- Calculation of the probability of encounter of a rock block with the structural or non-structural element(s) which is/are involved in each alternative scenario,  $P_{e,k}$ .

For this geometry, the probability of encounter of a rock with a lateral column  $P_{elc}$  is the double of the one obtained with a central column  $P_{ecc}$ :

$$P_{elc} = \min\left(\frac{2 l_c + d}{3 l_c + l_w}, 1\right) \quad [3.8]$$

$$P_{ecc} = \min\left(\frac{1 l_c + d}{3 l_c + l_w}, 1\right) \quad [3.9]$$

$$P_{ew} = \min\left(\frac{l_w + d}{l_c + l_w}, 1\right) \quad [3.10]$$

where  $P_{ew}$  is the encounter probability of a rock with a wall only.

- Development and iterative analyses of the finite element model FEM of the structure:

The FEM of the structure is developed omitting the destroyed element(s) for each scenario. The stress state is checked for each element section (columns and beams) and wherever the resistance is exceeded, the member(s) is/are considered destroyed and is/are removed from the FEM. Analysis is performed for the new model, until a new equilibrium state or total collapse is reached for the entire structure.

The developed finite element model of the building is shown in Figure 3.2.5. The software SAP v. 10 was used to this purpose.

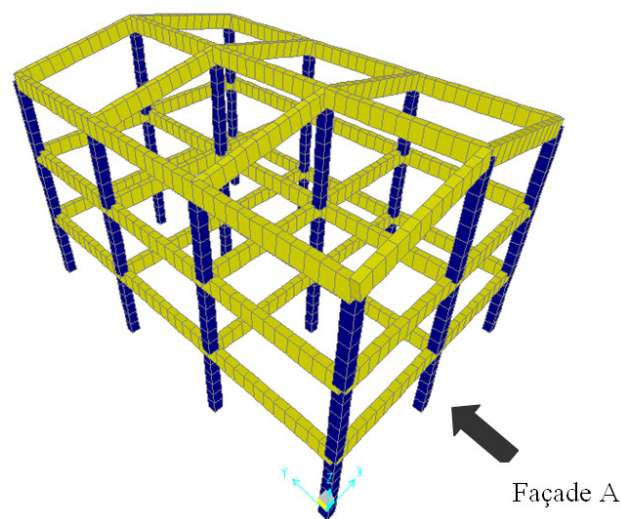


**Figure 3.2.5** Finite element model of the building

- Calculation of the damage index DI for the remaining undamaged structure as:

$$DI = \frac{\text{number of primary structural elements that fail}}{\text{total number of primary structural elements}} \quad [3.11]$$

The results are shown in Fig. 3.2.6 for every scenario.

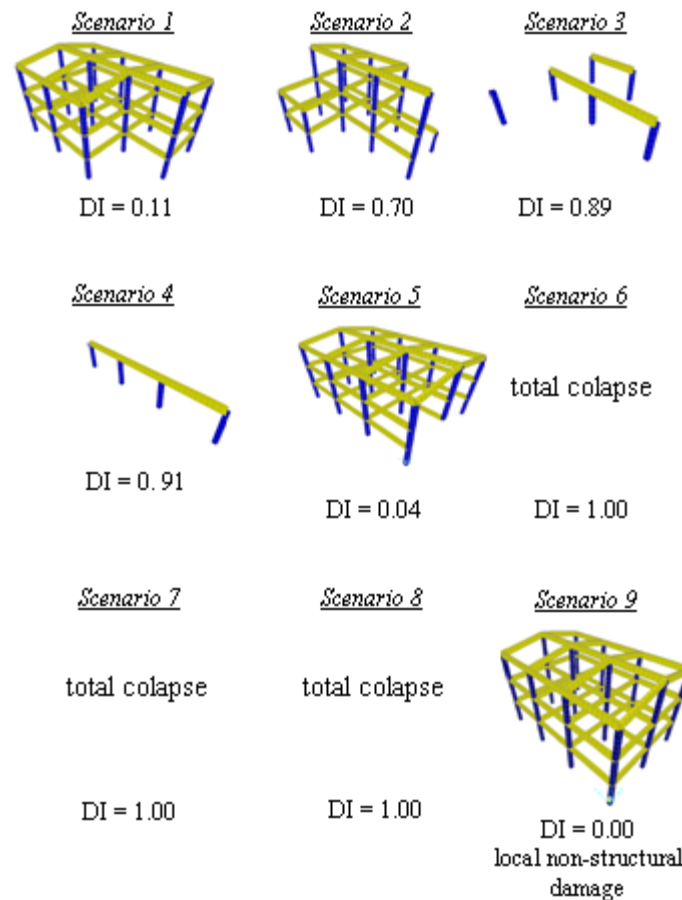


**Figure 3.2.6** Remaining undamaged structure and structural damage index  $DI$  that results for every impact scenario

Four damage states are thus proposed here: (1) non-structural damage: the impact causes the destruction of primary non-structural elements; (2) local damage: the impact causes the destruction of primary structural elements without further significant damage; (3) partial collapse: the impact causes the destruction of primary structural elements, whose loss initiates a progressive collapse of the structural frame leading to loss up to 30 % of the building; (4) extensive to total collapse: the impact causes the destruction of primary structural elements whose loss initiates a progressive collapse of the structural frame leading to physical loss greater than 30 % of the building.

- Calculation of the relative repair cost  $RRC$  in function of the damage index  $DI$  as:

$$RRC = \frac{\text{recovery cost}}{\text{value of building}} = f(DI) \leq 1 \quad [3.12]$$

To determine the function that correlates the  $RRC$  with the  $DI$ , proper damage scales based on historical events of rockfalls or other type of accidental events (e.g. earthquake) may be used. A proposed damage scale, which is provided by Whitman et al. (1973) is adapted and used here, as shown in Figure 3.2.7.

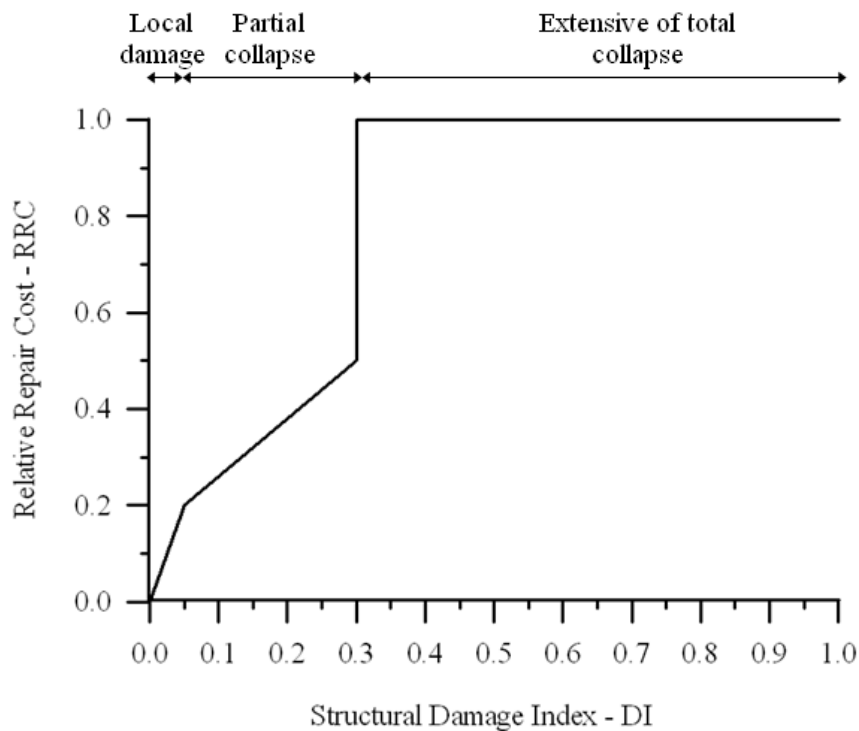


**Figure 3.2.7** Correlation of RRC with the DI

### 3.2.2 Quantification of the vulnerability using a damage index

The quantification of the vulnerability is made using the index:

$$V(R_{ij}) = \sum_{k=1}^k (P_{e,k} \times RRC_k) \leq 1 \tag{3.13}$$

where,

$V(R_{ij})$ : vulnerability for a rock block with a magnitude “i” and velocity “j”,

$P_{e,k}$ : encounter probability of a rock with a possible structural and non-structural element of the building “k” that may be struck by a rock block of magnitude “i”,

$RRC_k$ : relative recovery cost that corresponds to the struck of a possible structural and non structural element of the building “k” by a rock block of magnitude “i” and velocity “j”.

For the investigated building, Eq. (2.13) takes the form:

$$V(R_{ij}) = P_{elc} \times RRC_{lc} + P_{ecc} \times RRC_{cc} + P_{ew} \times RRC_w \leq 1 \tag{3.14}$$

where,

$RRC_{lc}$ : relative repair cost for impact on a lateral column,

$RRC_{cc}$ : relative repair cost for impact on a central column,

$RRC_w$ : relative repair cost for impact on a wall.

The results are shown in Table 3.2.1.

**Table 3.2.1** Vulnerability values for the investigated building in function of the rock velocity and diameter.

d (m)	m (kg)	v (m/s)															
		0.5	1.0	1.5	2.0	2.5	3.0	3.5	4.0	4.5	5.0	5.5	6.0	6.5	7.0	7.5	8.0
0.20	10	0.00	0.00	0.00	0.00	0.00	0.00	0.00	0.00	0.00	0.00	0.00	0.00	0.00	0.00	0.00	0.00
0.40	84	0.00	0.00	0.00	0.00	0.00	0.00	0.00	0.00	0.00	0.00	0.00	0.00	0.00	0.00	0.00	0.00
0.60	283	0.01	0.01	0.01	0.01	0.01	0.01	0.01	0.01	0.01	0.01	0.01	0.01	0.01	0.01	0.01	0.01
0.80	670	0.01	0.01	0.01	0.01	0.01	0.01	0.01	0.01	0.01	0.01	0.01	0.01	0.01	0.05	0.05	0.05
1.00	1308	0.01	0.01	0.01	0.01	0.01	0.01	0.01	0.01	0.01	0.01	0.01	0.05	0.05	0.05	0.26	0.26
1.20	2261	0.01	0.01	0.01	0.01	0.01	0.01	0.01	0.06	0.06	0.30	0.30	0.30	0.30	0.30	0.30	0.30
1.40	3590	0.01	0.01	0.01	0.01	0.01	0.07	0.07	0.34	0.34	0.34	0.34	0.34	0.34	0.34	0.34	0.34
1.60	5359	0.01	0.01	0.01	0.01	0.07	0.07	0.37	0.37	0.37	0.37	0.37	0.37	0.37	0.37	0.37	0.37
1.80	7630	0.01	0.01	0.01	0.08	0.08	0.41	0.41	0.41	0.41	0.41	0.41	0.41	0.41	0.41	0.41	0.41
2.00	10467	0.01	0.01	0.01	0.09	0.45	0.45	0.45	0.45	0.45	0.45	0.45	0.45	0.45	0.45	0.45	0.45
2.20	13931	0.01	0.01	0.09	0.09	0.49	0.49	0.49	0.49	0.49	0.49	0.49	0.49	0.49	0.49	0.49	0.49
2.40	18086	0.01	0.01	0.10	0.52	0.52	0.52	0.52	0.52	0.52	0.52	0.52	0.52	0.52	0.52	0.52	0.52
2.60	22995	0.01	0.01	0.11	0.56	0.56	0.56	0.56	0.56	0.56	0.56	0.56	0.56	0.56	0.56	0.56	0.56
2.80	28721	0.01	0.11	0.60	0.60	0.60	0.60	0.60	0.60	0.60	0.60	0.60	0.60	0.60	0.60	0.60	0.60
3.00	35325	0.01	0.12	0.64	0.64	0.64	0.64	0.64	0.64	0.64	0.64	0.64	0.64	0.64	0.64	0.64	0.64
3.20	42871	0.01	0.13	0.67	0.67	0.67	0.67	0.67	0.67	0.67	0.67	0.67	0.67	0.67	0.67	0.67	0.67
3.40	51423	0.01	0.13	0.71	0.71	0.71	0.71	0.71	0.71	0.71	0.71	0.71	0.71	0.71	0.71	0.71	0.71
3.60	61042	0.01	0.75	0.75	0.75	0.75	0.75	0.75	0.75	0.75	0.75	0.75	0.75	0.75	0.75	0.75	0.75
3.80	71791	0.01	0.79	0.79	0.79	0.79	0.79	0.79	0.79	0.79	0.79	0.79	0.79	0.79	0.79	0.79	0.79
4.00	83733	0.01	0.82	0.82	0.82	0.82	0.82	0.82	0.82	0.82	0.82	0.82	0.82	0.82	0.82	0.82	0.82
4.20	96932	0.01	0.86	0.86	0.86	0.86	0.86	0.86	0.86	0.86	0.86	0.86	0.86	0.86	0.86	0.86	0.86
4.40	111449	0.01	0.90	0.90	0.90	0.90	0.90	0.90	0.90	0.90	0.90	0.90	0.90	0.90	0.90	0.90	0.90
4.60	127348	0.17	0.94	0.94	0.94	0.94	0.94	0.94	0.94	0.94	0.94	0.94	0.94	0.94	0.94	0.94	0.94

### 3.2.3 Development of fragility curves

Fragility curves provide a graphic expression of the probability of exceeding a given damage state under a certain hazardous event. They are very useful when the performance of a building under a damaging event is governed by important uncertainties, thus the potential extent of the damage should be evaluated for different magnitudes (or intensities) of the hazardous event using probabilistic terms. To this purpose representative damage states which are associated with the consequences (i.e. financial cost, people safety etc.) should be defined. Fragility curves might be empirical, judgmental or analytical, depending on how the damage state is evaluated for a given magnitude (or intensity) of the hazardous event. The proposed methodology for the evaluation of fragility curves due to rockfalls is analytical, given that the potential damage for the buildings is calculated through the analytical simulation and evaluation of their performance after the first impact, using the finite element method.

The vulnerability of a structure to rockfalls expresses the expected loss due to the impact of a rock block of a certain magnitude and velocity. To evaluate it in quantitative terms, a function has to be defined that correlates both parameters with the probability of exceeding a certain response (i.e. damage) level, also accounting for the uncertainty of the impact location. This function may be described using sets of fragility curves. Based on this, in this paper, fragility curves will be generated for a range of rock diameters in function of the rock velocity taking into account the uncertainty of the impact location. The developed algorithm to this purpose is shown in Figure 3.2.8.

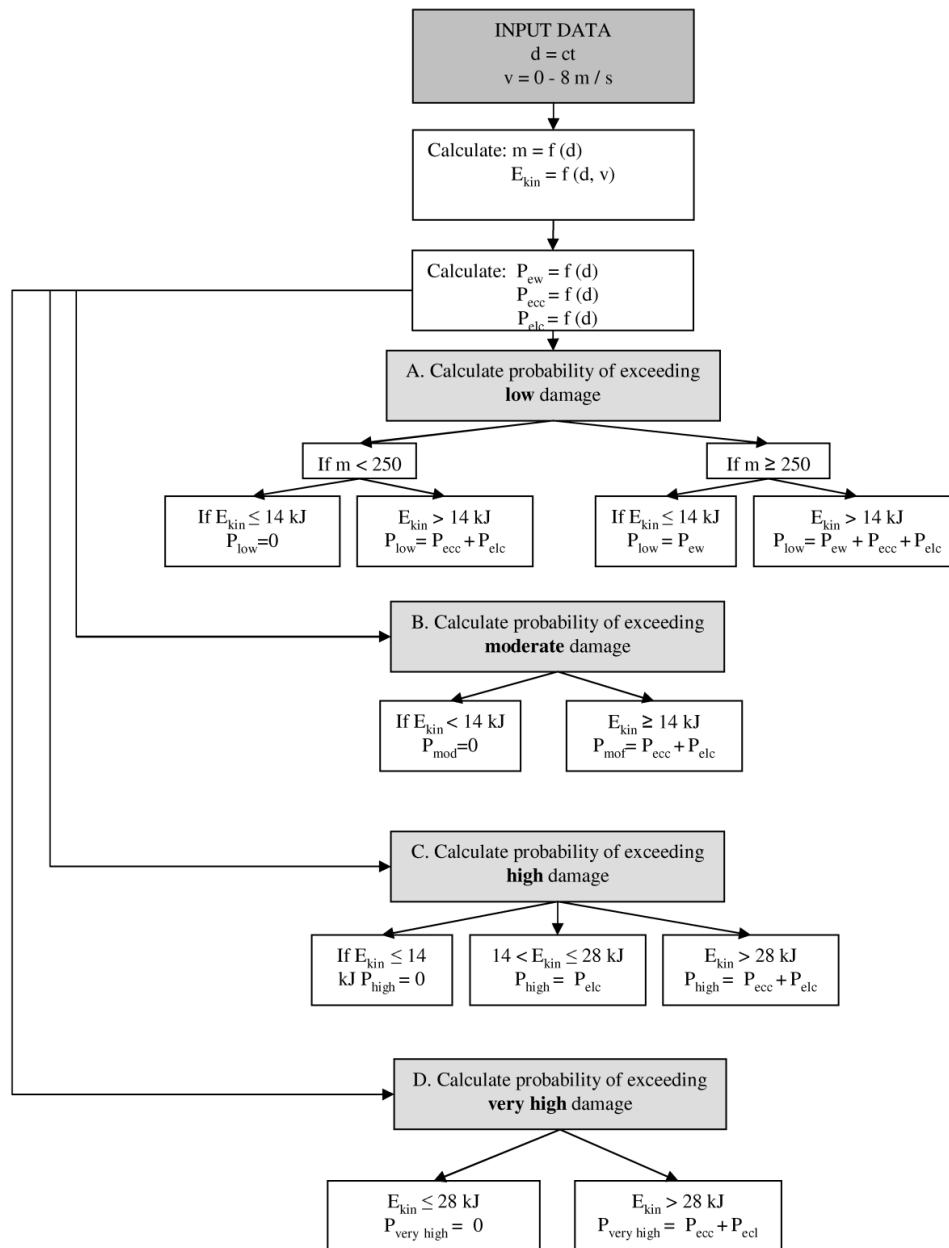


**Figure 3.2.8** Algorithm for the calculation of the probability of each damage state

The probability of exceedance for each damaged state is calculated in function of the probability of impact on a certain location of the structure (a structural or a non-structural element), on which depends the potential for a damage state. The final damage state is also determined by the rockfall energy, which according to given thresholds (see section 3.2.1) is sufficient to damage one or more basement columns at the impact. Consequently, for the considered building, every curve of the Fig. 3.2.9 is drawn considering 3 points, defined by the probability of exceedance for a damage state (calculated as described in Fig. 3.2.8) and the block diameter that, for a given velocity, corresponds to the 3 energy thresholds which are sufficient to damage of 1, 2 or 3 and more basement columns, leading to the different damage

states. Linear performance was considered for intermediate diameters, for simplicity. The results are shown in Figure 3.2.9 for a range of velocities and rock block diameters.

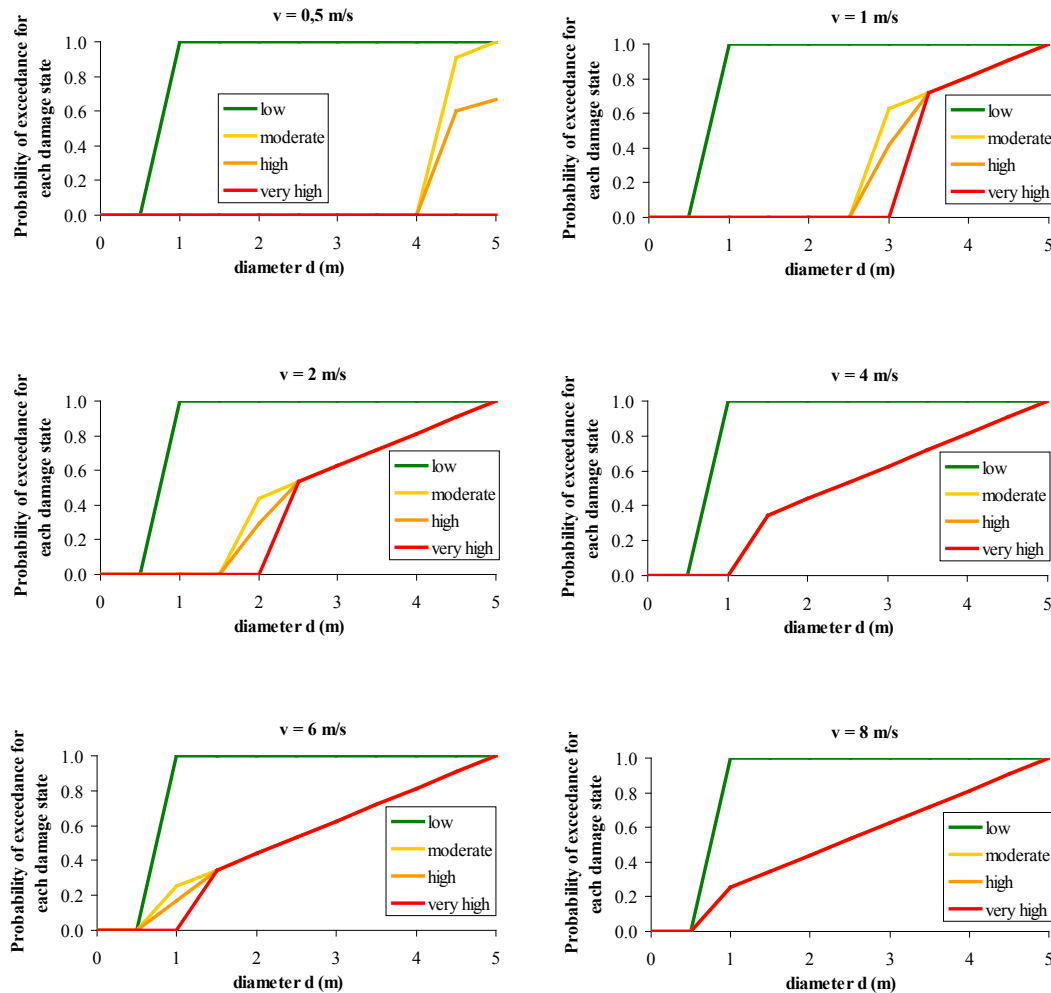


**Figure 3.2.9** Fragility curves for different rock velocities

The proposed methodology maybe applied at site-specific scale for the calculation of the vulnerability of an individual building, in the case of a single block impact on it. This situation is what might be expected in areas affected by low to moderate rockfall activity. It might be useful, for example, when the risk for an individual building must be evaluated for an owner or an insurance company, or for areas developed with a limited number of buildings mainly situated at the first line next to the slope, as for example in the case of Santa Coloma in Andorra (Corominas, 2005) where a small number of typologies should be analyzed.

The development of class representative fragility curves, based on the statistical elaboration of the results for individual buildings at a zone (considering uncertainties in geometric dimensions, material properties...) is an approach that has been already followed in the domain of seismic vulnerability (Polese et al., 2008) and similar methods may be developed for the generalisation of the results.

### 3.3 VULNERABILITY MODEL FOR ROCKFALL PROTECTION GALLERIES (ETHZ)

#### 3.3.1 Introduction

A vulnerability model for rockfall protection galleries is described in this section. The described model has been developed as part of a project sponsored by the Swiss Federal Road Authority (ASTRA). Further details about the model and the work carried out as part of this project are described in Schubert et al. (2005), Schubert and Straub (2008), Schubert (2009) and Schubert et al. (2010).

The generic framework used is based on a guideline document (JCSS 2008) developed by the Joint Committee on Structural Safety (JCSS) that describes the framework and principles for risk based engineering decision making. This framework has been described and used in other work areas of the SafeLand project, notably WP 2.1 (Deliverable D2.4 – Guidelines for landslide susceptibility, hazard and risk assessment and zoning) and WP 5.1 (Deliverable D5.3 – Quantitative risk-cost-benefit analysis of selected mitigation options for two case studies). The following provides a brief description of the framework.

The risk assessment for a given system is facilitated by considering the generic representation shown in Figure 3.3.1.

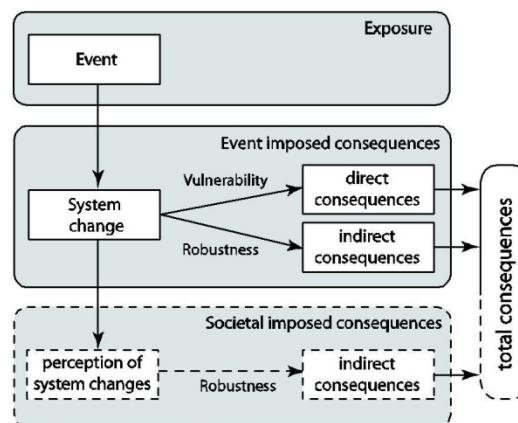


**Figure 3.3.1** Generic representation used for the risk assessment of a system

The exposure to an engineering facility is represented as a set of different exposure events acting on the constituents of the facility. The constituents of the facility can be considered as the first defence of the facility in regard to the exposures. The damages of the constituents are considered to be associated with direct consequences. Direct consequences may include monetary losses, loss of lives, damages to the qualities of the environment or just changed characteristics of the constituents. Direct consequences, are thus defined as all marginal (not considering loss of system functionality) consequences associated with damages or failures of the constituents of the system. Based on the combination of events of constituent failures and the corresponding consequences, follow-up or indirect consequences may occur. Indirect consequences may be caused by e.g. the sum of monetary losses associated with the constituent failures and the physical changes of the facility as a whole caused by the combined effect of constituent failures. The indirect consequences in risk assessment play a

major role and their modeling should be carefully considered. Typically the indirect consequences evolve spatially beyond the boundaries of the facility and also have a certain sometimes even postponed development in time. The vulnerability of the system characterizes the risk associated with the direct consequences and the robustness characterizes the degree to which the total risk is increased beyond the direct consequences.

### 3.3.2 Definition of the exposure for rockfall protection galleries

#### 3.3.2.1 *Probabilistic modeling of rock-fall frequency*

Due to the highly site specific nature of rock-fall phenomena, in general no or only little generally applicable statistical data is available. In addition, assessments by geologists are traditionally of a qualitative or a semi-quantitative nature and cannot be directly applied in a quantitative risk assessment. It is thus required to process the provided information and to address the significant uncertainties in the models explicitly. In the following a possible interpretation of the available information is developed and it is demonstrated how the model uncertainties can be included in the analysis in a quantitative manner. These uncertainties can then be reduced by updating the model based on observations or the results of more detailed geological assessments of the investigated area.

Most loads on structures due to natural hazards are best described by their exceedance frequency or probability. In the case of rock-fall hazards, a power-law is commonly applied to describe the exceedance frequency of detached rock volume, see e.g. Gutenberg et al. (1949), Dussauge-Peisser et al. (2002), Hovius et al. (1999) or Hungr et al. (1999). It should be noted that this function is purely empirically-based and has no physical or mathematical foundation. However, due to a lack of alternatives, the power-law is applied in the following. The exceedance frequency of detached rock volume  $V$  is thus defined as:

$$H_V(v | a, b) = a \cdot v^{-b} \quad [3.15]$$

with  $a$  and  $b$  being the statistical parameters describing the shape of the exceedance frequency function. The corresponding frequency density function is obtained as:

$$h_V(v | a, b) = \frac{\partial(-H_V(v | a, b))}{\partial v} = a \cdot b \cdot v^{-b-1} \quad [3.16]$$

Frequently, the geologist provides an estimation of the occurrence frequency for different ranges of detached volume. This information can be plotted in an exceedance frequency diagram (when transforming the occurrence to an exceedance frequency). In Figure 3.3.2, the estimated range of frequencies for one range of rock volume (denoted by “block fall”) is plotted in grey. This represents the information provided by the geologist. The uncertainty in this estimate can then be quantified by fitting a probability density function to the estimated frequency, as illustrated in Figure 3.3.2.

From the geological assessments, distributions can now be fitted for all volume ranges in analogy to the one illustrated in Figure 3.3.2. The parameters  $a$  and  $b$  describing the exceedance frequency can then be estimated using a maximum likelihood estimator (MLE), see Lindley (1965) or Faber (2009).

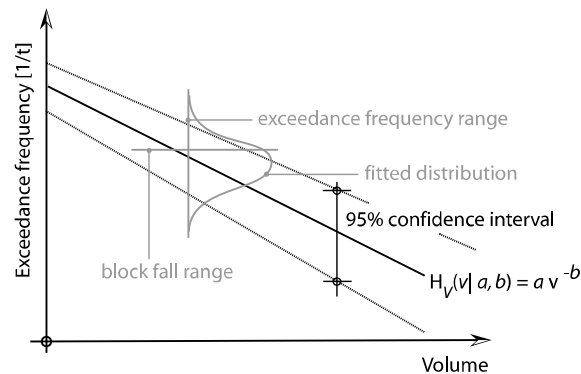


**Figure 3.3.2** Exceedance frequency of detached rock volume in a log-log scale.

The information matrix obtained from the MLE yields the standard deviations and the correlation factor of the joint Normal-distributed parameters  $a$  and  $b$ , enabling the calculation of the confidence interval, Faber (2009). The unconditional frequency density function is calculated as:

$$h_V(v) = \int_{-\infty}^{\infty} \int_{-\infty}^{\infty} h_V(v|a,b) \cdot f_{a,b}(a,b) da db \quad [3.17]$$

### 3.3.2.2 Uncertainties in frequency modelling

There are various sources for epistemic uncertainties in large-scale models, preventing an exact prediction of the exceedance frequency for a particular site:

- Statistical uncertainty: The parameters of the large-scale models are derived empirically from data-sets. Because of the limited size of these data sets, the estimated parameters are subject to statistical uncertainty.
- Measurement uncertainty: Measurements and recordings of the geological properties are typically subject to uncertainty and observations of rock-fall events are often incomplete and biased and must rely on local experts. As an example, rocks on a road will generally be reported and documented, but those that missed the road may often not be.
- Model uncertainty: Extrapolation of the statistical models to areas other than those for which observations are available leads to additional uncertainty as the geological and topographical characteristics will be different for these areas. GIS-based models will take into account some of these parameters, but the omitted parameters will lead to an uncertainty on the model predictions.
- Model uncertainty: Although the power-law is commonly assumed, it has not been justified by phenomenological considerations. Thus, it is not ensured that the parametrical model accurately represents the actual behaviour.
- Spatial variability: Rock-fall frequency varies in space. The observations represent an average over an area and the resulting parameter values, therefore, do not reflect the variations from the average.
- Temporal variability: Rock-fall frequency varies in time. When working with annual frequencies, the seasonal changes do not affect the analysis, but the frequency may change over the years or may be dependent on extreme events (e.g., earthquakes). However, in certain instances, e.g., when temporal closure of the road is considered as

a risk reduction measure, seasonal variations must be explicitly addressed by the analysis.

How can these uncertainties be quantified? Statistical uncertainty can be quantified by using standard statistical methods such as Bayesian analysis. Measurement uncertainty can generally be estimated when the data collection method is known. Unfortunately, no simple analytical method is available for estimating model uncertainties. A solution is to rely on expert opinion, i.e., to ask experts about their confidence in the models. It is also possible to compare the model with observations which have not been used in the calibration of the model (model validation) or to compare different models. Furthermore, it is possible to include additional parameters in the formulation of the exceedance frequency. The model uncertainties are then reduced while the statistical uncertainties increase, but the latter can then be estimated analytically.

### 3.3.2.3 *Updating the exceedance frequency*

When rock-fall events are observed or when the number of fallen rocks is counted, the parameters  $a$  and  $b$  describing the exceedance frequency can be updated using Bayes' rule. The posterior probability of  $a$  and  $b$  is obtained as:

$$f_{ab}''(a, b | n_R) = P(n_R | a, b) f_{ab}'(a, b) c_1 \quad [3.18]$$

where ' indicates the prior and '' the posterior distribution.  $n_R$  is the number of observed rocks larger than a specified volume  $v_n$  and  $P(n_R | a, b)$  is the probability of observing  $n_R$  rocks as calculated with the prior model with parameter values  $a$  and  $b$ . For the simple case when the falling process is not considered and all detached rocks are counted,  $P(n_R | a, b)$  is calculated from Equation (3.18) as

$$P(n_R | a, b) = \frac{H_v(v_n | a, b)^{n_R}}{n_R!} e^{-H_v(v_n | a, b)} \quad [3.19]$$

### 3.3.2.4 *Modeling the falling process*

Once the rock-fall process has initiated and the boundary conditions for a falling, rolling, bouncing or sliding movement are given, various models are available to calculate the falling process. These can be divided into trajectory and distribution models. Most models simplify the problem by assuming that the mass of the stone is concentrated in one point or by neglecting the mass of the stone. Such models are called lumped mass models. Rigorous models take the shape and the volume of the rock into account. The latter models provide, in general, more accurate results. A list of different rock-fall calculation programs can be found in Heidenreich (2004). The important input parameters to the models are the profile of the slope and the restitution coefficients, which are measures for the dissipated energy of a falling rock mass at ground contact. These are calculated as the ratio between the post and the pre-impact values of the normal and tangential velocity components, Giani et al. (2004). The values of these coefficients depend on the geology, the morphology, the structure and the vegetation of the contact surface.

The simulations yield a distribution of the impact energy on the gallery. By performing calculations for all volumes  $V$  the probability density function of the energy  $E$  at the gallery  $G$  conditional on the detached volume  $v$ ,  $f_E^G(e|v)$ , is obtained. The joint frequency density function of the volumes and energies of the rocks hitting the gallery  $G$  is then:

$$h_{EV}^G(e, v) = f_E^G(e|v) \cdot h_V(v) \quad [3.20]$$

The joint exceedance frequency is determined by integration of Equation (3.20):

$$H_{EV}^G(e, v) = \int_e^\infty \int_v^\infty f_E^G(e|v) h_V(v) dv de \quad [3.21]$$

For the calculation of the reliability of a protection system, the extreme value distribution, i.e. the distribution of the annual maxima rather than the frequency is of interest. By assuming that rock-fall events follow a Poisson process, this probability distribution function can be obtained as

$$\begin{aligned} F_{EV}^G(e, v) &= 1 - \left( 1 - \frac{H_{EV}^G(e, v)^0}{0!} e^{-H_{EV}^G(e, v)} \right) \\ &= 1 - e^{-H_{EV}^G(e, v)} \end{aligned} \quad [3.22]$$

Differentiation of Equation (3.22) yields the probability density function of the impact:

$$f_{EV}^G(e, v) = \frac{\partial^2 F_{EV}^G(e, v)}{\partial e \partial v} \quad [3.23]$$

Figure 3.3.3 illustrates the marginalized exceedance frequency and the probability of rock-fall volumes.

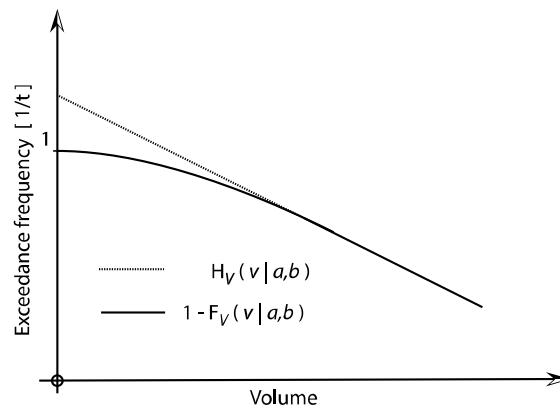


**Figure 3.3.3** Illustration of the marginalized exceedance frequency and the marginalized exceedance probability.

Note that the transformation from the frequency distribution to the density distribution must be performed for the combined energy-volume distribution and not for the distribution of detached volume. Consider a situation where rock-fall events are very frequent but only a small percentage of the rocks reach the gallery. If in Equation (3.20) the probability density function of the maximal volume is used (instead of the frequency density), a very high probability of no-impact in the considered time range results. However, this neglects the high frequency of rocks detached.

### *3.3.2.5 Uncertainties in rockfall trajectory*

The factors that contribute to the uncertainty in the prediction of the rockfall trajectory include the topography, its mode of motion (free fall, rolling, bouncing or sliding) and the characteristics of the surfaces of the rock and the ground. Existing numerical tools model this uncertainty by means of crude Monte Carlo simulation (MCS). The impact is the most intricate part of the falling process and its modelling is associated with large uncertainties. The modelling cannot account for the variability in the ground material (particularly in zones covered with vegetation) and the local geometry of the ground and the rock. These uncertainties are inherent to the model and can therefore be considered as aleatory. In addition, there is an epistemic uncertainty because of the limited basis for estimating the model parameters. Additional epistemic uncertainty is due to the simplified modelling of the slope profile at the impact location. In many applications, the profile surface in the models is generated from a digital elevation model (DEM) with limited resolution and between the points provided by the DEM the terrain is assumed to be linear. If the model is 2-dimensional, the reduction to a single plane is an additional source of epistemic uncertainty.

### *3.3.2.6 Impact modeling*

On many galleries a protective cushion layer is present on top of the concrete structure, a compound of sand and gravel, which mitigates so-called hard impacts and reduces the energy transmitted between the rock and the concrete. During the impact the protective cushion layer dissipates energy of the rock mass and shares the load to a larger area. Hard impacts generate high frequent waves with high amplitudes producing locally high damages. During a soft impact the cushioning layer between the rock and the cushion layer will be plastically deformed. According to FE-calculations of impacts by Bucher (1997), the interaction between the stiffness of the structure and the impact load can be neglected. Hence it is possible to calculate the behavior of the structure separated from the impact. A procedure for the calculation of static equivalent loads for the dynamic structural analysis of impact loads is formulated and verified by tests in Montani and Descoedres (1996).

## **3.3.3 Resistance modelling for rockfall protection galleries**

Several models for the resistance of rockfall protection galleries can be found in literature. A model for the punching resistance of slabs (without shear reinforcement) has been described in Muttoni (2003). An analytical model for the impact load capacity of rockfall protection galleries considering their dynamic response has been developed in Schellenberg (2008) based on a system of multiple degrees of freedom. This model is briefly described in Section 3.3.4.1.

## **3.3.4 Development of vulnerability curves for rockfall protection galleries**

### *3.3.4.1 Modelling of the vulnerability of rockfall protection galleries*

The detachment process and the falling process are highly site specific and the challenge is to develop a model in a generic sense. A vulnerability curve gives the probability for a certain predefined state of an object, conditional on one or more descriptive indicators. Without loss

---

of generality, the predefined state can in principle be any damage or failure state (sometimes also denoted as limit states) which is of interest and which may contribute to the total risk. In general, vulnerability curves are described by the descriptive indicators and thus, the dimension of the vulnerability curve is determined by the number of indicators which are used to describe the damage or failure state, i.e. the vulnerability of the object. In the simplest case, only one indicator is used to describe the vulnerability of an object.

The development of vulnerability curves is necessary if generic hierarchical probabilistic models are developed; they allow the calculation of the damage state conditional on given or predefined conditions of the system. The vulnerability curve can in many cases be calculated apart from the calculation of the exposure and can be later implemented in the entire probabilistic model. For this purpose the interfaces between the exposure model and the vulnerability model have to be defined. In this case the characteristic of the conditional independence of the vulnerability can be used. In general, the meaning of the vulnerability can be described with the total probability theorem:

$$P(A) = \sum_{i=1}^n P(A|B_i) P(B_i) \quad [3.24]$$

The term  $P(A|B_i)$  in equation (10) can be interpreted as the vulnerability. This term gives the probability for the event  $A$  (e.g. a failure of damage state), conditional on the indicator  $B$ .

Let  $B$ , for example, be the velocity of a stone at the impact location on the protection gallery and  $A$  the failure event which can be denoted by  $F$ ; then a typical vulnerability curve is shown in Figure 4.

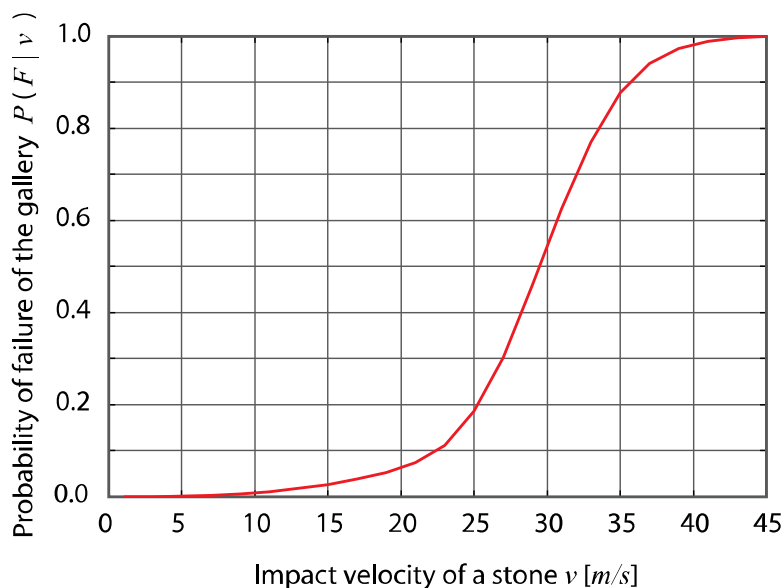


**Figure 3.3.4** Simplified example for a vulnerability curve of a rockfall protection gallery.

On the x-axis in Figure 4 the impact velocity of a stone at the impact location on the rockfall protection gallery is shown. The impact velocity is the only relevant indicator which is considered in this simplified example. On the y axis the probability of failure  $P(F|v)$  for the

gallery is shown. The probability of failure of the gallery, given that the velocity of the stone is 30 m/s is in the example in Figure 4 equal to 0.55.

Figure 3.3.4 shows a strong simplification of the reality. It is obvious that many different indicators, such as the characteristics of the stone and the gallery contribute significantly to the probability of failure of the gallery. The vulnerability curves for the rockfall protection galleries are thus more complex and multidimensional. By using the following five indicators the vulnerability curves for rockfall protection galleries can be calculated:

- Impact velocity at the impact location
- Mass of the falling stone
- Year of construction of the gallery
- Thickness of the concrete ceiling of the protection gallery
- Thickness of the cushion layer on the protection gallery

The indicators Year of the construction of the gallery and the thickness of the ceiling of the protection gallery are both aggregated indicators. They contain other relevant indicators such as material properties and properties of the reinforcement. However, due to the aim to develop generic vulnerability curves and due to limited computational times and resources, these indicators are only implicitly considered. This is not a general limitation but since such information can often hardly be obtained, it is reasonable to use such aggregated indicators.

The indicator year of construction contains information on the material properties of the concrete and the reinforcement bars. Depending on the requirements on the current generation of the codes and standards different concrete and steel qualities with different properties are used. The aggregated indicator thickness of the concrete ceiling is used for both, to model the thickness itself but also to consider the reinforcement ratio. Here, it can be assumed that the same amount of reinforcement has been installed that in the concrete compression zone of the gallery ceiling a plastic stress block will develop and that this plastic stress block has a size that no compression reinforcement is required in the ceiling. In this sense the whole cross section of the concrete ceiling is utilized completely in the limit state.

Since the design values of the concrete compression strength and the design values of the yield strength of the reinforcement changed over the last decades depending on the different code generation, also the reinforcement ratio changed.

For the calculation of the vulnerability curve a physical model is used. Different models for calculation the resistance of an impact on a concrete slab are available in the literature. Here, a model which was developed specifically for the impact on rockfall protection galleries was used. This deterministic model is described in detail in Schellenberg (2008). In the following only a broad overview on the model is given.

The model assumes a three mass oscillator and considers two different limit states, i.e. bending failure of the concrete slab and punching failure at the impact location. Punching failure at the columns due to an overloading is not considered by the model. The model was tested and calibrated through testing on a scale 1:2.

The developed computational model corresponds to a dynamic system with multiple degrees of freedom and is defined by the following form:

$$p = \mathbf{M} \ddot{y} + \mathbf{C} \dot{y} + \mathbf{K} y \quad [3.25]$$

$\mathbf{M}$  in Equation (3.25) is a matrix consisting of the three different masses of the system. The mass  $M_1$  corresponds to the mass of the impacting stone. The mass  $M_2$  is the mass of the considered punching cone in the slab due to the loading and  $M_3$  is the mass of the surrounding structure of the rockfall protection gallery.

Thus,  $\mathbf{M}$  is given by:

$$\mathbf{M} = \begin{bmatrix} M_1 & 0 & 0 \\ 0 & M_2 & 0 \\ 0 & 0 & M_3 \end{bmatrix} \quad [3.26]$$

$\mathbf{K}$  in Equation (3.25) is the stiffness matrix of the system. The stiffness matrix is described by three different non linear springs. The first spring  $K_1$  represents the characteristics of the cushion layer on the gallery. The second spring  $K_2$  represents the shear behavior at the critical section in the concrete ceiling and the third spring  $K_3$  represents describes the bending stiffness of the global system.

$$\mathbf{K} = \begin{bmatrix} K_1 & -K_1 & 0 \\ -K_1 & K_1 + K_2 & -K_2 \\ 0 & -K_2 & K_2 + K_3 \end{bmatrix} \quad [3.27]$$

For the bearing capacity of the gallery the damping  $\mathbf{C}$  is of less importance since a failure event in general will occur during the first load peak. However, the components of the damping will be briefly described here. Damping effects result mainly due to the used building material in the gallery.  $\mathbf{C}$  consists of three different components whereas  $C_1$  represents the damping of the cushion layer,  $C_2$  the local damping of the gallery at the impact location and  $C_3$  global damping effects of the entire gallery. The matrix  $\mathbf{C}$  can be written as:

$$\mathbf{C} = \begin{bmatrix} C_1 & -C_1 & 0 \\ -C_1 & C_1 + C_2 & -C_2 \\ 0 & -C_2 & C_2 + C_3 \end{bmatrix} \quad [3.28]$$

The equations for the calculation of the components of the matrix  $\mathbf{M}$ ,  $\mathbf{K}$  and  $\mathbf{C}$  and are given in Schellenberg (2008) and will not be repeated here. For the calculation of Equation (3.25) time step integration is used. The time steps  $\Delta t \leq 1[ms]$  are small in comparison to the total loading time  $\approx 12[ms]$ . The small time steps allow a simplified integration without disturbance of the convergence characteristics. The calculation can be performed by using any standard math software. Since no closed analytical solution is available for the punching and bending failure a Monte Carlo simulation for the calculation of the failure probability was used (see e.g. Melchers (2002)). The probabilistic model for the input parameters of the model is given in Table 3.3.1. The stiffness and concrete compression strength was modeled by using the

considerations given in JCSS (2001). The values of the parameters required for modelling the concrete compressive strength for different code generations for Switzerland are given in Table 3.3.2. The characteristics of the reinforcement steel are given in Table 3.3.3.

**Table 3.3.1 Probabilistic model for the calculation of the vulnerability curves.**

<i>Parameter</i>	<i>Description</i>	<i>Mean value</i>	<i>COV</i>	<i>Distribution</i>
$\alpha$	<i>Factor of the modal mass <math>M_3</math></i>	0.33	0.12	<i>Lognormal</i>
$k_w$	<i>Factor of the global stiffness of the gallery</i>	60	0.12	<i>Lognormal</i>
$\zeta_2$	<i>Damping coefficient of the damping behaviour.</i>	0.05	0.1	<i>Lognormal</i>
$\zeta_3$	<i>Damping coefficient of the bending behaviour.</i>	0.015	0.1	<i>Lognormal</i>
$\gamma_g$	<i>Specific weight of the cushion layer [kN / m<sup>3</sup>]</i>	20	0.15	<i>Normal</i>
$K_{10}$	<i>Initial stiffness of the cushion layer [N / mm]</i>	30000	0.1	<i>Normal</i>
$K_{1,max}$	<i>Max. stiffness of the cushion layer [N / mm]</i>	500000	0.1	<i>Normal</i>
$\varphi$	<i>Inner friction angle of the cushion material</i>	33	0.1	<i>Normal</i>
$c_1$	<i>Damping constant of the cushion material [Ns / m]</i>	7000	0.14	<i>Normal</i>
$A_{sg}$	<i>Max. steel strain [%o]</i>	55	0.09	<i>Normal</i>

**Table 3.3.2** Model for the concrete compression strength for different code generations.

Code	Representative concrete	Distribution	Parameter		Moments <sup>[N / mm<sup>2</sup>]</sup>	
			$\lambda$	$\xi$	$\mu$	$\sigma$
SIA162:1956	BN 350	Lognormal	2.9	0.14	18.35	2.58
SIA162:1968	BN	Lognormal	3.03	0.24	21.30	5.18
SIA162:1989	BN	Lognormal	3.03	0.24	21.30	5.18
SIA162:1993	B35/25	Lognormal	3.38	0.16	29.75	4.78
SIA262:2003	C30/37	Lognormal	3.63	0.14	38.20	6.15

**Table 3.3.3** Model for the steel strength for different code generations.

Code	Representative steel	Distribution	Parameter		Moments <sup>[N / mm<sup>2</sup>]</sup>	
			$\lambda$	$\xi$	$\mu$	$\sigma$
SIA162:1956	II a)	Lognormal	6.02	0.07	412.60	28.92
SIA162:1968	III a)	Lognormal	6.23	0.05	508.40	25.44
SIA162:1989	S500	Lognormal	6.33	0.07	562.53	39.43
SIA162:1993	S500	Lognormal	6.33	0.07	562.53	39.43
SIA262:2003	B500B/A	Lognormal	6.33	0.07	562.53	39.43

In order to develop generic vulnerability curves some assumptions have to be made. These assumptions will be discussed in the following. The materials used in the gallery are given in Table 3.3.2 and Table 3.3.3. They represent the most common building materials for galleries in this time. Aging effects such as concrete or steel corrosion are not considered. It is implicitly assumed that the maintenance of the gallery was conducted in an optimal manner.

In the current state of the model from Schellenberg (2008) it is assumed that the rocks hit the gallery in the middle of the slab. The impact location plays a role in the bearing capacity of a gallery roof. However, as an approximation it can be assumed that a hit in the middle of the roof represents all possible locations. It should be noted that all these assumptions are in general not necessary to make but they reduce the computational time for a generic model significantly.

Additionally, it is assumed that the roof of the gallery is fixed on one side and has a free support on the other side. This assumption has an influence on the modal mass  $M_3$  in the model. Both assumptions are idealizations of the reality since both supports act like springs with different stiffness values in reality. Thus, a coefficient of variation of 0.12 of the factor  $\alpha$  was used in the model.

The ratio between the span length of the concrete slab was determined with 0.9, i.e. that the span length perpendicular to the road is slightly smaller than the one in the direction of the road. In Figure 3.3.5 an illustration of the system is given.

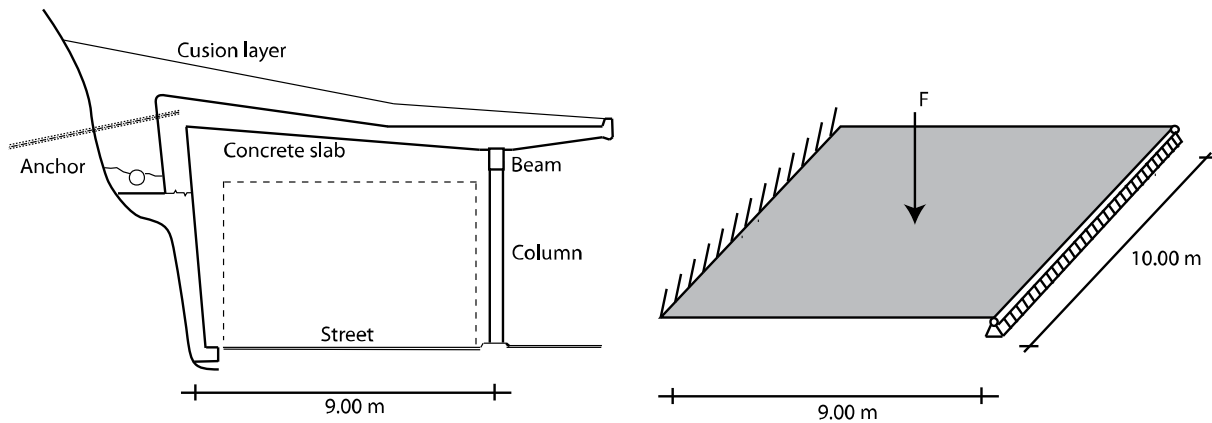


**Figure 3.3.5** Schematic illustration of the rockfall protection gallery.

All the assumptions made in the model introduce a model uncertainty. This is considered by using a log normal distributed random variable in the model  $X_{vul} \sim LN(1, 0.15)$ .

A more detailed modeling of the gallery is in principle possible by using the described approach. However, this is slightly depending on the approach. Here, a generic model is proposed which can be used for a large portfolio of rockfall protection galleries. Additionally, it is questionable if the assumptions and simplifications made in the vulnerability model really contribute significantly to the overall uncertainties in the entire rockfall model. The assumptions and uncertainties in the detachment model and falling model might dominate the entire analysis and thus one can gain not too much by using a more detailed vulnerability model.

Some of the made assumptions are necessary and by using simplified approaches such as event tree formulations are based on expert opinion and a lot of assumptions are made implicitly without having the chance to improve the model in the future.

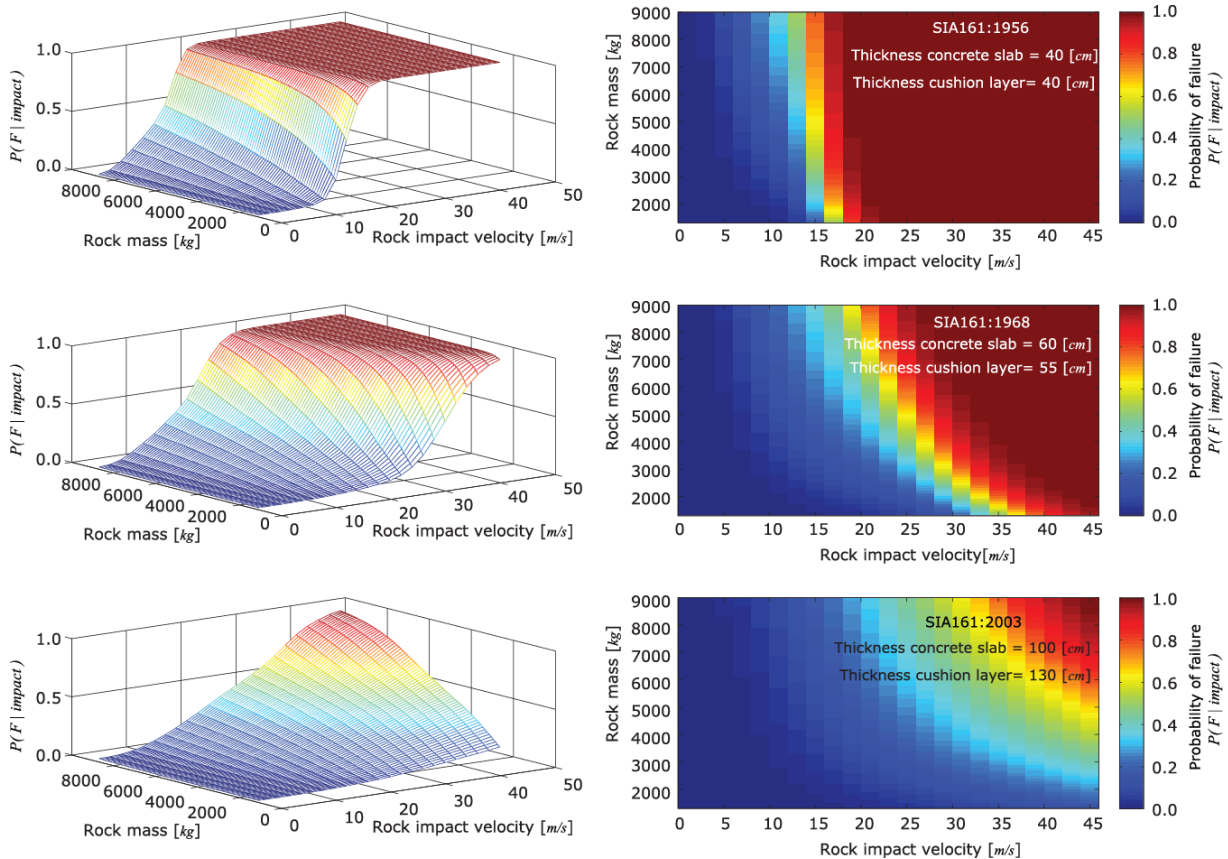


**Figure 3.3.6** Two and three-dimensional illustration of vulnerability curves for different thickness values for the concrete slab and the cushion layer.

By using the above described equations and assumptions, the vulnerability curves for the rockfall protection galleries can be calculated. Three different examples are given in Figure 3.3.6.

The figures on the right hand side show a two dimensional projection of the vulnerability curves into the mass velocity space of the impacting stones. The colors in Figure 3.3.6 represent the probability of failure. On the left hand side the same illustrations in the three dimensional space are given.

In Figure 3.3.6 the significant influence of the thickness of the concrete slab and the height of the cushion layer can be seen. The gallery with a thickness of 0.4m is very sensitive to the impact velocity. Stones with a velocity of more than 25m/s will lead to failure event.

With an increase of the thickness of the slab and an increase of the thickness of the cushion layer, the probability of failure decreases for events with a stone velocity of 25m/s. The resistance against punching and bending failure is increased.

An example of the influence of different code generations is given in Figure 3.3.7. Even though that not only the material changes with new code generations but also the concept of

design it can be assumed that the load bearing behavior in reality is similar, since the model does not influence the reality. It can be assumed that the modern codes reflect the real load bearing capacity better. Otherwise there would be no need to exchange a design concept in a code. Therefore, it is reasonable to calculate the failure probability for all code generation and construction years with the same physical model while the material properties changed over time.

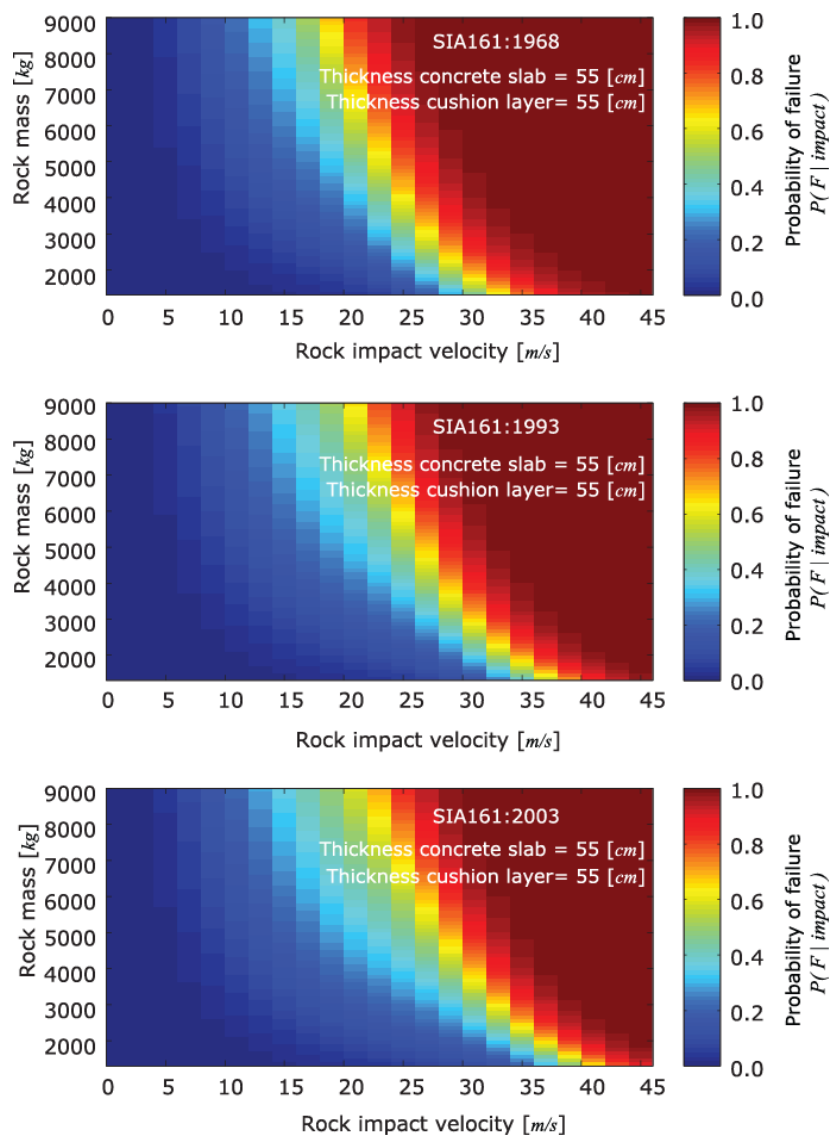


**Figure 3.3.7** Two dimensional illustration of the vulnerability curves for protection galleries from different code generations.

In Figure 3.3.7 the influence of the different material properties over time can be seen. It is interesting to see that the probability of failure is decreased over time – which seems to be reasonable. However, it can also be seen that the uncertainties in the vulnerability curves increases.

As mentioned before, the real advantage of the formulation is that a generic model can be established; for this purpose a Bayesian Network was used. This Network is shown in Figure 3.3.8. The node annual maximum of the detached rock mass contains the outcome of the detachment model. The node Impact velocity of the detached rock mass contains the outcome of the model for the falling process and the node impact considered the probability that a detached rock impacts the gallery. In principle a link between the node Annual detached rock mass and the node impact velocity is necessary. However, depending on the used falling process model, this link disappears. A lump mass approach for example calculates the impact velocity independent of the mass of the stone.

The node failure of the gallery contains the vulnerability curves of the rockfall protection galleries. In this project 280 different vulnerability curves have been calculated. For each vulnerability curve, 2369 different combinations of the impact velocity and the rock mass have been considered. The failure probability of a gallery with different characteristics was calculated by using a crude Monte Carlo simulation a total of 663320 times. This model was then connected with MS- Excel so that the calculation with the Bayesian Network can be performed automatically. A screenshot of this calculation is given in Figure 3.3.8. In the Excel sheet the expected value of the annual probability of failure  $E[P(F)]$  of a gallery with known specific characteristics is calculated.

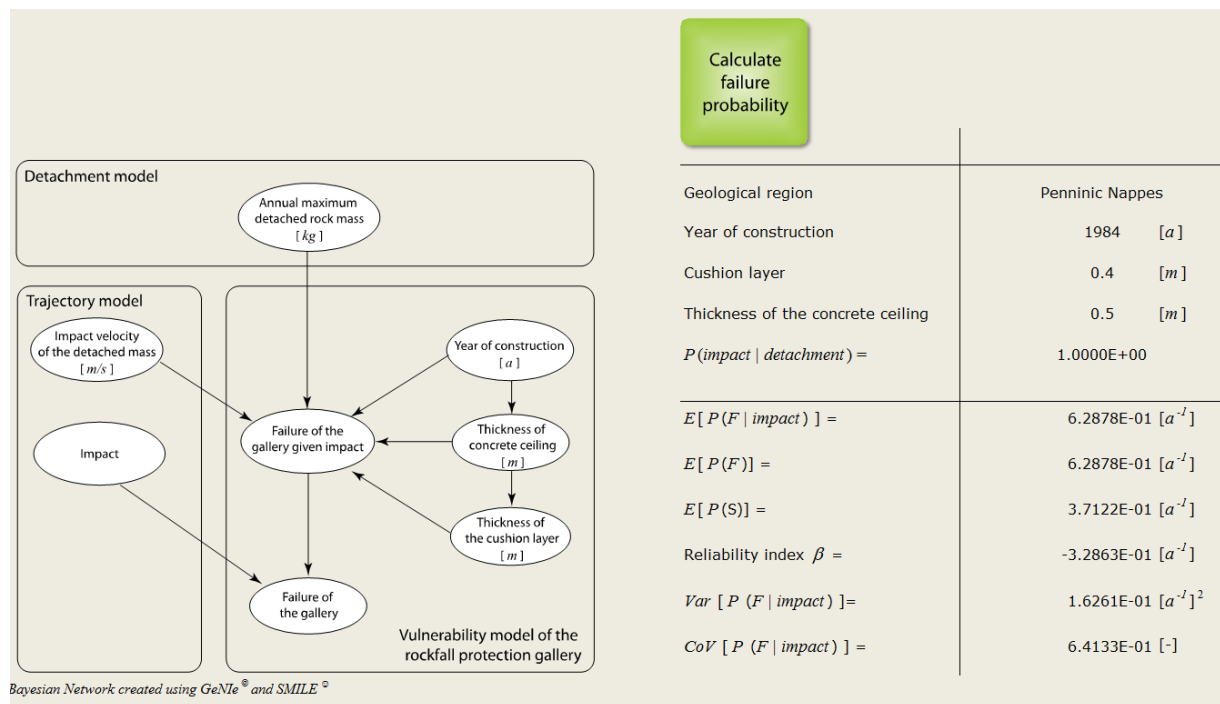


**Figure 3.3.8** Calculation of the probability of failure of the gallery.

## 4 PHYSICAL VULNERABILITY TO FAST MOVING LANDSLIDES

### 4.1 INTRODUCTION

Fast moving landslides are phenomena whose maximum expected velocity, during their paroxysmal phase, corresponds to class 5 to 7 as established by Cruden and Varnes (1996).

In most of the encountered cases, these landslides, which are generally first-failure phenomena, are associated with the most severe damage to buildings and infrastructures, usually resulting to the complete destruction of any element within their path. Even when the initial landslide body is relatively small, its final volume may be very large because of their capability to cover large distances in a very short time involving part of the material encountered on the slope. The risk is then very high owing to the high magnitude of the landslide due to its mass and velocity and the exposition which may be very high too due to the long runout of the soil mass which can propagate even over relatively flat areas (Picarelli 2010).

Essentially, three kinds of mobile behavior are commonly perceived during the movement of rapid landslides:

- slide, in which the sliding mass moves as a block without or with minor disaggregation
- slide-flow, in which the sliding mass moves partially as a block and is partially disaggregated into debris with rapid, flow-like motion and
- flow, in which the sliding mass fully disaggregates into debris, and moves extremely rapidly as granular flow.

Consequently, fast landslides are grouped into three types: slide, slide-flow, and debris flow (Wen et al., 2004).

### 4.2 METHODOLOGY FOR BUILDINGS AT LARGE SCALE (1:5,000) (UNISA)

#### 4.2.1 Introduction

##### Zoning purposes

The *vulnerability maps* at large scale can be useful in land-use planning as well as in the design phase of large engineering structures.

##### Definition of physical vulnerability at medium scale

In the adopted procedure at large scale, the physical vulnerability was defined as “*the degree of loss to a given building resulting from the occurrence of a fast-moving landslide of a given intensity*”. It is expressed on a scale from 0 (no damage) to 1 (total loss).

#### 4.2.2 Analysis and zoning at large scale

Most of the existing approaches for vulnerability analysis of structures potentially impacted by fast-moving landslides do not distinguish between the types of processes, the physical mechanism or the structural resistance of the endangered objects (Glade 2003; Fuchs et al., 2007). More importantly, information regarding the process intensity is often missing or only described semi-quantitatively. In particular for fast movements, few quantitative relationships

have been proposed in the scientific literature between intensities and vulnerability values. Fuchs et al. (2007), among others, used data from well-documented debris flow event in Austria Alps to derive quantitative vulnerability function applicable to brick masonry and concrete buildings, estimating debris flow intensity as a function of mean velocity and height of the impacting debris front. Faella and Nigro (2003), on the other hand, deduced the flow impact velocities through the interpretation of the main collapse mechanisms observed in several buildings impacted by the flowslides (Hutchinson, 1988) during the hydrogeological disaster occurred on 5<sup>th</sup> and 6<sup>th</sup> May 1998 in the town of Sarno (Campania region, southern Italy).

On the basis of the suggestions given by the above cited authors, the proposed procedure to assess the vulnerability of buildings potentially impacted by flow-like fast moving landslides at large scale is articulated in the following steps:

- a) detection of buildings at risk;
- b) definition of buildings' occupancy (residential, commercial, industrial, etc.) and typology (masonry, reinforced concrete, etc.);
- c) collection of information on past damages and losses;
- d) estimation of landslide intensity (i.e. the mean velocity of the impacting front) via results of numerical modelling of flowslides' propagation stage;
- e) estimation of the physical vulnerability of the buildings impacted by fast-moving landslides.

In particular, with reference to a given sample area, the elements at risk can be firstly identified by using accurate digital topographic map at 1:5,000 scale and, then, distinguished on the basis of their occupancy type (recovered in the municipal urban-plan). Once identified the type of elements at risk, it must be attributed to the *i*-facility the own *degree of loss* (namely the vulnerability  $V_i$ ) that is lawful to attend owing to the actions applied to a given element at risk by a phenomenon from rapid to extremely rapid (Cruden and Varnes, 1996), as is summarised in the Table 4.2.1.

**Table 4.2.1** Vulnerability of a single building on the basis of its occupancy type.

Type of building	Vulnerability value $V_i$
<i>A) Residential buildings</i>	*
<i>B) Public-use buildings</i>	1.00
<i>C) Historical, architectonics and monumental buildings</i>	1.00

With regards to the residential buildings instead, according to Faella (2005) and neglecting the role played by the flow direction (normal or tangential) impacting the structures, four probability of structural collapse were associated to the theoretical velocity corresponding to vulnerability values. For masonry buildings, in particular, it can be assumed that:

- if  $v \geq 5$  m/s  $\Rightarrow$  Very high probability of collapse (total loss),  $V_i = 1$ ;
- if  $v < 5$  m/s  $\Rightarrow$  High probability of collapse,  $V_i = 0.8$ .

For reinforced concrete frame buildings, on the other hand:

- if  $v \geq 10$  m/s  $\Rightarrow$  Very high probability of collapse (total loss),  $V_i = 1$ ;

- if  $7 \leq v < 10$  m/s  $\Rightarrow$  High probability of collapse,  $V_i = 0.8$ ;
- if  $3 \leq v < 7$  m/s  $\Rightarrow$  Medium probability of collapse,  $V_i = 0.5$ ;
- if  $v < 3$  m/s  $\Rightarrow$  Low probability of collapse,  $V_i = 0.2$ .

The estimation of the velocity  $v$  (i.e. the intensity) of the impacting flowslides can be obtained by modelling, thanks to the availability of Digital Elevation Models with squared cells of 5 m by 5m, the propagation stage of the flowslides. Then, by selecting the maximum value of the local flowslide velocities furnished as output by the numerical model and pertaining to the cells surroundings a given building, it is possible to associate a probability of collapse (or the  $V_i$  value) to the same building taking into account its typology (masonry or reinforced concrete). Finally, for zoning purposes, a nominal scale can be introduced as shown in Table 4.2.2.

**Table 4.2.2** Nominal scale of vulnerability values

Vulnerability value	Nominal scale
$0 < V_i < 0,25$	<i>Low</i>
$0,25 \leq V_i < 0,50$	<i>Modest</i>
$0,5 \leq V_i < 0,75$	<i>Medium</i>
$0,75 \leq V_i < 1$	<i>High</i>
$V_i = 1$	<i>Total loss</i>

### 4.3 IMPACT FORCES AGAINST FIXED OBSTACLES (UNISA)

In the field of the risk mitigation strategies related to the occurrence of flow-like fast-moving landslides (Hutchinson, 2005), “passive” measures allows the reduction of the vulnerability of the exposed buildings via the construction of control works (barriers, check dams, etc.) or the reinforcement of the superstructures. More precisely, the first types of measures allow the deviation of the landslide path – during the propagation stage – so avoiding the impact with the exposed buildings; with the second ones, on the contrary, the aim is to increase the strength of the buildings depending on the impact occurrence. For a proper design of these measures, the estimation of the force generated during the impact at the contact between the front of the fast landslide and the impacted element (assumed as a fixed obstacle) is needed. For the estimation of the force acting at the impact of the fast-moving landslide against a fixed obstacle, the following three approaches are suggested in the scientific literature (Lo, 2000;):

- *Empirical methods*: the dynamic component of the impact force is proportional to the static one (Lichtenan, 1973; Armanini, 1993; Scotton e Deganutti, 1997);
- *Analytical methods*: the impact force is proportional to the square of the velocity and the pressure  $p$  is assumed as a constant along the height of impacting front (Hung et al., 1984; Du et al., 1987; Matsushita e Ikeya, 1992).
- *Hybrid methods*: they can be considered as a linear combination of the above described methods (Voellmy, 1955; Sheidegger, 1975, ORDINANZA N. 1991 Commissario di Governo per l’Emergenza Idrogeologica nella Regione Campania, 2001).

In order to check the capability of these methods to adequately predict the value of the impact force, several numerical analyses were carried out via a commercial code PFC–2D (Itasca Consulting Group, 2004) implementing a Distinct Element Method – DEM (Fig. 4.3.1).

The DEM model of the impacting debris mass (2.00 m in width x 4.00 m in length x 1.00 m in height) is composed of 9,005 rigid particles having diameters ranging between 15 mm and 30 mm, bi-dimensional porosity  $n$  equal to 0.20 and solid mass density  $\rho_s$  of 2,600 kg/m<sup>3</sup>. Moreover, for each of the three assumed values of the velocity  $v$  of the impacting front ( $v_1 = 1$  m/s,  $v_2 = 4$  m/s e  $v_3 = 15$  m/s), different values of both the coefficient of the inter-particle friction and the contact stiffness are considered for the analyses purposes. The impacted obstacle, in turn, is modelled as a fixed “wall” element of 3 m in height while three different values of the normal stiffness at the particle-obstacle contact are taken into account.

The results of the numerical analyses (Vitolo, 2009) highlighted that, for a given stiffness of the impacting debris mass, the peak value of the impact force increases – while the duration of the impulsive phase decreases – as the stiffness of the obstacle increases (and vice-versa). Similarly, the above peak value increases as the coefficient of inter-particle friction increases, for a given value of the normal stiffness at the particle-obstacle contact.

Moreover, for fixed values of the stiffness at the contacts particle-particle and particle-obstacle, the magnitude of the peak impact force attained during the impulsive phase as well as its duration, are a function of the shape of the front (planar or convex) of the debris mass; on the contrary, the value of the impulse associated to this force remains practically unchanged (fig. 4.3.2).

Finally, according to Vitolo (2009), the analytical formula which seems to better predict the mean values of the force against the obstacle (Fig. 4.3.3) is that given by the hybrid method, namely:

$$F_{med}^n = \frac{1}{2} \rho_c g h_0^2 b + \rho_c v^2 h_c b \cos^2 \theta \quad [4.1]$$

where

- $\rho_c$  debris mass density;
- $v$  debris mass velocity;
- $\theta$  angle of the flow direction with respect to the axis normal to the impacted surface;
- $g$  acceleration of gravity;
- $h_0 = h_c + d$ , height of the impacted surface;
- $b$  width of the impacted surface;
- $h_c$  height of the debris mass;
- $d$  depth of the laying plane of the obstacle with respect to the topographic surface.

This result seems to be of a particular concern considering that the value of this force can be used within procedures aimed at estimating the vulnerability of buildings to fast-moving landslides at site-specific scale (1:2,000).

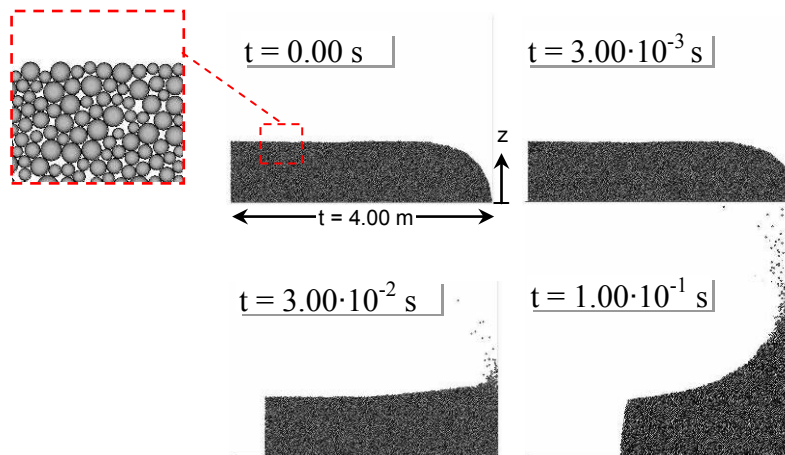


**Figure 4.3.1** Simulation of the debris evolution.



**Figure 4.3.2** Time history of the impact force  $F_n$  of a debris front having a convex or a planar shape.

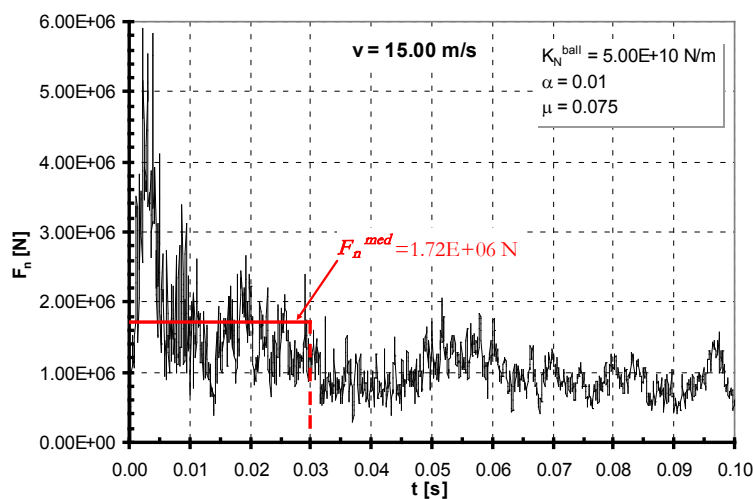


**Figure 4.3.3** Time history of the impact force  $F_n$  in the case of a debris front having a convex shape and mean value  $F_n^{med}$  of the impulsive phase.

## 4.4 METHODOLOGY FOR BUILDINGS AT SITE SPECIFIC TO LOCAL SCALES (AMRA)

### 4.4.1 Introduction

This report describes part of the model for damage impact evaluation, GIS aided, of the building structures hit by fast mud landslides developed at the PLINIVS Study Centre of the University of Naples on behalf of AMRA within the Safeland Project supported by the European Union.

In particular, the behavior of buildings under dynamic load due to rapid landslide (as debris flow) is here investigated. Vulnerability classes for prominent structural and non-structural elements of the building are defined, and the limit load for each of these is computed by limit state analysis related with experimental tests. The weight of each elementary vulnerability and their possible combinations are investigated to estimate the global vulnerability and define buildings typological classes. This represents the core element of the landslide impact model developed at PLINIVS Centre for AMRA.

Among the different types of landslides, those characterized by a fast flow represent by far the most dangerous for the buildings and especially for the population.

The pressure exerted on the walls of the affected buildings is almost always able to cause, even at the limits of the invaded area, the collapse of non-structural elements and the damage due to the invasion of the flow inside the building, while in the presence of high speed a strong probability of serious damage to structures is likely to occur, which in some cases leads to the collapse of the building.

It has been observed from previous events that the buildings response to the stress induced by a landslide does not depend only on the strength characteristics of the structure, but also by the “resistance hierarchies” between structure and “secondary” elements such as windows and infill panels. In order to simulate the real behavior of buildings it should be therefore investigated at first the individual elementary vulnerabilities (structures, infill panels, window frames) and then vulnerability curves corresponding to different combinations of the element resistance should be traced.

The risk of “casualties”, otherwise than earthquakes, is greater for people who are outside the buildings, while inside of them this is very high only for those who are on the ground floor.

### 4.4.2 Action on the buildings

The dynamic pressure acting on the buildings struck by a fast landslide is here treated as a static equivalent lateral load. In order to define the building stress due to landslides, the main parameters are the height of landslide’s front and the impact dynamic pressure.

Within the invaded area, buildings and other structures along the landslide flow path are stricken by a dynamic pressure  $p$  identified by the classical relation:  $p = k \cdot d \cdot v^2$ , where  $d$ =flow density;  $v$  = flow speed;  $k$  =0.5. Speed is either derived from hazard analysis or assessed taking into account the characteristics of a specific area. The pressure applied to affected structures is considered as evenly distributed throughout the front’s height, therefore, for instance, the stress on a building will generally affect its lower parts (first level, entirely or partially), but might also hit in some cases the second floor.

---

### 4.4.3 Damage scale

Vulnerability can be defined as the probability of a specific building category to suffer a damage of defined level caused by landslide of assigned strength. To properly face this issue an unambiguous definition of what is meant by “damage” is then needed, especially for what concerns the “physical” damage, which is the first and most important factor in the impact assessment and risk analyses.

A descriptive damage scale has been set, five severity levels, depending on the damage to structures, non-structural elements, equipments and furniture are considered, taking also into account the time required to restore functions of damaged elements. The descriptive classification of damage levels varies according to each category of exposed elements and is reported in Table 4.4.1.

*Table 4.4.1 Damage scale for rapid landslides*

<b>DAMAGE SCALE</b>				
<b>damage level</b>		<b>damage description</b>	<b>works needed to rehabilitate</b>	<b>time to rehabilitate</b>
<b>0</b>	<b>NO DAMAGE</b>			
<b>1</b>	<b>NEGLIGIBLE SLIGHT</b>	Negligible structural damage: tiny lesions, detachment of small pieces of plaster, falling of small stones. Breakthrough of large or weak window frames badly maintained. Mild localized invasion of flow within the building. Moderate damage to furniture, furnishings and any object is in the first floor	No extraordinary repairs	Within 24 hours after the event
<b>2</b>	<b>MODERATE</b>	Moderate structural damage: large and deep lesions, detachment of large parts of plaster. Severe damage to nonstructural elements. Breakthrough of windows mildly resistant Flooding inside the building. Major flooding in basements if any. Moderate damage to the infill in r.c. buildings Damage to interiors (flooring, fixtures etc) Major damage to furniture and any object is in the first floor	Removal of debris seeped into the building Low maintenance works Repair or replacement of damaged windows Check and repair facilities. Repair or replacement of damaged furniture	Within 7÷15 days after the event
<b>3</b>	<b>HEAVY</b>	Severe structural damage: Many wide and deep lesions, local plasticity of the structural elements. Possible collapse of non-structural elements Breakthrough of windows even if strong. Severe damage to the infill walls in reinforced concrete buildings, in a few cases total collapse of infill walls. Major flooding inside the building. Total invasion of any full basements Severe damage to interior finishes (flooring, fixtures, equipment) Severe damage to furniture, facilities, furnishings and any object is in the first floor	Removal of debris seeped into the building Major maintenance works. Structural repair and reinforcement. Checking and/or partial installation of the facilities. Replacement of windows. Repair or replacement of damaged furniture	Within 15÷45 days after the event
<b>4 - 5</b>	<b>VERY HEAVY DESTRUCTION</b>	Very serious structural damage. Many severe injuries, partial or total collapse of the structure. Even total collapse of the building. Breakthrough of infill walls even if strong. Major flooding with total invasion of ground floor and basements. Total destruction of facilities, finishes and everything is in the ground floor, in some cases even in the first floor. In some cases collapse of the ceiling between ground level and basement.	Total or partial demolition. New building construction Removal of debris and area arrangement with no rebuilding.	More than 45 days (even several months) after the event.

#### 4.4.4 Building vulnerability

Global modeling of the building behavior subject to landslide is a complex issue, as it is determined by the vulnerability level of three elements for R.C. buildings (structural frames, infill panels and openings in the front), and by the vulnerability level of two elements for masonry buildings (masonry walls and openings in the front). The global vulnerability level depends on these factors, but also on the hierarchical strength relations between them and on the combination of their vulnerability levels.

To better understand this aspect it is possible to use the analysis of the observed damage due to previous debris flow events (i.e. Sarno 1998). It has been seen, for instance, that for the majority of R.C. buildings the infill panels failed and the ground floors flooded, while no relevant damages were reported to the structural frames. This is because the infill panels collapse does not allow transmitting the fluid's pressure onto the frame. Hence the R.C. columns are stressed only on the limited surface represented by the face of the column since the fluid flows around the column and it is not able to exert the pressure required for its collapse, (Fig. 4.4.1). For fluid height within the first floor the dynamic pressure required to knock down a R.C. column of standard resistance is quite high.

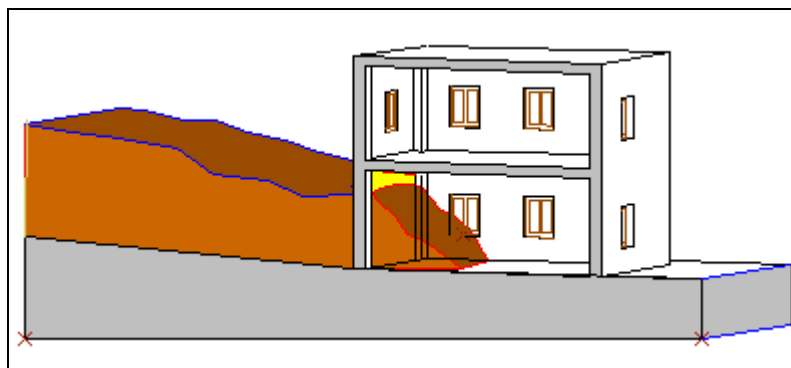


*Figure 4.4.1 R.C. building with weak infill walls*

In support to this theory, a limit state analysis has been carried out on the column, the results of which have fully corroborated empirical observations.

The results of the analysis show that weakly reinforced columns with sizes similar to those generally used in weak not a-seismic buildings, stressed exclusively on their surface, did not collapse unless high landslide's speed values (unlikely to occur in reality) were applied. However it should be also underlined that in certain cases the collapse of the structural frame might be the consequence of the impact with a missile, i.e. a solid body of relevant mass swept away by the landslide, such as motor vehicles, uprooted trees or bulky rocks. In the above-mentioned cases, dynamic pressure is not to be regarded as evenly distributed, since the pressure peak converges on relatively limited area (generally a  $25 \times 25 \text{cm}^2$  area is considered), therefore the likelihood of collapse is very high, even in cases of low speed. The collapse is mainly due to a fragile shear mechanism if the impact is near to the bottom or to the top of the column, while is due to a bending mechanism if the impact occurs near the center of the column.

A different behavior is shown by buildings with well-connected tuff masonry infill walls without openings, which offer an effective resistance to the advancing flow. In these cases the

greater strength of the wall is a vulnerability reduction factor as long as the pressure values remain low and, as a result, no fluid infiltrations occur so that the damage is almost irrelevant. When pressure values are higher, however, resistant infill walls turn out to be a negative factor, since they transmit onto the column the load resulting from the pressure exerted throughout the entire wall. As a result the stress values reached on the column increase considerably and it can realistically provoke its collapse especially when the structural frame is not designed to resist to lateral loads. It goes without saying that a collapse of the structural frame is far more detrimental to the whole building, with a total damage far heavier compared to a flooding of the ground floor. Given a stricken building front, the collapse probability is higher for central columns than corner columns, since they benefit from the stiffening contribution of infill walls orthogonal to the stricken front.

The hypothesis of a wall without openings in the example above is certainly not typical, since the case of a wall with one or more openings is far more frequent. It has been observed that the total vulnerability of a building is strongly conditioned by the infill walls resistance however this depends in its turn on the type and size of front's openings. In almost all cases, openings are the weakest element of a building and therefore they might collapse for low dynamic pressure values, determining the breakthrough of the opening and the infiltration of flow into the building. However this very circumstance originates a decrease in pressure that is proportional to the whole percentage and therefore a reduction of the likelihood that the wall collapses.

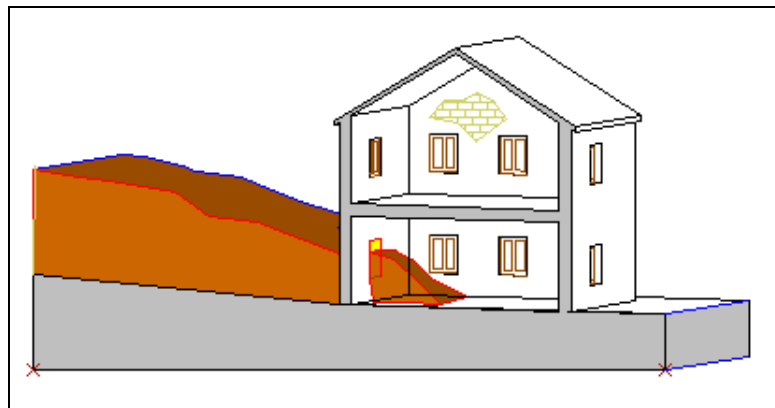


*Figure 4.4.2 Masonry building – weak window and strong wall*

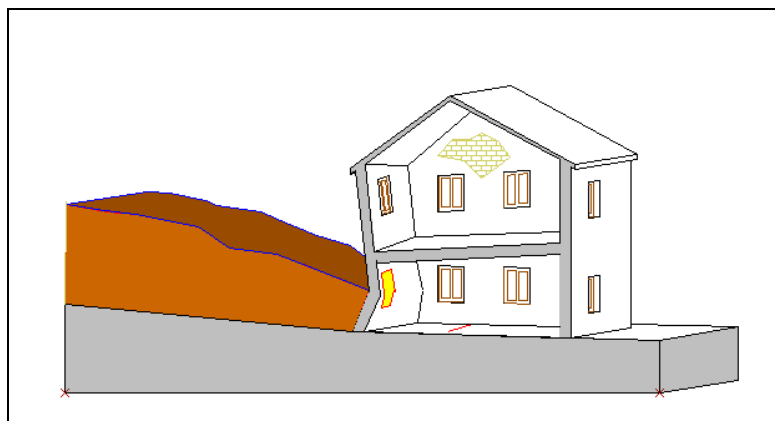


*Figure 4.4.3 Masonry building – strong window and weak wall*

On the other hand, if the whole percentage is low and the opening frame is provided with highly resistant screening (for example, anti-intrusion armored locks), openings do not collapse and the wall behaves similarly to a wall without openings. Vulnerability Type classification for different elements is reported next.

#### 4.4.4.1 *Main structure vulnerability*

For each construction type the analysis aimed at identifying the features which help to enhance or reduce the vulnerability level. Compared to masonry structure buildings, the behavior of frame buildings when undergoing dynamic pressure exerted by either a landslide or a flood is totally different. Therefore within a vulnerability classification, two different categories can be identified: buildings with continuous structure (typically masonry) and buildings with framed-structure and infill walls (reinforced concrete or steel). For each category three vulnerability type classes have been identified (A, B and C for masonry, D, E and F for framed structure) depending on construction typological characteristics. Definitions are reported in Tables 4.4.2 and 4.4.3.

**Table 4.4.2** *Vulnerability classes for masonry buildings*

MASONRY BUILDINGS VULNERABILITY	
CLASS	typology
<b>A</b>	Weak small buildings wood-structures, seasonal or permanent, with low-stiffness walls Masonry buildings with load-bearing walls badly connected and/or with thickness less than 25 cm, made with air bricks or irregular stone and bad quality mortar. Light precast buildings with corrugated or insulated steel sheet bearing panels
<b>B</b>	Strong wood buildings, permanent with stiff walls Masonry buildings with strong, well joined walls with thickness more than 30 cm and less than 50cm
<b>C</b>	Masonry buildings with strong, well joined walls with thickness more than 50 cm made with strong terra-cotta bricks or tuff or irregular stone and good quality mortar. Rigid ceilings

**Table 4.4.3** *Vulnerability classes for frame buildings*

FRAME BUILDINGS VULNERABILITY	
CLASS	typology
<b>D</b>	Light precast buildings with corrugated or insulated steel sheet infill panels and steel frame not braced R.c. buildings not-aseismic, designed for vertical loads, with weak frame, bad quality concrete and low percent of reinforcing steel bars
<b>E</b>	Light precast buildings with corrugated or insulated steel sheet infill and steel braced frame. R.c. buildings not-aseismic, designed for vertical loads. R.C. buildings with light frame and beams with span larger than 4 m
<b>F</b>	Strong steel braced frame structures Strong r. c. Buildings, a-seismic or not, with max 5m span and distance between floors less than 4 m

#### 4.4.4.2 *Infill walls vulnerability*

As mentioned above, the response of a framed building in the event of a flood/landslide lateral action depends also on the resistance of infill walls, for which a typological vulnerability classification can be established based on material and thickness (typically between 25 and 40 cm) and on the joint to the structural frame. Definitions are reported in Table 4.4.4.

**Table 4.4.4** *Vulnerability classes for infill walls in framed buildings*

INFILL WALLS	
CLASS	typology
<b>A</b>	Corrugated or insulated steel sheet infill panels. Wood panels . Light brick walls with less than 25cm thick
<b>B</b>	Terra-cotta air brick walls with more than 25 and less than 35cm thick Lightweight concrete brick walls with more than 25 and less than 35cm thick Tuff walls with more than 25 cm thick , non-regular elements and ineffective connections to the frame
<b>C</b>	Not-reinforced or weakly reinforced concrete walls, well connected to the frame Air brick or full brick walls , more than 35 cm thick and well connected to the frame Lightweight concrete brick walls , more than 35 cm thick and well connected to the frame Tuff walls , more than 35 cm thick , with regular joint texture and well connected to the frame

#### 4.4.4.3 *Openings vulnerability*

It has been observed that the expected damage does not depend exclusively on the structural type of the buildings, but it is determined by opening frames typology, dimension and resistance. This aspect is particularly important when the dynamic pressure is not such to cause a structural damage. The vulnerability of the opening frames is related to three factors: size, material and the presence of a protection screen. A wide glass door without any protection is the vulnerability top limit, whereas a relatively small frame provided with an effective anti-intrusion protection can be considered as the lowest level of a vulnerability scale. A series of experimental breakthrough tests have been carried out to test the resistance of casings (Zuccaro et al. 2000, Spence et al. 2004a, b, Zuccaro et al. 2008).

A first attempt of vulnerability classification is provided in the Table 4.4.5. It is a useful tool in assessing the expected damage, however it should be deemed as not complete and susceptible of improvement.

**Table 4.4.5** *Vulnerability classes for openings*

OPENINGS VULNERABILITY		
CLASS	typology	size
<b>A</b>	Weak Pvc (not protected or in bad condition)	large or medium
	Weak wood (not protected or in bad condition)	large or medium
	Weak aluminium (not protected or in bad condition)	large or medium
<b>B</b>	Weak Pvc (not protected or in bad condition)	small
	Weak wood (not protected or in bad condition)	small
	Weak aluminium (not protected or in bad condition)	small
	Strong Pvc manteined	large
	Strong wood manteined	large
	Strong aluminium manteined	large
	wood + aluminium	large
<b>C</b>	Strong Pvc manteined	medium or small
	Wood + aluminium	medium or small
	Aluminium manteined	small
	Strong aluminium manteined	medium or small
	steel	any

#### 4.4.5 Mechanisms and critic collapse load

In Tables 4.4.2 and 4.4.3 vulnerability building classes have been set; a probable collapse limit has to be associated to each of them (i.e. load bearing for masonry or infill panel in R.C. buildings). The analysis has been carried out, assessing the damage detected in buildings hit by mudflows. Unfortunately a systematic analysis of the damage based on the typological characteristics of stricken buildings has been rarely carried out; available damage surveys are rather limited. Therefore vulnerability analyses have been carried out working on simple collapse mechanisms, limit state Theoretical Calculation Model have been used comparing the results with a set of loading tests carried out during previous research projects (Zuccaro et al. 2000), which enabled to simulate the building's behavior in relation to the increment of the dynamic pressure of the hitting flow. A number of buildings models representing each of the typological classes assumed (Tables 4.4.2 and 4.4.3), both in masonry and reinforced concrete, has been set, and then laterally loaded with a pressure evenly applied on a wall's area, so that the collapse load value has been computed for each model. Calculations have been performed several times, modifying geometrical parameters (number of floors, distance between walls, height of intermediate landing, etc.) and construction characteristics (wall's construction material, floor's stiffness, connections between walls, etc.).

Similar computations have been carried out on reinforced concrete buildings, varying, besides the number of floors, the inter-story height, the frame stiffness, the reinforcement percentage, the thickness of infill panels and the connection between infill and frame. A specific computational procedure was developed, based on the probability of triggering the most common mechanisms of collapse as a function of lateral pressure and typological characteristics. The possible crisis situations considered for R.C. buildings are (see Table 4.4.6 for details):

- The loaded infill wall resists to the impact and transmits the load onto the concrete frame; if this one has no filled fields along the orthogonal frame, plastic hinges might arise in the joints.
- In the loaded infill wall, a bending mechanism is triggered.
- The loaded infill wall collapses due to the concentrated impact with an object swept away by the flow.

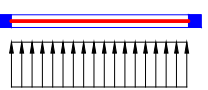
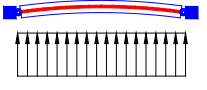
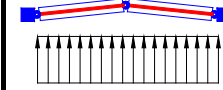
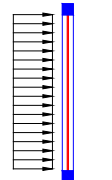
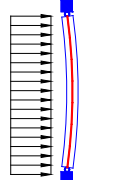
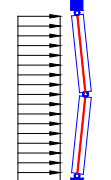
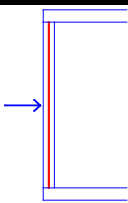
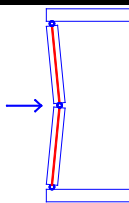
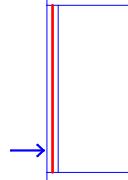
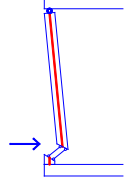
- A pillar collapses due to the concentrated impact in the central zone with an object swept away by the flow (bending mechanism)
- A pillar collapses due to the concentrated impact in the bottom or in the top zone with an object swept away by the flow (shear fragile mechanism)
- Many pillars collapse leading to the breakdown of the building.

The possible crisis situations for masonry buildings are:

- The loaded wall resists and transmits the impact load on the perpendicular wall (good connection) in which a shear mechanism is triggered.
- A bending mechanism along a horizontal or vertical axis is triggered in the loaded wall.
- A tilting mechanism is triggered in the loaded wall.
- A local collapse of the wall crops up due to the impact with an object carried away by the fluid (concentrated load)
- Multiple mechanisms on walls are triggered, bringing to the collapse of the building.

In the following section, we discuss about all the mechanisms used.

*Table 4.4.6 Collapse mechanism in concrete buildings*

INFIL WALLS MECHANISM IN R.C. BUILDINGS			
	PHASE 1	PHASE 2	PHASE 3
BENDING MECHANISM AROUND VERTICAL AXIS			
BENDING MECHANISM AROUND HORIZONTAL AXIS			
PILLAR MECHANISM IN R.C. BUILDINGS			
	PHASE 1	PHASE 2	
PILLAR COLLAPSE MECHANISM DUE TO CONCENTRATED IMPACT (BENDING)			
PILLAR COLLAPSE MECHANISM DUE TO CONCENTRATED IMPACT (SHEAR)			

#### 4.4.5.1 *Horizontal bending mechanism*

Firstly we discuss the out-of-plane bending mechanism around vertical axis in a masonry building wall.

With reference to the proposed model the symbolism used is reported hereafter:

- $W$  live load of the wall
- $P_v$  vertical load on the top of macro-element
- $P_o$  roof static horizontal push of the top of macro-element
- $L_A$  length of macro-element A;
- $L_B$  length of macro-element B;
- $X_{gi}$  distance of center of gravity of the general macro-element compared to its pole;
- $H$  maximum response of the wall or the horizontal restraint
- $S_l$  thickness of wall
- $\alpha_0$  horizontal load multiplier

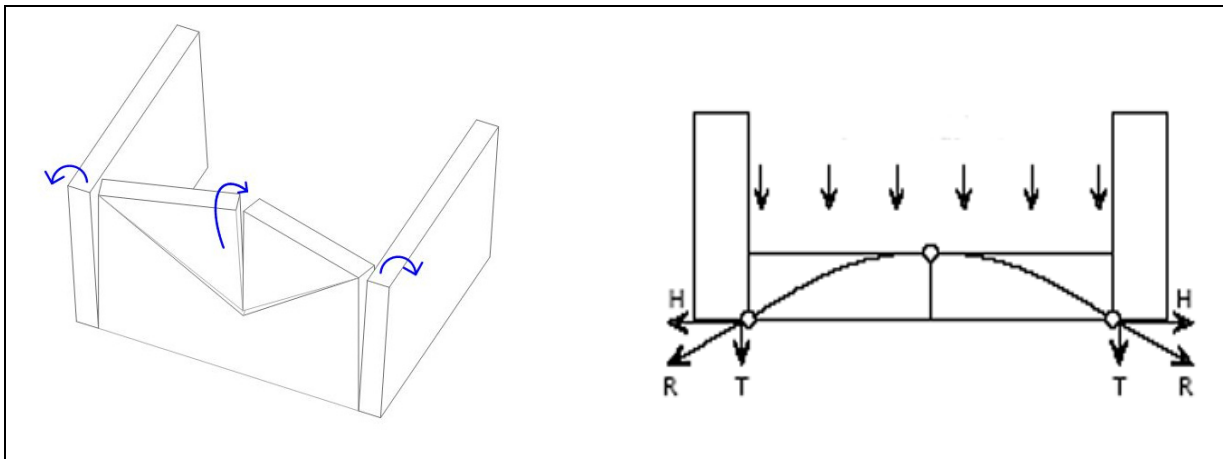


**Figure 4.4.4** *Horizontal bending mechanism*

The collapse mechanism (Fig. 4.4.5) is activated by the formation of three cylindrical hinges that define the macro-elements involved in the mechanism.

Each element can rotate around the hinge axis placed in correspondence to the lateral walls, while rotating also around the internal hinge C, whose position is not univocally determined and depends on the presence of openings and on the geometry of the wall involved in the kinematics.

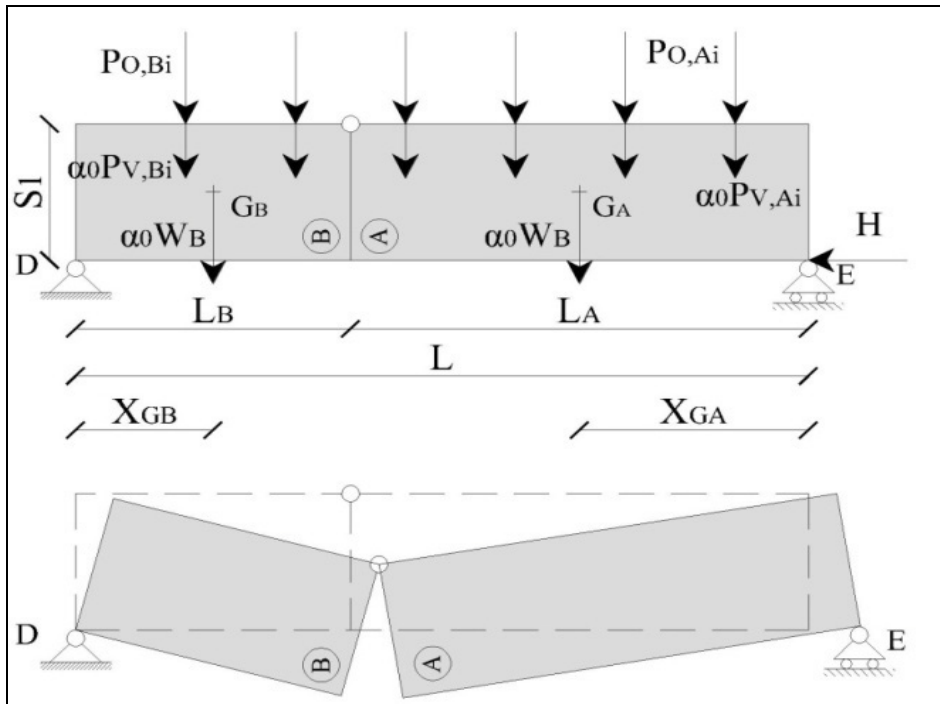


Figure 4.4.5 Horizontal bending mechanism - detail of actions

The rigid body B is constrained in D from a hinge having the following condition:

$$u_D = 0; \quad v_D = 0; \quad \varphi_D = 1 \quad [4.2]$$

while for the compatibility, internal hinge C imposes the following conditions:

$$\begin{cases} u_{CB} = u_{CA} \\ v_{CB} = v_{CA} \end{cases} \Leftrightarrow \begin{cases} \varphi_D S_1 = u_E - \varphi_E S_1 \\ -\varphi_D L_B = -\varphi_E L_A \end{cases} \quad [4.3]$$

rotation  $\varphi_D$  being positive and unitary:

$$\begin{cases} \varphi_D S_1 = u_E - \varphi_E S_1 \\ -\varphi_D L_B = -\varphi_E L_A \end{cases} \Leftrightarrow \begin{cases} S_1 = u_E - \varphi_E S_1 \\ -L_B = -\varphi_E L_A \end{cases} \Leftrightarrow \begin{cases} S_1 = u_E - \varphi_E S_1 \\ \varphi_E = \frac{L_B}{L_A} \end{cases} \Leftrightarrow \begin{cases} u_E = S_1 \left( 1 + \frac{L_B}{L_A} \right) \\ \varphi_E = \frac{L_B}{L_A} \end{cases} \quad [4.4]$$

The constraint in E imposes the following kinematic conditions:

$$u_E = S_1 \left( 1 + \frac{L_B}{L_A} \right); \quad v_E = 0; \quad \varphi_E = \frac{L_B}{L_A} \quad [4.5]$$

It is therefore possible to represent the generalized displacements of both elements B and A respectively as:

$$(u_D; v_D; \varphi_D) = (0; 0; 1)$$

$$(u_E; v_E; \varphi_E) = \left( S_1 \left( 1 + \frac{L_B}{L_A} \right); 0; \frac{L_B}{L_A} \right) \quad [4.6]$$

In order to apply the virtual works theorem, the virtual displacements of the points where the forces of the system are applied are determined for both directions as:

$$\delta_{GB_y} = v_D + \varphi_D x_{GB} = \varphi_D x_{GB} = -x_{GB} \quad [4.7]$$

$$\delta_{GA_y} = v_E - \varphi_E x_{GA} = -\frac{L_B}{L_A} x_{GB} \quad [4.8]$$

$$\delta_{O,By_i} = v_D + \varphi_D x_{O,Bi} = \varphi_D x_{O,Bi} = -x_{O,Bi} \quad [4.9]$$

$$\delta_{O,Ay_i} = v_E - \varphi_E x_{O,Ai} = -\frac{L_B}{L_A} x_{O,Ai} \quad [4.10]$$

$$\delta_{Hx} = x_E = S_1 \left( 1 + \frac{L_B}{L_A} \right) \quad [4.11]$$

Applying the virtual works theorem leads to the following equations:

$$-\alpha_0 W_A \delta_{GA_y} - \alpha_0 W_B \delta_{GB_y} - \alpha_0 \sum_{i=1}^n P_{V,Ai} \delta_{O,Ay_i} - \alpha_0 \sum_{i=1}^n P_{V,Bi} \delta_{O,By_i} - \sum_{i=1}^n P_{O,Ai} \delta_{O,Ay_i} + \quad [4.12]$$

$$- \sum_{i=1}^n P_{O,Bi} \delta_{O,By_i} - H \delta_{Hx} = 0$$

$$\alpha_0 W_A x_{GA} + \alpha_0 W_B \frac{L_B}{L_A} x_{GB} + \alpha_0 \sum_{i=1}^n P_{V,Ai} x_{O,Ai} + \alpha_0 \sum_{i=1}^n P_{V,Bi} \frac{L_B}{L_A} x_{O,Bi} + \sum_{i=1}^n P_{O,Ai} x_{O,Ai} + \quad [4.13]$$

$$+ \sum_{i=1}^n P_{O,Bi} \frac{L_B}{L_A} x_{O,Bi} - HS_1 \left( 1 + \frac{L_B}{L_A} \right) = 0$$

$$\alpha_0 \left[ W_A x_{GA} + W_B \frac{L_B}{L_A} x_{GB} + \sum_{i=1}^n P_{V,Ai} x_{O,Ai} + \sum_{i=1}^n P_{V,Bi} \frac{L_B}{L_A} x_{O,Bi} \right] = HS_1 \left( 1 + \frac{L_B}{L_A} \right) - \sum_{i=1}^n P_{O,Ai} x_{O,Ai} + \quad [4.14]$$

$$- \sum_{i=1}^n P_{O,Bi} \frac{L_B}{L_A} x_{O,Bi}$$

$$\alpha_0 = \frac{HS_1 \left( 1 + \frac{L_B}{L_A} \right) - \sum_{i=1}^n P_{O,Ai} x_{O,Ai} - \sum_{i=1}^n P_{O,Bi} \frac{L_B}{L_A} x_{O,Bi}}{\left[ W_A x_{GA} + W_B \frac{L_B}{L_A} x_{GB} + \sum_{i=1}^n P_{V,Ai} x_{O,Ai} + \sum_{i=1}^n P_{V,Bi} \frac{L_B}{L_A} x_{O,Bi} \right]} \quad [4.15]$$

The meaning of the symbols is shown in Figure 4.4.5 above. The evaluation of collapse multiplier in eq. (4.15) requires determining the push  $H$ , representing the resistance offered by orthogonal bracing walls in conjunction with anchoring systems opposing to analyzed displacement typology. The model used for  $H$ -push estimation is related to the rotation of a portion of the bracing wall.

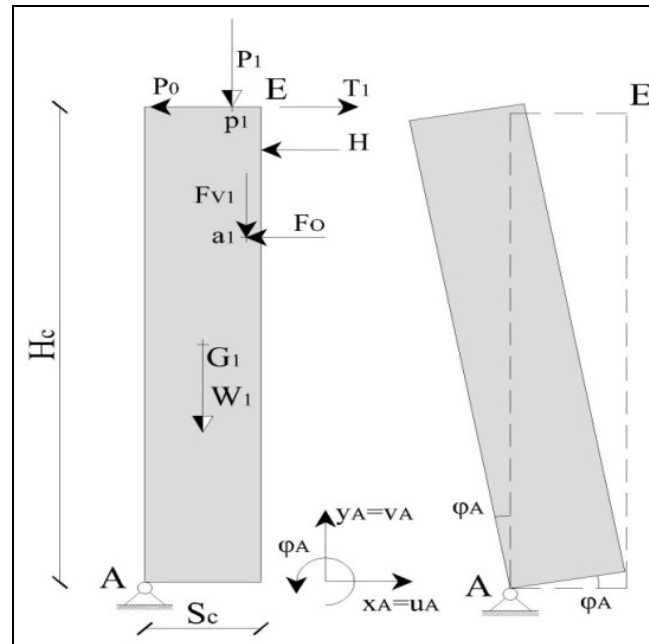


**Figure 4.4.6** *Overturning of orthogonal walls*

With reference to the figure 4.4.6, the stabilizing moment and the overturning moment are respectively equal to:

$$M_S = W_1 \frac{S_c}{2} + F_{v1} x_{a1} + P_1 x_{p1} + T_1 H_c \quad [4.16]$$

$$M_R = H y_H + F_o y_o + P_o H_c \quad [4.17]$$

A multiplier of collapse is obtained from equality between both terms:

$$W_1 \frac{S_c}{2} + F_{v1} x_{a1} + P_1 x_{p1} + T_1 H_c = H y_H + F_o y_o + P_o H_c \quad [4.18]$$

with

$$H = \frac{1}{y_H} \left( W_1 \frac{S_c}{2} + F_{v1} x_{a1} + P_1 x_{p1} + T_1 H_c - F_o y_o - P_o H_c \right) \quad [4.19]$$

In Eq. (4.19) used for the evaluation of  $H$  push, the terms represent weights and actions transmitted by the horizontal structures and are assessed by defining a conventional length of about one meter for the bracing wall.

The position of the  $H$  push is equal to:

$$y_H = H_c - \varepsilon \cdot b$$

[4.20]

The value is known only after fixing  $b$  dimension, which represents the height of the wall area involved in the horizontal bending mechanism, and the  $\varepsilon$  value (generally 0.33).

#### 4.4.5.2 *Vertical bending mechanism*

The mechanism of vertical bending is examined for walls with monolithic behavior.

With reference to the proposed models in the following paragraphs, the symbolism used is reported hereafter:

- $i=1 \dots n$  number of floors;
- $W_i$  live load of the wall at  $i$ -th floor
- $N$  generic vertical load on the top, supposed axial
- $Y_{gi}$  height of center of gravity of the wall at  $i$ -th floor compared to its pole;
- $S_i$  thickness of wall at  $i$ -th floor
- $a_0$  horizontal load multiplier
- $H_A$  height of macro-element A wall compared to its pole;
- $H_B$  height of macro-element B wall compared to its pole;
- $F_{vi}$  vertical component of vault's or arc's push on the wall at  $i$ -th floor;
- $F_{oj}$  horizontal component of vault's or arc's push on the wall at  $i$ -th floor;
- $P_i$  weight of the floor loading the wall at  $i$ -th floor, computed proportionally to the area of influence;
- $T_i$  maximum value of the resistance of a tie (if present) at the top of wall at  $i$ -th floor;
- $y_{ai}$  vertical height from the pole of the application point of vault's or arc's push on the wall at  $i$ -th floor;
- $x_{ai}$  horizontal distance from the pole of the application point of vault's or arc's push on the wall at  $i$ -th floor;
- $x_{pi}$  horizontal distance from the pole of the application point of floor's load at the top of wall at  $i$ -th floor.

The connection at the top of the wall prevents overturning, but in any case the walls stressed by horizontal actions can exhibit critical vertical instability (Fig. 4.4.7). The wall can withstand the bending stress only if the normal stress is such that the resultant is always internal to the cross section. In other words, the combination of vertical and horizontal actions determines a vertical arch-effect. In the hypothesis that the resultant is external to a section of the wall, it determines the origin of a cylindrical hinge, with a location initially undetermined that allows the triggering of the mechanism.

The determination of the collapse multiplier is important to identify the geometry of the macro-elements interested by the mechanism of vertical bending, in order to create a geometric model as real as possible. In general, the position of the cylindrical hinge that is formed within the wall section where the resultant of vertical and horizontal actions is not contained in its geometry, is not initially determined and it is necessary to consider the collapse multiplier for different positions of the cylindrical hinge and find the minimum value to be associated with activation of the mechanism.

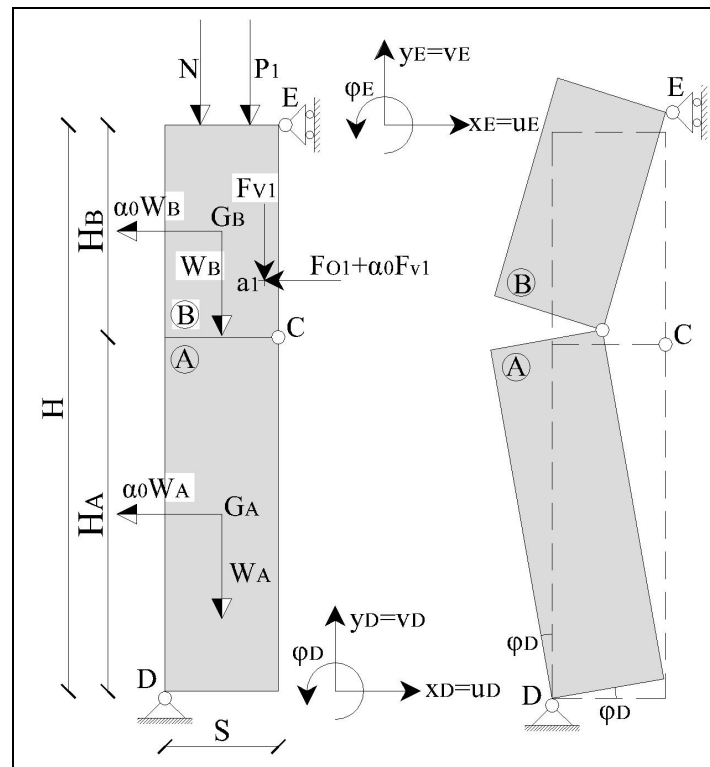


Figure 4.4.7 Vertical bending mechanism - detail of actions.

The mechanism considered below concerns a single floor monolithic wall. The boundary conditions needed to activate the local collapse mechanism are characterized by a wall hinged to the base and the presence of a sliding constraint that completely prevents any horizontal movement at the top. The combination of vertical and horizontal actions may be such as to form a cylindrical hinge needed to activate the mechanism whose position is not identified. The loads on the wall are represented by the weights transferred by structures and superstructures, by static pushes and horizontal forces due to landslide event and calculated as the product of the value of the vertical action.

Once identified the boundary conditions and loads acting on the system, it is possible to proceed to the identification of the cylindrical hinge that correspond to the minimum value of the collapse multiplier. The formulation of the collapse multiplier is obtained with reference to the system shown in Figure 4.4.4. The general displacement parameters describing the kinematics of the system are derived from congruence conditions imposed by the constraints. Given a generic point P belonging to a rigid body whose coordinates are respectively x and y, its displacement components  $U_p$  and  $V_p$  can be expressed in terms of displacement components  $U_0$  and  $V_0$  of the reference point O and its rotation  $\phi_0$  around it. Assuming a counter clockwise (positive) rotation, we have:

$$u_p = u_0 - \phi_0 y \quad v_p = v_0 - \phi_0 x \quad [4.21]$$

For the system in Figure 4.4.7 we can evaluate the components of generalized displacements for the two bodies A and B, parts of the whole wall, taking into account the boundary conditions described above. In particular, the rigid body A is bound by a hinge at point D

whose boundary conditions require zero movement in both x and y directions and an assumed counterclockwise rotation (positive):

$$u_D = 0; \quad v_D = 0; \quad \varphi_D = \varphi_D = 1 \quad [4.22]$$

The internal hinge C requires as a consistency condition, that the displacements along x direction are equal, then the rotation around the pole E is equal to:

$$u_{CA} = u_{CB} \Rightarrow -\varphi_D H_A = \varphi_E H_B \Rightarrow \varphi_E = -\frac{H_A}{H_B} \varphi_D = -\frac{H_A}{H_B} \quad [4.23]$$

while vertical displacement at point E is expressed as:

$$v_E = \varphi_D S_1 = S_1 \quad [4.24]$$

So, the components of the generalized displacements in E are given as:

$$u_E = 0; \quad v_E = S_1; \quad \varphi_E = -\frac{H_A}{H_B} \quad [4.25]$$

Then the generalized displacements of the two rigid bodies A and B can synthetically be represented as:

$$(u_D; v_D; \varphi_D) = (0; 0; 1) \quad [4.26]$$

$$(u_E; v_E; \varphi_E) = \left( 0; S_1; -\frac{H_A}{H_B} \right) \quad [4.27]$$

The application of the virtual works principle requires calculating the virtual displacements of the application points of the forces acting on the system in both directions, thus, assuming:

$$H_B = \frac{H}{\beta}; \quad W_B = \frac{W}{\beta} \quad [4.28]$$

One gets:

$$H_A = H - H_B = H - \frac{H}{\beta} = \left( \frac{\beta - 1}{\beta} \right) H; \quad W_A = \left( \frac{\beta - 1}{\beta} \right) W \quad [4.29]$$

$$\frac{H_A}{H_B} = \left( \frac{\beta - 1}{\beta} \right) H \frac{\beta}{H} = (\beta - 1) \quad [4.30]$$

$$\begin{cases} \delta_{GAx} = u_D - \varphi_D y_{GA} = -y_{GA} = -\frac{H_A}{2} = -\frac{H}{2} \left( \frac{\beta - 1}{\beta} \right) \\ \delta_{GAy} = v_D + \varphi_D x_{GA} = \varphi_D x_{GA} = \frac{S_1}{2} \end{cases} \quad [4.31]$$

$$\begin{cases} \delta_{GBx} = u_E - \varphi_E y_{GB} = \frac{H_A}{H_B} y_{GB} = \frac{H_A}{H_B} \left( -\frac{H_B}{2} \right) = -\frac{H_A}{2} = -\frac{H}{2} \left( \frac{\beta - 1}{\beta} \right) \\ \delta_{GBy} = v_E + \varphi_E x_{GB} = S_1 - \frac{H_A}{H_B} x_{GB} = S_1 - \frac{H_A}{H_B} \left( -\frac{S_1}{2} \right) = \frac{S_1}{2} \left( 2 + \frac{H_A}{H_B} \right) = \frac{S_1}{2} (1 + \beta) \end{cases} \quad [4.32]$$

$$\begin{cases} \delta_{a1x} = u_E - \varphi_E y_{a1} = \frac{H_A}{H_B} (-y_{a1}) = -\frac{H_A}{H_B} y_{a1} = -y_{a1} (\beta - 1) \\ \delta_{a1y} = v_E + \varphi_E x_{a1} = S_1 - \frac{H_A}{H_B} (-x_{a1}) = S_1 + \frac{H_A}{H_B} x_{a1} = S_1 + x_{a1} (\beta - 1) \end{cases} \quad [4.33]$$

$$\delta_{ny} = v_E + \varphi_E x_n = S_1 - \frac{H_A}{H_B} (-x_n) = S_1 + \frac{H_A}{H_B} x_n = S_1 + x_n (\beta - 1) \quad [4.34]$$

$$\delta_{p1y} = v_E + \varphi_E x_{p1} = S_1 - \frac{H_A}{H_B} (-x_{p1}) = S_1 + \frac{H_A}{H_B} x_{p1} = S_1 + x_{p1} (\beta - 1) \quad [4.35]$$

Applying the virtual works principle one gets:

$$-\alpha_0 W_A \delta_{GAx} - \alpha_0 W_B \delta_{GBx} - \alpha_0 F_{v1} \delta_{alx} - F_{o1} \delta_{alx} - W_A \delta_{GAy} - W_B \delta_{GBy} - F_{v1} \delta_{aly} + \\ - N \delta_{ny} - P_1 \delta_{p1y} = 0 \quad [4.36]$$

$$\alpha_0 W_A \frac{H}{2} \left( \frac{\beta - 1}{\beta} \right) + \alpha_0 W_B \frac{H}{2} \left( \frac{\beta - 1}{\beta} \right) + \alpha_0 F_{v1} y_{al} (\beta - 1) + F_{o1} y_{al} (\beta - 1) - W_A \frac{S_1}{2} + \\ - W_B \frac{S_1}{2} (1 + \beta) - F_{v1} [S_1 + x_{al} (\beta - 1)] - N [S_1 + x_n (\beta - 1)] - P_1 [S_1 + x_{p1} (\beta - 1)] = 0 \quad [4.37]$$

$$\alpha_0 W \left( \frac{\beta - 1}{\beta} \right) \frac{H}{2} \left( \frac{\beta - 1}{\beta} \right) + \alpha \frac{W}{\beta} \frac{H}{2} \left( \frac{\beta - 1}{\beta} \right) + \alpha_0 F_{v1} y_{al} (\beta - 1) + F_{o1} y_{al} (\beta - 1) - W \left( \frac{\beta - 1}{\beta} \right) \frac{S_1}{2} + \\ - \frac{W}{\beta} \frac{S_1}{2} (1 + \beta) - F_{v1} [S_1 + x_{al} (\beta - 1)] - N [S_1 + x_n (\beta - 1)] - P_1 [S_1 + x_{p1} (\beta - 1)] = 0 \quad [4.38]$$

$$\alpha_0 \left[ W \frac{H}{2} \left( \frac{\beta - 1}{\beta} \right) \left[ \left( \frac{\beta - 1}{\beta} \right) + \frac{1}{\beta} \right] + F_{v1} y_{al} (\beta - 1) \right] = -F_{o1} y_{al} (\beta - 1) + W \frac{S_1}{2} \left( \frac{\beta - 1}{\beta} \right) \left[ 1 + \frac{(1 + \beta)}{(\beta - 1)} \right] + \\ + F_{v1} [S_1 + x_{al} (\beta - 1)] + N [S_1 + x_n (\beta - 1)] + P_1 [S_1 + x_{p1} (\beta - 1)] = 0 \quad [4.39]$$

$$\alpha_0 \left[ W \frac{H}{2} \left( \frac{\beta - 1}{\beta} \right) \left[ \left( \frac{\beta - 1}{\beta} \right) + \frac{1}{\beta} \right] + F_{v1} y_{al} (\beta - 1) \right] = W \frac{S_1}{2} \left( \frac{\beta - 1}{\beta} \right) \left[ 1 + \frac{(1 + \beta)}{(\beta - 1)} \right] + \\ + S_1 (F_{v1} + N + P_1) + (\beta - 1) [F_{v1} x_{al} + N x_n + P_1 x_{p1} - F_{o1} y_{al}] \quad (36) \quad [4.40]$$

$$\alpha_0 = \frac{W \frac{S_1}{2} \left( \frac{\beta - 1}{\beta} \right) \left[ 1 + \frac{(1 + \beta)}{(\beta - 1)} \right] + S_1 (F_{v1} + N + P_1) + (\beta - 1) [F_{v1} x_{al} + N x_n + P_1 x_{p1} - F_{o1} y_{al}]}{\left[ W \frac{H}{2} \left( \frac{\beta - 1}{\beta} \right) \left[ \left( \frac{\beta - 1}{\beta} \right) + \frac{1}{\beta} \right] + F_{v1} y_{al} (\beta - 1) \right]} \quad [4.41]$$

For the evaluation of the collapse multiplier, we need to identify the location of the hinge C that divides the wall into two macro-elements indicated as A and B. The position of the hinge is not uniquely determined, for each position corresponds to a different value of  $\alpha_0$ . To re-evaluate the minimum value of the collapse multiplier, we should find the associated  $\beta$  value.

#### 4.4.5.3 *Plate bending mechanism*

The plate bending mechanism describes the behavior of a wall with well-connected borders, so that it is possible to consider each bound as a not-perfect fixed edge.

The plate is subdivided into two separated 1m-width stripes respectively along the x and y directions, where bending stresses are calculated considering the not-perfect fixed edge constraint condition with the distributed load proportionally assigned to the stripes according to the ratio between vertical and horizontal size.

The limit state considered is the critical value of side constraints, leading to the creation of cylindrical hinges.

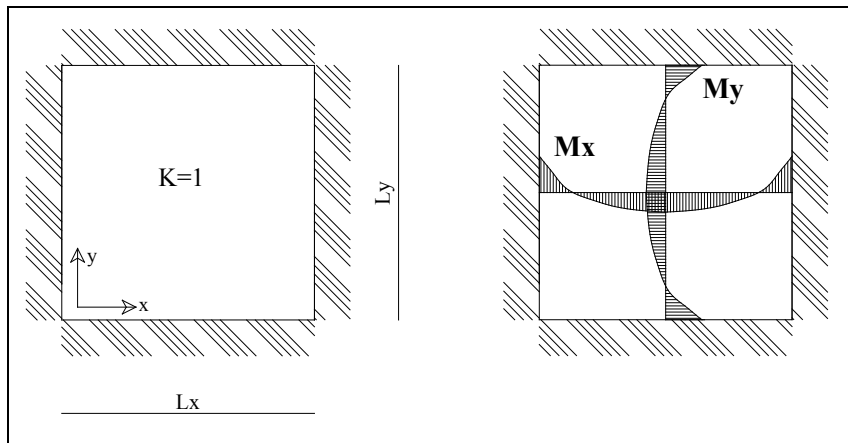


**Figure 4.4.8** *Plate bending mechanism.*

With reference to fig. 4.4.8 and 4.4.9, the adopted relations are:

$$p_x = p_{tot} \frac{L_y^4}{kL_x^4 + L_y^4} \quad [4.42]$$

$$p_y = p_{tot} - p_x \quad [4.43]$$

$$M_x = \frac{1}{16} p_x L_x^2 \quad ; \quad M_y = \frac{1}{16} p_y L_y^2 \quad [4.44]$$

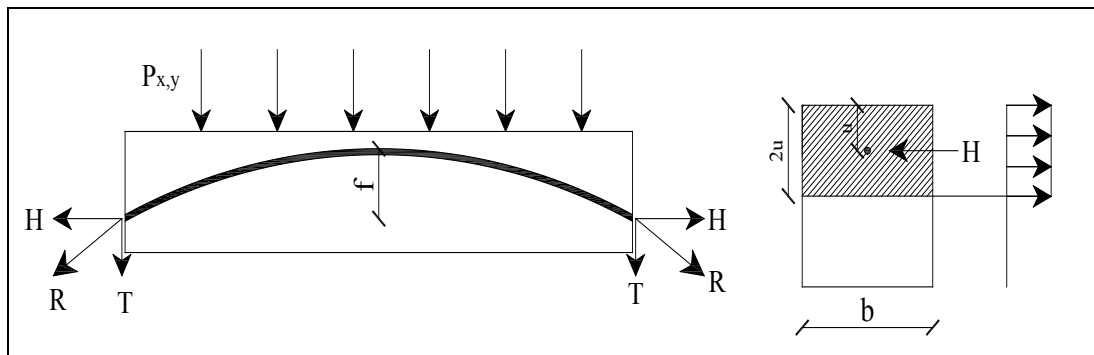


**Figure 4.4.9** Plate bending mechanism- scheme adopted to calculate the limit moment  $M_u$

$$M_u = 2ub\sigma_r f; u_{\max} = s/4; f = (s - 2u_{\max}) = s/2; M_u = \frac{F_k \cdot s^2}{4} \quad [4.45]$$

$$p_u = p_{tot} : \text{Max}(M_x, M_y) = M_u \quad [4.46]$$

Where :

$s$  : thickness of wall

$k$  : partition coefficient of the total load (depend by the constrain conditions. It's assumed  $k=1$ )

$p_{tot}$  : total distributed load

$p_x$  : part of the total distributed load that is assigned to the band along x direction

$p_y$  : part of the total distributed load that is assigned to the band along y direction

$L_x$  : x direction length

$L_y$  : y direction length

$M_x$  : Bending moment along x on the border line

$M_y$  : Bending moment along y on the border line

$\eta_d$  : dynamic coefficient depending on the dissipation capacity of the rock missile and on the ratio between the missile mass and the mass of the stricken structure.

$Fk$  : characteristic compression resistance of wall

$M_u$  : wall's limit deflecting moment

$p_u$  : critical flow pressure

In this way the limit load that causes the disconnection in the joint and the triggering of the mechanism is computed. This critic point is not a collapse point, since it needs more load to rotate the disconnected parts of the wall.

This model can be used to calculate the limit load for masonry buildings walls or infill walls in R.C. buildings, but in the first case it needs to consider the vertical load due to the floors.

#### 4.4.5.4 Column bending mechanism

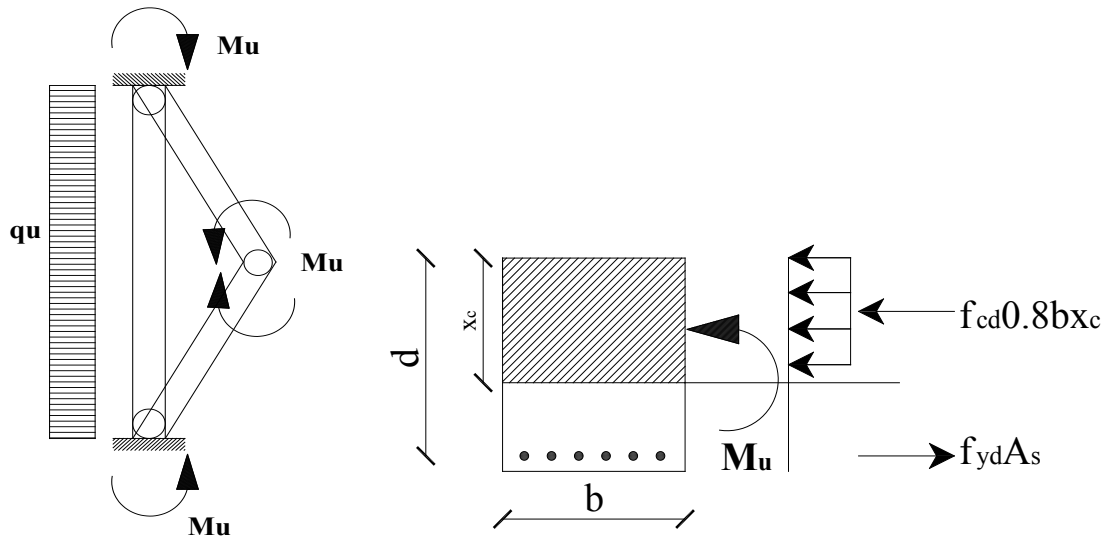


**Figure 4.4.10** Column bending mechanism - scheme adopted to calculate the limit moment  $M_u$ .

The static scheme is constituted by a column fixed at the ends and subjected to a uniformly distributed load  $q$ . The collapse mechanism is triggered by the formation of three plastic hinges, at the ends and in the midspan respectively, where the bending moments reach the ultimate value  $M_u$ .

The application of the kinematic theorem of the limit analysis allows determining the uniformly distributed collapse load  $q_u$  of the column:

$$q_u = 16 \frac{M_u}{h^2} \quad [4.47]$$

Where

- $q_u$  - the total distributed load
- $h$  - height of column
- $M_u$  - column's limit deflecting moment

The limit moment  $M_u$  can be found, with reference to figure 4.4.10.

$$0.8 f_{cd} b x_c = f_{yd} A_s \quad x_c = \frac{f_{yd} A_s}{0.8 f_{cd} b d} \quad [4.48]$$

$$M_u = 0.8 f_{cd} b x_c (d - 0.4 x_c) = f_{yd} A_s (d - 0.4 x_c)$$

#### 4.4.6 Numeric elaborations

The pressure collapse value is calculated for each of the kinematic limit states and for both masonry and R.C buildings.

For masonry buildings, the triggering of “plate” mechanism was considered as severe damage limit state, resulting in a D3 damage, while the triggering of the first bending mechanism on the wall (horizontal or vertical) was considered as the limit state of collapse, resulting in a D4-D5 damage.

The procedure was iterated by varying the geometric, typological and mechanical characteristics of the model assumed, as shown in Tables 4.4.7 and 4.4.8. The variation ranges of these characteristics are chosen according to the most frequent building types in the areas under study (the areas in Campania Region with a high level of hazard).

*Table 4.4.7 Masonry model parameters.*

<b>Masonry model varying parameters</b>	
<b>L</b>	Width of wall
<b>Th</b>	Thickness of wall (with gradual decreasing for upper levels)
<b>H</b>	Inter-storey height (height of the wall )
<b>Lh</b>	Size of the slab resting on the wall
<b>Nw</b>	Nr. of windows or doors
<b>Sw</b>	Size of the openings
<b>Nf</b>	Nr. Of floors
<b>Sl</b>	Kind of slab structure
<b>Typ</b>	Typology of masonry texture

*Table 4.4.8 Reinforced concrete model parameters.*

<b>R.C. model varying parameters</b>	
<b>Nw</b>	Nr. of windows or doors
<b>Sw</b>	Size of the openings
<b>L</b>	Width of infill wall
<b>Th</b>	Thickness of infill wall
<b>H</b>	Inter-storey height
<b>Lh</b>	Size of the slab resting on the frame
<b>b</b>	column cross section base
<b>h</b>	column cross section height
<b>Af</b>	Reinforcing steel cross section area
<b>Fcd</b>	Concrete breaking strain (normal compression)
<b>Fyd</b>	Steel breaking strain (normal traction)
<b>Fkm</b>	Masonry breaking strain (normal compression)
<b>ym</b>	Infill wall density

An example of the results corresponding to the case of a wall belonging to three-floors building, having a width of 5 m and two openings, and other parameters varying, is reported in Table 4.4.9.

**Table 4.4.9** Sample table of speed of flow (m/s) results obtained for the masonry model. .

<b>Flow speed (m/s) bringing to limit load (density of flow = 15 kn/mc)</b>										
		Full brick masonry			Regular cut tuff Masonry			Irregular stone masonry		
		Th = 30	Th= 40	Th= 60	Th = 30	Th= 40	Th= 60	Th = 30	Th= 40	Th= 60
Wooden beam slab	H = 300	0,83	1,38	1,70	0,81	1,35	1,65	0,84	1,42	1,75
	H = 350	0,79	1,34	1,66	0,78	1,30	1,60	0,80	1,38	1,71
	H = 400	0,99	1,51	1,71	0,97	1,46	1,65	1,01	1,55	1,77
Steel beam with terra-cotta infill slab	H = 300	0,97	1,55	1,87	0,96	1,52	1,83	0,98	1,58	1,92
	H = 350	0,92	1,49	1,81	0,91	1,46	1,76	0,93	1,52	1,86
	H = 400	1,15	1,63	1,82	1,14	1,58	1,76	1,17	1,67	1,87
R. C with terra-cotta infill slab	H = 300	1,19	1,79	2,12	1,18	1,76	2,08	1,19	1,81	2,16
	H = 350	1,12	1,70	2,03	1,11	1,68	1,99	1,12	1,73	2,07
	H = 400	1,33	1,75	1,94	1,31	1,71	1,88	1,34	1,80	1,99

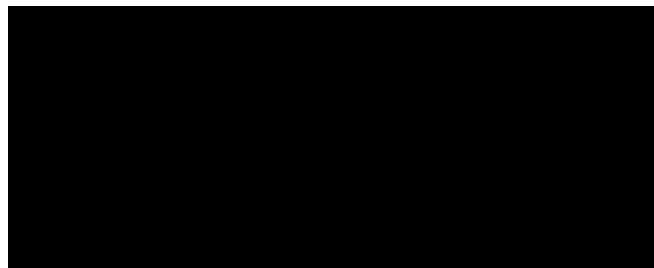
3 storey building, wall width = 5m; height of flow equal to interstorey distance

Th = thickness of wall; H = interstorey distance;

From the interpretation of the results obtained for all the performed calculations, the pressure values corresponding to the collapse state D4-D5 have been defined for the three classes of masonry buildings (A, B, C). In Table 4.4.10, for each class we report the ranges of variation and the mean values of pressure and the corresponding velocity (assuming a flow density of 15 kN/m<sup>3</sup> and the height of flow front equal to the interstorey height).

Similarly, for R.C. buildings, the “plate” mechanism for the infill panels corresponding to a severe damage limit state (D3) and the bending mechanism on the column, corresponding to a collapse limit state (D4-D5), have been considered.

Also in this case the procedure was iterated by varying the geometric, typological and mechanical characteristics of the calculated model. The variable parameters are reported in Table 4.4.8. An example of the results corresponding to the case of a frame mesh with a width of 5 m and two openings is reported in Tables 4.4.11 and 4.4.12.

**Table 4.4.10** Collapse values of speed (m/s) for each vulnerability class (masonry structure)

**Table 4.4.11** Sample table of speed of flow (m/s) results obtained for column in the RC frame model. .  
See Table 4.4.7 for abbreviations.

<b>COLUMN</b>											
<b>Flow speed bringing to limit load (density of flow = 15 kn/mc)</b>											
			fcd = 12 N/mm <sup>2</sup>			fcd = 16 N/mm <sup>2</sup>			fcd = 20 N/mm <sup>2</sup>		
			H= 30	H= 40	H= 50	H= 30	H= 40	H= 50	H= 30	H= 40	H= 50
<b>interstorey height = 300</b>	fyd = 200 (N/mm <sup>2</sup> )	poor reinforcement	2,23	2,24	2,25	2,62	2,63	2,64	2,96	2,97	2,98
		medium reinforcement	2,70	2,72	2,73	3,19	3,20	3,22	3,61	3,62	3,63
		strong reinforcement	3,08	3,11	3,13	3,65	3,68	3,70	4,14	4,17	4,18
	fyd = 220 (N/mm <sup>2</sup> )	poor reinforcement	2,33	2,34	2,35	2,75	2,76	2,76	3,11	3,12	3,12
		medium reinforcement	2,82	2,84	2,86	3,33	3,35	3,37	3,78	3,80	3,81
		strong reinforcement	3,22	3,26	3,28	3,81	3,85	3,87	4,33	4,36	4,38
	fyd = 240 (N/mm <sup>2</sup> )	poor reinforcement	2,43	2,44	2,45	2,86	2,88	2,88	3,24	3,25	3,26
		medium reinforcement	2,93	2,96	2,98	3,47	3,50	3,51	3,94	3,96	3,97
		strong reinforcement	3,34	3,39	3,42	3,97	4,01	4,03	4,51	4,55	4,57
<b>interstorey height = 350</b>	fyd = 200 (N/mm <sup>2</sup> )	poor reinforcement	1,91	1,92	1,92	2,25	2,26	2,26	2,54	2,55	2,55
		medium reinforcement	2,31	2,33	2,34	2,73	2,75	2,76	3,09	3,11	3,12
		strong reinforcement	2,64	2,67	2,69	3,13	3,15	3,17	3,55	3,57	3,58
	fyd = 220 (N/mm <sup>2</sup> )	poor reinforcement	2,00	2,01	2,02	2,35	2,36	2,37	2,66	2,67	2,68
		medium reinforcement	2,42	2,44	2,45	2,86	2,88	2,89	3,24	3,25	3,26
		strong reinforcement	2,76	2,79	2,81	3,27	3,30	3,32	3,71	3,74	3,75
	fyd = 240 (N/mm <sup>2</sup> )	poor reinforcement	2,08	2,09	2,10	2,45	2,47	2,47	2,78	2,79	2,79
		medium reinforcement	2,52	2,54	2,56	2,98	3,00	3,01	3,38	3,39	3,41
		strong reinforcement	2,87	2,90	2,93	3,40	3,44	3,46	3,87	3,90	3,91
<b>interstorey height = 400</b>	fyd = 200 (N/mm <sup>2</sup> )	poor reinforcement	1,67	1,68	1,68	1,97	1,97	1,98	2,22	2,23	2,23
		medium reinforcement	2,02	2,04	2,05	2,39	2,40	2,41	2,71	2,72	2,73
		strong reinforcement	2,31	2,34	2,35	2,74	2,76	2,77	3,11	3,12	3,14
	fyd = 220 (N/mm <sup>2</sup> )	poor reinforcement	1,75	1,76	1,76	2,06	2,07	2,07	2,33	2,34	2,34
		medium reinforcement	2,11	2,13	2,15	2,50	2,52	2,53	2,83	2,85	2,86
		strong reinforcement	2,41	2,44	2,46	2,86	2,89	2,90	3,25	3,27	3,28
	fyd = 240 (N/mm <sup>2</sup> )	poor reinforcement	1,82	1,83	1,84	2,15	2,16	2,16	2,43	2,44	2,44
		medium reinforcement	2,20	2,22	2,24	2,60	2,62	2,63	2,95	2,97	2,98
		strong reinforcement	2,51	2,54	2,56	2,98	3,01	3,02	3,38	3,41	3,43

**Table 4.4.12** Sample table of speed of flow (m/s) results obtained for infill walls in the RC frame model.

<b>INFILL WALLS</b>									
<b>Flow speed (m/s) bringing to limit load (density of flow = 15 kn/mc)</b>									
	light air bricks			Regular cut tuff Masonry			Full brick masonry		
	Th = 30	Th = 40	Th = 60	Th = 30	Th = 40	Th = 60	Th = 30	Th = 40	Th = 60
H=300	0,75	1,00	1,25	0,85	1,13	1,42	0,98	1,31	1,64
H=350	0,79	1,05	1,31	0,89	1,19	1,48	1,03	1,37	1,71
H=400	0,84	1,11	1,39	0,95	1,27	1,58	1,10	1,46	1,83

wall width = 5m ; height of flow equal to interstorey distance

Th = thickness of wall; H = interstorey distance ;

From the interpretation of the obtained results, the pressure values corresponding to the collapse state D4-D5 have been defined for the three classes of R.C. buildings (D, E, F). In Tables 4.4.13 and 4.4.14, for each class, we report the ranges of variation and the mean values of pressure and the corresponding velocity (assuming a flow density of 15 kN/m<sup>3</sup>).

**Table 4.4.13** Collapse speed (m/s) values for each vulnerability class (RC frame structure)

<b>R.C. collapse flow speed (m/s)</b>			
(density = 15Kn/mc)			
Class	min	central	max
D	1,7	2,3	2,9
E	2	2,9	3,5
F	2,7	3,7	4,6

**Table 4.4.14** Collapse speed (m/s) values for each vulnerability class (RC infill walls)

<b>Masonry collapse flow speed (m/s)</b>			
(density = 15Kn/mc)			
Class	min	average	max
A	0,7	1,1	1,6
B	1,4	1,9	2,3
C	2,2	2,4	2,6

#### 4.4.7 Missiles

All the loads considered until now are equally distributed, however during a fast-flowing landslide event often the density of the moving mass is not homogeneous, and frequently the flow sweeps objects that represent concentrated masse, e.g. boulders, garbage bins, vehicles etc. The impact of these objects can be computed as a concentrated load on the building's wall or infill panel or column, since the impact surface can represent less than 25x25 cm<sup>2</sup>. The intensity of this load is proportional to the carried mass and to the square of the speed. This kind of phenomenon is called "missile" and has to be treated in a specific way, because it's

evident that the intensity of the strain on the structure is much higher than the load caused by the flow motion only, so the probability of failure for stricken structures is very high, even when flow speed is not very high.

For instance, the Italian code suggests, for urban roads, to consider a 500 kN force in case of vehicle impact against engineered structures (bridge pile, house walls facing the roads, etc.) due to normal traffic accident. It is reasonable to assume this load value for a medium-sized car (150 kN mass) dragged by flow hitting a building at 2.8 m/s speed (about 10 km/h), taking into account the rate of energy dissipated by the deformation of the vehicle.

#### 4.4.7.1 Walls

In case of impact on a wall (both a masonry building resistant wall and an infill panel in RC building), the crisis can be caused by bending or shear mechanism, but generally the shear mechanism is more frequent, unless the impact occurs in the middle of a large wall.

Assuming the force concentrated in the middle of the wall height, the wall bending model adopted is:

$$V_x = V_{tot} \frac{L_y^4}{kL_x^4 + L_y^4} \quad [4.49]$$

$$V_y = V_{tot} - V_x \quad [4.50]$$

$$M_x = \frac{1}{2} \eta_d V_x L_x \quad ; \quad M_y = \frac{1}{2} \eta_d V_y L_y \quad ; \quad [4.51]$$

$$M_u = \frac{F_k \cdot s^2}{4} \quad [4.52]$$

$$V_u = V_{tot} : \text{Max}(M_x; M_y) = M_u \quad [4.53]$$

where:

$k$  : partition coefficient of the total load (depends on the constraint conditions and assumed to be equal to 1)

$V_{tot}$  : total missile action

$V_x$  : part of the total action that is assigned to the band along x direction

$V_y$  : part of the total action that is assigned to the band along y direction

$\eta_d$  : dynamic coefficient depending on the dissipation capacity of the missile and on the ratio between the mass of missile and the mass of stricken structure.

$Fk$  : characteristic compression resistance of the wall

$Lx$  : x dimension of the wall

$Ly$  : y dimension of the wall

$M_u$  : wall's limit deflecting moment

$V_u$  : crisis missile action

If the missile hits the wall near an edge (e.g. the bottom or the top), the bending moment is small, so the principal strain is shearing. In this case the collapse load can be evaluated in a simplified way by computing:

$$\text{shear resistant area:} \quad A_s = p \cdot th \quad [4.54]$$

$$\text{shear collapse strain:} \quad Tu = F_{vk} \cdot 2/3 \cdot A_s \quad [4.55]$$

$$\text{assuming from the Italian Code:} \quad F_{vk} = F_{vk0} + 0.4 \cdot \sigma_n \quad [4.56]$$

where:

$A_s$  : shear resistant area

$p$  : perimeter of the hit zone (25cm x 4) = 100 cm

$th$  : thickness of the wall

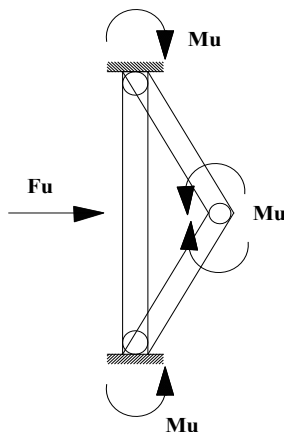
$F_{vk}$  : characteristic shear resistance of the wall

$F_{vk0}$  : characteristic shear resistance of the wall without compression strain

$\sigma_n$  : average normal strain due to vertical loads in the wall

#### 4.4.7.2 Columns

In case of impact on a column, the crisis is mostly due to a shear mechanism. Nevertheless, a bending mechanism can be triggered by a missile hitting in the middle of a thin column. Both cases are examined.



The bending crisis is due to the three plastic hinges mechanism. The first limit state considered is the crisis of the extremity joints, with the creation of two hinges (damage state), and afterwards, with the creation of a third plastic hinge in the center of the column (collapse state). The limit load is given by:

$$V_u = 10 \frac{M_u}{L} \quad [4.57]$$

where:

$M_u$  : column limit deflecting moment

$V_u$  : crisis missile action

The value of  $M_u$  is calculated as for the limit flow on columns.

If the impact occurs near the end of the edge of the column, or the column is stubby, the bending stress is inessential, and shear strain is predominant.

In this case the shear crisis is due to the fragile collapse of column in the zone stricken by the missile.

The **damage limit** of stress in the shear reinforcement is:

$$V_{Rsd} = 0.9 \cdot d \cdot \frac{A_{sw}}{s} \cdot f_{yd} \cdot \frac{\sqrt{2}}{2} \quad [4.58]$$

The **damage limit** of stress in the concrete is:

$$V_{Rcd} = 0.9 \cdot d \cdot b_w \cdot \alpha_c \cdot \frac{f'_{cd}}{2} \quad [4.59]$$

where :

- $A_{sw}$  : shear reinforcement area  
 $d$  : height of column cross section  
 $b_w$  : width of column cross section  
 $s$  : distance between two consecutive reinforcements stirrup;  
 $\sigma_n$  : average normal strain due to vertical loads in the column  
 $f'_{cd}$  : reduced compressive strength of concrete (  $f'_{cd} = 0,5 \cdot f_{cd}$  )  
 $f_{yd}$  : limit strength of reinforcement  
 $\alpha_c$  : increasing coefficient equal to:
 

$1 + \sigma_n / f_{cd}$	if $0 \leq \sigma_n < 0,25 f_{cd}$
$1,25$	if $0,25 f_{cd} \leq \sigma_n \leq 0,5 f_{cd}$
$2,5(1 - \sigma_n / f_{cd})$	if $0,5 f_{cd} < \sigma_n < f_{cd}$

The crisis is achieved when the missile action is equal to minimum value between  $V_{Rsd}$  and  $V_{Rcd}$ .

The **collapse limit** of stress in the shear reinforcement and concrete are respectively:

$$V_{Rsk} = 0.9 \cdot d \cdot \frac{A_{sw}}{s} \cdot f_{yk} \cdot \frac{\sqrt{2}}{2} \quad [4.60]$$

$$V_{Rck} = 0.9 \cdot d \cdot b_w \cdot \alpha_c \cdot \frac{f_{ck}}{2} \quad [4.61]$$

Where:

- $f_{ck}$  : characteristic compressive strength of concrete  
 $f_{yk}$  : yield strength of reinforcement

The crisis is achieved when the missile action is equal to minimum value between  $V_{Rsk}$  and  $V_{Rck}$ .

#### 4.4.8 Combination of elementary vulnerability

All the possible combinations of the three elementary vulnerabilities involved in the R.C. structures were examined, and the limit loads related respectively to the damage states D2, D3 and D4-5 were estimated according to the damage definitions reported above.

The results are given in table 4.4.15, where in the 4<sup>th</sup>, 5<sup>th</sup> and 6<sup>th</sup> columns, the hierarchic order of collapse is shown. It is important to note that the results have to be considered as a preliminary achievement of vulnerability assessment and the estimated limit values could be

improved. The prominent issue of this kind of study is the introduction of the hierarchy of vulnerability factors linked to the progression of damage on the different structural and non structural elements under increasing load.

The same analysis has been carried out for masonry; in this case, there are fewer combinations since the elements considered in the hierarchic order of collapse are less numerous (Table 4.4.16).

In Appendix II, some samples of vulnerability curves for R.C. and masonry buildings are given, which correspond to some of the combinations reported in tables 4.4.15 and 4.4.16.

**Table 4.4.15** R.C. - Hierarchic order of collapse for structural and non structural elements involved (values of speed are in m/s).

Flow speed limit values for all the possible combination between structure, infill and openings vulnerability class														
COMBINATIONS			COLLAPSE HIERARCHY			D2			D3			D4-D5		
openings	infill	frame	openings	infill	frame	MIN	AVER.	MAX	MIN	AVER.	MAX	MIN	AVER.	MAX
A	A	D	1	2	3	0,37	0,45	0,63	0,70	1,00	1,40	1,70	2,40	2,90
A	A	E	1	2	3	0,37	0,45	0,63	0,70	1,00	1,40	2,00	2,90	3,50
A	A	F	1	2	3	0,37	0,45	0,63	0,70	1,00	1,40	2,71	3,79	4,60
A	B	D	1	->	2	0,37	0,45	0,63	0,86	1,22	1,48	0,86	1,22	1,48
A	B	E	1	2	3	0,37	0,45	0,63	0,95	1,20	1,60	2,00	2,90	3,50
A	B	F	1	2	3	0,37	0,45	0,63	0,95	1,20	1,60	2,71	3,79	4,60
A	C	D	1	->	2	0,37	0,45	0,63	0,86	1,22	1,48	0,86	1,22	1,48
A	C	E	1	->	2	0,37	0,45	0,63	1,02	1,48	1,79	1,02	1,48	1,79
A	C	F	1	2	3	0,37	0,45	0,63	1,20	1,50	1,90	1,38	1,94	2,35
B	A	D	1	2	3	0,52	0,80	1,00	0,70	1,00	1,40	1,70	2,40	2,90
B	A	E	1	2	3	0,52	0,80	1,00	0,70	1,00	1,40	2,00	2,90	3,50
B	A	F	1	2	3	0,52	0,80	1,00	0,70	1,00	1,40	2,70	3,81	4,60
B	B	D	1	2	3	0,52	0,80	1,00	0,86	1,22	1,48	0,86	1,22	1,48
B	B	E	1	2	3	0,52	0,80	1,00	0,95	1,20	1,60	2,00	2,90	3,50
B	B	F	1	2	3	0,52	0,80	1,00	0,95	1,20	1,60	2,71	3,79	4,60
B	C	D	1	->	2	0,52	0,80	1,00	0,86	1,22	1,48	0,86	1,22	1,48
B	C	E	1	->	2	0,52	0,80	1,00	1,02	1,48	1,79	1,02	1,48	1,79
B	C	F	1	2	3	0,52	0,80	1,00	1,20	1,50	1,90	1,38	1,94	2,35
C	A	D	->	2	3	0,59	0,84	1,17	0,59	0,84	1,17	1,70	2,40	2,90
C	A	E	->	2	3	0,59	0,84	1,17	0,59	0,84	1,17	2,00	2,90	3,50
C	A	F	->	2	3	0,59	0,84	1,17	0,59	0,84	1,17	2,70	3,81	4,60
C	B	D	1	->	2	0,82	0,97	1,15	0,86	1,22	1,48	0,86	1,22	1,48
C	B	E	1	2	3	0,82	0,97	1,15	0,95	1,20	1,60	2,00	2,90	3,50
C	B	F	1	2	3	0,82	0,97	1,15	0,95	1,20	1,60	2,71	3,79	4,60
C	C	D	->	->	1	0,76	1,07	1,30	0,76	1,07	1,30	0,76	1,07	1,57
C	C	E	1	->	2	0,82	0,97	1,15	1,02	1,48	1,79	1,02	1,48	1,79
C	C	F	1	2	3	0,82	0,97	1,15	1,20	1,50	1,90	2,70	3,79	4,60

S.L.D : Limit state of damage - S.L.U : Limit state of collapse

**Table 4.4.16** MASONRY - Hierarchic order of collapse for structural and non structural elements involved (values of speed are in m/s).

Flow speed (m/s) limit values for all the possible combination between structure and openings vulnerability class													
COMBINATIONS		COLLAPSE HIERARCHY			D2			D3			D4-D5		
openings	walls	openings	walls S.L.D	walls S.L.U	MIN	AVER.	MAX	MIN	AVER.	MAX	MIN	AVER.	MAX
A	A	1	2	3	0,37	0,45	0,63	0,52	0,73	0,97	0,63	0,97	1,63
A	B	1	2	3	0,37	0,45	0,63	0,89	1,26	1,55	1,41	1,63	1,83
A	C	1	2	3	0,37	0,45	0,63	1,41	1,63	1,83	1,63	2,00	2,45
B	A	->	1	2	0,45	0,61	0,81	0,45	0,61	0,81	0,53	0,81	1,37
B	B	1	2	3	0,52	0,80	1,00	0,89	1,26	1,55	1,41	1,63	1,83
B	C	1	2	3	0,52	0,80	1,00	1,41	1,63	1,83	1,63	2,00	2,45
C	A	->	1	2	0,45	0,61	0,81	0,45	0,61	0,81	0,53	0,81	1,37
C	B	->	1	2	0,75	1,06	1,30	0,75	1,06	1,30	1,18	1,37	1,53
C	C	1	2	3	0,82	0,97	1,15	1,41	1,63	1,83	1,63	2,00	2,45

S.L.D: Limit state of damage - S.L.U : Limit state of collapse

A final vulnerability classification of building will derive from the critical analysis of these tables, grouping the combinations in vulnerability classes, according to the collapse load values, and then pointing out the typological characteristics of each class.

A first attempt of grouping the combinations is shown in fig 4.4.11 (R.C.) and in fig. 4.4.13 (Masonry). The interpolated vulnerability curves for each group are reported in fig 4.4.12 (R.C.) and 4.4.14 (Masonry).

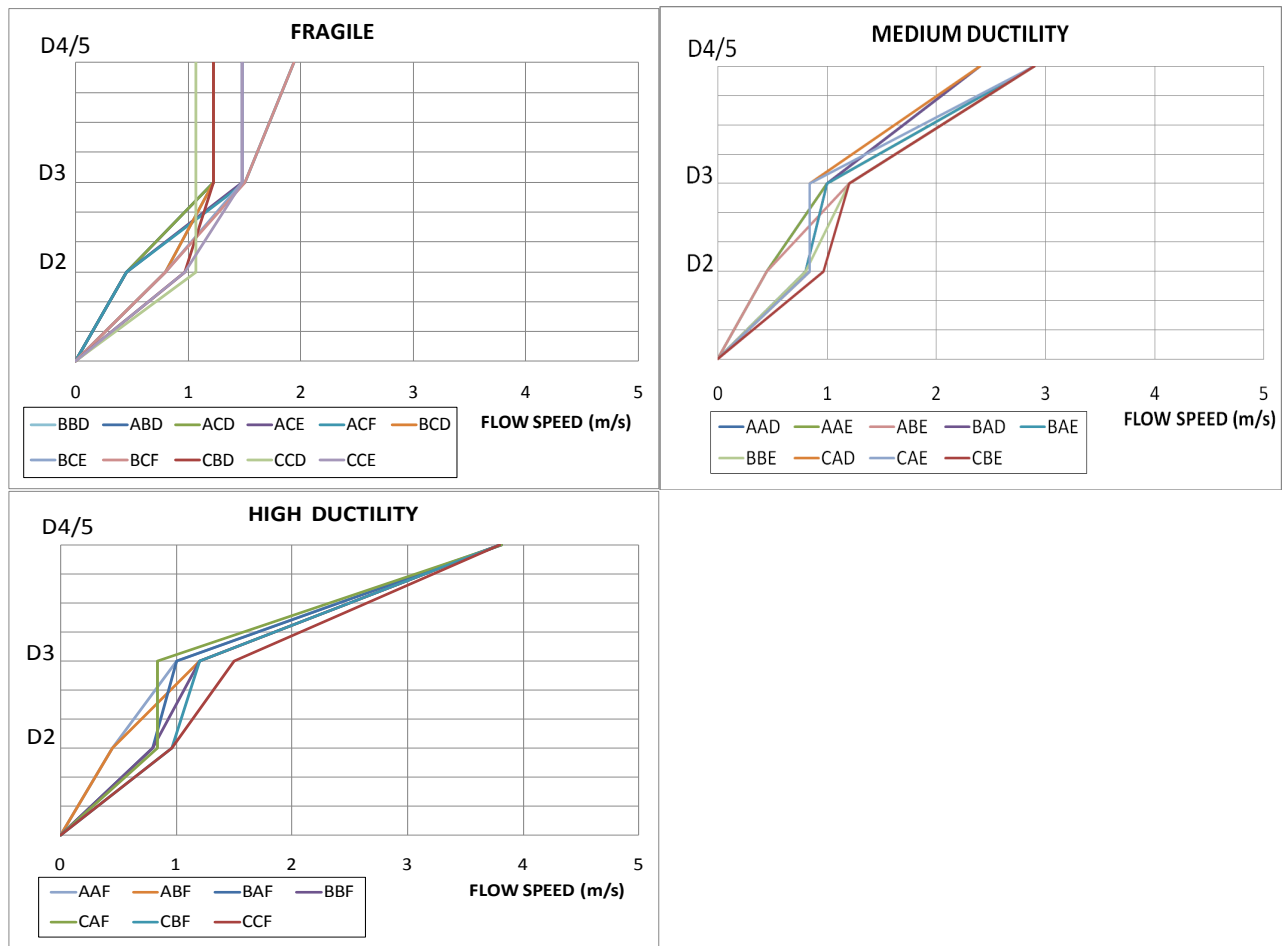


Figure 4.4.11 R. C.: Vulnerability diagrams of each group of combinations.

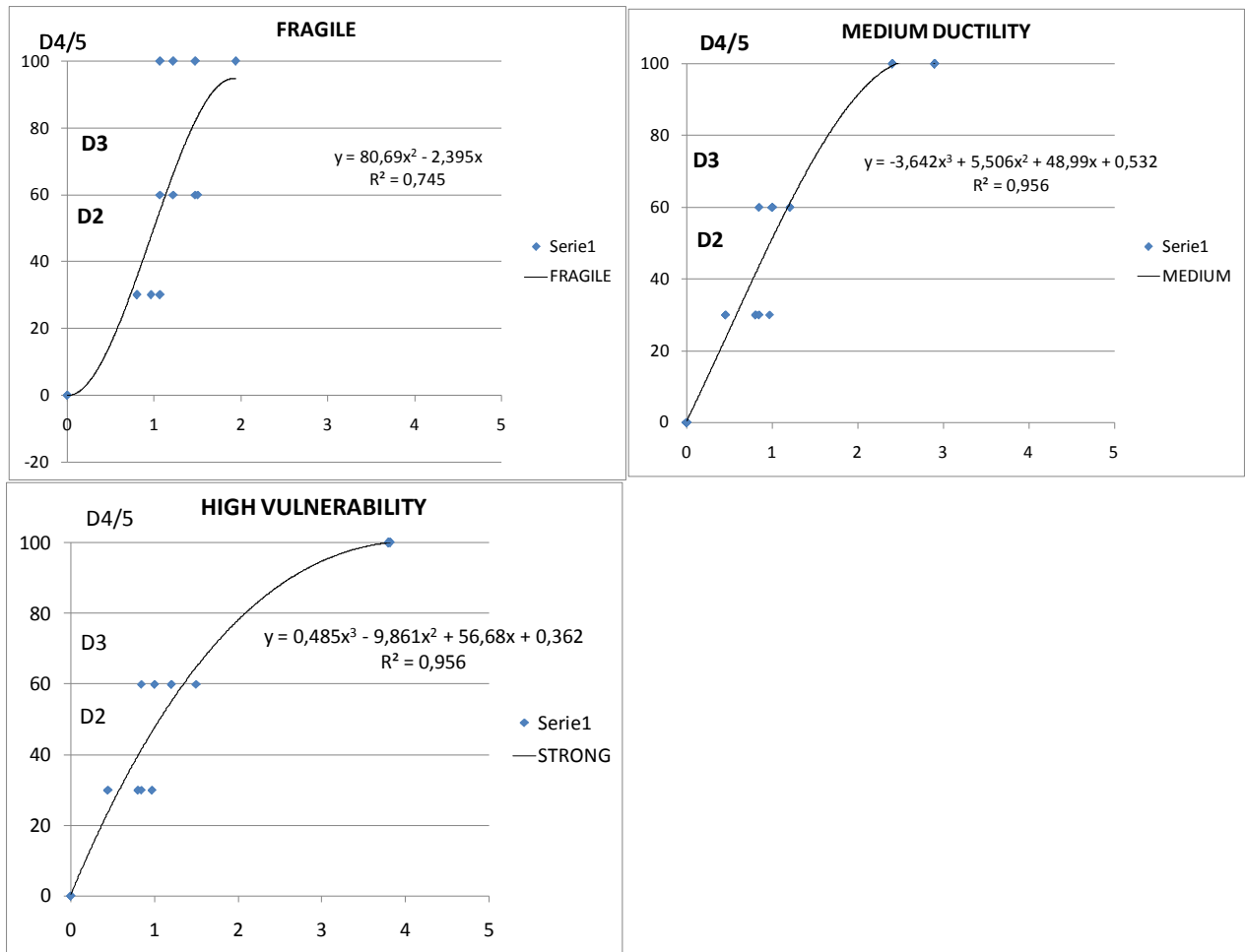


Figure 4.4.12 R. C.: Vulnerability curves obtained by interpolating the values of each group of combinations.

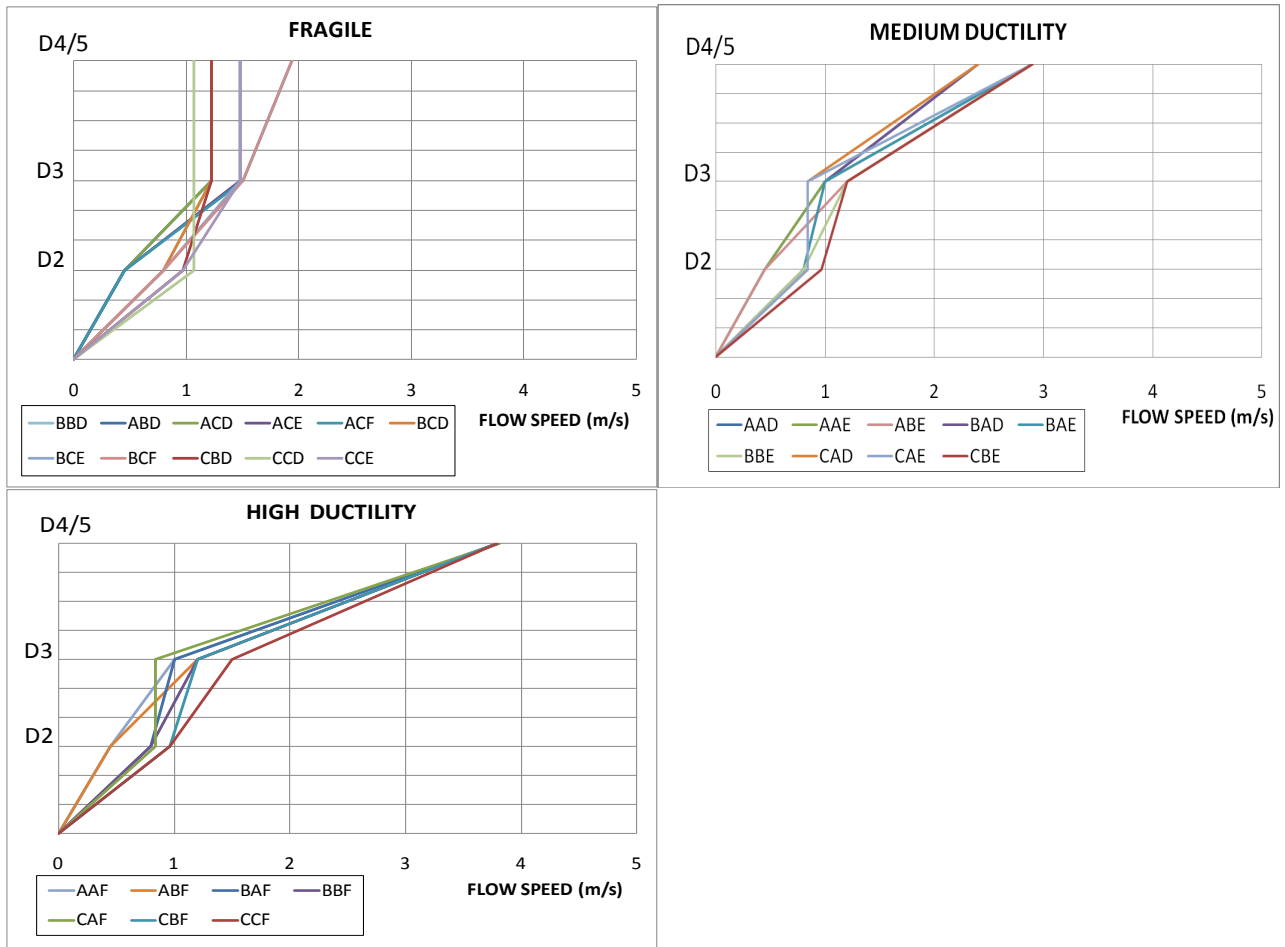
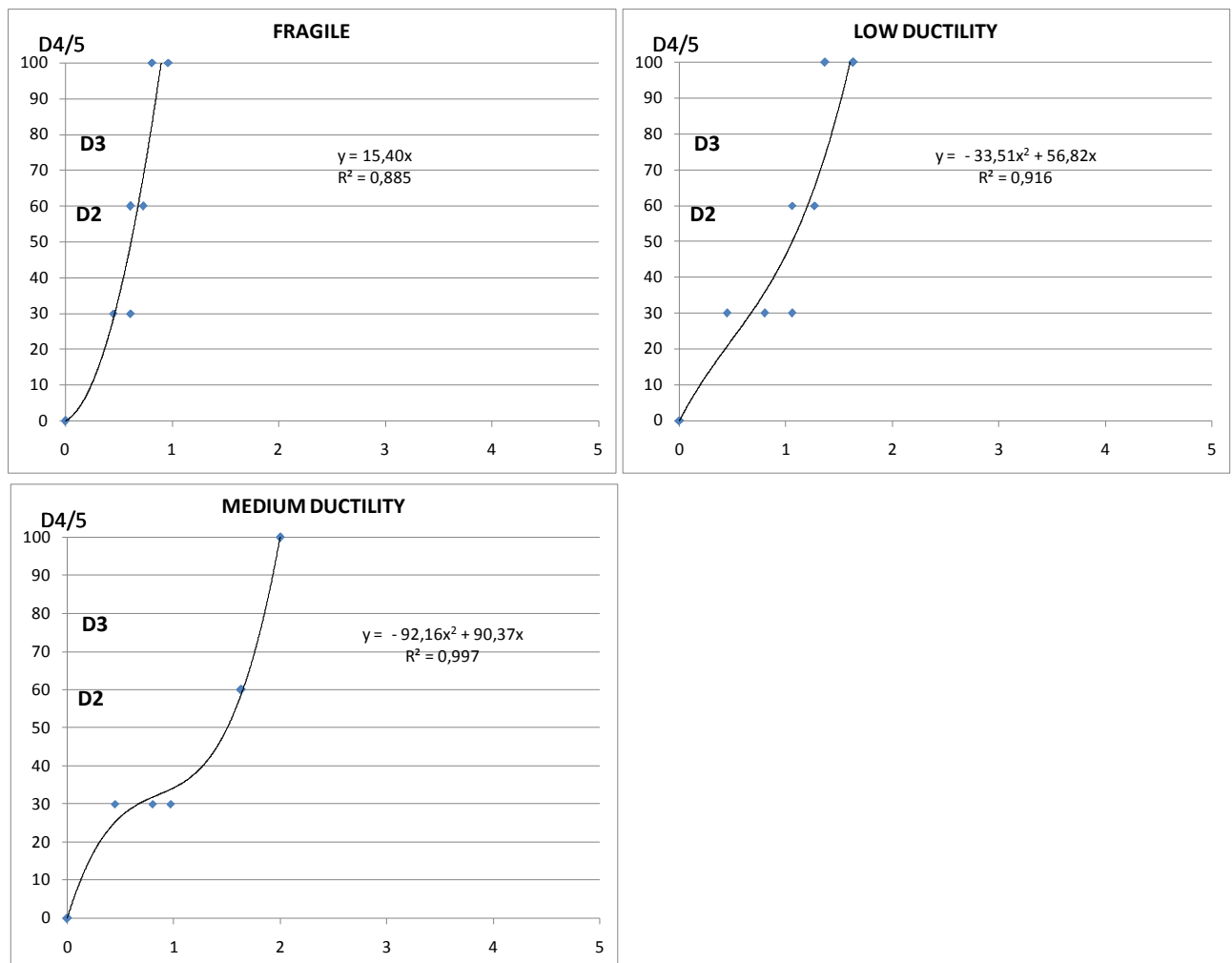


Figure 4.4.13 MASONRY: Vulnerability diagrams of each group of combinations.



**Figure 4.4.14** MASONRY: Vulnerability curves obtained by interpolating the values of each group of combinations.

#### 4.4.8.1 Conclusions

A first attempt of systematizing the behavior of buildings under fast landslide flow impact is made. The effort was finalized to analyze the vulnerability of the whole building starting from the combination of the building elements. This is achieved by estimating the vulnerability of each element and tracing the “path” that leads to the collapse. The curves have been obtained by iterating the elaboration, by varying the typological characteristic of the buildings (according to the most diffuse characteristic of the local heritage in Campania region) and by deriving the range of load values responsible for first damage and collapse. The procedure has been applied assuming the most common input values: height of the flow equal to the inter-story height, density equal to 1.5 KN/m<sup>3</sup> etc. Extrapolation to other input conditions can be easily achieved in order to generalize the procedure toward the creation of an abacus of vulnerability curves according to different density, height of the flow, etc.

## 4.5 METHODOLOGY FOR ROADS/ DEBRIS FLOW (TRL-AUTH-UPC)

### 4.5.1 Introduction

Published fragility curves for the vulnerability assessment of roads due to debris flow are not known to the authors in the literature. While there were several possible approaches available, including an analytical approach, the divergence of such approaches led to the proposal that engineering judgment should be applied to the problem.

The method is based on the completion of a questionnaire (see Appendix I) that was sent to those who have been involved with debris flows and their impact upon roads in the recent past. The questionnaire was designed to interrogate practitioners as to their views on the following relevant areas:

1. The probability of a given volume of debris causing damage exceeding a set level on a given road type. Respondents were requested to give probabilities for six debris flow volumes (between  $<10\text{m}^3$  and  $100,000\text{m}^3$ ), selected to give a broad view of the hazards involved, for each of:
  - Two road types: high speed and local.
  - Three damage states: limited, serious and destroyed.This gave the potential to construct two sets of preliminary fragility curves, one set for each road type with each set comprising three curves and each curve built up from six debris flow volume-probability data points. This approach is not dissimilar to that which has been used in earthquake engineering studies (e.g. ATC-13, 1985) in the past.
2. Their relevant experience: ranked from zero (no experience) to 10 (extensive experience).
3. Their confidence in the probability estimates for each debris flow volume: ranked from zero (none) to 10 (absolute).
4. The frequency of each debris flow volume in their geographical region: every year, 1 in 10 years, every 10s of years and every 100s of years.
5. Optional questions were also asked to establish the views of respondents on the debris flow volumes, the road types and the damage states used in the questionnaire.

It is clear that the judgment of an individual or self-selected group of individuals is unlikely to be either independent or free of bias: such bias might, for example, include that imposed by experience in a particular geographical region and/or their professional environment. Accordingly a large number of experts was targeted from geographically diverse areas of the World and from industry, academia and government bodies. A total of 176 questionnaires was sent by the three organisations involved in this work.

It has been assumed that the volume of landslide debris refers to the volume of landslide deposited at the level of the road.

## 4.5.2 Road Characterization

Many different classifications of roads could potentially be considered. Key factors that must be examined are the construction type and associated stiffness and ductility (bituminous/asphaltic, reinforced concrete, unreinforced concrete and unpaved), the speed of the traffic (e.g. <30, 50, 80, 110 km/h), and the number of traffic and other lanes. However, in order to reduce the questionnaire down to a reasonable size some considerable simplification was clearly needed.

Primarily it was decided that, for the purposes of this exercise, all roads could be considered to be relatively stiff and brittle (stiffness for example is unlikely to drop much below 1 to 2 GPa). In order to further simplify the analysis roads have been simply divided into low and high speed roads, characterized as follows:

- High speed: speed limit between 80 and 110km/h and one or more running lane in each direction, most likely in conjunction with a hard strip or hard shoulder.
- Local (or low speed) roads: speed limit typically <50km/h on a single-carriageway (one lane for each traffic direction) or single-track. This category is intended to encompass both paved (bituminous, unreinforced or reinforced concrete) and unpaved constructions.

While there is clearly a gap between the speed limits of the two classes of road this reflects the transition between local roads and high speed roads which is by no means clear cut. It is accepted that some respondents naturally will have considered such roads under the different categories. However, we consider that this is most likely to reflect the reality of the situation which is that in some countries and regions such roads are more closely aligned with the definition of local roads and in others they are more closely aligned with the definition of high speed roads.

## 4.5.3 Damage States and Definitions

The damage states considered in the questionnaire are defined in Table 4.5.1 and range from the type of damage that is unlikely to radically affect the passage of vehicles, at least on high speed roads, to that which causes longer term damage and restrictions to the speed and/or passage of traffic.

**Table 4.5.1** *Damage state definition*

<b>Damage State</b>	<b>High Speed Roads</b>	<b>Local Roads</b>
P1 (Limited damage)	Encroachment limited to verge/hardstrip	Partial blockage of carriageway
P2 (Serious damage)	Blockage of hardstrip and one running lane	Complete blockage of carriageway and/or damage to ancillaries
P3 (Destroyed)	Complete blockage of carriageway and/or repairable damage to surfacing	Complete blockage of carriageway and/or damage to surfacing. For unpaved roads the surfacing may remain damaged but passable at reduced speeds post clean-up

#### 4.5.4 Description of Probabilities

Respondents to the survey were requested to use their expert judgement to assess the probability of each damage state being exceeded using the qualitative descriptor codes given in Table 4.5.2. The descriptors have been coded A to G in order to assist with completion of the Probability Tables, and correspond to probability values that have been subsequently used to construct the fragility curves.

Respondents were asked to use the qualitative descriptors “Highly Improbable” and “Extremely Unlikely with caution, and only where an extensive, high quality dataset supports the classification.

**Table 4.5.2** *Description of probabilities*

<b>Qualitative Descriptor</b>	<b>Description</b>	<b>Qualitative Descriptor Code</b>	<b>Values for Analysis</b>
Highly improbable	Damage state almost certainly not exceeded, but cannot be ruled out	A	0.000001
Improbable (remote)	Damage state only exceeded in exceptional circumstances	B	0.00001
Very unlikely	Damage state will only be exceeded in very unusual circumstances	C	0.0001
Unlikely	Damage state may be exceeded, but would not be expected to occur under normal circumstances	D	0.001
Likely	A good chance the damage state may be exceeded under normal circumstances	E	0.01
Very likely	Damage state expected to be exceeded	F	0.1
Extremely likely	Damage state almost certainly exceeded	G	1.0

#### 4.5.5 Response to the questionnaire

In total the questionnaire was sent to 176 experts and, of those, 47 responded by completing the questionnaire giving a response rate of 27%. The responses were received from 17 countries as detailed in Table 4.5.3 and illustrated in Figure 4.5.1.

*Table 4.5.3 Respondents broken down by country.*

<b>Country</b>	<b>Number of Experts</b>	<b>Percentage</b>
UK	16	34%
Greece	11	23%
Canada	2	4%
Ireland	2	4%
Italy	2	4%
New Zealand	2	4%
Spain	2	4%
Andorra	1	2%
Hong Kong	1	2%
Netherlands	1	2%
Norway	1	2%
Poland	1	2%
Romania	1	2%
Republic of Korea	1	2%
Slovenia	1	2%
Switzerland	1	2%
UAE	1	2%
<b>Total</b>	<b>47</b>	

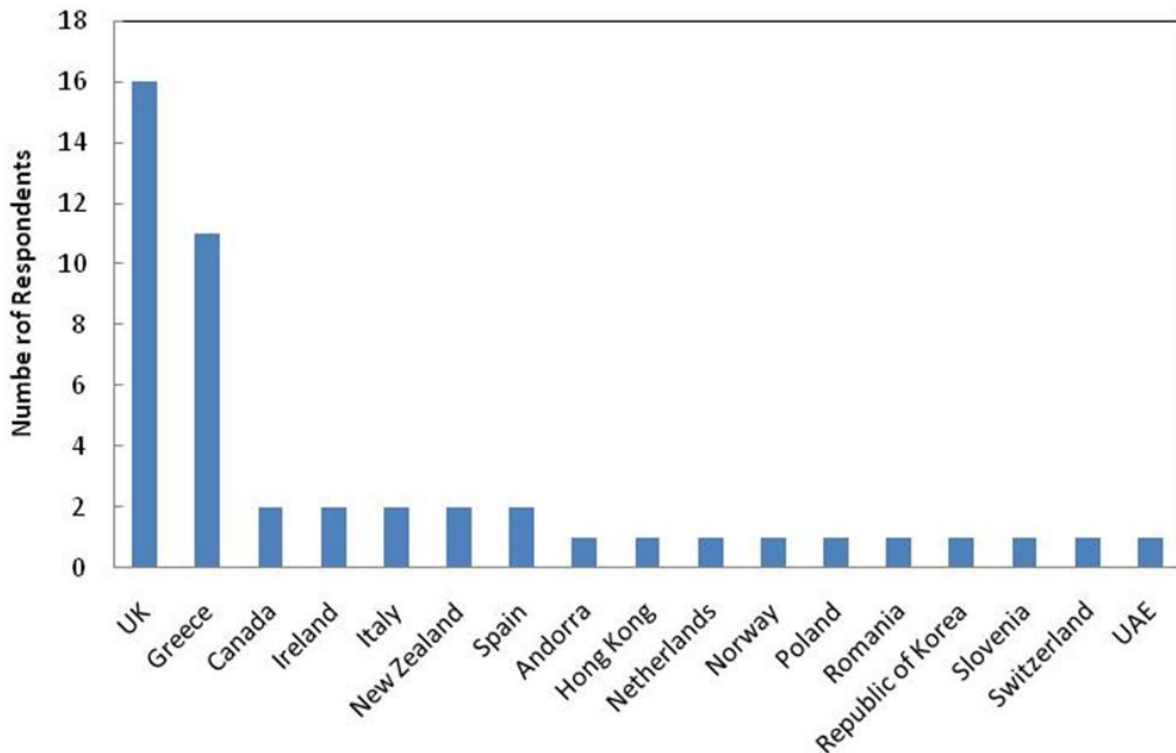


*Figure 4.5.1 Respondents by country.*

The background of the respondents is detailed in Table 4.5.4 and illustrated in Figure 4.5.2.

*Table 4.5.4 Respondents broken down by background.*

<b>Background</b>	<b>Number of Experts</b>	<b>Percentage</b>
Academic	15	32%
Government	8	17%
Industry	24	51%
<b>Total</b>	<b>47</b>	

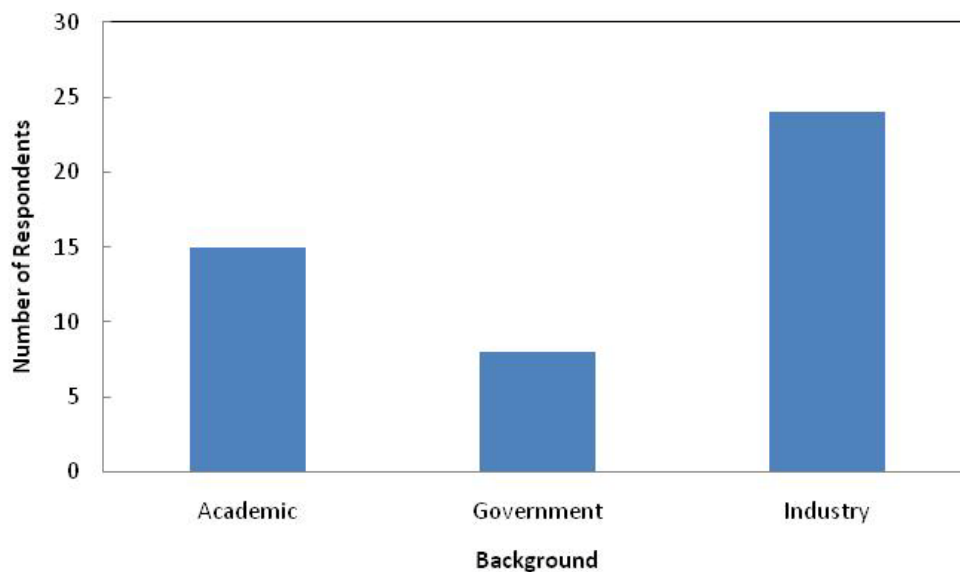


**Figure 4.5.2** Respondents by background.

#### 4.5.6 The basic data

As with all data a reality, or ‘sense’, check is advisable. In terms of what might be expected from the probability data, Figure 4.5.3 illustrates the way in which one might anticipate the basic data should plot. For smaller landslide volumes, the majority of the responses plot to the left hand side while for larger volumes, the majority of the data plot to the right hand side. For the intermediate damage state, the majority of the data plots somewhere between these two extremes. In addition, for Limited Damage, one might anticipate that the data would be skewed slightly to the right as more events would be expected to induce such a state. Similarly for the Destroyed category, one might expect the data to be skewed slightly to the left as fewer events would be likely to induce this extreme state.

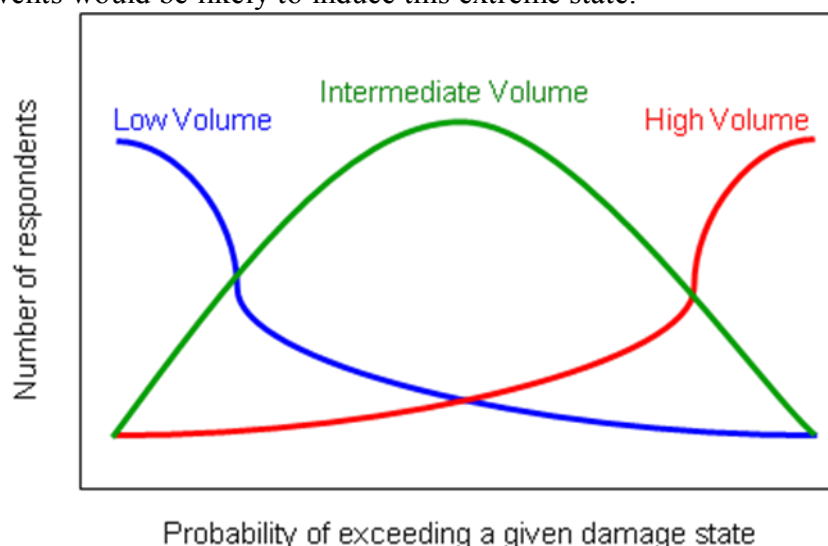


**Figure 4.5.3** An idealized plot of the probability of exceeding a given damage state against the frequency of response illustrating how the data might be expected to appear and to thus provide an immediate ‘sense’ check.

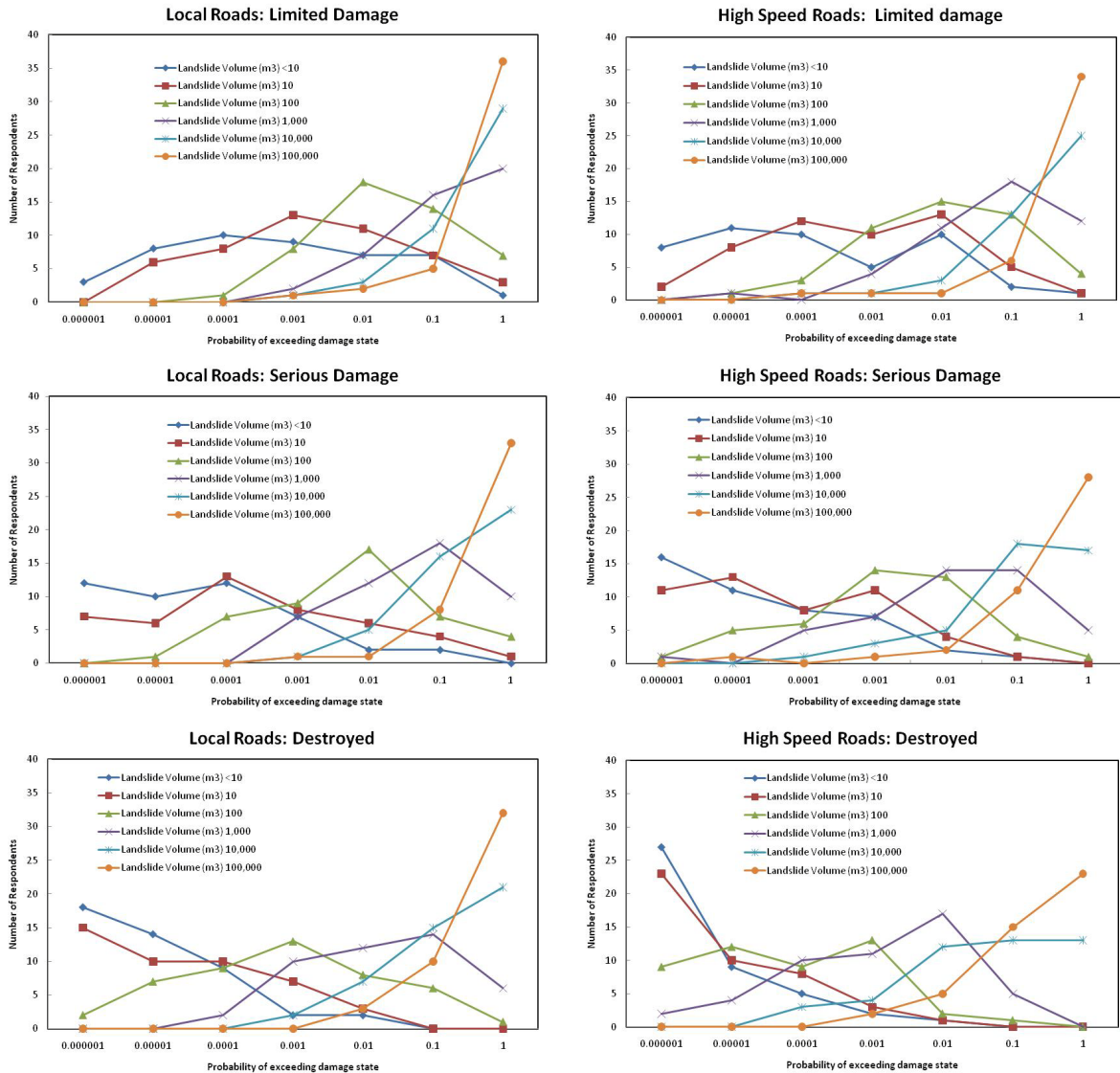
The data from the questionnaire responses (Figure 4.5.4) shows that in broad terms, it makes sense. While there is a greater or lesser degree of scatter and/or variation from the norm set-out in Figure 4.5.3, most of the data broadly follows the illustrated and the variations from it described above.

It is a relatively straightforward matter to construct preliminary fragility curves from the average of the probability responses at each volume, at each damage state and for both high speed roads and local roads as illustrated in Figure 4.5.5. These curves have the basic attributes of typical fragility curves. In broad terms these curves and the data that underpin them make sense. The curves for local roads generally show that smaller landslides have a greater probability of exceeding a given damage state than for high speed roads. Indeed, those for high speed roads generally show little effect at small landslide volumes, below a few hundred cubic meters.

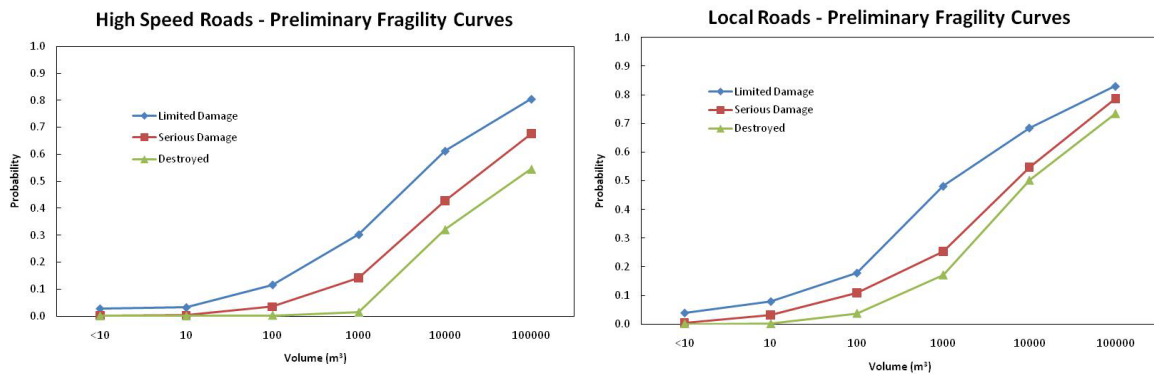
However, there are also one or two issues that are apparent from the data presented, not least the fact that the mean probabilities do not reach unity. This is an inevitable facet of using the average of the responses as the maximum possible response coincides with the desired termination point of each curve (a volume at which exceeding the given damage state is inevitable and the probability is unity).

Figure 4.5.6 illustrates the same data with standard Excel<sup>TM</sup> curve-fitting applied (third order polynomial for Limited Damage states and fourth order polynomial for Severe Damage and Destroyed states). In particular the individual curves show better separation than the illustration in Figure 4.5.6 and the differences between high speed and local roads especially at lower volumes are clearer.

Using such curve-fitting techniques allows a degree of extrapolation of the data to higher volume/probabilities. However, over application of such extrapolation tends to distort the curve at lower volumes and in Figure 4.5.6 this has been limited strictly to avoid such distortions.



**Figure 4.5.4** Probability of exceeding each damage state on each type of road plotted against the number of responses by for each landslide volume.



**Figure 4.5.5** Fragility curves for high speed and local roads.

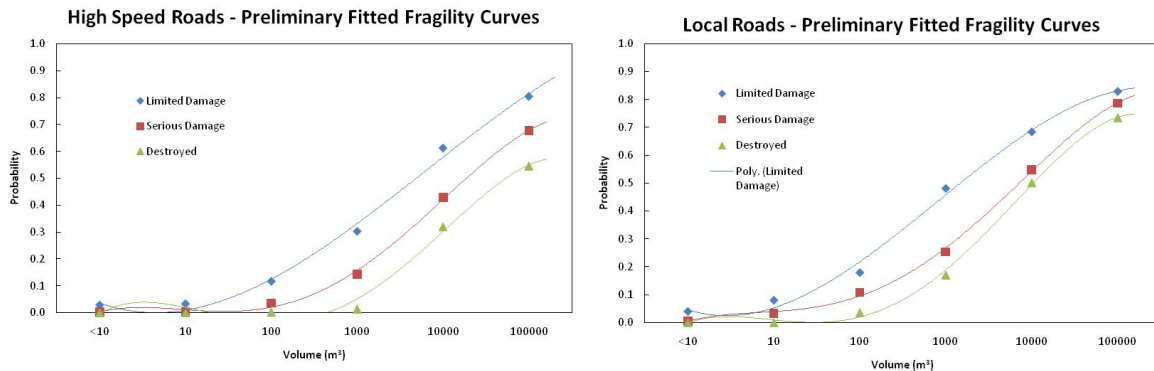


**Figure 4.5.6** Preliminary curve-fitted fragility curves for high speed and local roads.

It is thus interesting to manually extrapolate the data presented in Figure 4.5.5 by a further logarithmic cycle of volume (Figure 4.5.7). This has been achieved by visually judging the appropriate value of probability at 1,000,000 m<sup>3</sup> in order to maintain the broad appearance and trend of the curves. It is noticeable that, even when the volume is increased to 1,000,000 m<sup>3</sup> in this way none of the fragility curves reaches unity; only that for Limited Damage for local roads reaches a value of around 0.95.

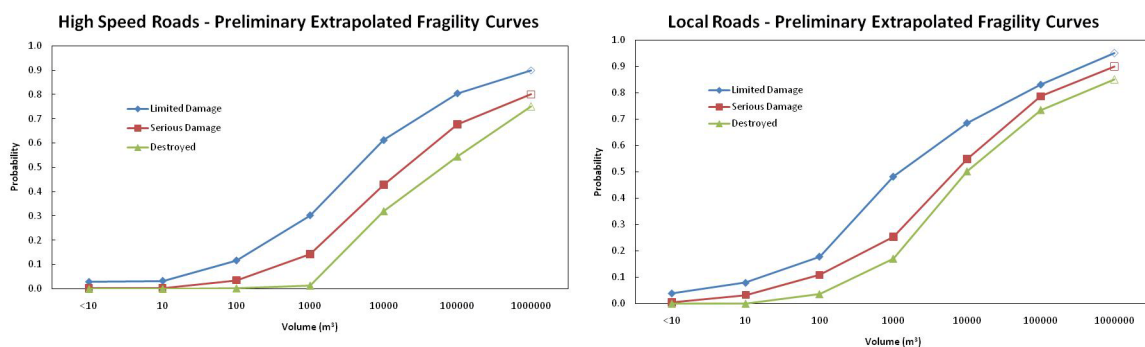


**Figure 4.5.7** Extrapolated fragility curves for high speed and local roads.

#### 4.5.7 Experience of the Respondents

Clearly the experience of the respondents is a critical metric in terms of understanding, evaluating, analyzing and interpreting this data. The respondents were asked to assess their experience on a scale of zero (no experience) to 10 (extensive experience). The results of their assessments are summarized in Figure 4.5.8. It is clear that the scores of this self-assessment weight towards the higher end of the range, as might be expected from a sample of respondents who were selected for their known expertise in this area.

It thus seems potentially appropriate to place a greater confidence in the responses received from those who reported that their level of experience was higher than the average. In order to do so a number of approaches can be taken.

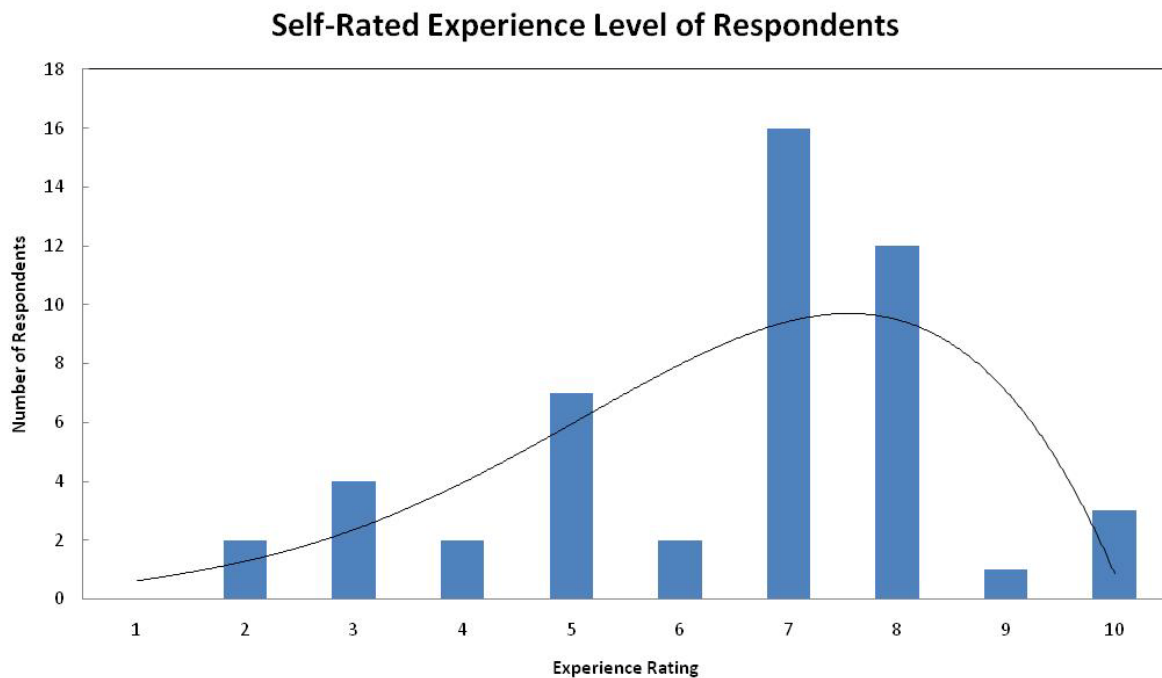


**Figure 4.5.8** Respondents self-assessment of their experience in the subject area addressed in the questionnaire. The fitted curve is an Excel™-generated fourth order polynomial.

Firstly, a weighting approach may be taken. However, care is needed to ensure that the sample is weighted rather than the individual responses; otherwise bias will be introduced into the results. (Weighting the individual responses will, depending upon the precise approach taken, either increase or decrease the individual probabilities contained within the questionnaires for those with higher expertise, the converse for those with lower levels of expertise. There is no logical justification for such a change and this should therefore be avoided.) Weighting the sample may be done as follows:

$$p = \frac{\sum_{i=1}^n p_i E_i}{\sum_{i=1}^n E_i} \quad [4.62]$$

Where  $p$  is the weighted mean probability of a particular damage state being exceeded,  
 $p_i$  represents the individual responses of the probability of a particular damage state being exceeded,  
 $E_i$  represents the individual responses in terms of self-assessed experience, and  
 $n$  is the number of responses.

However, there does remain a question as to what a weighted average means and statistical advice (B Sexton, Pers. Comm.) indicates that the results should be treated with a degree of caution.

This approach yields fragility curves as illustrated in Figure 4.5.9. It is clear that the sample weighting process, in this case, yields lower probabilities of given damage states being exceeded by a given volume of event than those derived from the full data set.

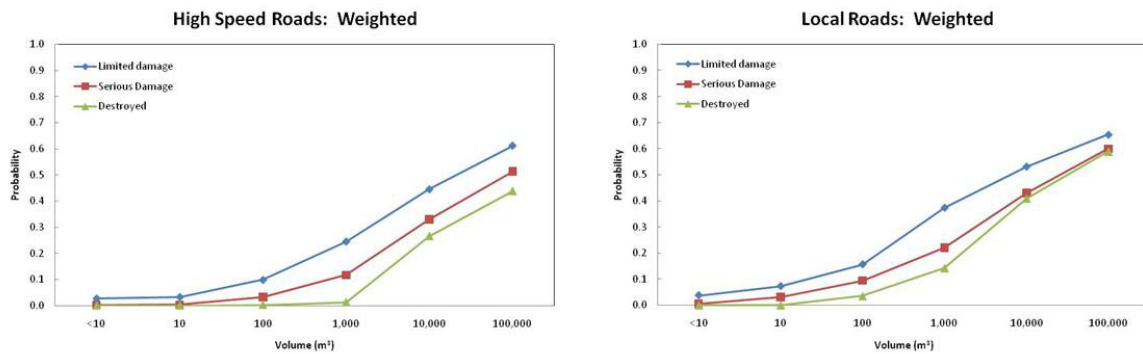


**Figure 4.5.9** Fragility curves constructed from the weighted average of the responses.

The second approach involves rejecting the data from those respondents reporting less experience, leaving only that from those who assessed themselves as more experienced in this area. A cursory examination of the data presented in Figure 4.5.8 would indicate that taking the data from those who judged their experience level as seven or above would be a suitable manner in which to proceed. Statistical advice (B Sexton, Pers. Comm.) indicates that approximately only the upper 25% should be examined. This implies that the analysis should be undertaken for those judging their experience level as eight or above (33% of respondents, out of whom only 8% judged their experience at level nine or above). However, plotting the data led to a rather confused picture and to the conclusion that the 16 responses corresponding to the 33% of respondents reporting their experience level to be eight or above were insufficient to present a coherent picture. The resulting analysis of the data from the 32 (65%) respondents who assessed their experience level as seven or above is presented in Figure 4.5.10.

As for the weighting approach, the resulting fragility curves, as illustrated in Figure 4.5.10, yield lower probabilities of given damage states being exceeded by a given volume of event than those derived from the full data set.

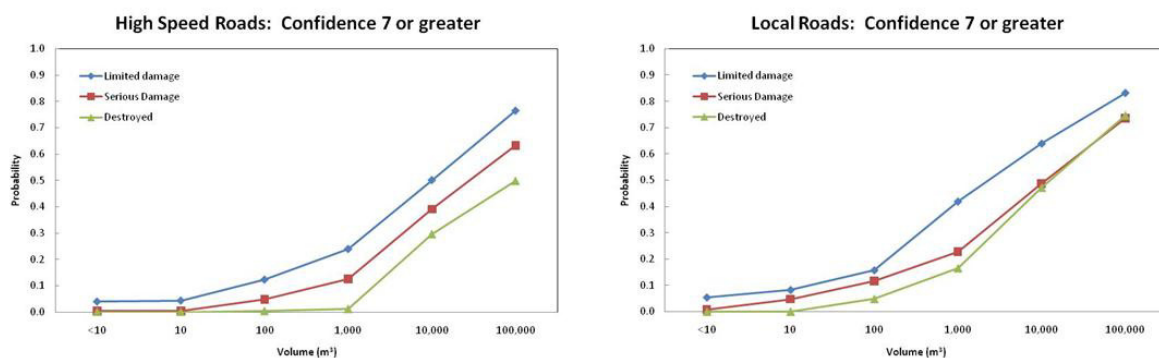


**Figure 4.5.10** Fragility curves constructed from the responses of those who assessed their experience as seven or above.

These results may be interpreted in two ways:

1. The more ‘expert’ respondents present a more considered and cautious approach to determining the probability levels assigned to each volume and damage state.

2. The data set is restricted to the extent that the results become less robust.

On balance, while the former interpretation is attractive in terms of reinforcing the inherent validity of the data set, the authors are more inclined towards the second interpretation, not least as their experience of the larger volume events (up to 100,000 m<sup>3</sup>) indicates that the probabilities should be tending towards unity.

#### 4.5.8 Further Interpretation of the Data

The data points that make up the fragility curves presented above represent the mean responses of either the entire sample or of a cohort (or sub-sample) within the full sample. As such it is both necessary and desirable to examine the statistical variation in the data.

In order to do this the standard deviation may be assessed and the curves representing the mean plus and minus one standard deviation plotted alongside the mean curve (Figure 4.5.11); these represent the bounds within which 68% of the data falls.

The lines at zero and unity are important as probability states outwith these bounds are purely of a statistical nature and have no meaning in terms of the relative likelihood of a damage state being reached. Where the curves extend beyond these conceptual limits it is clear that there is a wide range within the reported data.

It is clear, albeit to varying degrees, that the standard deviation of the probability of a given damage state being reached or exceeded, increases with the volume of the event considered.

This is not altogether surprising as larger events occur less frequently and thus the collective experience of the respondents may be expected to be both less and more variable; both factors with the potential to increase the range of responses. This increase in the variation in responses seems to be more marked as the damage level increases, seemingly indicating a high level of confidence on the part of the respondents to questions relating to the probability of low volume events creating high damage states. Again this result conforms to what might reasonably be expected.

#### 4.5.9 Completing the Curves

The curves illustrated in Figure 4.5.5 do not stretch between zero and unity. Attempts have been made to adjust the curves by manually extrapolating along the landslide volume axis to 1,000,000m<sup>3</sup> (Figure 4.5.7). However, even using that process the curves do not reach to unity as would be expected if they had been derived from a modelling process in which a constraint would have been placed upon the results in order to ensure such a result.

Using the current approach it is inevitable that the mean probability of each damage state being reached or exceeded is less than unity unless all of the respondents return such a value – this seems more than a little unlikely. This then begs the question of how to account for such an inevitable, and seemingly contradictory, facet of the results. It is a simple matter to ‘force’ the fragility curves to reach to unity by a straightforward ratio approach (the forced probability at any value of landslide volume,  $p_{if} = p_i \cdot [1/p_n]$  where  $p_i$  is the mean probability and  $p_n$  is the mean probability at the maximum value of landslide volume) (Figure 4.5.12).

In order to determine whether such an approach can be justified one must examine the more detailed responses of the respondents to the questionnaire and in particular the responses of those where a probability of unity was assigned to the combinations of landslide volume and damage state (Figure 4.5.13).

---

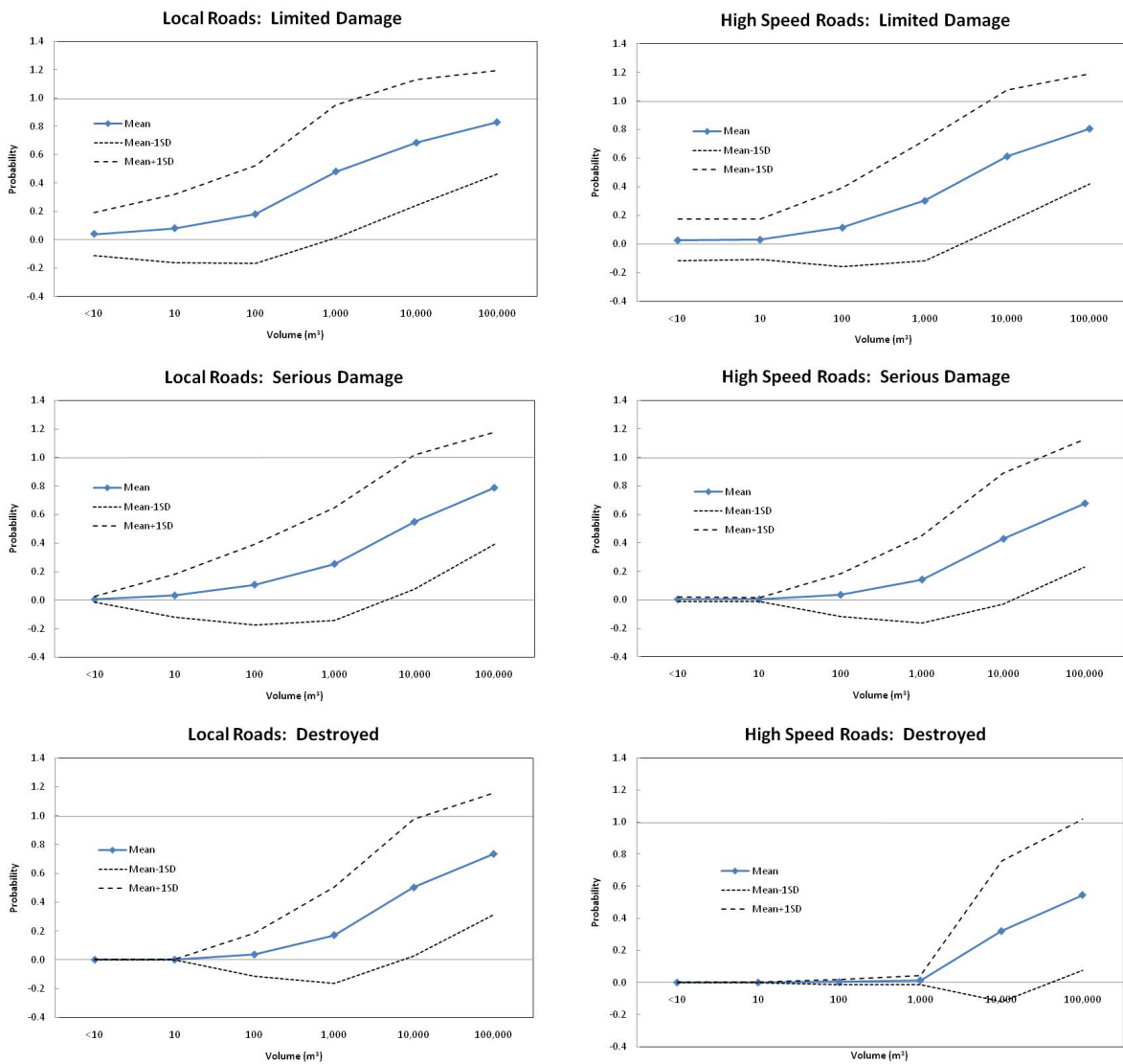


**Figure 4.5.11** Fragility curves showing the mean and the mean plus and minus one standard deviation.

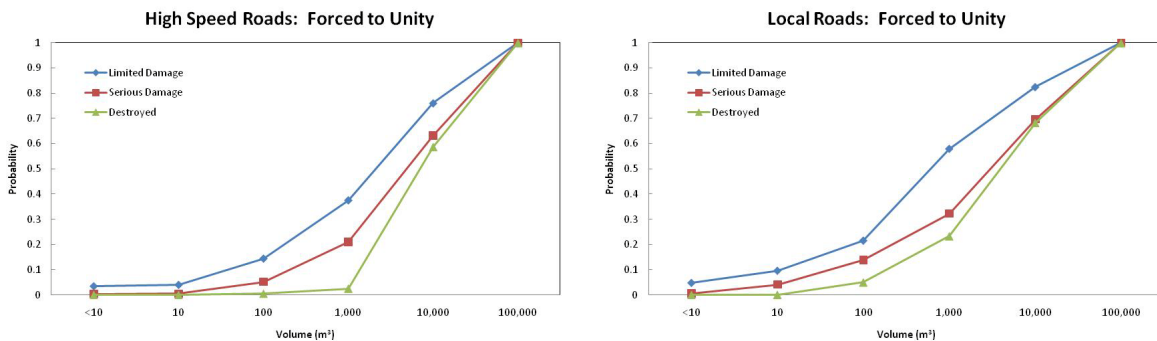


**Figure 4.5.12** Fragility curves forced to unity.

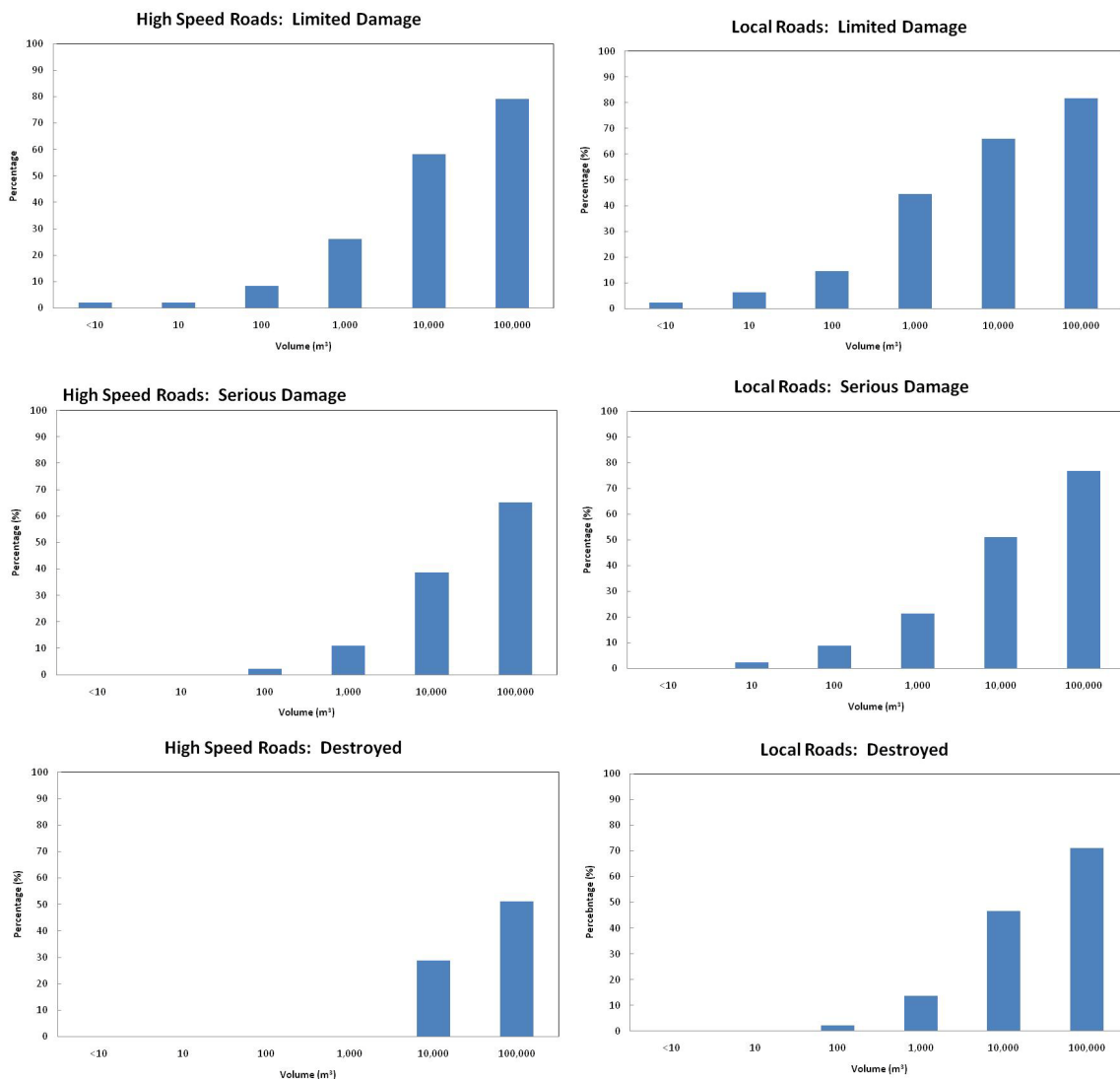


**Figure 4.5.13** Percentage of respondents assigning a probability of unity.

These data illustrate, as might be anticipated, that the number of responses assigning a probability of unity increases markedly with landslide volume while decreasing with increased damage state severity. Most importantly, by the time high landslide volumes are considered the majority of respondents return a value of unity for the likelihood of a given damage state being reached or exceeded. This lends some considerable justification to the approach of ‘forcing’ the curves to reach unity.

While Figure 4.5.12 illustrates the effect of forcing the preliminary fragility curves of Figure 4.5.5 to unity, Figure 4.5.7 illustrates the effect of manually extrapolating the fragility curves to the next order of magnitude in terms of landslide volume (i.e. 1,000,000m<sup>3</sup>). The next logical step is to combine these two actions as illustrated in Figure 4.5.14. The curves illustrated therein do conform to the ‘s’-shape generally perceived as being correct for fragility curves.

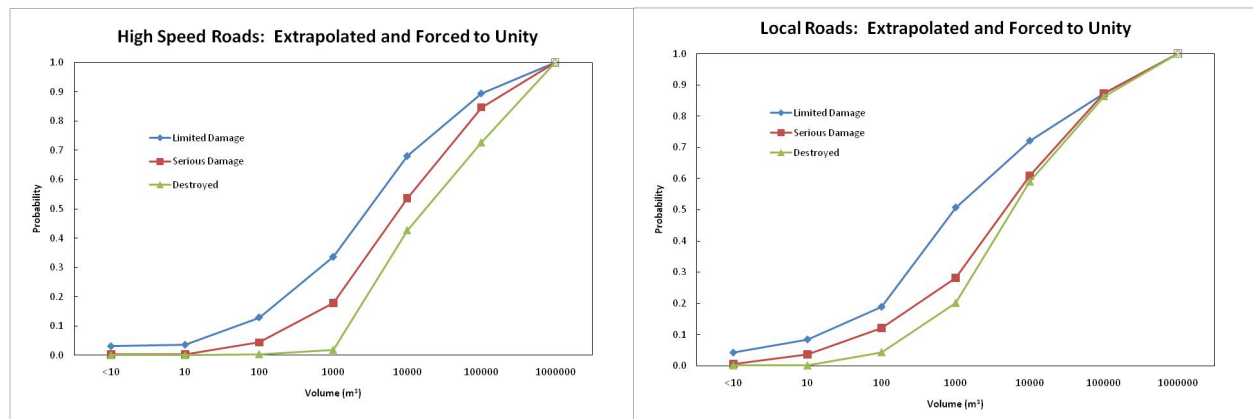


*Figure 4.5.14 Extrapolated fragility curves forced to unity.*

#### 4.5.10 Geographical Variations

The 47 respondents to the questionnaire were from 17 different countries (Table 4.5.3 and Figure 4.5.1). However, a large proportion of these were from the UK (16) and Greece (11). As the severity and frequency of debris flow events varies significantly on a global basis it is instructive to undertake a separate analysis for the data derived from respondent from the UK, Greece and the Rest of the World (20) (Figure 4.5.15).

The curves prepared from the responses of UK-based individuals broadly exhibit slightly higher probabilities for larger landslide volumes while those for derived from the responses of individuals based in the Rest of the World exhibit slightly lower probabilities, compared to the curves derived from all response (Figure 4.5.4). The data from respondents based in Greece exhibit more scatter in the data than is evident from the other data sets and it seems likely that this is a function of the smaller data set, which may well be too small to derive a consistent pattern.

The observed variations are however rather small and, notwithstanding the above comments, it is concluded that the variations between the responses based on geographical location are too small to derive any significant variation. The counterpoint to this is, of course, that the data seem to be broadly geographically consistent and thus it seems sensible to analyse the data set as a single entity as has been done in the preceding sections.

#### 4.5.11 Variations in Background

The backgrounds of the respondents to the questionnaire varied between academia (15), government (8) and industry (24) (Table 4.5.4 and Figure 4.5.2). It is instructive to assess whether membership of one of these groupings affects the results and thus the data for each group is analyzed separately (Figure 4.5.16).

As was noted in Section 4.5.10 for the dataset derived from those based in Greece, the data set for Government people seems to be too small to draw any meaningful conclusions from as the scatter is more significant than that for other data sets. Much as for the UK and Rest of the World data sets (see Section 4.5.10), the data set for those from Academia seems to give slightly higher probabilities of a given damage state being reached or exceeded by larger

landslide volumes while that from those based in Industry seems to give slightly lower probabilities, compared to the curves derived from all response (Figure 4.5.4).

The observed variations are however rather small and, notwithstanding the above comments, it is concluded that the variations between the responses based on the background of respondents are too small to derive any significant variation. The counterpoint to this is, of course, that the data seems to be broadly consistent by background and thus it seems sensible to analyse the data set as a single entity as has been done in the preceding sections.

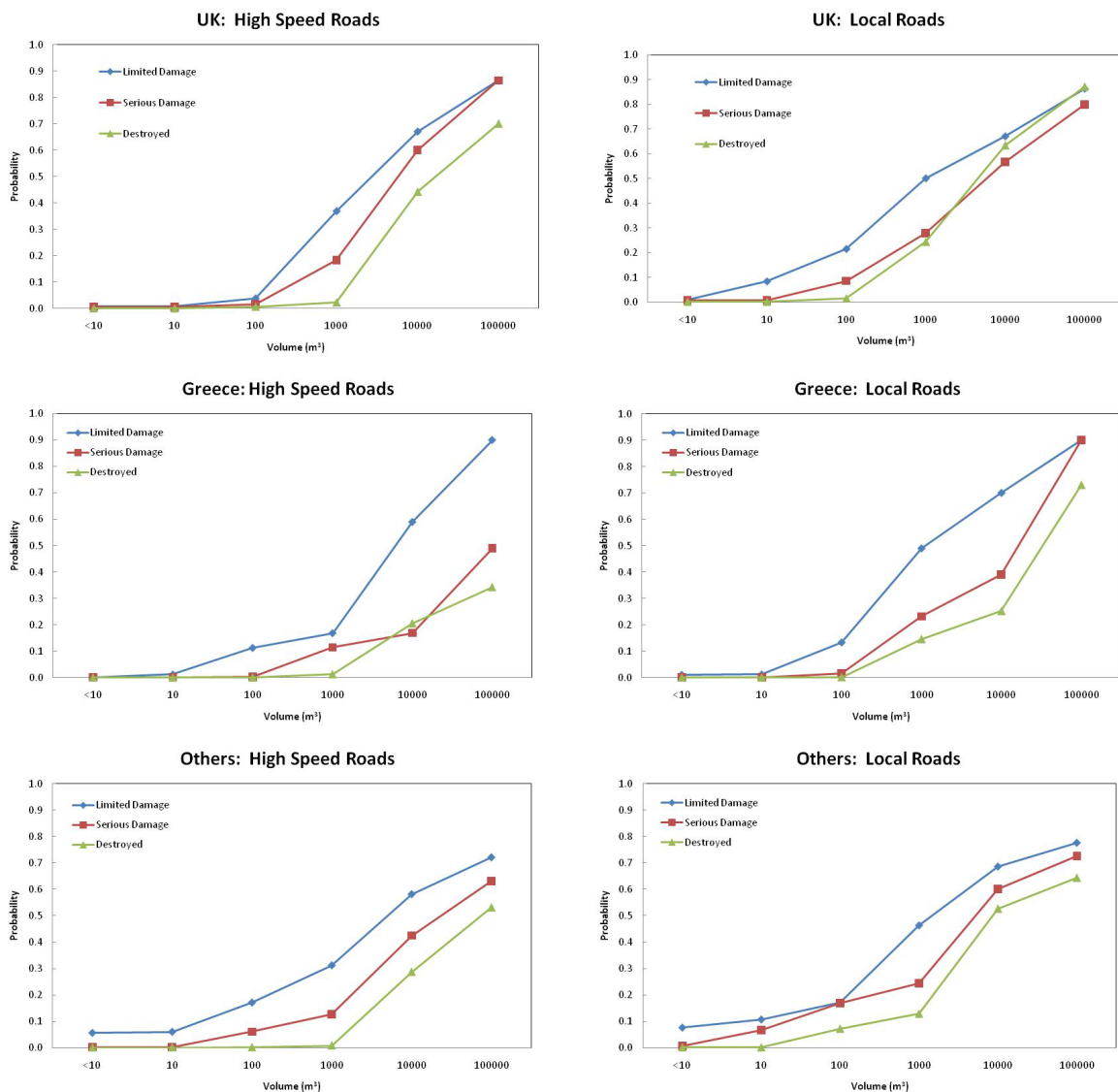


**Figure 4.5.15** Fragility curves constructed from the responses of those from the UK, Greece and the Rest of the World (Others).

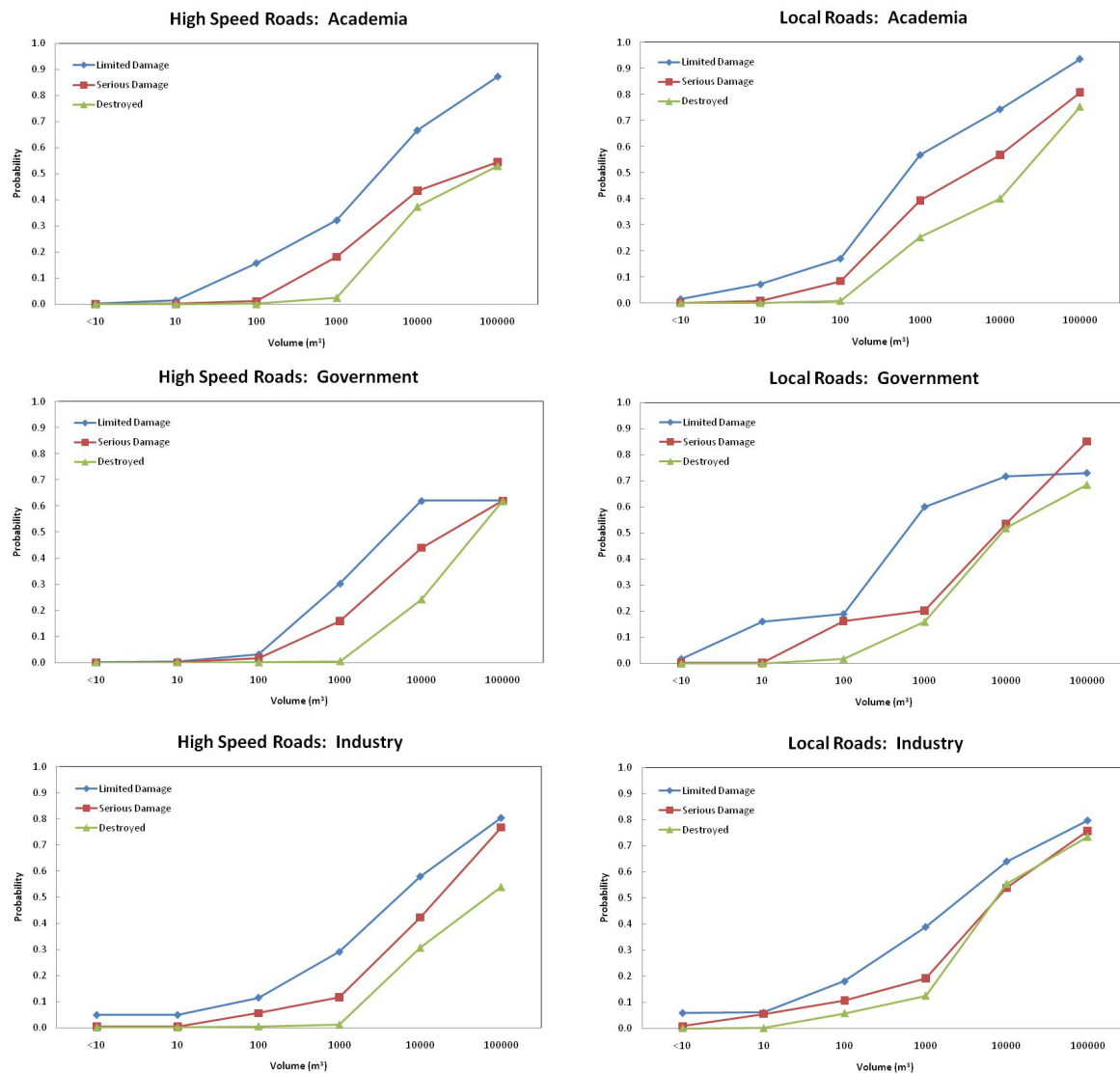


**Figure 4.5.16** Fragility curves constructed from the responses of those from academia, government and industry.

#### 4.5.12 Confidence Ratings

Each respondent was asked to rate their confidence on a scale of 0 to 10 for each of the landslide volumes for which they were asked to provide estimates of the probability of such events causing the given damage states to be exceeded. The data is plotted in Figures 4.5.17.

As might be expected the confidence of respondents for low volume events is markedly higher than for high volume events, reflecting the higher frequency of low volume events.

Indeed, examination of the individual charts for each landslide volume considered (Figure 4.5.17) indicates that:

- For low volume events, the distribution of the responses is skewed to the right (high confidence).
- For medium volume events ( $1,000\text{m}^3$  to  $10,000\text{m}^3$ ), the distribution becomes broadly normal.

- For high volume events ( $100,000\text{m}^3$ ), the distribution shows signs of beginning to skew to the left (lower confidence).

This data is presented in three-dimensional form in Figure 4.5.18. If the tentative pattern described in the bulleted list above were to be perfectly formed, then the surface of the plot would exhibit a ridge from high landslide volume/low confidence to low landslide volume/high confidence (i.e. a line trending roughly south-south-east to north-north-east on the graph).

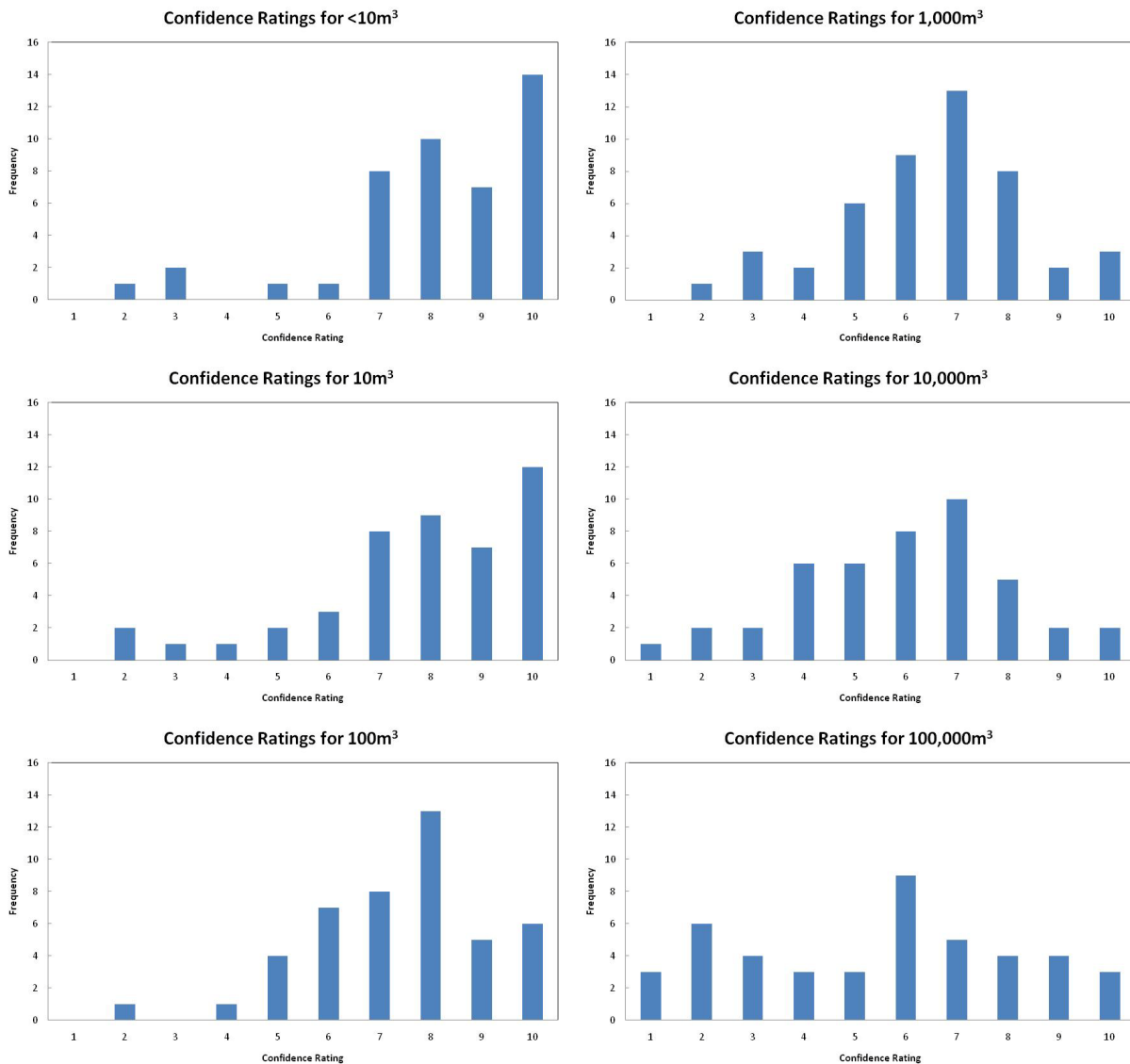


**Figure 4.5.17** Self-assessed confidence ratings relative to given event volumes.

This is not so clearly replicated in Figure 4.5.18 and may be indicative of two features of the data.

First, that confidence in the very small landslide volumes (e.g.  $<10\text{m}^3$ ) is not so consistently high as it is for slightly larger volumes (e.g.  $100\text{m}^3$ ), perhaps because events of such small

volume have little influence upon the infrastructure and professionals are rarely called upon to visits such sites as only a relatively straightforward clean-up operation is usually required. Second, and noting that the skew to the left in the distribution of the responses for the largest landslide volume is not fully formed, it seems that it would be useful as was suggested by a small number of respondents to the questionnaire to include landslide volumes up to 1,000,000m<sup>3</sup>. It is assumed that returns for such a volume would skew further to the left and complete the ridge pattern described above. This lends some validity to the extrapolation of the data to this higher value of landslide volume (see Figures 4.5.7 and 4.5.14).

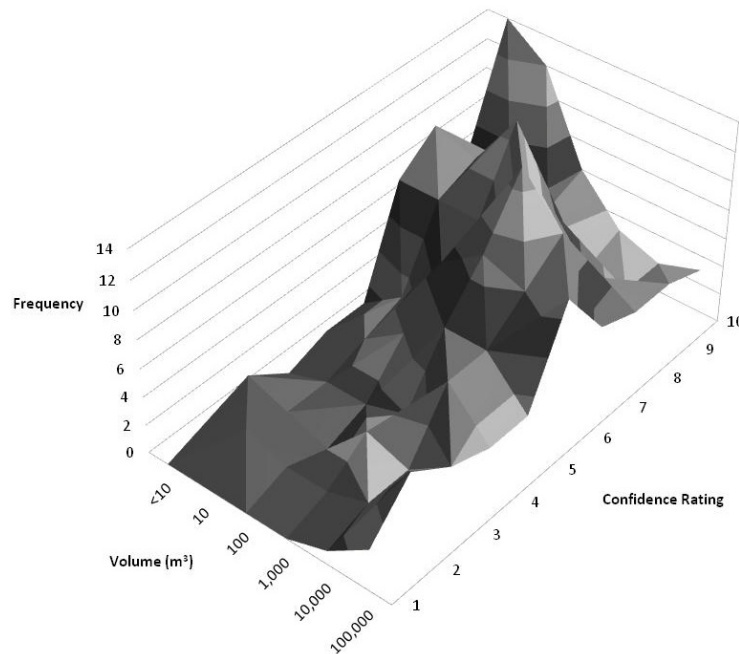


*Figure 4.5.18 Self-assessed confidence ratings relative to given event volumes.*

### 4.5.13 Frequency of Events

Each respondent was asked to state the expected frequency of occurrence of each size of event in their region on a scale of annually to centuries. The data, plotted in Figure 4.5.19, broadly conforms to what might reasonably be expected. The annual frequency data implies that higher volume events are much less frequent than smaller volume events within this period. As the period considered increases to 10 years, through decades to centuries the larger volume events progressively play a greater role and become anticipated within the given period. For frequencies of a century or more the data broadly indicate that one or more events of all volumes would be expected to occur, on a probabilistic basis, within that timeframe. This does not mean that the numbers of each event size would be the same, merely that at least one of each of these events would be anticipated.

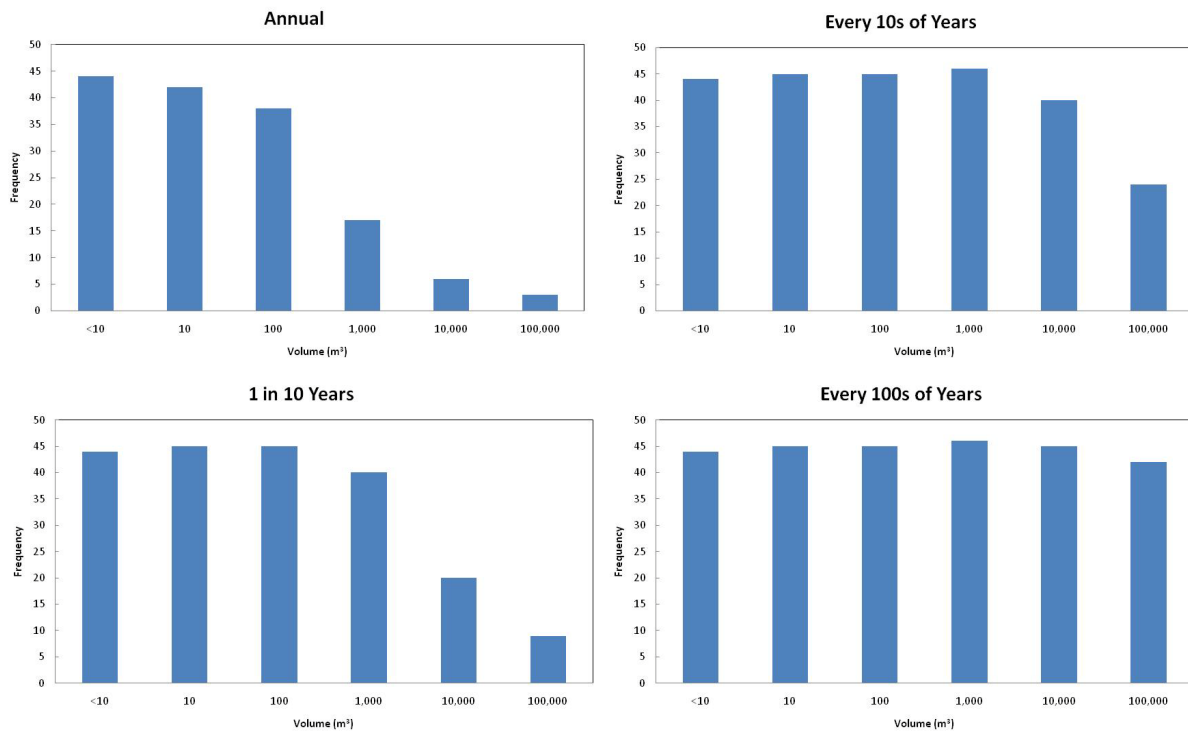


**Figure 4.5.19** Frequency of events in the respondents' regions.

#### 4.5.14 Qualitative Responses

Each respondent was invited to make comments in response to three text questions that were posed, as follows:

1. *For the purposes of the development of fragility curves do you consider the proposed landslide volumes appropriate? Do the proposed volumes cover most scenarios?*
2. *Roads have been divided into two categories: high speed and local. Initially this was driven by road speed limits that are in operation; however, they correspond well to road construction. That is, high speed roads are typically designed, constructed, and maintained to a higher quality than local roads, due to a need for improved safety and performance. In your opinion, is this two-tier classification sufficient or does it represent an over-generalisation?*
3. *Do the damage state definitions given adequately describe the damage state levels? i.e. Does blockage of the hardstrip and one running lane on a high speed road constitute "moderate damage"?*

The questions were posed to allow respondents to make comments upon the form of the questionnaire and thus to provide a degree of validation, or otherwise, of the approach taken and also to inform the approach taken to the analysis of the data.

With respect to **Question 1**, the respondents were generally supportive of the approach taken. There were two points raised that bear further discussion. The first of these is that the landslide volumes would have been better presented as ranges. The authors' view in drafting the questionnaire was that this was clear and sufficiently implicit that <math>10\text{m}^3</math>, <math>100\text{m}^3</math>, <math>1,000\text{m}^3</math>, etc. meant <math>10-99\text{m}^3</math>, <math>100-999\text{m}^3</math>, etc. With the benefit of hindsight this could have

been more clearly articulated, albeit that it does not appear to have had an adverse impact upon the resulting data.

A small number of correspondents suggested that a higher volume, corresponding to 1,000,000m<sup>3</sup>, be included while one respondent suggested yet another volume category corresponding to >1,000,000m<sup>3</sup>. The limitation placed on the size of event in the questionnaire seemingly relates to the authors' experience and background in Europe and it is accepted that application in some parts of Asia requires that larger volumes be considered. The authors have gone some way towards addressing this by extrapolating the fragility curves to 1,000,000m<sup>3</sup> on a manual basis.

A small number of respondents seemed not to have appreciated that the questionnaire considered only debris flows and wrote of the need to consider different probabilities for slides and rockfalls. Notwithstanding this their responses to the numerically answered questions remained consistent with both the authors' knowledge of the individuals and the broader data set as applied to debris flow.

With respect to **Question 2**, the respondents were generally supportive of the approach taken. However, some respondents did call for additional classes of road. These ranged from the addition of single track roads to the introduction of additional classes for both dual-carriageway roads and motorways: it is certainly not clear to the authors how this latter action would have added value to the work. One respondent suggested that the classification should be predicated on the law of a particular country, but it is extremely difficult to see how the laws or standards of each nation could be accommodated within a single classification system. One respondent gave a detailed description of a four-tier system before noting that for most, if not all practical purposes, it could be reduced to two.

Telling within the responses were those who are, or have recently been, employed by the organisations responsible for the routine maintenance and operation of road networks. Without fail they accepted the distinction between high speed and local roads as being rational. One of those clarified their comment by noting that no allowance for localised mitigating factors such as verge width, ditches and safety barriers had been made. Clearly these are factors that have a highly localised significance and should form part of a detailed site-specific assessment rather than a more generalised approach such as that presented here.

Although not without potential issues, the two-tier approach to road type appears to have achieved a good balance - covering the different types of road, keeping both the questionnaire sufficiently simple and sufficiently short that busy professionals were able to respond, and ensuring that the analysis was both manageable and understandable.

With respect to **Question 3**, the respondents were generally supportive of the approach taken. However, a typographical error in which the phrase 'moderate damage' was used in the text questions and 'serious damage' in the main part of the questionnaire may have caused some confusion.

Notwithstanding this most of the negative comments were in respect of wishing to see more damage categories. Included in this were some issues that are perhaps more appropriately dealt with at a site-specific level. This would of course have generated a more complex questionnaire that would be considerably more time-consuming to complete with the additional ramifications noted above.

Interestingly, one respondent noted that the damage criteria were reflective of those used by the Norwegian Road Authority to determine the need, or otherwise, for maintenance interventions.

---

Inevitably, in examining the responses to the three text questions a large number of competing statements were found. For example, some respondents felt that the blocking of a single lane of two-lane road was a relatively minor issue while other respondents felt that neither 'moderate' nor 'serious' damage did full justice to the situation.

#### 4.5.15 Comparison with Real Events

In order to assess the validity of the curves developed clearly a view must be taken on the most appropriate set of curves to consider. In light of the comments received from questionnaire respondents and reported in Section 4.5.14 the extrapolated curves forced to reach unity presented in Figure 4.5.14 are proposed. Events from both Scotland in the UK and the Republic of Korea are used.

In August 2004 two debris flow events occurred at Glen Ogle (Figure 4.5.20). These blocked the A85 strategic road, blocked culverts and other drainage features, and necessitated a full repair to the road pavement, safety barriers and parapets (Winter *et al.*, 2005; 2006). Some 20 vehicles were trapped by the events and 57 people were airlifted to safety; one vehicle was swept away in the latter stages of the event (Winter *et al.*, 2005). Figure 4.2.21 shows some of the key features of the two events. The smaller southerly and larger northerly events were estimated to have deposited around 3,200m<sup>3</sup> and 8,500m<sup>3</sup> in their respective debris lobes having been triggered by smaller translational slides of around 285 and 280m<sup>3</sup> (Milne *et al.*, 2009). The depositional figures are believed not to include material deposited on the road and it seems reasonable therefore to round these figures up to around 5,000 and 10,000m<sup>3</sup>.



**Figure 4.5.20** The northerly and larger of the two August 2004 debris flows at Glen Ogle.



**Figure 4.5.21** Aerial photographs (north to the top) showing the Glen Ogle debris flows of August 2004 showing key features (Licensed to Transport Scotland for PGA, through Next Perspectives<sup>TM</sup>): Left; 4km by 3km (12 tiles), National Grid Reference (NGR) of SW corner NN 560 250 or 2560 7250; Right; 1km by 1km (single tile), NGR of SW corner NN 570 260 or 2570 7260.

**KEY:**

1. Northerly debris flow: (a) potential source area(s), (b) debris track, (c) runout/debris fan and (d) subsequent carriageway repair;
2. Southerly debris flow: (a) potential source area(s), (b) debris track, (c) runout/debris fan and (d) subsequent carriageway repair;
3. Historic rock falls; and
4. Other debris flows assumed to have occurred in August 2004.

Figure 4.5.22 shows how these event volumes plot on the fragility curves originally derived in Figure 4.5.14. For the smaller ( $5,000\text{m}^3$ ) event the probability of the three damage states being exceeded for 'Limited Damage', 'Serious Damage' and 'Destroyed' are around 0.6, 0.4 and 0.3, while for the larger ( $10,000\text{m}^3$ ) event the probabilities are around 0.7, 0.55 and 0.4, in both cases for a High Speed Road. Certainly the damage caused by the larger event would have been described as exceeding the 'Destroyed' damage state using the scheme considered here, the probability of which is 0.4. Similarly the damage caused by the smaller event, although significantly less in terms of physical damage to the infrastructure, would also be classified as exceeding the 'Destroyed' damage state and this seems to be broadly reflective of the probability of 0.3 returned from Figure 4.5.22.

Events at the "Rest and be Thankful" (Winter *et al.*, 2008; 2010) are frequent and have certainly occurred on at least an annual basis over the preceding 20 to 25 years. The event magnitude is however, rather small, generally ranging between  $200$  and  $1,000\text{m}^3$ . Figures 4.5.23 and 4.5.24 illustrate the main hillside at the "Rest and be Thankful" and the detail of the October 2007 event at that location – on this occasion the volume of material deposited at

the A83 strategic road level was estimated by the road operating company to be around 400m. On-site observations indicate that it would be reasonable to use a figure of around 1,000m<sup>3</sup> for the total amount of material deposited.

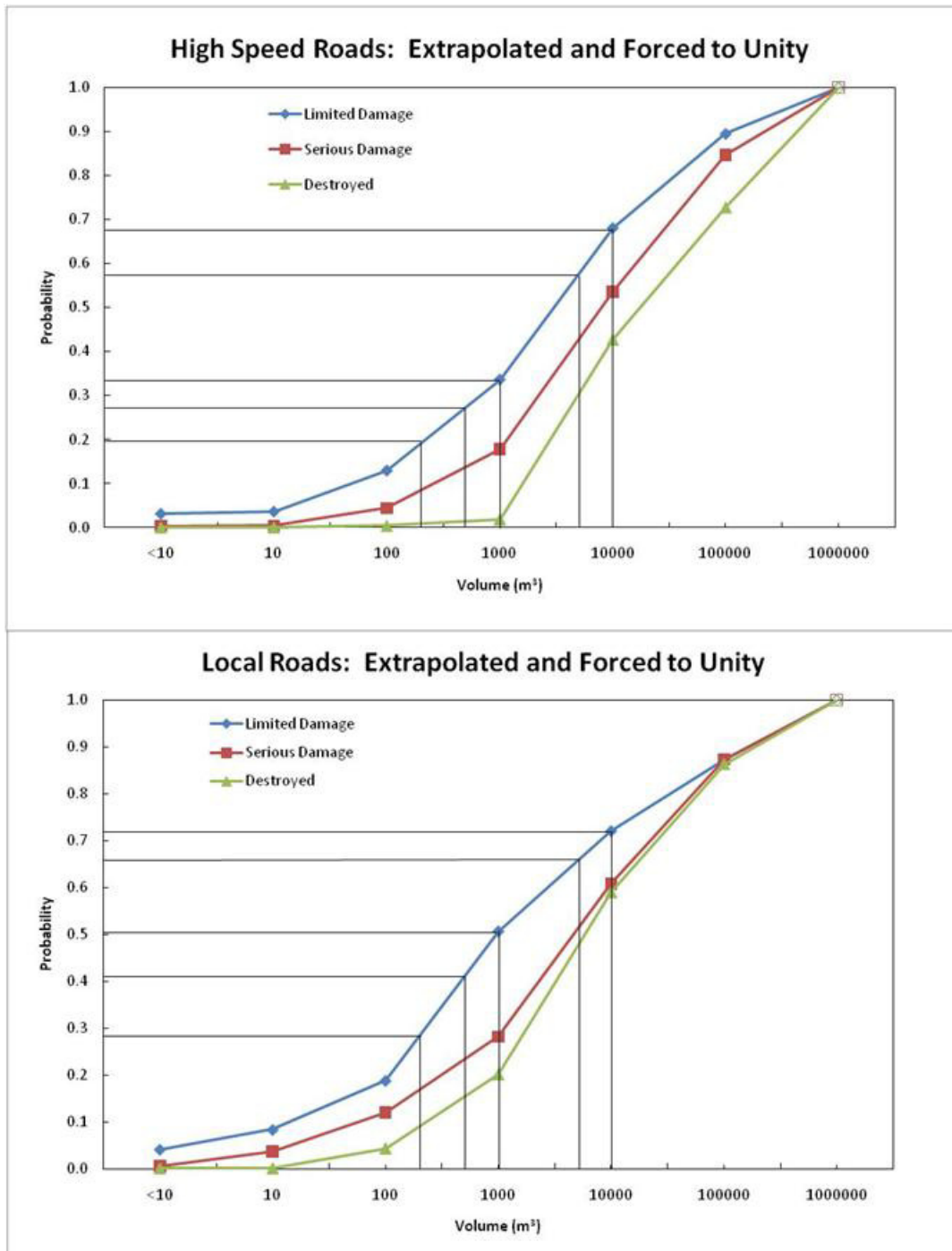


**Figure 4.5.22** The fragility curves of Figure 4.5.14 with vertical lines added at 200, 500, 1,000, 5,000 and 10,000m<sup>3</sup>. These lines are drawn horizontally across to the probability axis. In order to retain a degree of clarity only horizontal lines where the 'Limited Damage' curve is intersected are shown.



*Figure 4.5.23* General view of the main hillside at the Rest and be Thankful, including the October 2007 event.

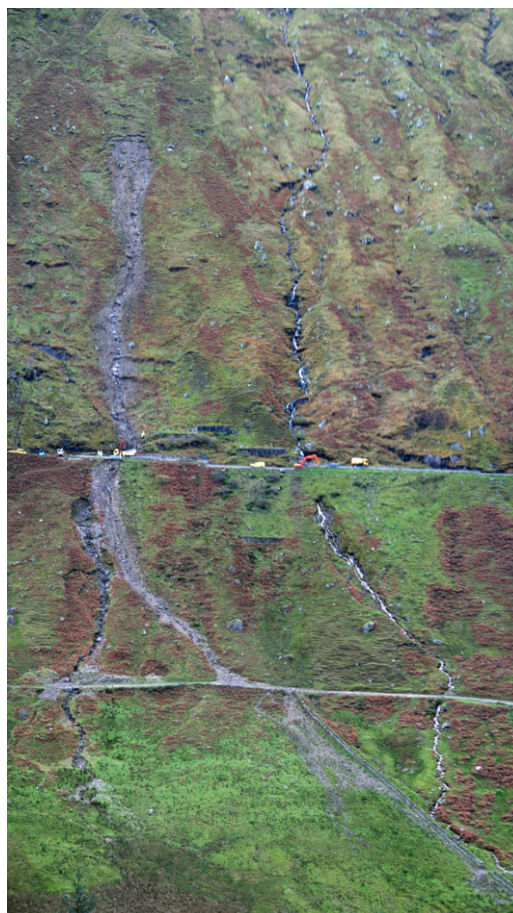


*Figure 4.5.24* Detailed view of the October 2007 event at the "Rest and be Thankful".

For smaller events the probabilities of the three damage states being exceeded for ‘Limited Damage’, ‘Serious Damage’ and ‘Destroyed’ of around 0.2, 0.05 and 0.01 (for smaller events the volume which may be as low as 200m<sup>3</sup>) and of 0.3, 0.2 and 0.02, for the larger October 2007 event (1,000m<sup>3</sup>), for High Speed Roads.

Following the October 2007 event the road was closed for some considerable period while major structural repairs were undertaken to the ground below the road, the observed effects exceeded the ‘Destroyed’ damage state. This does then beg the question as to how such a small event caused so much damage. In simple terms two events occurred. The flow above the road blocked the A83 and in isolation required clean-up and pavement repairs. However, it also blocked an open drain on the upslope side of the road which caused water to overtop the road and to erode a further wash-out-type failure below the road; it was this secondary event that did most of the damage (as described in more detail by Winter *et al.*, 2008).

In addition the profile of this road and some of the construction details, such as the aforementioned open drain, make an argument for describing this road as a Local Road (within the scheme described herein and notwithstanding the higher speed limit). Thus the probability of the ‘Destroyed’ damage state being exceeded by the initial 1,000m<sup>3</sup> flow is higher at around 0.2 (see Figure 4.5.22).

Three debris flow sites from the Republic of Korea (Lee and Winter, 2010) are also presented here, as follows:

- Seoul to Chuncheon National Road 46 (Figures 4.5.25 and 4.5.26).
- Seoul to Chuncheon National Highway tunnel portals (Figures 4.5.27 and 4.5.28).
- Seoul to Gangnung Highway at Pyeong-chang Services (Figures 4.5.29 and 4.5.30).



**Figure 4.5.25** Debris flow site from July 2009 at the Seoul to Chuncheon National Road 46 in the Republic of Korea. The barrier was erected after the event to protect the road from the effects of further flows while the concrete drainage channels were badly damaged during the event.



**Figure 4.5.26** Source area for a debris flow site from July 2009 at the Seoul to Chuncheon National Road 46 in the Republic of Korea.

Each of the three Korean sites corresponds to a High Speed Road and the volumes were up to 5,000m<sup>3</sup> for Seoul to Chuncheon National Road 46, 500 to 1,000m<sup>3</sup> for Chuncheon National Highway Tunnel Portals, and 10,000m<sup>3</sup> for Seoul to Gangnung Highway at Pyeong-chang Services.

The corresponding probabilities of the states ‘Limited Damage’, ‘Serious Damage’ and ‘Destroyed’ being exceeded are therefore:

- Seoul to Chuncheon National Road 46: 0.6, 0.4 and 0.3.
- Seoul to Chuncheon National Highway tunnel portals: 0.3, 0.2 and 0.02.
- Seoul to Gangnung Highway at Pyeong-chang Services: 0.7, 0.55 and 0.4.

For the Seoul to Chuncheon National Road 46 the damage state corresponded to exceeding the 'Destroyed' category. This is reflected in the probability of such an occurrence of 0.3 (approximately one in three chance). It should also be noted that the damage that occurred was most likely exacerbated by the highly constrained nature of both the natural topography and by the channelling effect of the concrete drainage channels shown in Figure 4.2.25.



*Figure 4.5.27 Debris flow site from July 2009 above tunnel portals on the Seoul to Chuncheon National Highway in the Republic of Korea. The view is from the source area looking out over the tunnel portals.*



*Figure 4.5.28 Source area for a debris flow site from July 2009 above tunnel portals on the Seoul to Chuncheon National Highway in the Republic of Korea.*

Only minor damage was incurred at the Seoul to Chuncheon National Highway tunnel portals and this reflects the small volumes and a probability of 0.3 of the 'Limited Damage' state being exceeded. The road was not open at the time of the event and there is every possibility of both further and larger events that have the potential to exceed higher damage states.



**Figure 4.5.29** Debris flow site above the Seoul to Gangnung Highway at Pyeong-chang Services in the Republic of Korea. The view is of the flow channel above the road.



**Figure 4.5.30** Debris flow site above the Seoul to Gangnung Highway at Pyeong-chang Services in the Republic of Korea. The view is from the flow channel above the road looking at the services located on the opposite of the road.

Less detail is available for the event at Seoul to Gangnung Highway at Pyeong-chang Services, but the damage incurred exceeded at least the 'Serious Damage' state and, most likely, the 'Destroyed' damage state. Certainly significant remedial works constructed since

the flow occurred. The probability of the two damage states being reached or exceeded by the size of flow that occurred are 0.55 for 'Serious Damage' and 0.4 for 'Destroyed'. These seem to again be broadly reflective of the events rendering a one in two to 1 in 2.5 chance of the damage state being exceeded.

#### **4.5.16 Conclusions**

A survey of experts in the field of debris flow has been conducted to ascertain their views on a wide range of pertinent issues related to the construction of preliminary fragility curves for the effects of debris flows on roads.

Included in the questionnaire was the opportunity for the respondents to make 'free text' responses to defined questions. Their responses have been used, in part, to determine the form of analysis. Consequently the proposed fragility curves have been extrapolated to include events one order of magnitude greater than the largest considered in the questionnaire. In addition, this form of determining fragility curves renders it almost impossible for the probabilities to range from zero to unity; according the proposed fragility curves have been stretch to ensure such a spread.

The derived fragility curves have been compared to known events in Scotland (UK) and the Republic of Korea. In general the curves tend to give results that might be deemed 'sensible' with probabilities of around 0.3 to 0.55 being suggested for known damage states. Exceptions to this occur when detailed site characteristics introduce complexities that are not, and could not be, accounted for in the analysis.

The method of data acquisition and the perceived interpretations of the questionnaire for this first approach raise some interesting issues that are explored in the body of the report. Continued efforts are needed, potentially including the use of modelling and empirical data to further validate, and potentially improve, the curves reported herein.

## **5 PHYSICAL VULNERABILITY TO SLOW MOVING LANDSLIDES**

### **5.1 INTRODUCTION**

It is generally admissible that damage to engineering structures resulting from the occurrence of rapid landslides such as debris flows and rock falls is generally the highest and most severe as it may lead to their complete destruction of any structure within the affected area. However, slow-moving slides (classes 1 to 4 according to Cruden and Varnes (1996) classification) that may include earth slides (both rotational and translational landslides), earth flows and debris slides may also have adverse effects on affected facilities that have sometimes been underestimated. Mansour et al. (2010) investigated the level of damage to different facilities caused from more than 50 cases of soil slides. They revealed that buildings and residential houses may sustain higher slide velocities and total displacements than the other facilities before experiencing serious damage while bridges were found to be the most vulnerable elements.

The damage caused by a slow moving landslide on a building is mainly attributed to the cumulative permanent (absolute or differential) displacement and it is concentrated within the unstable area. For instance, a slow moving slide may produce tension cracks due to differential displacement to a building (Fell et al., 2008) that may result to the partial or complete disruption of its serviceability and stability. These landslides can be occasionally reactivated or active (Leroueil et al., 1996) and in certain circumstances can be transformed into rapid landslides resulting in significant damage on structures both in and outside the landslide area.

Generally, the vulnerability of structures to slow moving slides may depend on several factors. Among them, some of the most pronounced are (a) the hazard level (b) the rate of movement (relative slow to extremely slow moving slides) (c) the triggering mechanism (intense rainfall, earthquake, erosion, construction activities etc), (d) the specific strength and stiffness characteristics of the exposed elements and, (e) their position in relation to the potential sliding surface, and (f) the type of materials controlling the movement.

### **5.2 METHODOLOGY FOR BUILDINGS AT SMALL SCALE (1:100,000) (UNISA)**

#### **5.2.1 Introduction**

##### Zoning purposes

The *vulnerability maps* at regional scale – showing the Municipalities most susceptible to landslide-induced damage – can be useful for the Authorities in charge of the land use planning and/or the disaster management planning. Moreover, they can represent a profitable tool for the engineers in evaluating possible constraints due to landslides in the development of large engineering projects.

### Definition of physical vulnerability at small scale

In the proposed procedure at small scale the physical vulnerability was defined as “*the ratio between the whole damageable vulnerable areas and the whole vulnerable areas of a given municipality*”.

### **5.2.2 Analysis and zoning at small scale**

A general framework of the proposed procedure is shown in Figure 5.2.1.

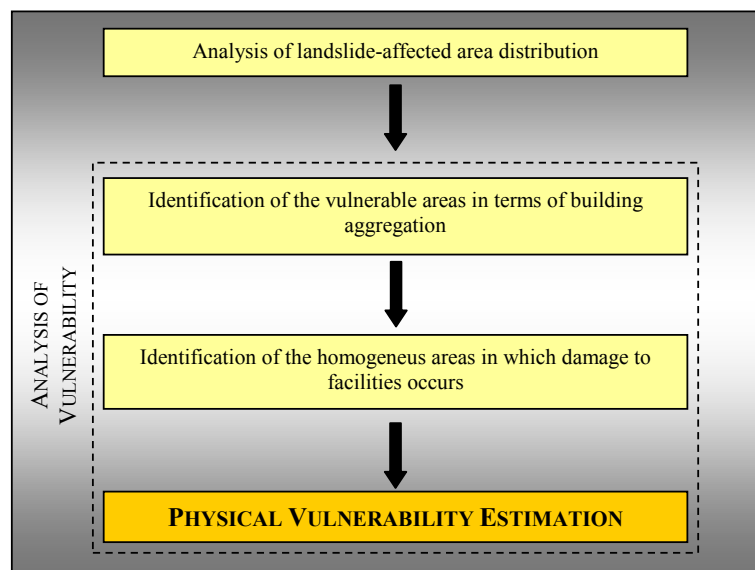


**Figure 5.2.1** General framework for the estimation of the physical vulnerability to slow-moving landslides at regional scale (modified from Pisciotta 2008).

According to the “consequence model” described by Wong et al. (1997), this framework was established considering that the expected damage to building aggregates can be related to several factors, often concomitant; among these, the spatial distribution of the phenomena and the density of built-up areas within a given territory.

On the basis of the general framework shown in Figure 5.2.1, the role played by some predisposing factors in determining the spatial distribution of the existing slow-moving landslide within the territory under study must be firstly investigated. In particular, these kind of studies are aimed to identify, via index-based methods (Soeters and van Westen, 1996; Coe et al., 2004) for instance, the geo-lithological complexes most prone to slow-moving landslides, i.e. the areas in which more damages to facilities might be expected at a parity of built-up areas density. Starting from the obtained results, further studies could be carried out for the identification, within a given geo-lithological complex, of areas in which a different homogeneous “landsliding character” (in terms of both the existence or not of groups of phenomena and the shape/size of landslide-affected area) can be recognised (Pisciotta, 2008). This latter analysis is helpful for the definition of different vulnerability scenarios for Municipalities located within homogenous contexts in terms of landsliding character, so

overcoming the difficulties associated with the definition of landslide intensity at regional scale.

The physical vulnerability at small scale, according to its definition, can be estimated with reference to the territories of some Municipalities (assumed as reference territorial units) chosen within homogeneous areas. The elements at risk, on the other hand, must be considered as aggregates. The intersection of the building aggregates with the landslide-affected areas – mapped in the landslide inventory map at 1:25,000 scale – allows the detection of the vulnerable built-up areas falling within the municipal territories.

Once detected the vulnerable built-up areas, physical vulnerability analyses needs the availability of a comprehensive database of landslide-induced damage; in particular, only damage whose severity affected the stability of the building superstructure (on the whole or a part of it) can be considered for the analysis purposes. Then, considering that elements at risk are identified in terms of building aggregates, the concept of “*Equivalent Damage*” (*ED*) must be introduced.

In particular, for a given vulnerable area, ED is expressed by the formula:

$$ED = (N_0 \text{ of buildings with damage}) \times (\text{Minimum building aggregation area}) \text{ [m}^2\text{]}$$

where *N<sub>0</sub> of buildings with damage* represents the number of damaged buildings within a vulnerable area while the *Minimum building aggregation area* is considered equal to the area occupied by a building aggregation of three houses. As a consequence, the equivalent damage of a vulnerable area can be evaluated referring to the smallest damaged exposed surface. It should be observed that this assumption could result in an overestimation of the effective damage occurred; however, this assumption allows the distinction of a large building aggregation from a small one with the same number of damaged buildings.

Finally, the physical vulnerability can be estimated by a further Index, called “Areal Index of Damage” *I<sub>D</sub>*, given by:

$$I_D = \frac{A_{AVD}}{A_{AV}} \cdot 100 \text{ [%]} \quad [5.1]$$

In the above expression *A<sub>AVD</sub>* is the sum of the Equivalent Damages referring to the vulnerable areas with detected damages of a given municipal territory; *A<sub>AV</sub>* is the whole urbanized area interacting with the landslides (i.e. the sum of the vulnerable areas) of a given municipal territory.

Finally, according to Galli and Guzzetti (2007), vulnerability thresholds (*V<sub>min</sub>* and *V<sub>max</sub>*) can be established, for each of the considered homogeneous areas, considering the curves respectively passing from the lowest and the highest value of the index *I<sub>D</sub>* referred to the considered municipal territories. An example is furnished by the application shown in the SafeLand deliverable D2.7 (Pitilakis et al. 2011).

Once the vulnerability curves are calibrated and validated for each homogeneous geo-environmental context, the corresponding threshold values can be used to predict the physical vulnerability of the built-up areas of municipal territories not included in calibration and validation analyses. Finally, the results can be summarised in “Landslide vulnerability zoning maps” showing the spatial distribution of the minimum/maximum values of the expected degree of damage to the vulnerable areas of the municipal territories.

## 5.3 METHODOLOGY FOR BUILDINGS AT MEDIUM SCALE (1:25,000) (UNISA)

### 5.3.1 Introduction

#### Zoning purposes

The *vulnerability maps* at medium scale can be useful in land use planning to select more suitable zones to be urbanised and to choose the alternative layouts of traffic facilities; moreover, they can be used to update the existing official maps made by River Basin Authorities within the “Hydrogeological Setting Plans” (Italian Law 365/2000).

#### Definition of physical vulnerability at medium scale

In the adopted procedure at medium scale the physical vulnerability was defined as “*the expected degree of damage to an aggregate, constituted by a given number of buildings, falling within an area affected by slow-moving landslides of a given intensity*”.

### 5.3.2 Analysis and zoning at medium scale

The proposed procedure for the analysis of the physical vulnerability at medium scale is based on a consequence model whose final product consists of vulnerability curves, i.e. the graphical relationship between the landslide intensity and the expected level of damage to a given buildings’ aggregate. The followed methodological approach consists of sequential steps (Fig. 5.3.1).

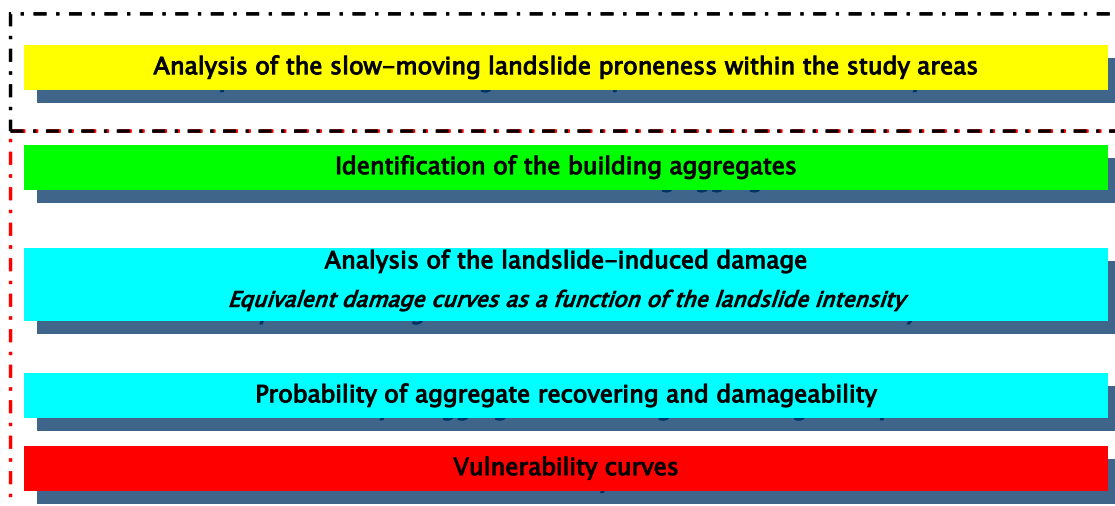


**Figure 5.3.1** General framework for the physical vulnerability analysis at medium scale (modified from Viscardi 2010).

First of all, the analysis of spatial distribution of slow-moving phenomena within study areas enables the main landslide typology, the prevailing state of activity and some other characteristics of the phenomena censored (e.g. probability density distribution of landslide-

affected areas) to be identified. The obtained results are useful to justify the actual spatial distribution of both elements at risk and induced damages to the same elements.

At the considered (medium) scale of analysis, a methodology based on geometrical consideration, is proposed to identify building aggregates. In particular, planar figures whose geometry is convex-outwards and therefore does not present any cusps on the perimeter, are sketched (as shown in yellow in Figure 5.3.2). Moreover:

- around each structure, taking into account the graphical error related to the working scale (1:25,000), a 25 m buffer can be considered, in order to also contemplate additional construction in the property (Maquaire et al. 2004);
- the distance between each building can be assumed to be not bigger than 100 m in order to avoid, amongst other things, the possibility to have well-extended aggregations in which non-urbanized areas prevail to the urbanized ones.

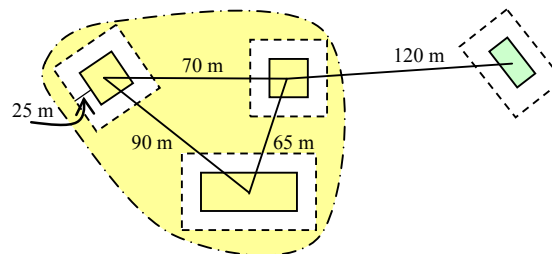


**Figure 5.3.2** Scheme for the determination of building aggregations (Ferlisi and Pisciotta, 2007)

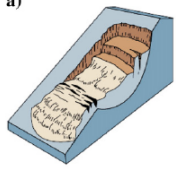
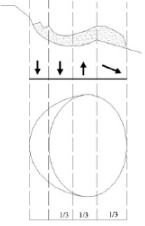
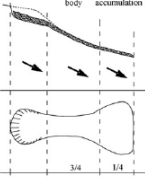
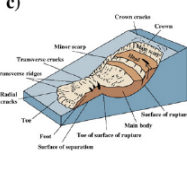
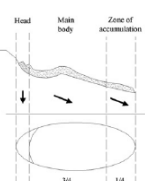
On the basis of the available data, this approach can be easily modified using additional information, such as occupancy type or typological characteristics of the buildings.

Once fixed the criteria for the identification of the elements at risk, the study must be focused on the analysis of the distribution of damage to the vulnerable elements (buildings' aggregates) in relation to their position within landslide-affected areas (i.e. at the head, in the main body, in the accumulation zone). The analysis can be carried out by using the available dataset of landslide-induced damages to properties and introducing simplified schemes aimed to define the geometrical partition of the landslide body (Fig. 5.3.3).

On the other hand, the equivalent damage ED of a given vulnerable area can be computed as the weighted average of the individual damage suffered by buildings belonging to areas affected by landslides.

On the basis of its definition, the physical vulnerability can be obtained by multiplying the Equivalent Damage by the spatial probability that a given aggregate interacts with a landslide as well as by the probability that it suffers a given level of damage. Then, the results can be used to obtain vulnerability curves, following a procedure similar to that adopted at small scale. After a validation process, minimum and maximum values of the vulnerability, for a fixed landslide-affected area, can be finally used for prediction purposes.

The final products of the analyses carried out are given by the physical minimum/maximum vulnerability zoning maps.

Rotational slide	Simplified scheme	Notes
		<p><b>Head:</b> as mapped by NBA LGV at 1:25,000 scale; mainly vertical downward ground displacements are supposed.</p> <p><b>Main body:</b> it covers 2/3 of the landslide (excluding the <i>head</i>). The first part (1/3) is characterised by vertical downward ground displacements; in the second part (1/3) vertical upward displacements are supposed.</p> <p><b>Zone of accumulation:</b> it represents the remaining 1/3 of the landslide body (excluding the <i>head</i>). The prevailing component of the ground displacements are supposed translational with the same slope angle as the topographic surface.</p>
		<p><b>Head:</b> as mapped by NBA LGV at 1:25,000 scale; ground displacements are supposed mainly translational with the same slope angle as the topographic surface.</p> <p><b>Main body:</b> it covers 3/4 of the landslide (excluding the <i>head</i>). Ground displacements are supposed mainly translational with the same slope angle as the topographic surface.</p> <p><b>Zone of accumulation:</b> it represents the remaining 1/4 of the landslide body (excluding the <i>head</i>). Ground displacements are supposed mainly translational with the same slope angle as the topographic surface.</p>
		<p><b>Head:</b> as mapped by NBA LGV at 1:25,000 scale; mainly vertical downward ground movements are supposed.</p> <p><b>Main body:</b> it covers 3/4 of the landslide (excluding the <i>head</i>). Ground movements are supposed mainly translational with the same slope angle as the topographic surface.</p> <p><b>Zone of accumulation:</b> it represents the remaining 1/4 of the landslide body (excluding the <i>head</i>). Ground movements are supposed mainly translational with the same slope angle as the topographic surface.</p>

**Figure 5.3.3** Simplified geomorphological schemes for different landslide typologies within the study area: a) rotational slide; b) earthflow; c) rotational slide–earthflow (Cascini et al. 2010).

## 5.4 METHODOLOGY FOR BUILDINGS AT DETAILED SCALE (1:2,000) (UNISA)

### 5.4.1 Introduction

#### Zoning purposes

The *vulnerability maps* at detailed scale can be useful to Engineers engaged in design activities aimed to mitigate the landslide risk via (active and/or passive) control works.

#### Definition of physical vulnerability at detailed scale

In the adopted procedure at detailed scale the physical vulnerability was defined as “*the expected degree of damage to a single building owing to the activation/reactivation of a slow-moving landslide of a given intensity*”.

### 5.4.2 Analysis and zoning at detailed scale

The main goal of the analyses carried out at detailed scale consists on the generation of vulnerability curves by combining the results of numerical analyses with those deriving from the use of damageability criteria adopted in the geotechnical practice. In this regard, it can be

observed that the reliability of the obtained results depends on: *i*) the quality of the input data to be used for the quantitative estimation of the parameters comparing in the adopted constitutive models or employed for the definition of the initial and boundary conditions of the problem at hand; *ii*) information achieved about the buildings at risk (in terms of their state of maintenance, structural typology of both superstructure and footing system, occupancy type, number of floors, etc.); *iii*) the completeness of the catalogue of damage data recorded to buildings after historical activation/reactivation of a given landslide displaced mass interacting with them.

A synthesis of the input data to be considered in order to characterise the landslide phenomenon and the elements at risk in activities aimed to the analysis and zoning of physical vulnerability at detailed scale is shown in Figure 5.4.1.

The methodological approach to be followed in the conceived procedure includes two main steps. The first one deals with the development of numerical analyses devoted to: *i*) the simulation of the groundwater regime during rainfall event of given intensity and duration; *ii*) the detection of the mean values of the shear strength parameters mobilized along the shear zones; *iii*) FEM stress-strain analyses. The second step consists on the interpretation of the output data of the stress-strain analyses via damageability criteria (Skempton and McDonald, 1956; Burland, 1995).

It is worth noting that the obtained results, calibrated on a well-documented case study (as shown in the application presented in the SafeLand deliverable D2.7, Pitilakis et al. 2011), can be profitably used to validate the fragility curves obtained via parametric numerical analyses.

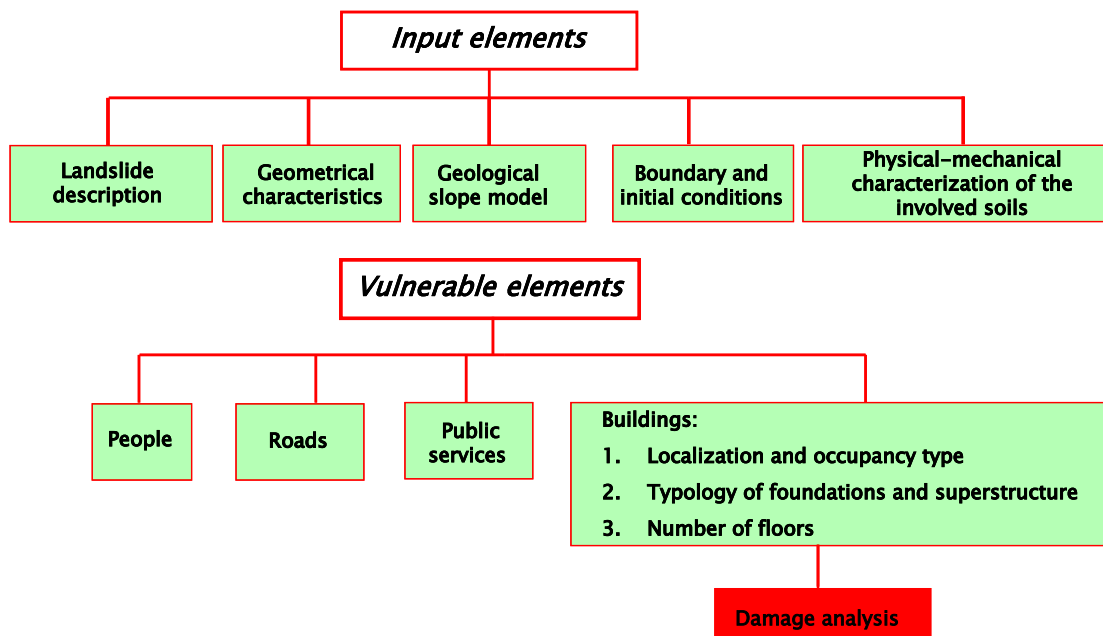


*Figure 5.4.1* Input elements to be considered for the characterization of a landslide at detailed scale and data to be recorded about vulnerable elements.

## **5.5 METHODOLOGY FOR BUILDINGS AT SITE SPECIFIC SCALE (AUTH)**

### **5.5.1 Earthquake triggered landslides**

Seismically triggered landslides represent one of the most important collateral hazards associated with earthquakes. They commonly account for a significant proportion of total earthquake damage related to human losses and damage to the built environment. Some of the most pronounced seismically induced landslides have occurred in Taiwan California, Japan, Italy, China and elsewhere, resulting to numerous casualties and tremendous (direct and indirect) damage to infrastructure.

Various methods of different complexity have been proposed to assess earthquake induced landslide hazards including the estimation of the probability of occurrence of a landslide, the factor of safety of a slope and the slope permanent displacement along a slip surface using Newmark type displacement methods or advanced numerical approaches. On the contrary, little work has been done on the quantification of the physical vulnerability due to earthquake triggered landslides. HAZUS (NIBS, 2004) multi-hazard loss estimation methodology may be considered an exception. Separate fragility curves, distinguishing between ground failure due to lateral spreading and ground failure due to ground settlement, and between shallow and deep foundations, were generated considering one combined Extensive/Complete damage state. However, the aforementioned methodology, exclusively based on expert judgment, involves a high degree of subjectivity and simplification as it does not account for the various landslide types and mechanisms, the building typology, the stiffness of the foundation and the different damage states.

### **5.5.2 Methodology**

The proposed methodology (Fotopoulou et al., 2011; Fotopoulou and Pitilakis, 2011), recognizing the need to improve the available background, may be applied for the vulnerability assessment of RC buildings subjected to earthquake triggered relative slow moving slides. It is principally based on a comprehensive set of numerical computations and statistical analysis. Figure 5.5.1 illustrates a schematic representation of the proposed framework. Building classification (foundation type, superstructure) constitute the capacity of the building. The earthquake demand, the landslide type and the relative location of the building to the potential unstable slope, constitute the deformation demand of the building. These two components (building capacity, deformation demand) can be considered as inputs to the simulation engine which is the third major component, i.e. the methodology for structural assessment. Structural response data obtained by analyzing the building capacity under the deformation demand is processed by the methodology for fragility curve generation to yield the results. Limit states, which are determined with respect to the building classification, properly selected empirical criteria and expert judgment, are required at this step. The final step of the methodology will result to the construction of the fragility relationships. Similar flowcharts may be defined for other triggering mechanisms (intense rainfall, erosion etc.). It is also possible to construct synthetic flowcharts combining different triggering mechanisms.

The vulnerability is defined through specific probabilistic fragility functions for specified limit states. The fragility curves are numerically estimated in terms of peak ground acceleration (PGA) at the “seismic bedrock”, versus the probability of exceedance of each

limit state. Alternatively, the permanent ground displacement at the slope area (that is a product of PGA) may be considered as an intensity parameter as it is generally better correlated to structural damage and allows for comparisons to non-earthquake related landslide damage to buildings. In terms of numerical simulation, a two-step uncoupled analysis is performed. In the first step, the differential permanent displacements at the building's foundation level are estimated using a FLAC2D (ITASCA Consultants, 2005) finite difference dynamic slope model. Gradually increasing acceleration time histories are applied at the base of the model to assess the building's foundation response and the associated ground displacements are computed accordingly. Then, the calculated differential displacements are statically imposed to building's model at the foundation level to assess the building's response for different ground landslide displacements induced by the earthquake. Limit states are defined in terms of a threshold value of building's material strain. The numerical (static time history) analyses of the buildings are performed through the fiber-based finite element code SEISMOSTRUCT (Seismosoft, 2007). The developed methodology is explored parametrically to different soil types (sand and clay soils corresponding to soil categories C and D of EC8), slopes geometries and building configurations allowing explicit consideration of various sources of uncertainties.

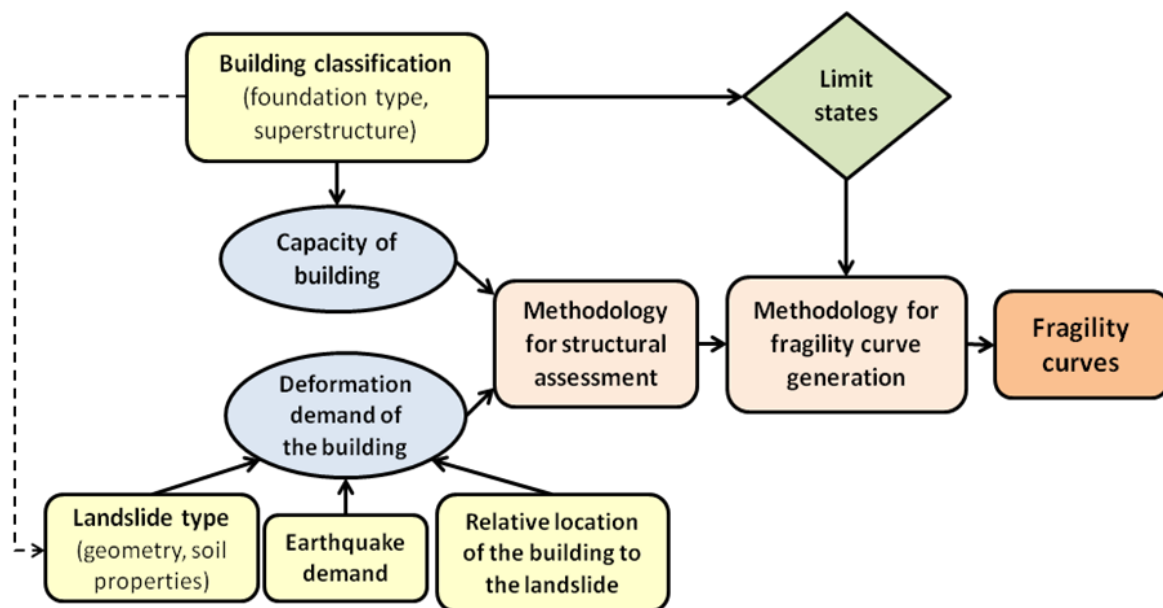


**Figure 5.5.1** Flowchart for the proposed framework of fragility analysis of RC buildings

In the following paragraphs, some key points of the proposed framework are highlighted:

- The landslide type is a crucial part of the proposed methodology as landslides of different types and sizes usually require different and complementary methods to estimate vulnerability. A relative slow moving, soil slide that will produce tension cracks due to differential displacement to a RC building, exposed to the landslide hazard, is considered in this study.
- The characteristics (amplitude, frequency content and duration) of the earthquake ground motion in relation to the soil dynamic properties and stratigraphy can significantly influence the derived deformation demand for the building. Material

damping, the impedance contrast between sediments and the underlying bedrock, and the characteristics of incident wavefield are considered to represent the governing factors for site amplification/attenuation (Kramer and Steward, 2004; Pitilakis, 2010). A fundamental period of the earthquake close to the natural period of the site can lead to resonance phenomena and, consequently, to an amplified energy content of the ground motion. Combining a low-frequency seismic input motion together with a resonance phenomenon in the low-frequency range, the slope failure potential assumes its highest values (Bourdeau et al., 2004)

- The relative location of the building to the landslide area is a very important contributing factor in estimating vulnerability. Landslides triggered by earthquakes tend to be clustered near ridge crests and hill slope toes. Peng et al. (2009) attributed this ridge- crest clustering to topographic effects, and the clustering at hill slope toes to dynamic pore-pressure changes in the water-saturated material of lower hill slopes. In this study, a building standing near the crest where the seismic ground motion due to topographic effects is generally amplified is assumed (Bouckovalas and Papadimitriou, 2005; Ktenidou 2010).
- For a landslide of given type, mechanism and intensity, the typology of the exposed structure is also a key factor in the vulnerability assessment methodology. Geometry, material properties, state of maintenance, code design level, soil conditions, foundation and structure details, number of floors etc. are among typical typological parameters which determine the capacity of the building to withstand the specified co-seismic landslide displacement. The response to permanent total and differential ground deformation depends primarily on the foundation type. A structure on a deep foundation (e.g., piles) compared to shallow foundations often has higher resistance ability and hence a lower vulnerability. For shallow foundations (Fig. 5.5.2), the distinction is between rigid and flexible/unrestrained foundation systems. When the foundation system is rigid, the building is expected rather to rotate as a rigid body and a failure mainly attributed to the loss of functionality of the structure is anticipated. In this case, the damage states are defined empirically, as there is limited structural demand to the members of the building (apart from possible P- $\Delta$  effects at larger rotations). On the contrary, when the foundation system is flexible, the various modes of differential deformation produce structural damage (e.g. cracks) to the building members (Bird et al., 2006) that can be estimated using an analytical procedure analogous to that of the response due to seismic ground motion.

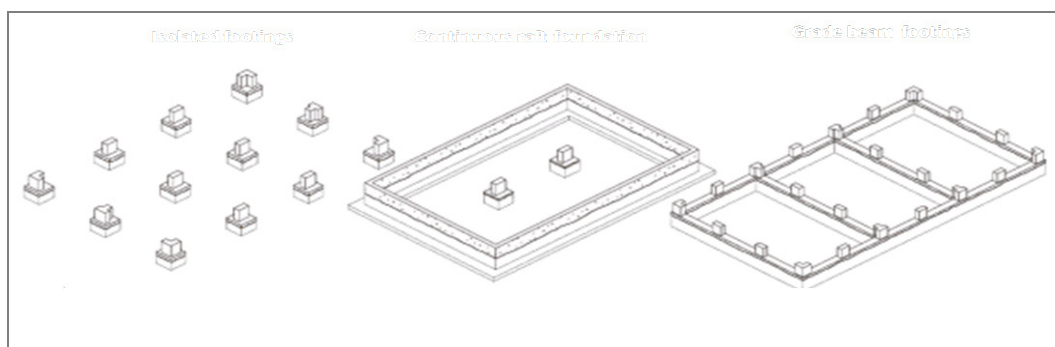


**Figure 5.5.2** Typical shallow foundation systems - Types and layout

- When building response to ground failure comprises structural damage, damage states can be classified using the same schemes used for structural damage caused by ground shaking. Limit states are defined in terms of limit value of a component's strain based on damage observation from previous earthquake events, the existing knowledge related to earthquake damage levels, and published tolerances for non-earthquake related foundation deformations (Crowley et al., 2004; Bird et al., 2006).
- In a probabilistic approach applied herein, the uncertainties related to the capacity of the building, the definition of the limit states and the deformation demand (differential permanent displacement) should be considered. The uncertainty in the displacement capacity is a function of the material properties, geometric properties, and the yield strain of steel and post-yield strain capacities of the steel and concrete. The uncertainty in the demand includes all of the variability associated with the ground motion estimation plus the additional uncertainties associated with the landslide type and size, the relative position of the building to the landslide area, the variability in soil parameters and stratigraphy and the uncertainty within the assessment of ground deformations.

### 5.5.3 Application

#### 5.5.3.1 *Deformation demand- Numerical analysis*

An application of the proposed methodology to an idealized case study is presented herein. To estimate the input differential displacements at the building's foundation level, we applied FLAC 2D finite difference model (ITASCA Consultants, 2005) (fig. 5.5.3) using an elastoplastic constitutive model with Mohr-Coulomb failure criterion, able to simulate large deformations for slope stability assessments. A small amount of Rayleigh damping (1 to 3%) is assigned to the model to account for the energy dissipation in the elastic range. The center frequency of the installed Rayleigh damping is selected to lie between the fundamental frequencies of the input acceleration time histories and the natural modes of the system. In the slope area, a fine grid discretization of 1m x 1 m is adopted, whereas towards the lateral boundaries of the model, where the accuracy requirements loosen, the mesh is coarser (2 m x 1.6 m). The model is 300m wide and 100 m high. It contains approximately 12600 elements. The slope height and inclination are 20m and 30° respectively. Free field absorbing boundaries are applied along the lateral boundaries while quiet (viscous) boundaries are applied along the bottom of the dynamic model to minimize the effect of reflected waves. In order to apply quiet boundary conditions along the same boundary as the dynamic input, the seismic motions must be input as stress loads combining with the quiet (absorbing) boundary condition. The soil type is selected to represent homogenous dry sand corresponding to soil category C of EC8; its material, physical and dynamic properties are provided in Table 5.5.1. A building is assumed to be located 3m from the slope crest. The building is modeled only by its foundation (uncoupled approach). The foundation width is 6m. Two different foundation systems are considered (Table 5.5.2): isolated footings and a uniform loaded continuous slab foundation. In the first case, the foundation is simulated with concentrated loads at the footings' links. The soil-structure interaction can be neglected in this case due to the flexibility of the foundation system. In the second case, the foundation system is modeled as a deformable elastic beam connected to the grid through appropriate frictional interface

elements that can approximate the potential Coulomb sliding and/or tensile separation of the beam. The static factor of safety of the slope is calculated through a limit equilibrium method as  $F_s=1.45$ .

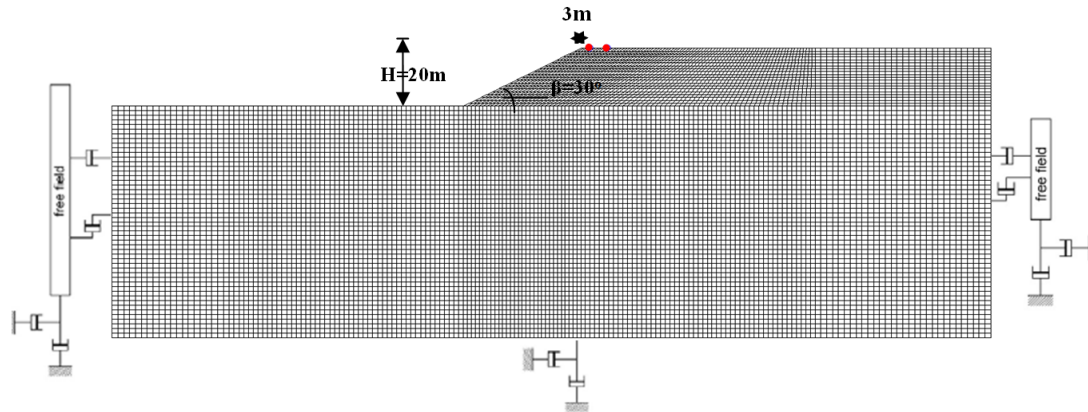


**Figure 5.5.3** *FLAC dynamic model*

**Table 5.5.1** *Soil properties*

Properties	SOIL C
Constitutive model	Mohr Coulomb
Dry density (KN/m <sup>3</sup> )	18
Vs (m/sec)	250
Poisson's ratio	0.3
Cohesion (KPa)	0
Friction angle (degrees)	36
N <sub>1(60)</sub>	21
Dr(%)	60

**Table 5.5.2** *Foundation properties*

Properties	Foundation system	
	Stiff foundation	Flexible foundation
Element	beam	
Length (m)	6	
Density (KN/m <sup>3</sup> )	24	
Young's modulus (KPa)	2.90E+7	
Moment of inertia I (m <sup>3</sup> )	0.0053	
Area (A) (m <sup>2</sup> )	0.4	
Load (KN/m)	Uniform distributed q=25KN/m <sup>2</sup>	Concentrated load P=50KN/m

Prior to the dynamic simulations, a static analysis is carried out to establish the initial effective stress field throughout the model. The dynamic input motion consists of SV waves vertically propagating from the base. Six different earthquake records are used as excitation for the dynamic analysis: (i) Valnerina (Cascia-L), Italy,  $M_s=5.8$ , 1979, (ii)

Athens (Kypseli-L), Greece, Mw=5.9, 1999, (iii) Montenegro-[TRA (EW)], former Yugoslavia, Mw=6.9, 1979 and (iv) Northridge (Pacoima Dam -L), USA, Ms=6.7, 1994, (v) Campano Lucano (Sturno-L), Italy, Mw=6.9, 1980 and (vi) Duzce (L), Turkey, Mw=7.2, 1999. They all refer to outcrop conditions. The selected records cover a wide range of seismic motions in terms of the seismotectonic environment, amplitude, frequency content and significant duration. Before applied along the base of the model, they are subjected to appropriate correction (baseline correction, filtering and tapering) to assure an accurate representation of wave transmission through the model. Note that due to the compliant base used in the model the appropriate input excitation corresponds to the upward propagating wave train that is taken as one-half the outcrop motion (Mejia and Dawson 2006). Figure 5.5.4 presents the normalized elastic response spectra of the input motions together with the proposed elastic design spectrum of EC8 for soil type A (rock).

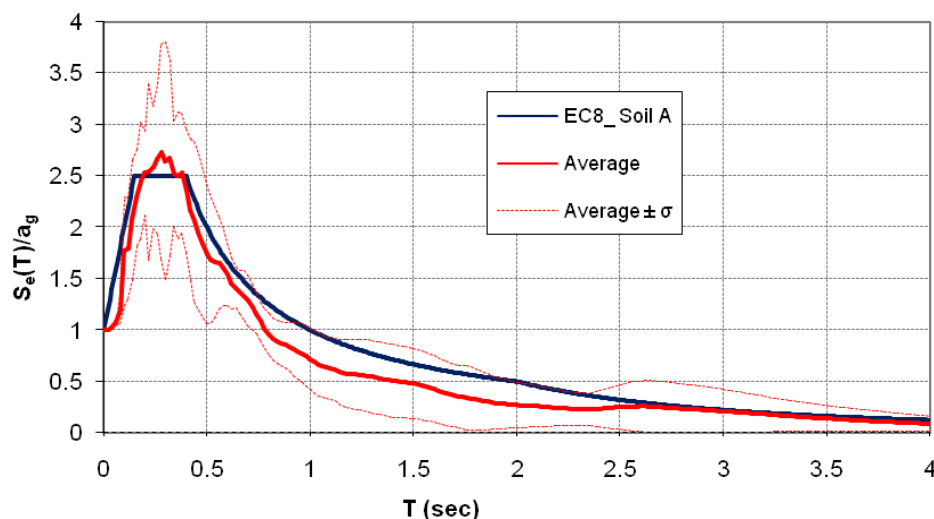


**Figure 5.5.4** Normalized average elastic response spectrum of the input motions in comparison with the corresponding elastic design spectrum for soil type A (rock) according to EC8.

The input accelerograms are scaled to five levels of peak ground acceleration (PGA=0.1, 0.3, 0.5, 0.7 and 0.9g) so as to assess the building response for different displacement magnitudes. This procedure will allow resulting in different damage states for the building and finally to be able to construct the corresponding vulnerability curves.

Figure 5.5.5 presents the maximum values of differential displacements for the building with flexible and stiff foundation system derived from the dynamic analysis by applying the different scaled accelerograms. It is observed that the specific characteristics (frequency content and duration) of the seismic ground motions can significantly influence the magnitude of the computed differential displacement at the foundation level. Figure 5.5.6 presents the maximum values of permanent ground displacement in relation to the corresponding differential displacements for the building with flexible and stiff foundation system. A strong, positive linear correlation between the two variables is detected. Thus, differential deformation can be easily determined by the residual maximum slope displacement using an appropriate linear relationship. It is worth noticing that when the soil structure interaction is considered, the differential horizontal displacements at the beam foundation are practically zero and the total differential displacement vector for the building is generally decreased.

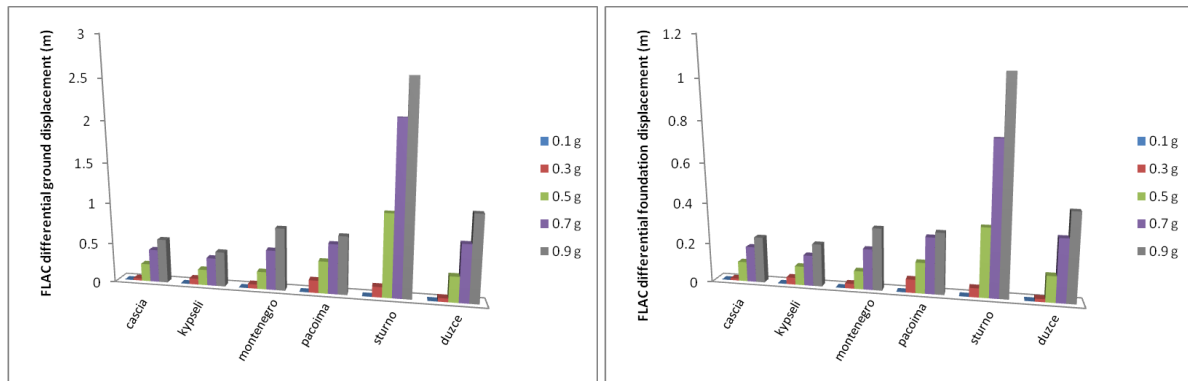


**Figure 5.5.5** Maximum values of differential displacement vector for buildings with flexible (left) and stiff (right) foundation system

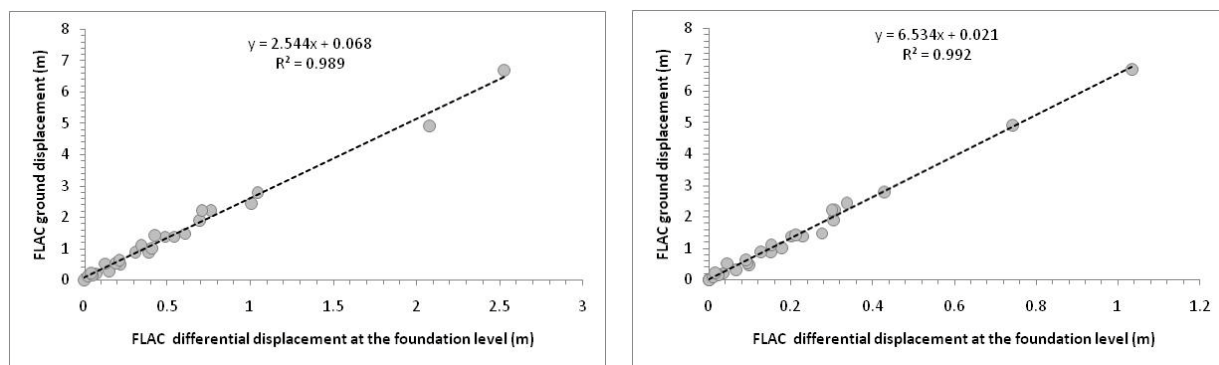


**Figure 5.5.6** Regression of differential displacement vector for buildings with flexible (left) and stiff (right) foundation system on the maximum computed permanent ground displacement

### 5.5.3.2 Comparison with simplified displacement methods

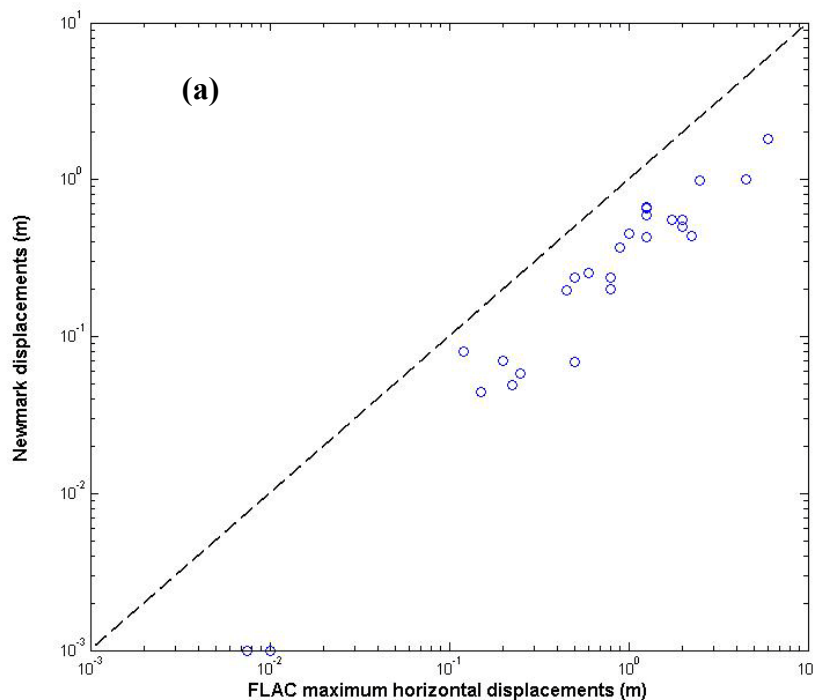
To validate the numerical results, they are compared, in terms of maximum permanent horizontal displacement, with the simplified Newmark-type displacement methods. The conventional Newmark rigid block model (Newmark, 1965; Jibson et al., 2003), as well as one of its improvements to account for the soil deformability using a coupled stick-slip deformable sliding block model (Bray and Travararou, 2007), are used to calculate permanent displacements of the slide mass.

Bray and Travararou (2007) displacement model captures the primary influence of the system's yield coefficient ( $k_y$ ), its initial fundamental period ( $T_s$ ), and the ground motion's spectral acceleration at a degraded period equal to  $1.5T_s$ . The input accelerograms applied to both methods are the scaled acceleration time histories recorded on rock multiplied by the site amplification factor  $S=1.15$  (as proposed in EC8 for subsoil class C), in an effort to conservatively approximate the equivalent acceleration time histories acting on the potentially sliding mass. The yield coefficient,  $k_y$ , is computed by applying the following relationship, as proposed in Bray (2007):

$$k_y = \tan(\varphi - \beta) + c / (\gamma \cdot H \cdot \cos 2\beta \cdot (1 + \tan \varphi \cdot \tan \beta)) \quad [5.2]$$

where:  $\varphi$ = friction angle,  $c$ = cohesion,  $H$ = height of the critical sliding surface and  $\beta$ = slope angle.

The results of the above methods are summarized in figure 5.5.7 (a) and (b) respectively in comparison with the co-seismic numerical displacements calculated herein. The direct application of Newmark rigid block approach is found to underestimate the computed displacements. This can be regarded as relevant considering that Newmark's method treats the potential landslide block as a rigid mass (no internal deformation) that slides in a perfectly plastic manner on an inclined plane, which is not realistic in our case. The results of fully coupled stick-slip deformable sliding block model introduced by Bray and Travararou are generally in good agreement with that of the dynamic analysis. In both cases, however, a large scatter on the predicted residual displacements is detected recognizing the need to adopt a fully probabilistic framework, as proposed in Bray and Travararou (Bray and Travararou, 2007).



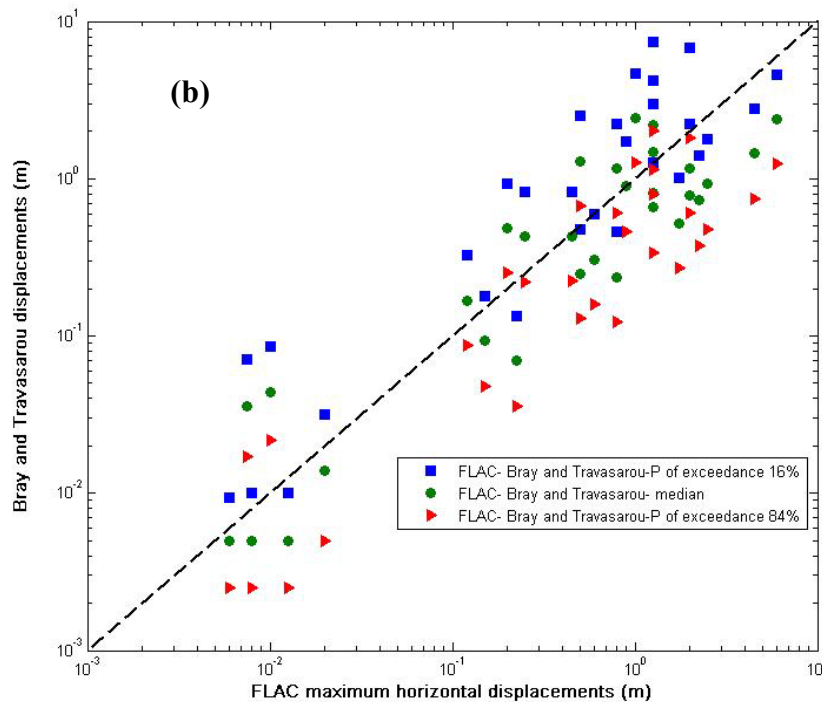


**Figure 5.5.7** Comparison between Newmark (a) and Bray and Travararou (b) displacements with maximum horizontal displacement from 2D dynamic analyses.

### 5.5.3.3 Numerical analysis of the building's response

The analyses of the buildings is conducted using the finite element code SeismoStruct (Seismostruct, Seismosoft 2007), which is capable of predicting the large displacement behavior of space frames under static or dynamic loading, taking into account both geometric nonlinearities and material inelasticity. Both local (beam-column effect) and global (large displacements/rotations effects) sources of geometric nonlinearity are automatically taken into account. The spread of material inelasticity along the member length and across the section area is represented through the employment of a fiber-based modeling approach, implicit in the formulation of SeismoStruct's inelastic beam-column frame elements. Static time-history analyses are performed for all numerical simulations. In particular, the differential permanent (ground or beam) displacement (versus time) curves, directly extracted from the FLAC dynamic analysis, are statically imposed at one of the RC frame supports.

Two reference single bay-single story RC buildings are considered that vary only in the foundation system: buildings with flexible foundation system (isolated footings) and buildings stiff but not completely rigid foundation system (continuous uniform loaded foundation of finite stiffness characteristics). The material properties assumed for the members of the reference RC buildings are described below. A uni-axial nonlinear constant confinement model (fig. 5.5.7(a)) is used for the concrete material ( $f_c=20\text{MPa}$ ,  $f_t=2.1\text{MPa}$ , strain at peak stress  $0.002\text{mm/mm}$ , confinement factor 1.2), assuming a constant confining pressure throughout the entire stress-strain range (Mander et al., 1988). For the reinforcement, a uni-axial bilinear stress-strain model with kinematic strain hardening (fig. 5.5.8(b)) is utilized ( $f_y=400\text{MPa}$ ,  $E=200\text{GPa}$ , strain hardening parameter  $\mu =0.005$ ). This simple model is

characterized by easily identifiable calibrating parameters and by its computational efficiency. The longitudinal reinforcement used is  $8\Phi 14$  ( $A=0.00123\text{m}^2$ ) for all the cross sections considered. All columns and beams have rectangular cross sections (0.40x 0.40m). The reference building's height and length are 3m and 6m respectively.

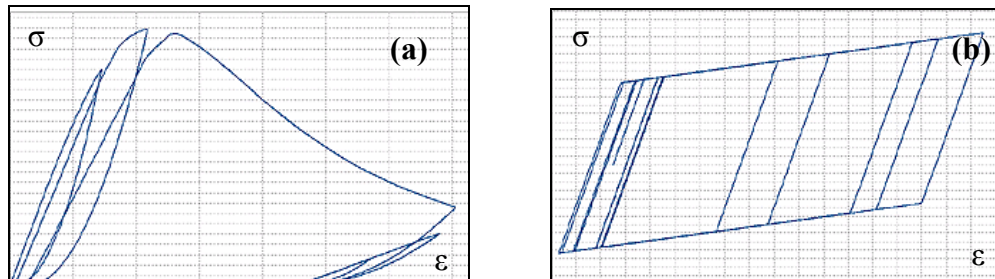


**Figure 5.5.8** Stress-strain models for concrete (a) and steel (b).

A sensitivity analysis is performed for the two reference building cases by varying, in a range of reasonable values, the yield strength of steel ( $f_y=210, 400, 500$  MPa), the compressive ( $f_c=16, 20, 30$  MPa) and tensile ( $f_t=2.0, 2.1, 3.0$  MPa) strengths of concrete, reinforcement bar size ( $\Phi 12, \Phi 14, \Phi 16$ ), the strain hardening parameter ( $\mu=0.005, 0.01$ ), the confinement factor (1.0, 1.2, 1.3) and the building height ( $H=3,4$  m) and length ( $L=5,6\text{m}$ ), together with the cross sections dimensions (30x30m, 40x40m, 50x50m), for progressively increasing levels of differential displacements extracted from the previous dynamic stress strain analysis for increasing level of input acceleration time histories. This analysis allows for indentifying the influence of different parameters on the structural response and proposing a preliminary probabilistic framework of the damage estimation.

The deformed shapes of buildings with flexible foundation system are essentially the same irrespective of the variability in the strength parameters and the level of demand, observation that is in accordance with that of Bird et al. (2005). The same trend is observed to the buildings with stiff foundation (Fig. 5.5.9). In both building typologies, a column failure mechanism is detected (see also Negulescu and Foerster, 2010). The reason is that the axial stiffness of the beams is generally much higher compared to the flexural stiffness of the columns. Moreover, in the case of buildings with flexible foundations, the applied differential displacement vector is mainly governed by the horizontal component that determines the deformation mode (fig. 5.5.9(a)). On the contrary, in buildings with stiff foundation system the applied displacements are practically vertical. Hence, it is concluded that the inclination of the applied differential permanent displacement constitutes a fundamental parameter in determining the deformed shape of the building when subjected to a permanent displacement at the foundation level.

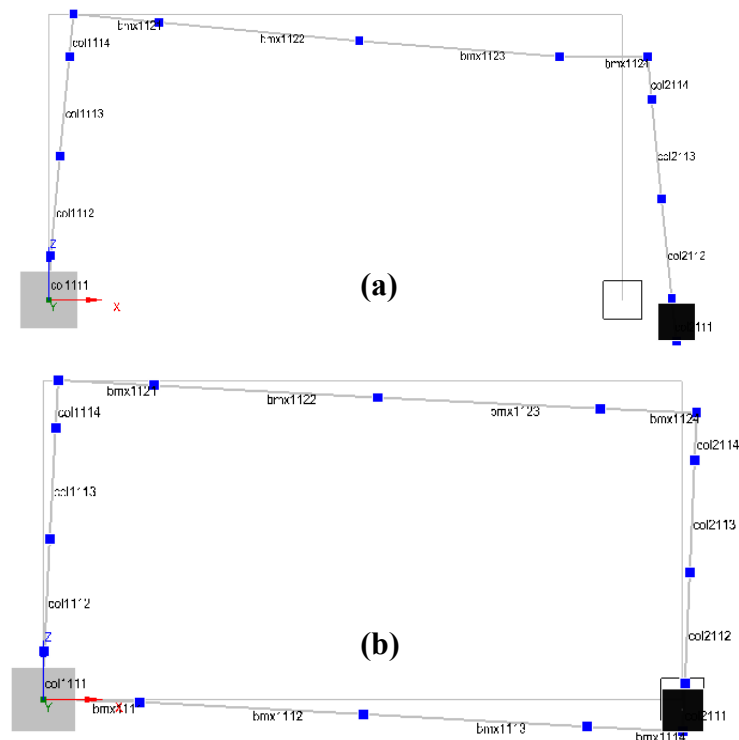


**Figure 5.5.9** Deformed shapes for buildings with flexible (a) and stiff (b) foundations

#### 5.5.3.4 Construction of fragility curves

We derived in this stage two sets of analytical fragility curves for single bay- single storey RC buildings with varying stiffness of the foundation system. Each curve provides the conditional probability of exceeding a certain limit or damage state under a range of seismic induced landslide events of given type and intensity. The landslide intensity is expressed in this work in terms of peak ground acceleration at the seismic bedrock that is the initial trigger of the slow moving slide. This will result to permanent differential displacements at the foundation level.

The probabilistic nature of the problem is treated by accounting for the variability associated with the building capacity (yield strength of steel, compressive and tensile strength of concrete, reinforcement bar size, strain hardening parameter, confining factor, building height and length and cross sections dimensions), as well as the variability in the demand, assuming different progressively increasing acceleration time histories that result in different permanent differential displacement magnitudes at the building's foundation links. In order to identify the building performance (damage) state and to construct the corresponding fragility curves, a damage index (DI) is introduced describing the steel and concrete material strains. Within the context of a fibre-based modelling approach, such as that implemented in SeismoStruct, material strains do usually constitute the best parameter for identification of the performance state of a given structure (Seismostruct, Seismosoft 2007). In all cases analyzed (900 in total), the steel material strain ( $\epsilon_s$ ) yields more critical results. Thus, it was decided to adopt only this parameter as a damage index hereafter for simplicity reasons. In this way, it is possible to establish a relationship between the damage index ( $\epsilon_s$ ) and the input motion intensity in

terms of the PGA values at the assumed seismic bedrock, for the two different building typologies and consequently to assign a median value of PGA to each limit state (Fig. 5.5.10). The next step is the definition of the damage or limit states. Based on the work of Crowley et al. (2004), Bird et al. (2005, 2006) and engineering judgment, 4 limit states (LS1, LS2, LS3, LS4) are defined. A qualitative description of each damage band for reinforced concrete frames is given in Table 5.5.3 while the limit state values finally adopted in quantitative terms are presented in Table 5.5.4. These concern exceedance of minor, moderate, extensive and complete damage of the building. The first limit state is specified as steel yielding that is the ratio between yield strength and modulus of elasticity of the steel material.

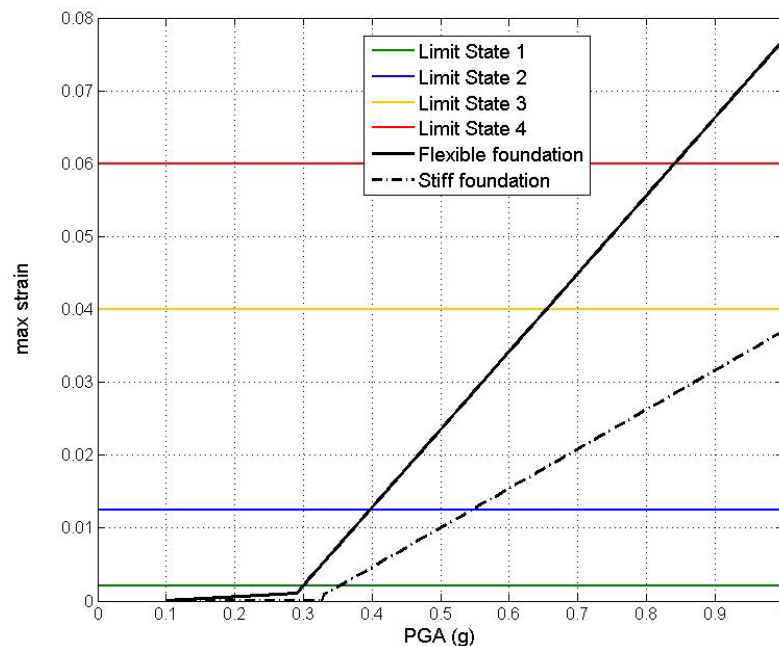


**Figure 5.5.10** PGA–damage index relationships for 1-story-1-story RC frame buildings with stiff and flexible foundation system

**Table 5.5.3** Structural damage state descriptions for RC frame buildings (after Crowley et al. 2004)

Structural damage band	Description
None to slight	Linear elastic response, flexural or shear type hairline cracks (<1.0 mm) in some members, no yielding in any critical section
Moderate	Member flexural strengths achieved, limited ductility developed, crack widths reach 1.0 mm, initiation of concrete spalling
Extensive	Significant repair required to building, wide flexural or shear cracks, buckling of longitudinal reinforcement may occur
Complete	Repair of building not feasible either physically or economically, demolition after earthquake required, could be due to shear failure of vertical elements or excessive displacement

**Table 5.5.4** Definition of Limit states for RC buildings

Limit state	Steel strain ( $\epsilon_s$ )
LS1	Steel bar yielding: 0.0011-0.0025
LS2	0.0125
LS3	0.04
LS4	0.06

In order to construct the fragility relationships, appropriate cumulative distribution functions, as the ones proposed in HAZUS (NIBS, 2004), that describe the fragility relationships have been generated. For structural damage, given peak ground acceleration PGA, the probability of exceeding a given limit state, SL<sub>i</sub>, is modeled as:

$$f(PGA) = \Phi \left[ \frac{1}{\beta_i} \ln \left( \frac{PGA}{\overline{PGA}_i} \right) \right] \quad [5.3]$$

Where:

- $\Phi$  is the standard normal cumulative distribution function,
- $\overline{PGA}_i$  is the median value of peak ground acceleration at which the building reaches the limit state, i,
- $\beta_i$  is the standard deviation of the natural logarithm of peak ground acceleration for limit state, i.

The median values of peak ground acceleration that correspond to each limit state can be defined for the threshold values of the aforementioned damage indexes as the values that corresponds to the 50% probability of exceeding each limit state. The standard deviation values [ $\beta$ ] describe the total variability associated with each fragility curve. Three primary sources contribute to the total variability for any given damage state (NIBS, 2004), namely the variability associated with the definition of the limit state value, the capacity of each structural type and the demand (seismic demand, landslide type, relative position of the structure to the landslide). Based on the work of Crowley et al. (2004), Bird et al. (2006) and HAZUS (NIBS, 2004) prescriptions, the uncertainty in the definition of limit states and the capacity are assumed to be equal to 0.4 and 0.25 respectively for both building typologies (with flexible and stiff foundation system) considered. The last source of uncertainty associated with the demand, is taken into consideration by calculating the variability in the results of numerical simulation carried out in Seismostruct for the computed differential displacement time histories. It should be mentioned that this variability is different for the two different building types. In particular, it is higher in the case of the buildings with flexible foundation system. The total uncertainty is estimated as the root of the sum of the squares of the component dispersions. The median (expressed in terms of peak ground acceleration PGA) and beta values of each limit state for the building with flexible and stiff foundation system are shown in Table 5.5.5.

**Table 5.5.5** Parameters of fragility functions

Limit State / Building type	Median PGA (g)				$\beta_i$
	LS <sub>1</sub> (g)	LS <sub>2</sub> (g)	LS <sub>3</sub> (g)	LS <sub>4</sub> (g)	
Flexible building	0.3	0.4	0.67	0.85	0.8
Stiff building	0.36	0.55	>0.9	>0.9	0.74

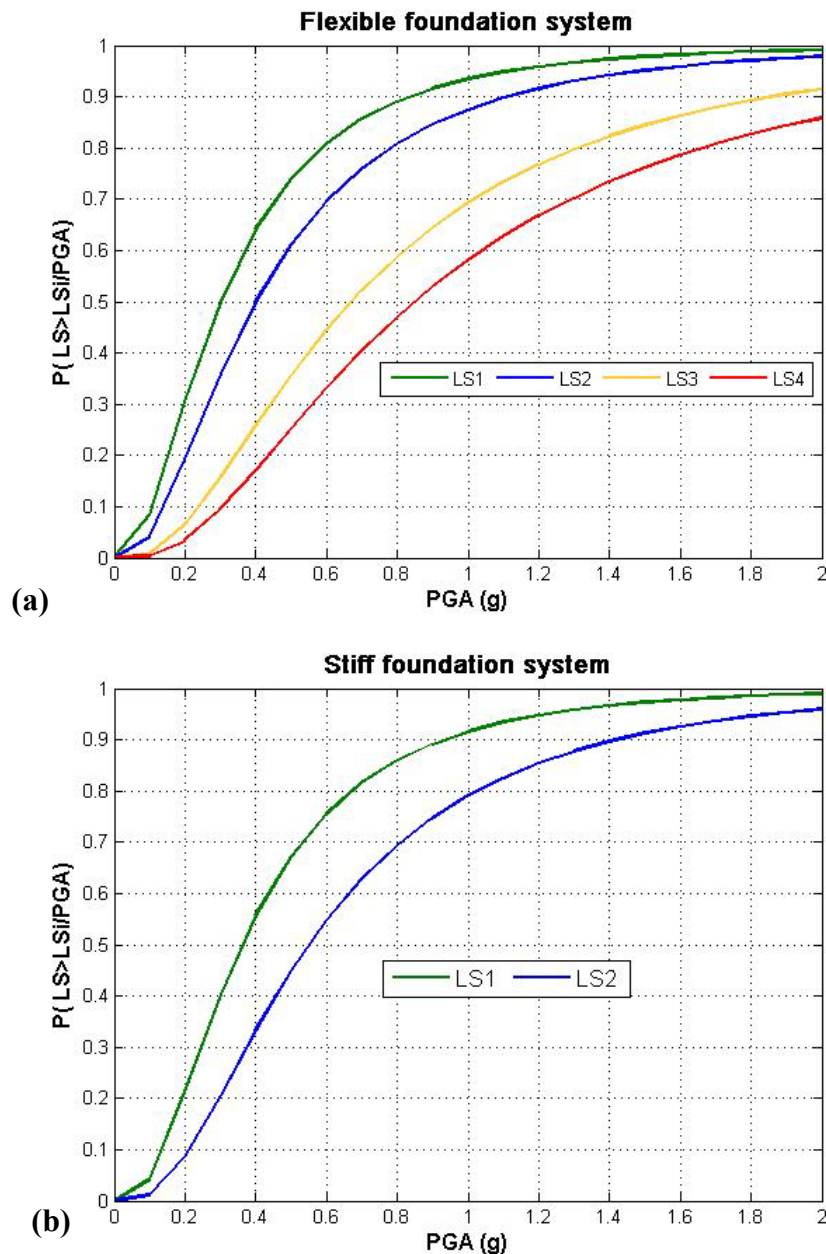


**Figure 5.5.11** Fragility curves for one bay- one storey RC buildings with flexible (a) and stiff (b) foundation system

Figure 5.5.11 illustrates the derived fragility curves for the two building typologies. As expected, the building with stiff foundation system sustain less damage due to earthquake induced slow moving slides compared to the building with the flexible foundation system. More specifically, only minor and moderate damages are possible for the former for the specified levels of deformation. It should be noticed that only the structural damage of the building members is considered in this study. The total damage (structural and non-structural) will be quite different (certainly larger) in case of the building with the stiff foundation as a considerable amount of damage may be attributed to the rotation of the whole building as a rigid body. In the latter, the damage can only be defined using empirical criteria and expert opinion. Furthermore, it is worth pointing out that the complex issue of combined ground shaking and ground failure due to landslide is not taken into account in the evaluation of the building 's vulnerability. The authors are planning to include this in a future work.

#### 5.5.4 Parametric study

In order to examine the influence of various parameters in assessing the vulnerability of RC frame buildings and increase the applicability band of the proposed methodology, an extensive parametric study is performed.

The parameters selected to vary are associated to:

- The geometry of the finite slope (slope height  $H$ , inclination  $\theta$ , distance to the seismic bedrock) (Fig. 5.5.12).
  - Slope height  $H=20, 40$  m
  - Distance to the seismic bedrock  $D= 80, 120$ m
  - Slope inclination  $\theta =f$  (Soil properties) =  $15^\circ, 30^\circ$
- The soil properties (soft or stiff clay and sand soils corresponding to soil categories B, C and D according to EC8) and constitutive laws for soil (Mohr Coulomb, strain softening)

##### Sandy soils:

$\varphi= 36^\circ$  (slope inclination  $30^\circ$ )

$\varphi= 20^\circ$  (slope inclination  $15^\circ$ )

##### Clayed soils:

Stiff  $\rightarrow c= 10$  KPa,  $\varphi= 25^\circ, \gamma=18$  KN/m<sup>3</sup> (slope inclination  $30^\circ$ )

Soft  $\rightarrow c= 5$  KPa,  $\varphi= 15^\circ, \gamma=17$  KN/m<sup>3</sup> (slope inclination  $15^\circ$ )

- The water table (dry, wet conditions) (Fig. 5.5.12)
  - Water table height  $H_w=80\%H$ ,
  - Dry conditions
- Foundation details (flexible or stiff shallow foundation)
  - Foundation width: 6, 12 m
  - Shallow foundation system: *flexible* (concentrated load to the footings), *stiff* (distributed load)
- Relative position of the building to the slope crest ( $L$ ) (Fig. 5.5.12)
  - Distance of the building to the slope's crest:  $L= H/10, H/6.67, H/5$ m

- Building typology (Figure 5.5.13)
  - Typical low rise RC frame buildings* (1, 3 storeys, 1÷2 bays)
    - Typical bay length: 6m
    - Typical storey height: 3m
- Building code (low and high code)
  - Low code:
    - Compressive strength of concrete:  $f_c = 16, 20$  MPa
    - Yield strength of reinforcement:  $f_y = 220, 400$  MPa
    - Reinforcement bar size  $\Phi 12, \Phi 14$
  - High code:
    - Compressive strength of concrete:  $f_c = 20, 30$  MPa
    - Yield strength of reinforcement:  $f_y = 400, 500$  Mpa
    - Reinforcement bar size  $\Phi 14, \Phi 16$
- Parameters of constitutive models for concrete and the reinforcement
  - Steel: bilinear stress-strain model with kinematic strain hardening
  - Concrete: nonlinear constant confinement model
- Dynamic time histories
  - Real acceleration time histories properly adjusted to satisfy the following criteria:
    - Free field accelerograms recorded at rock sites
    - Match the proposed elastic spectrum of EC8 for soil type A (rock)
    - Predominant frequencies vary from 1 to 5 Hz
    - Appropriate filtering, baseline correction and tapering
    - Damping: Rayleigh type varies from 1-5%
    - $PGA_{scaled} = 0.1, 0.3, 0.5, 0.7$  and  $0.9$  g at the base of the dynamic model

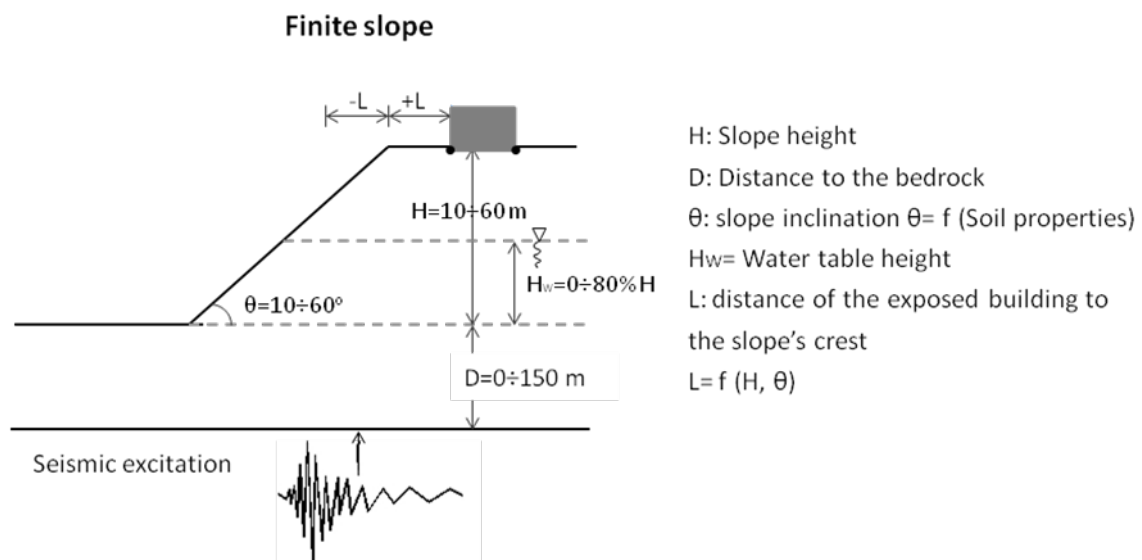


**Figure 5.5.12** Slow movements- Geometry of finite slope

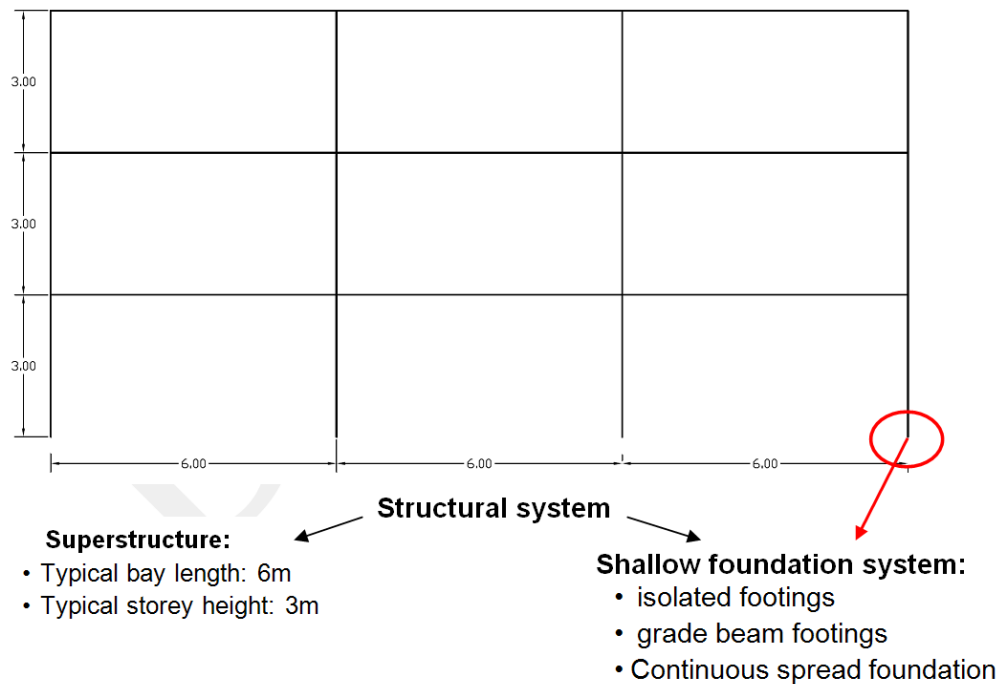


*Figure 5.5.13 Frame RC building's typology*

In the following, several examples in terms of fragility curves are presented revealing the sensitivity of different parameters to the building's response. It should be mentioned that these fragility curves are valid only for a specific combination of geometry, material properties and limit states. However, they allow for the identification and classification of the most influential factors in assessing the structure's vulnerability. Finally, although the results are limited by some of the idealizations and assumptions of the analysis, they should provide a useful starting point in the vulnerability assessment of affected buildings standing near the crest of precarious slopes providing the basis for more sophisticated numerical analysis for the particular governing conditions in selected real case studies (see Safeland Deliverable D2.7, Pitilakis et al. 2011).

#### *5.5.4.1 The effect of code level*

Fragility curves for low and high code design buildings impacted by slow moving landslides have been generated according to the proposed methodological framework. Bare RC frame buildings with flexible and stiff foundation system are investigated assuming the same geometrical and hydro-geological conditions ( $H=20\text{m}$ ,  $\beta=30^\circ$ , dry conditions, sand soil,  $V_s=250\text{m/sec}$ ). Considering that low code RC buildings are poorly constructed structures characterized by a low level of confinement, the limit steel strains needed to exceed post yield limit states should have lower values compared to high code, properly constructed RC buildings. As a consequence, it was decided to adopt different limit state values for exceedance of extensive and complete damage for low and high code frame RC buildings (Table 5.5.6) based on the work of Crowley et al. (2004) and Bird et al. (2005) and engineering judgement.

The corresponding fragility functions are depicted in figures 5.5.14 and 5.5.15 for buildings with stiff and flexible foundation system respectively.

**Table 5.5.6** Definition of Limit states for “low” and “high” code RC buildings

Limit state	Steel strain ( $\epsilon_s$ ) –low code	Steel strain ( $\epsilon_s$ ) –high code
LS1	Steel bar yielding	Steel bar yielding
LS2	0.0125	0.0125
LS3	0.025	0.04
LS4	0.045	0.06

It is observed that for the 1<sup>st</sup> and 2<sup>nd</sup> limit states, low and high code RC frame buildings experience quite similar performance. However, when extensive or complete damage to the building members is anticipated, the deviation in the building performance for low and high code design buildings is expected to increase resulting to higher vulnerability levels for low code buildings. This is due to the low levels of attainable limit strains assumed for low code building compared to high code, adequate confined structures. In the ensuing examples, “high code” design buildings are assumed.

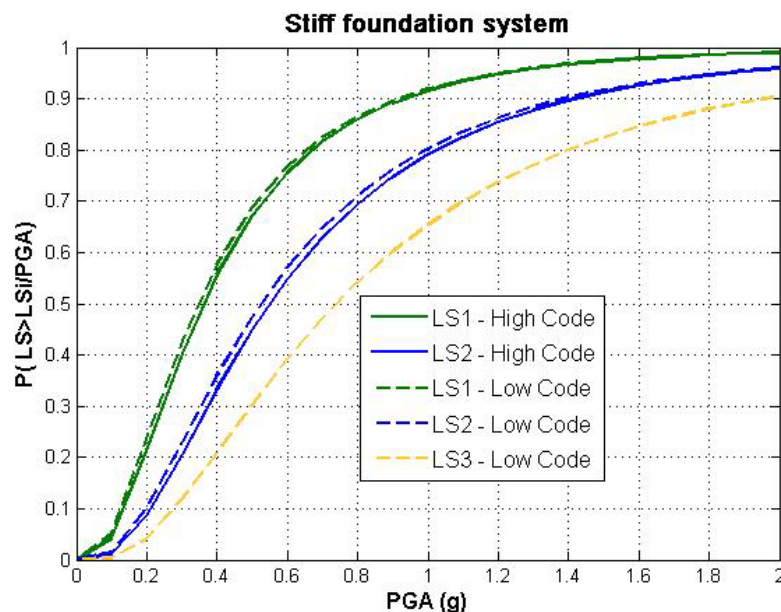


**Figure 5.5.14** Fragility curves for “low” code and “high” code one bay- one storey RC buildings with stiff foundation system

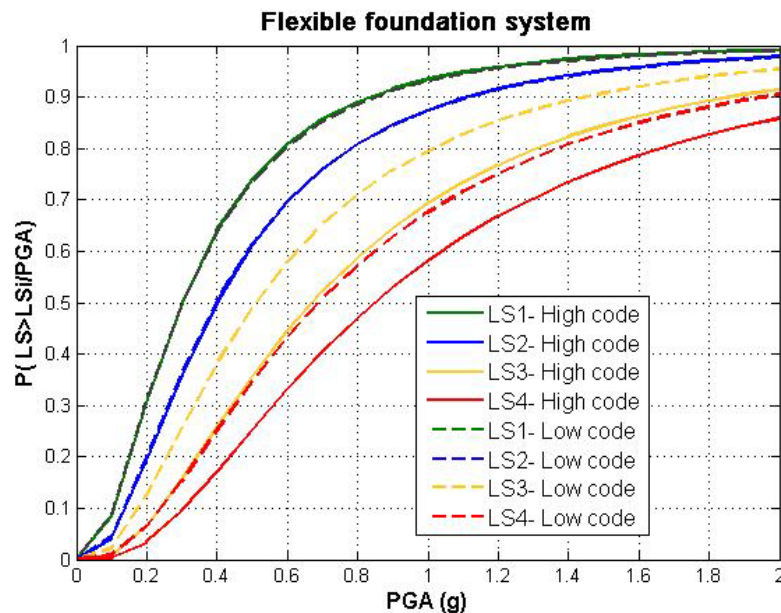


**Figure 5.5.15** Fragility curves for “low” code and “high” code one bay- one storey RC buildings with flexible foundation system

#### 5.5.4.2 The effect of slope geometry

Four different slope configurations are analysed in order to reveal the impact of slope height and inclination to the building’s performance level:

- H=20m,  $i=30^\circ$
- H=40m,  $i=30^\circ$
- H=20m,  $i=15^\circ$
- H=40m,  $i=15^\circ$

Slope inclination has been found to vary as a function of the soil properties. Hence, in the present study, we consider a stiff clay material ( $c=10$  KPa,  $\phi=25^\circ$ ,  $V_s=250$  m/s) for relatively steep slopes (inclination  $i=30^\circ$ ) and a soft clay soil ( $c=5$  KPa,  $\phi=15^\circ$ ,  $V_s=150$  m/s) for gentle slopes (inclination  $i=15^\circ$ ). In the cases presented herein, the single bay-single story RC frame building is assumed to be located  $H/6.67$  m from the crest.

Figures 5.5.16 and 5.5.17 illustrate the derived fragility curves for one bay- one storey RC buildings standing near the crest of a 20m and 40m high cliff for relatively steep and gentle slopes respectively. The comparison demonstrates that the higher the slope height and inclination, the higher the estimated vulnerability for the building. Worthy of note is the fact that the buildings founded on gentler slopes are expected to suffer less structural damage despite the softer soil conditions assumed.

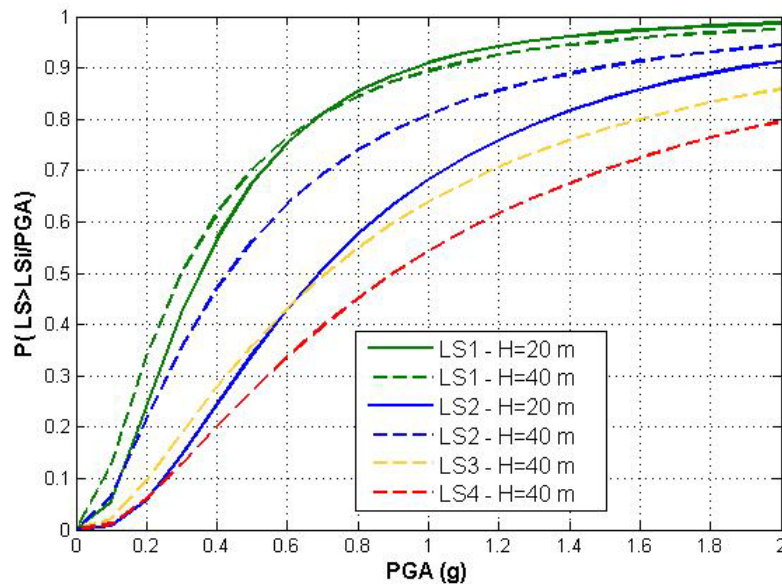


**Figure 5.5.16** Fragility curves for one bay- one storey RC buildings standing near the crest of a relatively steep (inclination  $i=30^\circ$ ) low-rise ( $H=20\text{m}$ ) and high-rise ( $H=40\text{m}$ ) cliff.

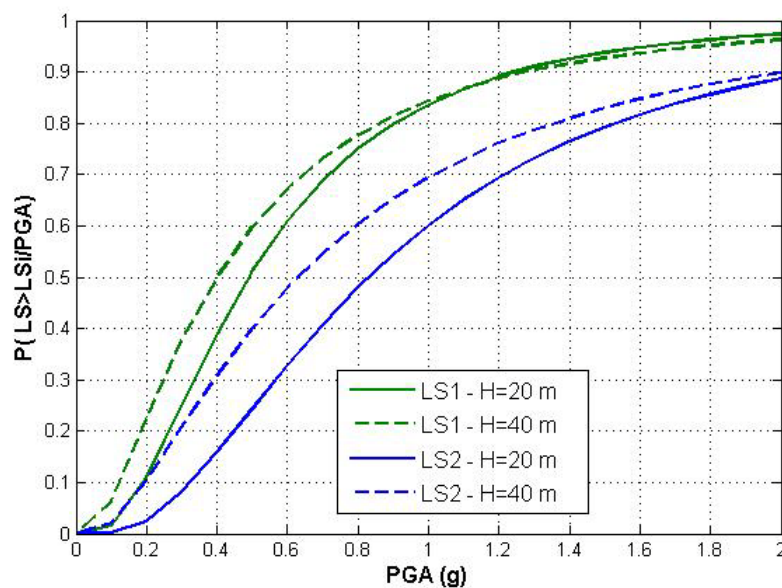


**Figure 5.5.17** Fragility curves for one bay- one storey RC buildings standing near the crest of a gentle (inclination  $i=15^\circ$ ) low-rise ( $H=20\text{m}$ ) and high-rise ( $H=40\text{m}$ ) cliff.

#### 5.5.4.3 The effect of distance from the crest

The computed differential ground displacements are generally decreased with the distance from the slope's crown. For instance, considering two dynamic slope models ( $H=40\text{m}$ ,  $\beta=30^\circ$ , sand soil,  $V_s=250\text{m/sec}$ ) that differ only in the location of the building in relation to the slope's crest and applying the Pacoima dam –I Northridge accelerogram at the assumed seismic bedrock scaled at  $\text{PGA}_{\text{scaled}}=0.5\text{g}$ , the differential ground displacements derived from

the dynamic analysis are shown in Figure 5.5.18. This is only for illustrative purposes as 6 different accelerograms scaled at 5 levels of PGA (as discussed previously) are applied at the base of the dynamic model. Finally, figure 5.5.18 presents the fragility curves for one bay-one storey RC building with flexible foundations standing 4m (H/10) and 6m (H/6.67) from the slope's crest, indicating the influence of the proximity of the structure to the potential unstable slope in estimating building's vulnerability.

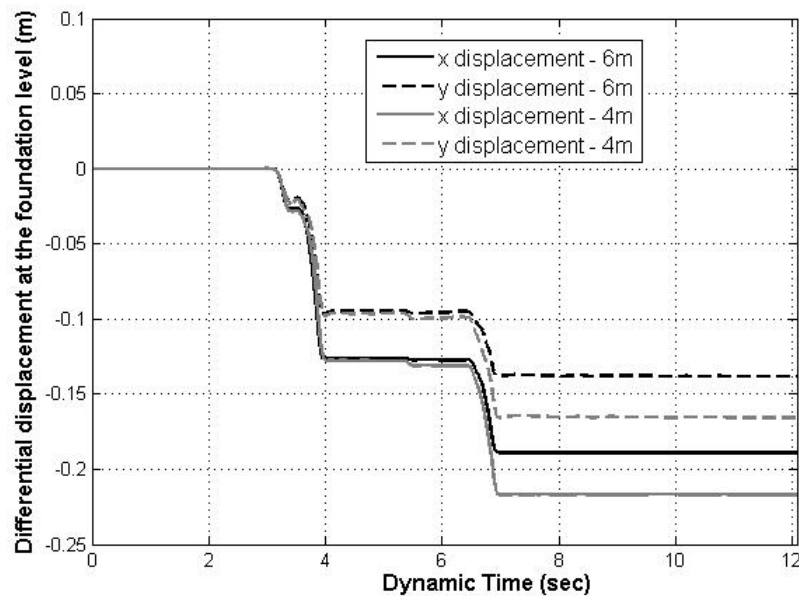


**Figure 5.5.18** Differential x and y ground displacements at the foundation level for buildings standing 4m and 6m from the crest

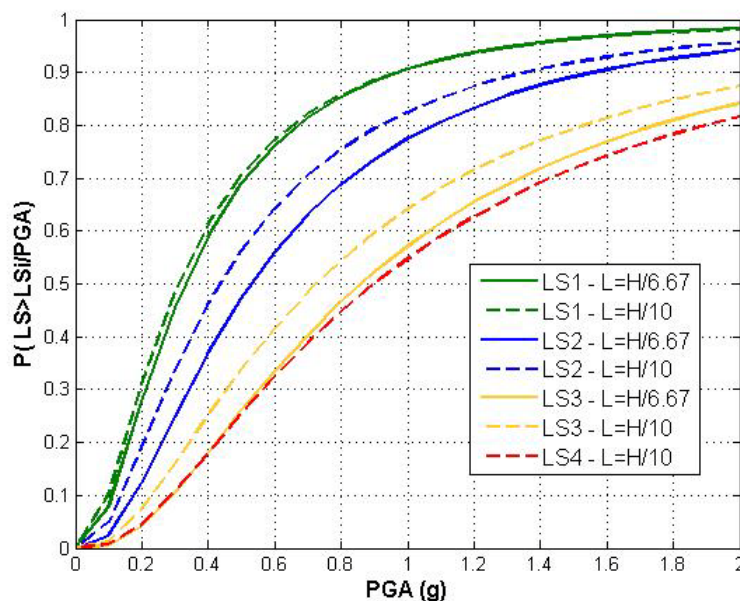


**Figure 5.5.19** Fragility curves for one bay- one storey RC buildings with flexible foundation standing 4m and 6m from the crest

#### 5.5.4.4 *The effect of water table level*

Fragility curves for buildings with dry and partially saturated soil conditions ( $H_w=80\%H$ ) for homogeneous sand and clay soils are illustrated in Figures 5.5.20 and 5.5.21 respectively. The slope dynamic models ( $H=20\text{m}$ ,  $\beta=30^\circ$ ,  $V_s=250\text{m/sec}$ ) vary only in the hydrological and soil conditions examined. A single bay-single story bare frame RC building with flexible foundation system standing 3m from the slope's crest is considered for all the analysis cases. For both sand and clayey soil conditions, the presence of water results into an increase in the total permanent ground displacement. However, the differential displacement imposed to the building foundation level is decreased in case of clayed soil yielding to lower vulnerability levels (fig. 5.5.21). The latter may be explained as follows: the presence of water is associated with the formation of a larger sliding surface that, in relation to the proximity of the structure to the slope's crest, involves a larger amount of total displacement but limited differential displacements for the building. On the contrary, for sand soils that generally distinguish smaller sliding masses, the presence of water results to larger differential deformation for the specified building (located 3m from the crest) and consequently to higher vulnerability levels.

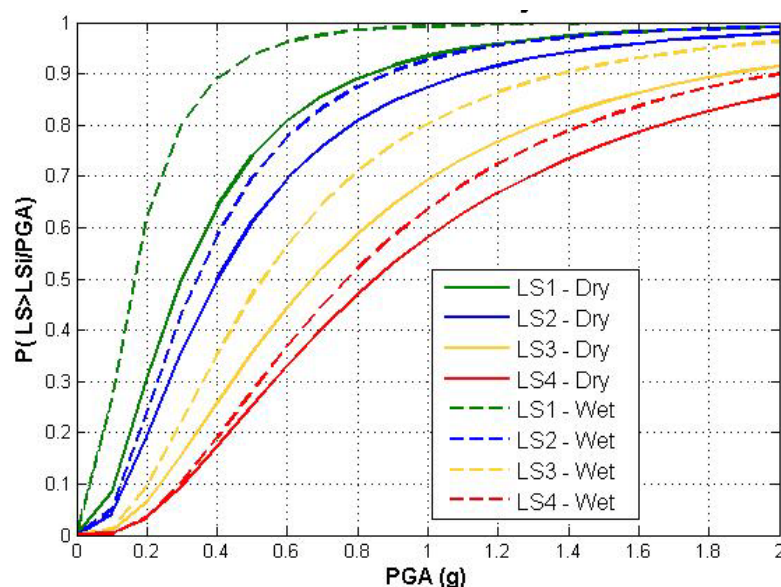


**Figure 5.5.20** Fragility curves for one bay- one storey RC buildings with flexible foundation with dry and partially saturated sand soil conditions ( $H_w=-4\text{m}$ )

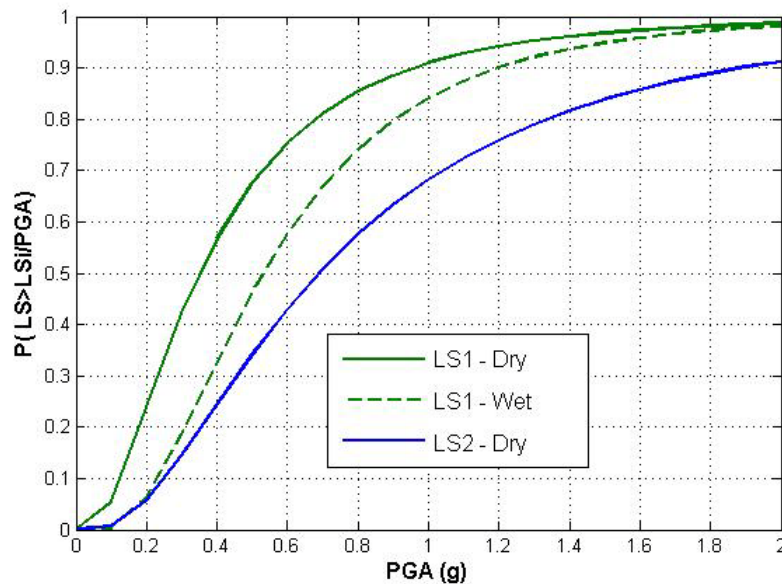


**Figure 5.5.21** Fragility curves for one bay- one storey RC buildings with flexible foundation with dry and partially saturated clay soil conditions

#### 5.5.4.5 The effect of soil type

The soil type (sand or clay) also plays a significant role in assessing building's vulnerability standing near the crest of potential precarious slopes. It is observed that slopes consist of clay material generally demonstrate an improved performance compared to sands when subject to permanent ground displacements. This is due to the inherent cohesive behavior of clay soil material. Figure 5.5.22 displays the derived fragility curves for 1b-1s bare frame RC buildings with flexible foundations lying 4m (H/10) from the slope's crest on medium dense/stiff sand and clay soil conditions representing soil category C according to EC8. The slope height and inclination considered are 40m and 30°.

#### 5.5.4.6 The effect of number of bays

Figure 5.5.23 presents the fragility curves for one bay and two bays-1 storey RC buildings founded on isolated footings, standing 3m from the slope's crest, considering the same hydro-geological and geometrical conditions ( $H=20\text{m}$ ,  $\beta=30^\circ$ , dry sand,  $V_s=250\text{m/sec}$ ). As shown in the figure, the two-bay frame building distinguishes an improved behavior compared to the one-bay structure with the same structural and stiffness characteristics. Hence, one-bay RC structures despite their simplicity are found to be adequately representative of the performance of real low rise RC frame buildings resulting on sufficient conservative fragility functions.

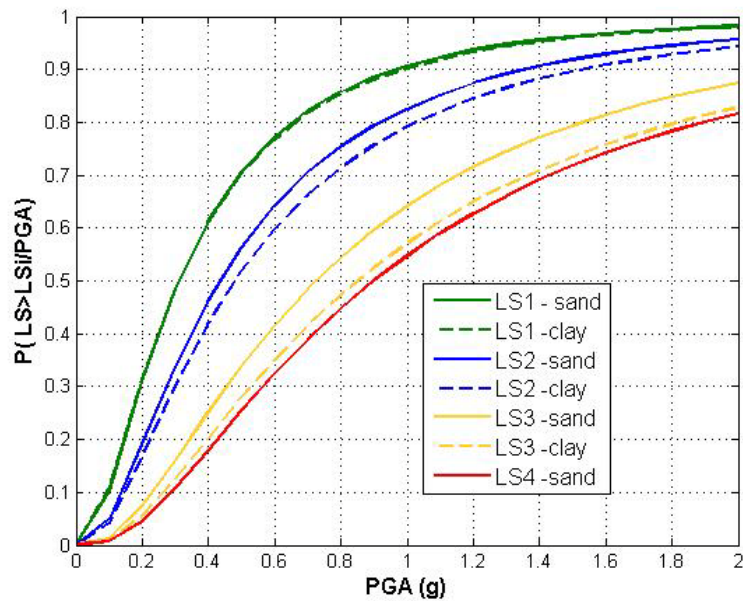


**Figure 5.5.22** Fragility curves for one bay- one storey RC buildings with flexible foundation on medium dense/stiff sand and clay soil conditions

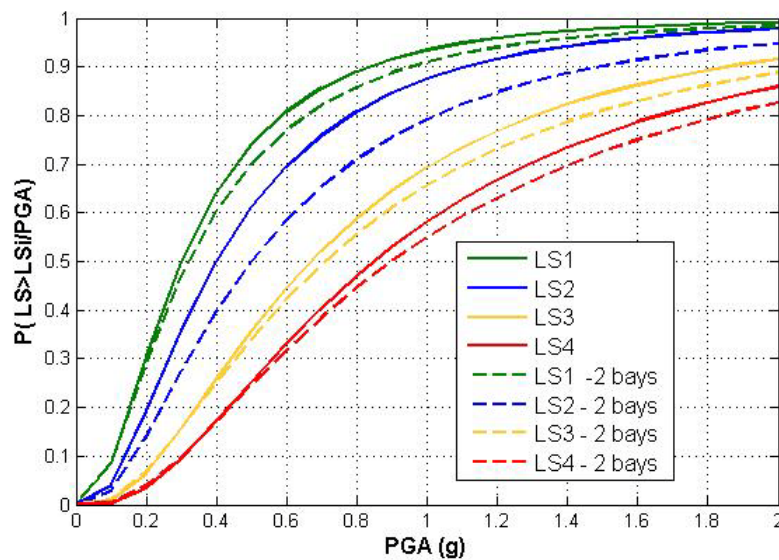


**Figure 5.5.23** Fragility curves for one bay- one storey and two bays-1 storey RC buildings with flexible foundation system

## **5.6 SITE SPECIFIC METHODOLOGY FOR VULNERABILITY ASSESSMENT OF RC BUILDINGS TO SLOW-MOVING EARTH SLIDES (BRGM)**

### **5.6.1 Introduction**

As mentioned in previous chapters, it appears that existing studies seldom propose a quantitative assessment of structural elements, when performing landslide risk analyses, although it is a key step towards the quantitative evaluation of risk from hazardous events. Whereas the seismic vulnerability of structures has been well studied over the past years and is constantly improving, several studies highlight the lack of quantitative indicators on the vulnerability of elements exposed to landslide hazards. The aim of this chapter is hence to present a methodology applicable for physical vulnerability assessment of RC buildings to slow-moving earth slides at the site specific scale, by means of analytical fragility curves and considering non earthquake triggering factors.

### **5.6.2 Methodology**

A flowchart similar to the one presented for earthquake-triggered landslides can be used (see Fig. 5.5.1), in which building capacity depends on the target building typology and where the earthquake demand is replaced by the slope motion, in order to derive the deformation demand of the building. Building capacity and deformation demand constitute the two main components to be used as inputs for structural response assessment (i.e. the third component of the methodology), with fragility curves as final output obtained through numerical simulations.

However, landslide hazard involves so many aspects that the methodology adopted here considers a specific scenario of a 2D single-bay single-storey reinforced concrete (RC) frame building exposed to a deep-seated earth-slide occurring within a finite slope.

A building located right above a finite slope (uphill configuration) is generally exposed to some damages due to slope failure zone nearby. This phenomenon has been highlighted by Cardinali et al. (2006) and Galli & Guzzetti (2007), who gathered significant data from the surroundings of Umbria in Central Italy. Thus, we have chosen to reproduce a similar configuration, e.g. a simple 2D RC frame structure located on a horizontal ground, at a distance  $L$  to a slope of angle  $\theta$ . In order to model a realistic landslide, we have used the empirical approach described by Duncan and Wright (2005) on slope stability analysis. Therefore we have defined a sliding zone within the slope, corresponding to the area where we impose a progressive displacement of magnitude  $A$ .

Regarding structural damage indicators, whereas some global indicators are widely used in seismic vulnerability assessment, no such criteria are yet available in the case of landslides. A number of authors have proposed local damage indicators based on allowable values of material strains (concrete and steel), in order to assess the vulnerability of structures subjected to differential ground deformations (Bird et al., 2006a,b; Negulescu & Foerster, 2010).

The approach proposed by Bird and co-workers (2006a,b), uses analytical solutions to assess the expected damage of existing RC frame buildings due to liquefaction-induced differential ground movements. It proposes equations in order to represent the deformational capacity of the critical column, by applying principles of displacement-based assessment, semi-empirical and semi-mechanical approaches, while the column deformational demand related to ground motions is derived geometrically. In this approach, the structure deformation is idealized in four cases considering differential vertical settlements and lateral movement associated with horizontal and vertical components. A first limit state is defined using concrete and steel yielding strains and geometrical properties of the section. The authors propose also a second and a third limit state, each one depending on the admissible strain values for both materials separately. Only bare reinforced concrete frame buildings are considered in this approach and the foundation deformation is assumed to be equal to the free-field deformation. Interesting conclusions arise from the results of this study regarding the damage mechanisms due to ground failure and the displacement demand of the floor columns. One important one concerns RC frame structures, for which the displacement demand is concentrated to the ground floor columns, as the upper stories generally rotate as a rigid body. Also, the authors show that for a single-bay case, deformations take place in the column rather than in the beam.

Several methods developed over the years are based on movements caused by structure settlements due to its own weight, and do not consider the external factors that could induce deformations (tunneling, excavations, ground heaving, liquefaction, etc.). These factors together with the crucial need for quantifying the deformations in case of key buildings (e.g. schools, hospitals, historical monuments) lead to using more sophisticated methods, such as finite elements (FEM), etc., in order to estimate settlement-induced damages.

Two trends can be observed in FEM calculations:

- Two-step uncoupled analyses, in which the soil and the structure are studied separately, and the soil settlements profile is imposed as input to the FEM model of the building;
- One-step coupled analyses, in which Soil-Structure Interactions (SSI) are modeled.

Interesting conclusions have been reached from FEM calculations with SSI:

1. The weight of the building tends to increase the general magnitude of the settlements that develop underneath.
2. The building stiffness may act to reduce differential settlements.
3. Depending on the building deformation mode (e.g. sagging or hogging), SSI effects may be more or less important, as lateral restraint provided by the ground may reduce the extent of tensile stresses in the building.
4. SSI modeling generally leads to reduced differential settlements for the building.

Contrary to SSI analyses, uncoupled analyses generally ignore the effects of the building weight and stiffness on the ground settlement profile, which can lead to inaccurate prediction of expected settlements. However, SSI analyses may often be too complex and time consuming for practical vulnerability assessment over wide areas (e.g. urban settlements).

In the present study, we adopt a methodology based on 2D uncoupled FEM analyses, consisting in:

1. Soil-Foundation Interaction (**SFI**) simulations with varying landslide and foundation features and using the FEM code GEFDYN (Aubry et al., 1986): the purpose is first to identify possible candidates for intensity measures, apart from the obvious parameter of landslide magnitude  $A$ , and second, to estimate the differential displacements resulting at ground surface, along the building's foundation level;
2. RC frame building response assessment, using the differential displacements obtained at the foundation level as input time histories for the fiber-based FEM code Seismostruct (Seismostruct, Seismosoft 2007).

In the next section, we describe the model parameters and numerical schemes considered for analysis, together with the parametric study carried out to identify the most relevant parameters, in order to predict the structural damage, as well as the methodology used to develop analytical fragility curves, that can be used to quantitatively evaluate the structural vulnerability to landslides at site scale.

### 5.6.3 Parametric study

#### 5.6.3.1 *General description of the study*

Different parameters that can influence the final structural response have been examined in this analysis and will be presented in the next sections:

- Slope geometry: inclination ( $\theta$ ), height ( $H$ );
- Soil features: sequence of sediment deposits, soft/stiff materials (clays/sands), dry/wet conditions;
- Landslide displacements: magnitude ( $A$ );
- Distance of the building to the slope crest ( $L$ );
- RC frame features: cross-section geometry, section reinforcement degree.

Regarding SFI analyses, a shallow stiff foundation type has been assumed (distributed load applied on the footings to simulate the building). As for the building typology, a typical low-rise RC frame (one bay-one storey) has been chosen for all analyses, considering a 4m bay length and a 3m storey height.

In order to estimate the differential displacements obtained at the bottom of the building's foundation level (first step of the methodology), we have performed 2D nonlinear full slope plane strain static SFI simulations with the FEM program GEFDYN.

#### 5.6.3.2 *Material properties for soil and structure*

For the different slope models, we assume four soil configurations with three sediment layers in which we vary the constitutive material properties. An elastoplastic Drucker-Prager (DP) constitutive behavior is assumed for all sediment layers. *Table 5.6.1* to *Table 5.6.2* sum up the different values adopted in the simulations.

**Table 5.6.1** Soil properties remaining constant for all configurations

<b>ALL configurations</b>			
Properties	Layer1	Layer2	Layer3
Constitutive model	DP	DP	DP
Bulk density (kg/m <sup>3</sup> )	2000	1900	1800
V <sub>s</sub> (m/s)	400	200	145
V <sub>p</sub> (m/s)	750	375	270
Porosity	0.3	0.3	0.3

**Table 5.6.2** Varying soil properties

<b>CLAY configuration</b>			
Properties	Layer1	Layer2	Layer3
Cohesion (kPa)	15	10	5
Friction angle (°)	25	20	15
Permeability (m/s)	10 <sup>-8</sup>	10 <sup>-8</sup>	10 <sup>-8</sup>
<b>SAND configuration</b>			
Properties	Layer1	Layer2	Layer3
Cohesion (kPa)	0	0	0
Friction angle (°)	40	35	30
Permeability (m/s)	10 <sup>-4</sup>	10 <sup>-4</sup>	10 <sup>-4</sup>
<b>CLAY-SAND configuration</b>			
Properties	Layer1 (clay)	Layer2 (clay)	Layer3 (sand)
Cohesion (kPa)	15	10	0
Friction angle (°)	25	20	30
Permeability (m/s)	10 <sup>-8</sup>	10 <sup>-8</sup>	10 <sup>-4</sup>
<b>SAND-CLAY configuration</b>			
Properties	Layer1 (sand)	Layer2 (sand)	Layer3 (clay)
Cohesion (kPa)	0	0	5
Friction angle (°)	40	35	15
Permeability (m/s)	10 <sup>-4</sup>	10 <sup>-4</sup>	10 <sup>-8</sup>

The stiff foundation system is modeled as a deformable elastic beam connected to the underlying soil grid through interface elements with elastoplastic Coulomb type behavior, which are able to simulate appropriately the potential sliding and/or tensile separation of the beam foundation relative to the soil. As only the foundation system is modeled, the weight of the building is assigned as a uniform distributed load of 25kN/m along the foundation beam. The foundation and interface soil-foundation features are presented in *Table 5.6.3*.

**Table 5.6.3** *Foundation and interface soil-foundation features*

<b>Foundation properties</b>	
Length (m)	4
Cross section (m <sup>2</sup> )	0.4 x 0.4
Moment of inertia (m <sup>3</sup> )	0.0053
Young Modulus (GPa)	29
<b>Interface properties</b>	
Shear stiffness (MPa)	1000
Normal stiffness (MPa)	1000
Cohesion (kPa)	0
Friction angle (°)	15

The 2D static SFI simulations have been carried out for each slope and soil configuration. The results are used in the second step as input for the structural response assessment, using the FEM program SeismoStruct (see §5.5.3.3 for details), in order to derive fragility curves, i.e. probability of reaching or exceeding some given damage limit states. The material properties used for structural response analysis are given in *Table 5.6.4*.

**Table 5.6.4** *Material properties for the RC frame*

<b>Concrete</b>	
Compressive strength $f_c$ (MPa)	20
Tensile strength $f_t$ (MPa)	2.1
Strain at peak stress (mm/mm)	0.002
Confinement factor	1
Specific weight (kN/m <sup>3</sup> )	24
<b>Reinforcement steel</b>	
Young Modulus (GPa)	200
Yield strength $f_y$ (MPa)	400
Strain hardening parameter	0.005
Specific weight (kN/m <sup>3</sup> )	78

### 5.6.3.3 *Damage state limits and analytical fragility curves*

Regarding the damage limit states adopted for analyses, we use the limit strain states given in *Table 5.6.5*. The description of the structural damages corresponding to these local damage indicators has already been detailed in *Table 5.5.3* of previous chapter. The first damage state, LS1 (slight damage), is directly connected to the yielding strain limit, which is here 0.002 for both concrete and steel. Post-yield damage states are chosen according to the quality of the construction.

**Table 5.6.5** Definition of Limit states considered for RC frame buildings in this study

Limit state	Structural Damage	Limit strain
LS1 (yielding)	None to slight	0.002
LS2	Moderate	0.0125
LS3	Extensive	0.04
LS4	Complete	0.06

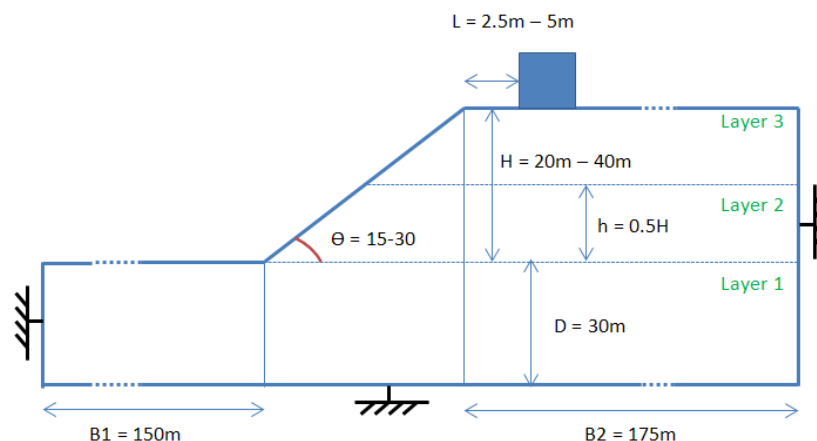
The analytical fragility curves giving the conditional probability of exceeding a specific limit state or level of damage are derived over a range of relevant hazard intensity values. Each fragility curve is obtained by counting, for different values of imposed hazard intensity parameter, the number of situations out of the total computed cases, that have led to the desired limit damage state  $LS_i$ ; these probabilities can then be fitted into a curve, usually representing the cumulative function of a standard normal cumulative distribution  $\phi$ , as described by Shinozuka (1998) and Shinozuka et al. (2000). The functional form is given as:

$$P(LS > LS_i | X) = \phi \left( \frac{1}{\beta_i} \ln \frac{X}{\alpha_i} \right) \quad [5.4]$$

where  $\alpha_i$  and  $\beta_i$  represent respectively the median and standard deviation (dispersion) values for damage state  $LS_i$  and  $X$  is the chosen hazard intensity parameter (e.g. landslide magnitude, differential settlement, etc.).

#### 5.6.3.4 Description of the full slope SFI modeling

Eight slope configurations have been assumed, which features are recalled in *Figure 5.6.1* and *Table 5.6.6* and for which we consider a constant basal layer thickness  $D$  of 30m. The important sizes of the left and right lateral extensions of the slope models are here to prevent discrepancies due to the lateral boundaries with respect to displacements developing during the analysis.

**Figure 5.6.1** Model features considered for full slope SFI simulations

The first simulations performed have shown that the spatial extent of the phenomenon is quite limited in space, and that consequently, most of the settlements are due to the motion of the landslide's crest. Consequently, this zone has been carefully meshed and surfaces located farther from it have been coarsely meshed, in order to reduce computation time. Mesh features are detailed in *Figure 5.6.2*.

In the sliding area, we impose a downward progressive uniform displacement vector, which direction is parallel to the slope's one. *Figure 5.6.3* shows one of the model meshes, where mesh refinement near the foundation is particularly noticeable.

**Table 5.6.6** Slope model features for SFI analyses

Configuration Name	H (m)	$\theta$ (°)	L (m)
m1	20	15	2.5
m2	20	30	2.5
m3	40	15	2.5
m4	40	30	2.5
m5	20	15	5
m6	20	30	5
m7	40	15	5
m8	40	30	5

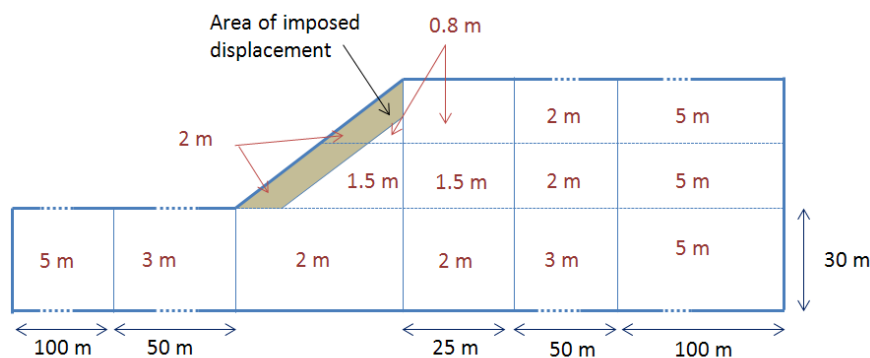


**Figure 5.6.2** Characteristic lengths used for unstructured triangle elements of the mesh: the foundation zone is finely meshed for accuracy purposes.

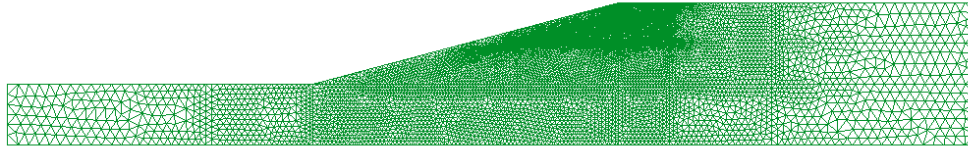


**Figure 5.6.3** GID mesh for model parameters  $h=40\text{m}$ ,  $\theta=15$  and  $L=2.5\text{m}$

In the next section, we will present the results obtained with the different models, by varying the parameters listed in section 5.6.3.1.

#### 5.6.3.5 Results of the parametric study

##### ***Effect of the slope height***

The differential displacement resulting on the foundation is mainly caused by the movement of the nearest part of the landslide area (distance to the building). However, as the magnitude of the imposed displacement increases, the displacement of the slide bottom has an increasing influence on the differential settlement of the building. Hence, the height of the sliding surface is a parameter with increasing importance as the magnitude of the slide increases.

The fragility curves for  $h=20\text{m}$  and  $h=40\text{m}$  are presented on *Figure 5.6.4*. We see that the vulnerability of the building increases with the slope height  $h$ . For LS2 damage state, the intersection of fragility curves may be due to insufficient number of simulations carried out.

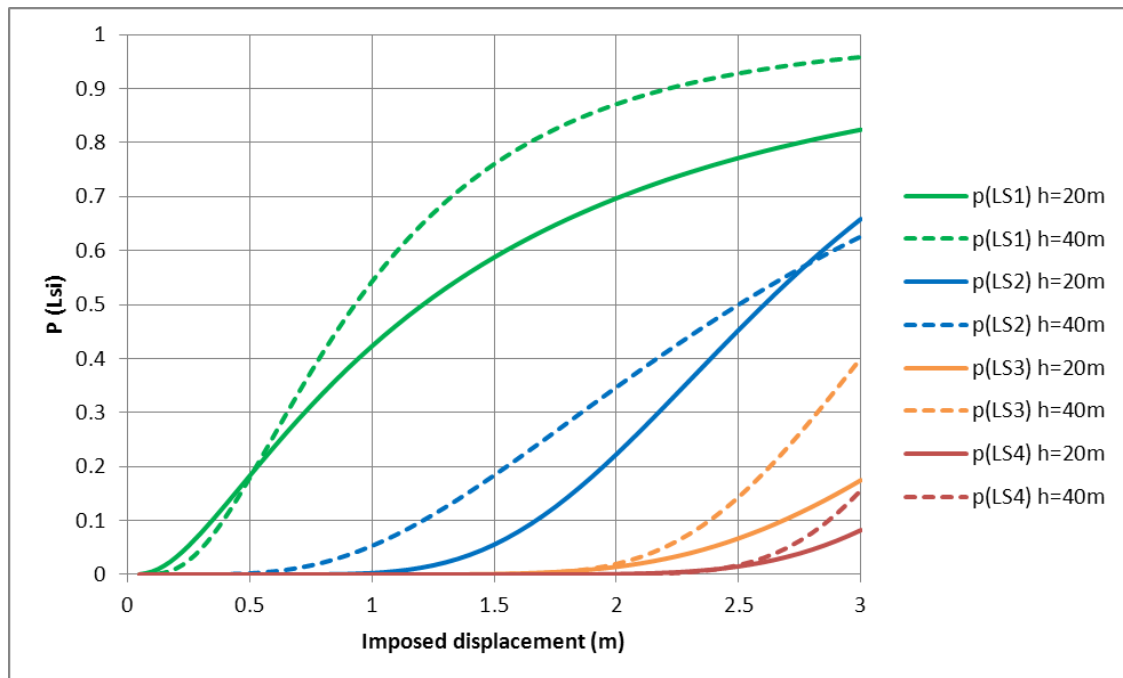


**Figure 5.6.4** Fragility curves obtained for a one bay-one storey RC frame building when varying slope height ( $h=20\text{m}$  and  $40\text{m}$ )

### Effect of the slope inclination

Figure 5.6.5 shows the fragility curves obtained when varying the slope angle. As expected, a landslide occurring on a steepest slope produces more damages to the building.

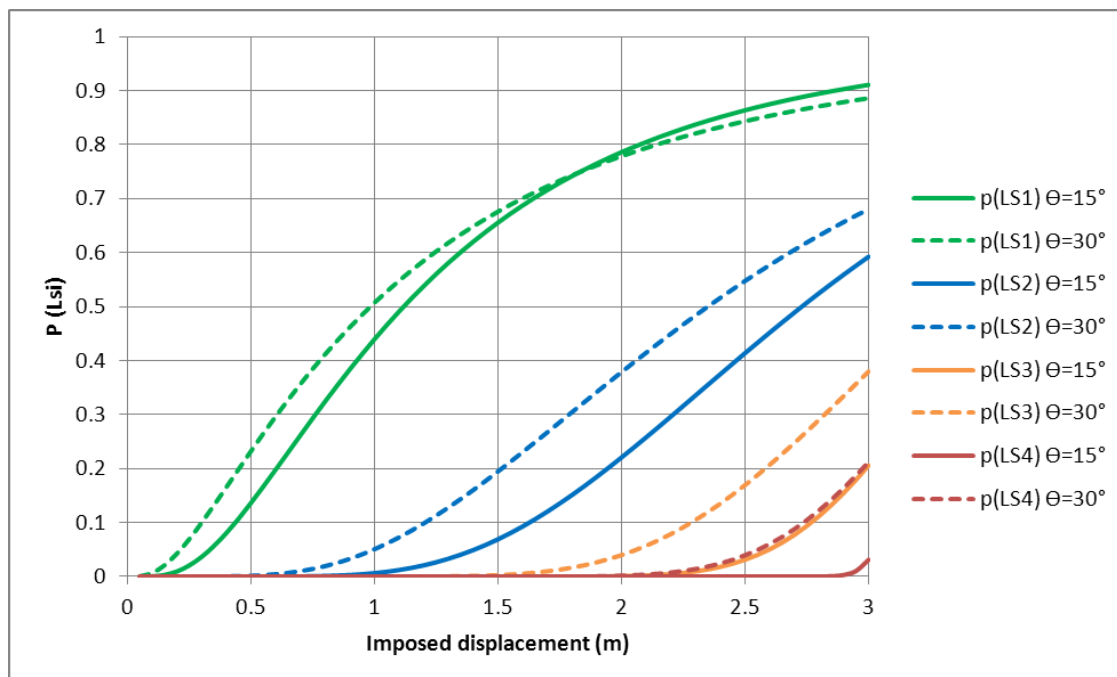


**Figure 5.6.5** Fragility curves obtained for a one bay-one storey RC frame building when varying slope inclination ( $\theta=15^\circ$  and  $30^\circ$ ).

### ***Effect of the building distance from the slope crest***

The performed simulations show that the distance from the slope crest is a parameter which has a great influence on the settlements resulting on the foundation. In *Figure 5.6.6*, we see for instance that a building located very close to the earth slide edge and exposed to a slide of magnitude 1.5m, will reach damage state LS1 in more than 95 % of the cases.

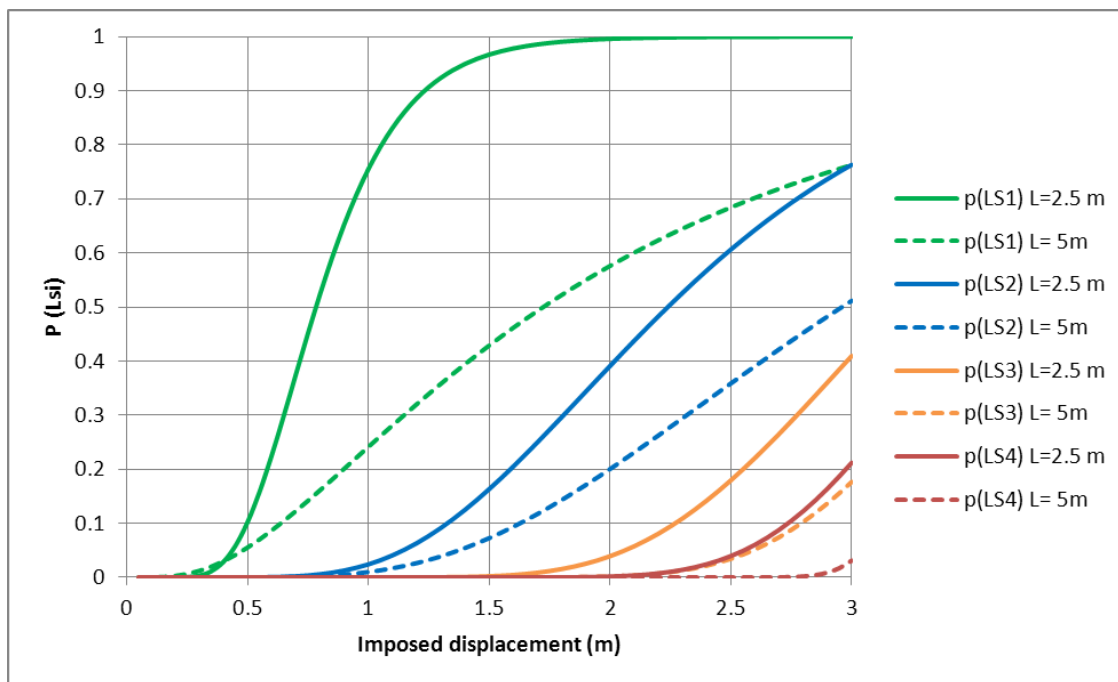


**Figure 5.6.6** Fragility curves obtained for a one bay-one storey RC frame building when varying building distance from the slope crest ( $L=2.5\text{m}$  and  $5\text{m}$ ).

### ***Effect of the soil material properties***

As four different soil configurations have been tested in simulations, the fragility curves obtained in this section are probably less accurate than those obtained for the other parameters, because only 16 simulations have been performed for each soil configuration in this case (instead of 32). As a consequence, we also present unsmoothed probability of damage in the following charts.

In *Figure 5.6.7* and *Figure 5.6.8*, we present the fragility curves obtained respectively for damage states LS1 and LS2 and for the 4 soil configurations. First, we note that clay configuration is producing more damage on the building than the sand one. Moreover, for relatively low soil displacement ( $<0.8\text{m}$ ), the unsmoothed probability of damage LS1 for “clay” and “sand-clay”, and for “sand” and “clay-sand” are very close. As mentioned before for slides with relatively small magnitude, differential settlements are mainly caused by the movement of the nearest part of the landslide area. Thus, in this displacement range, “clay” and “sand-clay” models (resp. “sand” and “clay-sand”) whose third layer is constituted of clay (resp. sand) present the same behavior.

Finally, as the magnitude of the slide increases, the influence of layers 1 and 2 on the differential settlement increases: this is the reason why fragility curves for “clay-sand” and “sand-clay” models intersect for LS1.

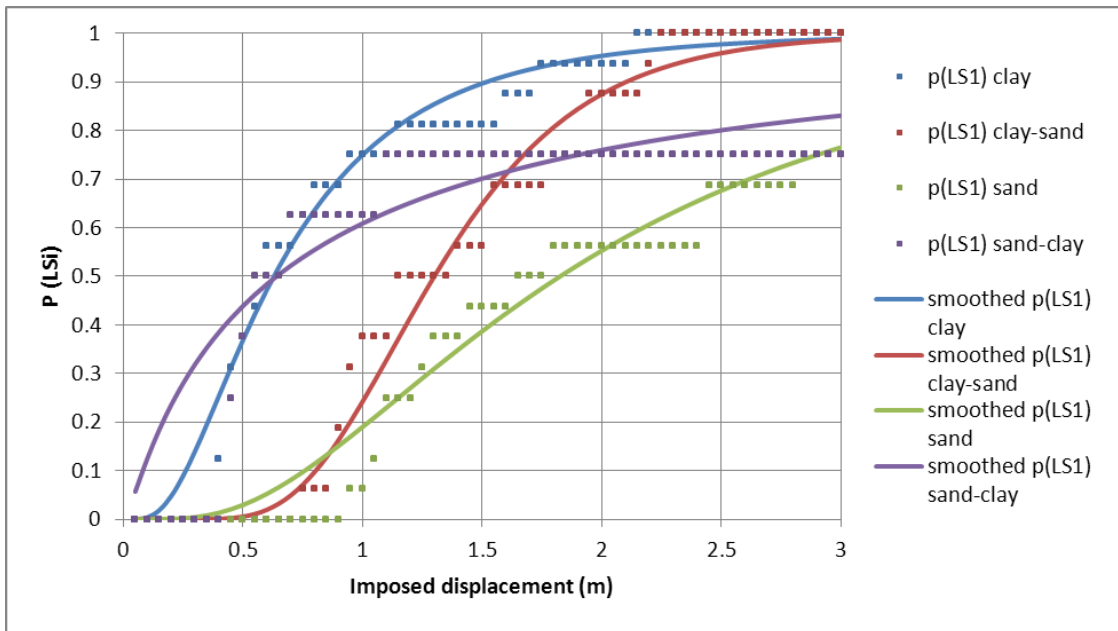


Figure 5.6.7 Fragility curves obtained for damage state LS1, considering a one bay-one storey RC frame building and varying soil configurations.

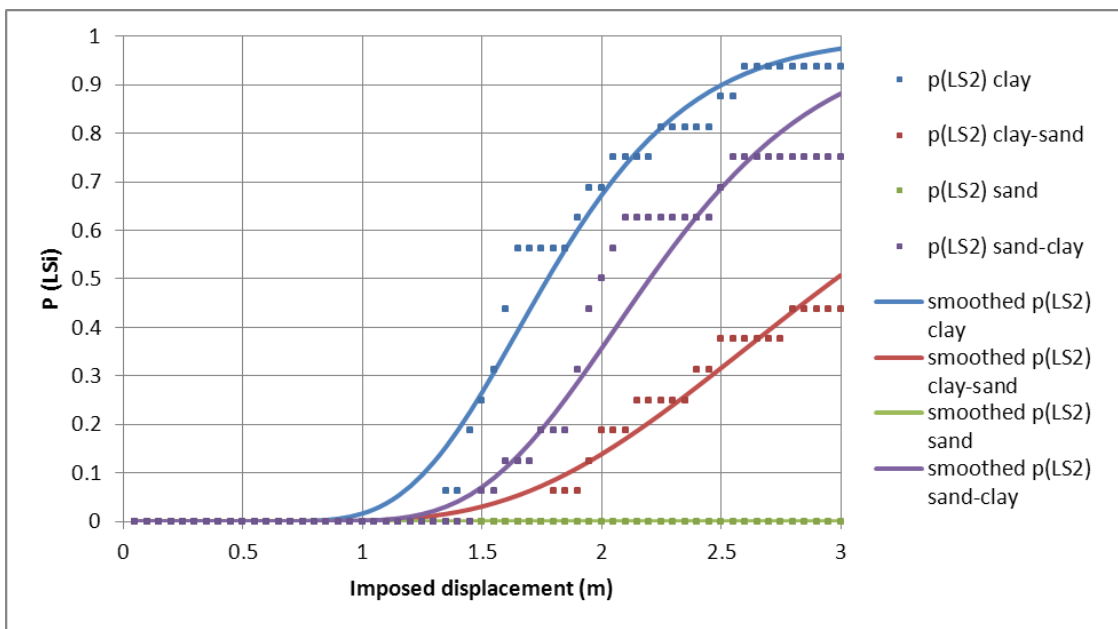
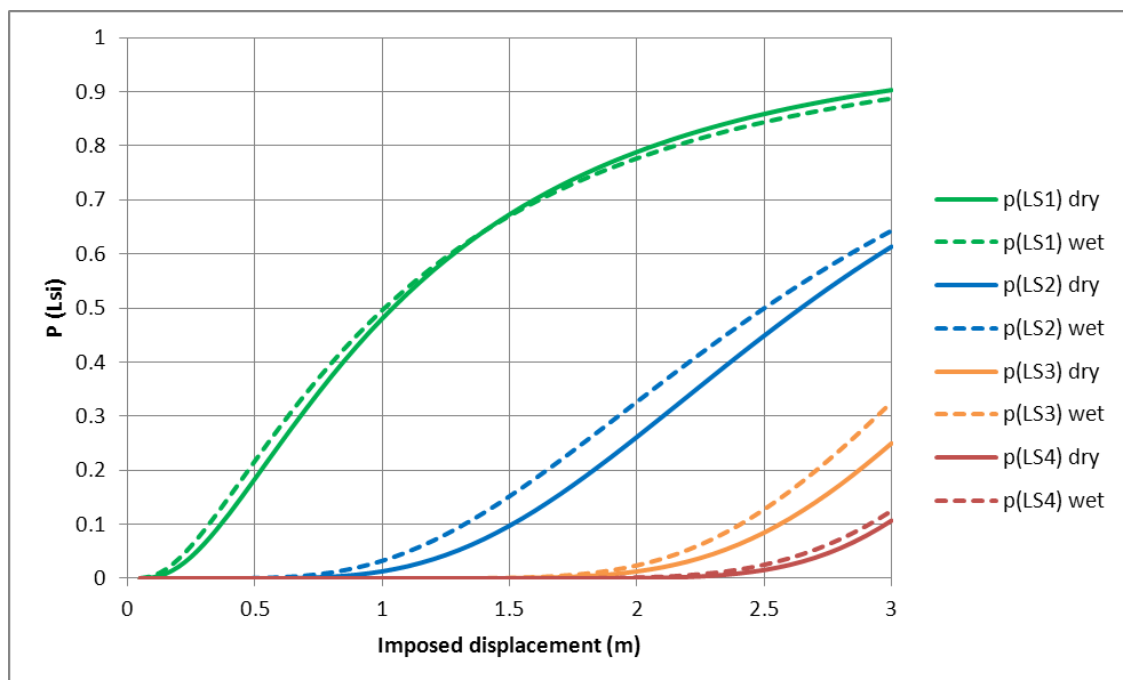


Figure 5.6.8 Fragility curves obtained for damage state LS2, considering a one bay-one storey RC frame building and varying soil configurations.

### *Effect of the hydraulic condition (dry/wet)*

Heavy rainfalls are often considered as the main trigger of landslides, due to buoyancy effects when pore fluid pressures increase. In this study, we assume a porous medium (30% porosity) with two hydraulic conditions: a first one with no water (dry materials) and a second with a water table level located at 80% of the slope height (saturated materials underneath the water table and dry materials above).

In *Figure 5.6.9*, we see that the vulnerability of the building is slightly increased by the presence of pore water.



**Figure 5.6.9** Fragility curves obtained for a one bay-one storey RC frame building when varying hydraulic conditions (dry or partially saturated materials).

## 5.7 METHODOLOGY FOR ROADS (AUTH)

The existing HAZUS (NIBS, 2004) fragility functions for roads provide the conditional probability of reaching or exceeding a certain damage state, under a range of ground failure events of given type and intensity. They result from a combination of expert judgmental models and empirical models based on statistical analysis of damage data from previous events (Giovinazzi and King, 2009). They are defined with respect to road classification and permanent ground displacement (PGD) due to landslides, liquefaction and fault rupture. Two different types of curves are given, for roads with two traffic lanes (urban roads) and roads with four or more lanes (major/highway roads) (figs. 5.7.1a and 5.7.1b respectively). Five damage states are defined, a qualitative description of these is given in Table 5.7.1. The medians and dispersions of these curves for each damage state are presented in Table 5.7.2.

**Table 5.7.1** *Damage state definition for roads in HAZUS*

Damage States	Description
ds1. None	-
ds2. Slight/Minor Damage	slight settlement (few cm) or offset of the ground
ds3. Moderate Damage	moderate settlement (several cm) or offset of the ground
ds4. Extensive Damage	major settlement of the ground (few m)
ds5. Complete Damage	major settlement of the ground (i.e., same as ds4).

**Table 5.7.2** *Damage algorithms for roadways (from HAZUS, NIBS 2004)*

Permanent Ground Deformation			
Components	Damage states	Median (m)	$\beta$
Major Road	slight/ minor	0.30	0.7
	moderate	0.60	0.7
	extensive/complete	1.50	0.7
Urban Road	slight/ minor	0.15	0.7
	moderate	0.30	0.7
	extensive/complete	0.60	0.7

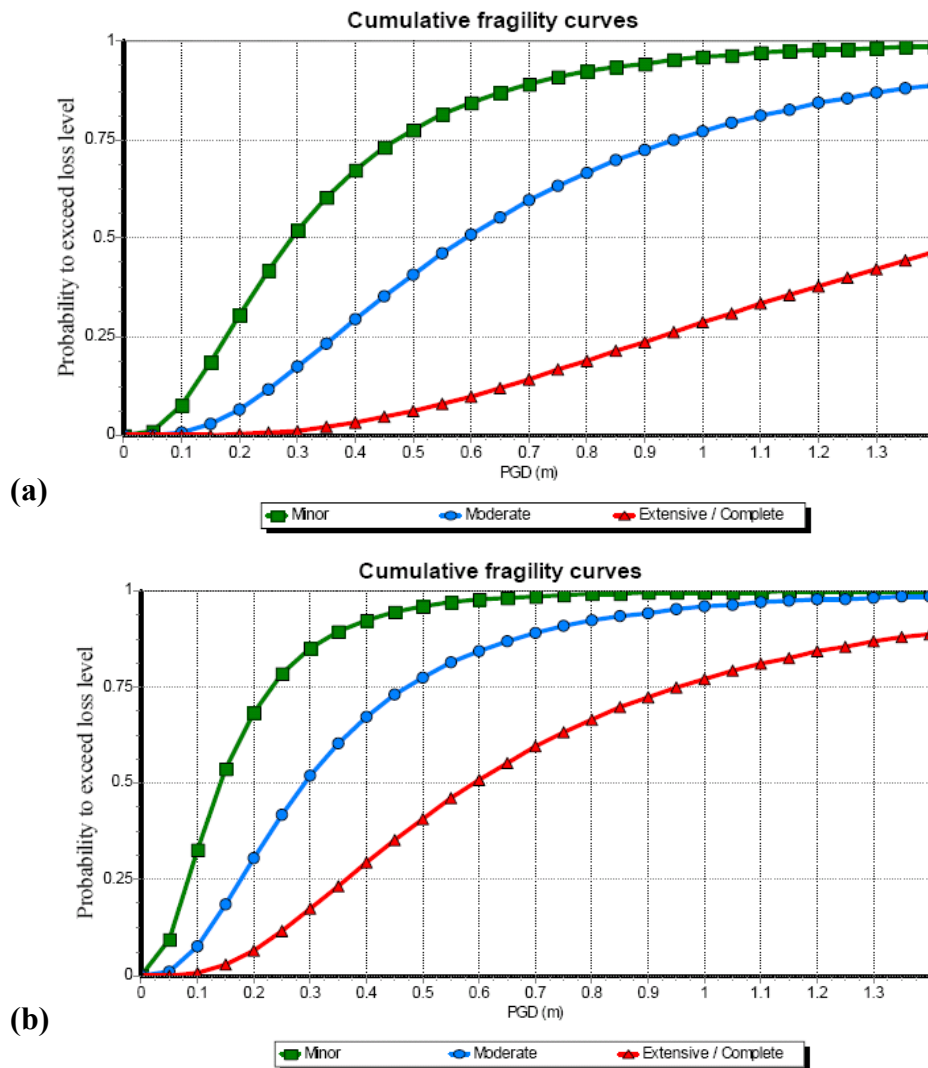


**Figure 5.7.1** Fragility curves at various damage states (a) for Highways and (b) for Urban roads (NIBS, 2004).

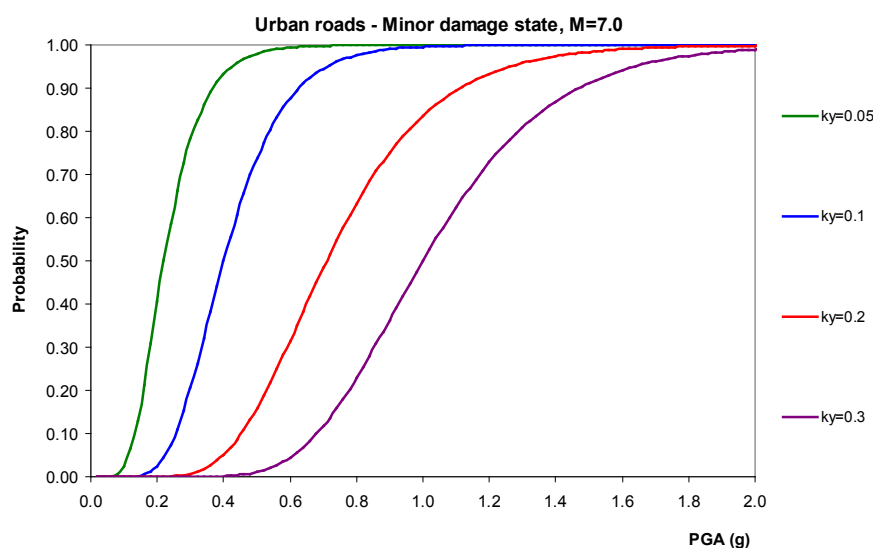
The aforementioned curves are the only ones available in the literature for estimating the vulnerability of roads due to landslides. They have shown to give in most cases a realistic assessment of the expected damage level (Azevedo et al., 2010). However, they comprise a generalized approach that does not take into account the specific characteristics of soil and local topography. In the framework of WP2.2-D2.5, it is attempted to propose fragility curves for roads in case of earthquake triggered slides as a function of peak ground acceleration (PGA) considering the characteristics of the slope (i.e. yield coefficient  $k_y$ ). In this respect, the existing HAZUS curves are modified using the Bray and Travarasrou (2007) model (eq. 5.5) that relates the seismic permanent ground displacement PGD with the PGA (peak ground acceleration of the ground motion, i.e.  $S_a(T_s=0)$ ) for the Newmark rigid sliding block case ( $T_s=0$ ):

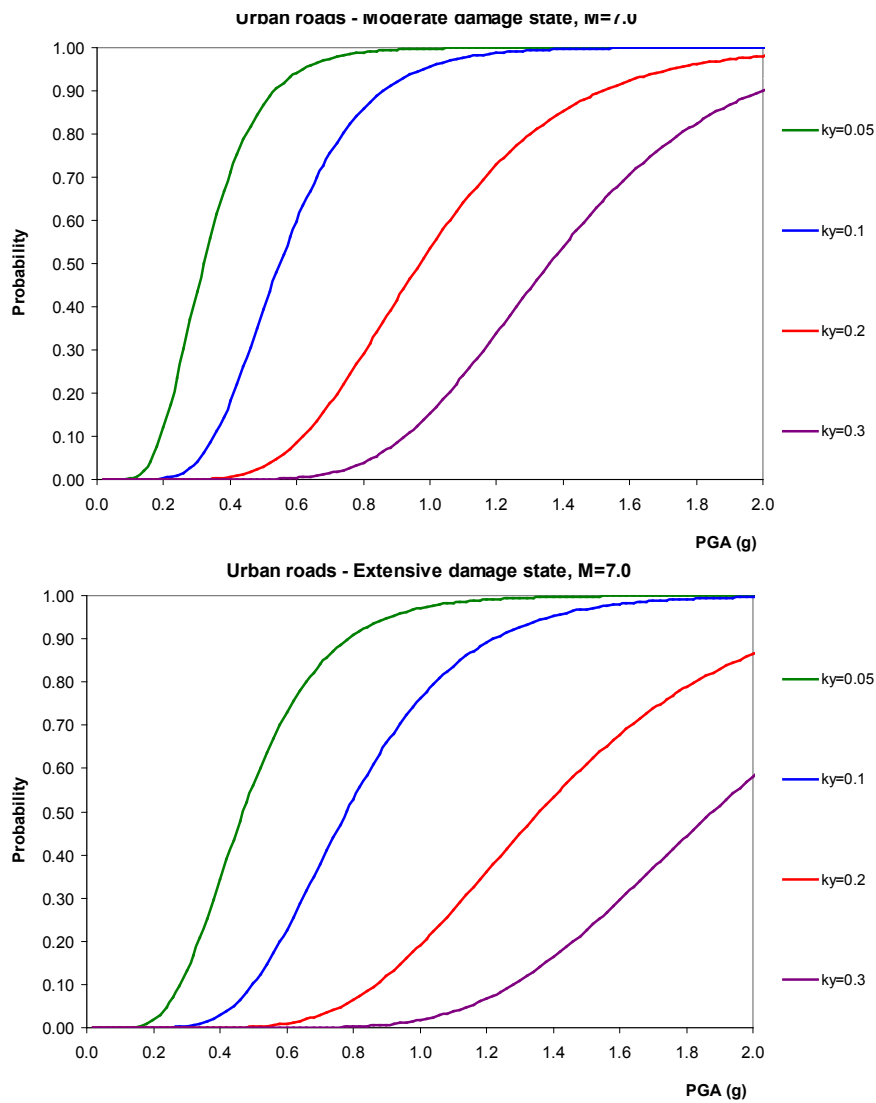
$$\ln(\text{PGD}) = -0.22 - 2.83 \ln(k_y) - 0.333 (\ln(k_y))^2 + 0.566 \ln(k_y) \ln(\text{PGA}) + 3.04 \ln(\text{PGA}) - 0.244 (\ln(\text{PGA}))^2 + 0.278(M - 7) \pm \varepsilon \quad [5.5]$$

In particular, using the existing fragility curves, the exceedance probabilities of each damage state are calculated for the corresponding PGD values that are derived for a range of PGA values based on the aforementioned relationship. Then a lognormal distribution is fitted on each curve and the median and standard deviation parameters ( $\beta$ ) are estimated. It is noted that the  $\beta$  values are considered to be the same for all the damage states in each case. Representative fragility curves are provided in Table 5.7.3 for different values of  $k_y$  (0.05, 0.1, 0.2, 0.3) and a given earthquake moment magnitude ( $M_w=7.0$ ). The derived fragility curves for the different  $k_y$  values are compared for the minor, moderate and extensive/complete damage states in figures 5.7.2 and 5.7.3 for urban and major roads respectively. We see that vulnerability is lower when  $k_y$  is increasing, that is when the specific slope characteristics are considered.

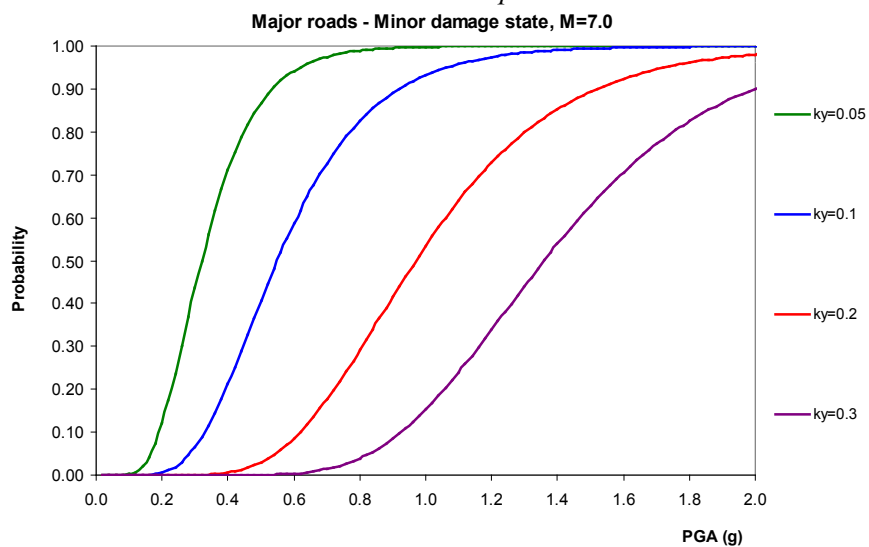
**Table 5.7.3** Proposed damage algorithms for roadways on slope ( $M=7.0$ ).

		Peak Ground Acceleration							
Components		$k_y=0.05$		$k_y=0.1$		$k_y=0.2$		$k_y=0.3$	
	Damage states	Median (g)	$\beta$	Median (g)	$\beta$	Median (g)	$\beta$	Median (g)	$\beta$
Major Road	slight/ minor	0.32		0.55		0.97		1.36	
	moderate	0.47	0.40	0.78	0.40	1.36	0.35	1.88	0.30
	extensive/complete	0.83		1.34		2.22		2.90	
Urban Road	slight/ minor	0.22		0.40		0.71		1.00	
	moderate	0.32	0.40	0.55	0.35	0.97	0.35	1.36	0.30
	extensive/complete	0.47		0.78		1.36		1.88	





*Figure 5.7.2 Fragility curves at various damage states and different yield coefficients ( $k_y$ ) for urban roads on slope.*



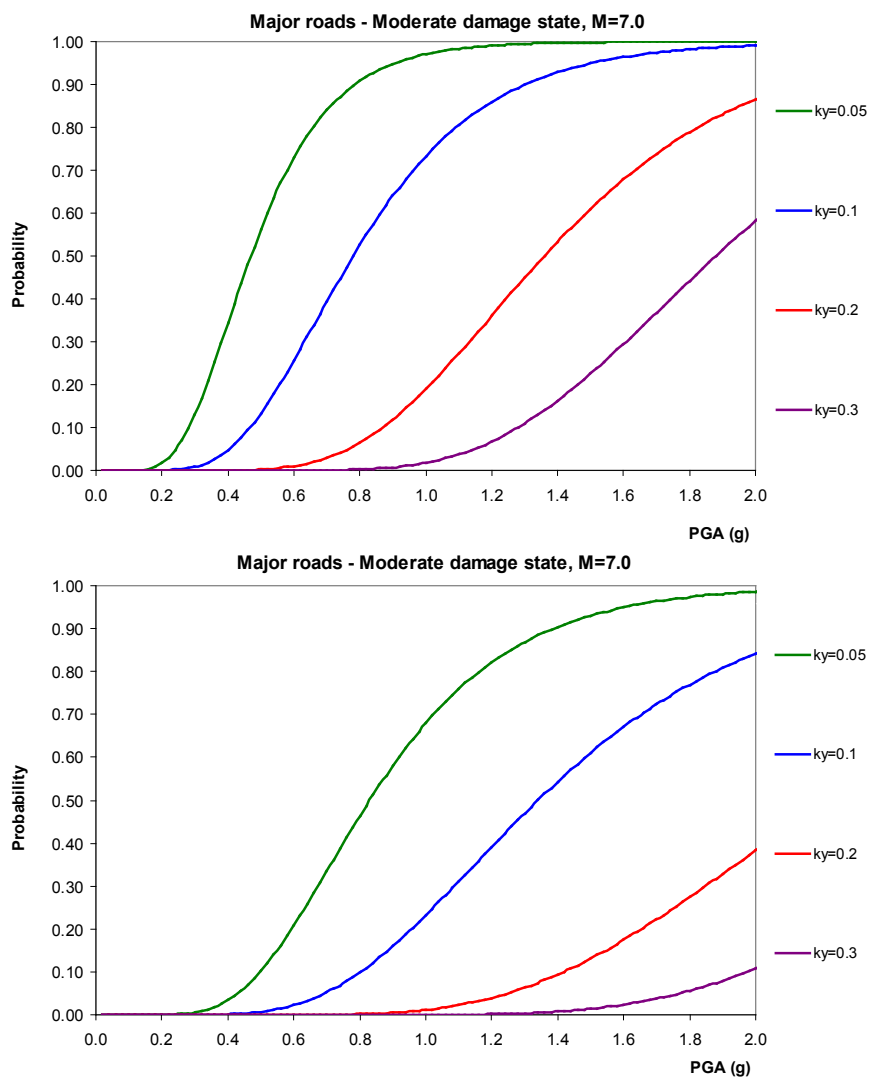


**Figure 5.7.3** Fragility curves at various damage states and different yield coefficients ( $ky$ ) for major roads on slope.

## 6 PHYSICAL VULNERABILITY TO FAST AND SLOW MOVING LANDSLIDES

### 6.1 METHODOLOGY FOR PIPELINES (AUTH)

#### 6.1.1 Analytical approach

Landslides can severely affect underground lifelines such as buried gas and water pipelines. There have been a number of attempts to quantify the resulting deformations and limiting conditions leading to pipeline failure (e.g. Swanson and Jones 1982; Sweeney et al. 2004; Terzi et al. 2008, etc.). Regardless of whether the pipeline starts within the unstable soil mass, or is impacted by debris flow originating from elsewhere, the main principles of the problem are the same: the pipeline will be subjected to loading over a defined length determined by the width  $B$  of the unstable soil zone and its angle relative to the pipeline (Fig. 6.1.1). Ultimately the pipeline may come to a stable deformed shape where the continued active loading from the slide is equilibrated by the membrane tension in the pipeline in addition to the passive resistance (Randolph et al, 2010).

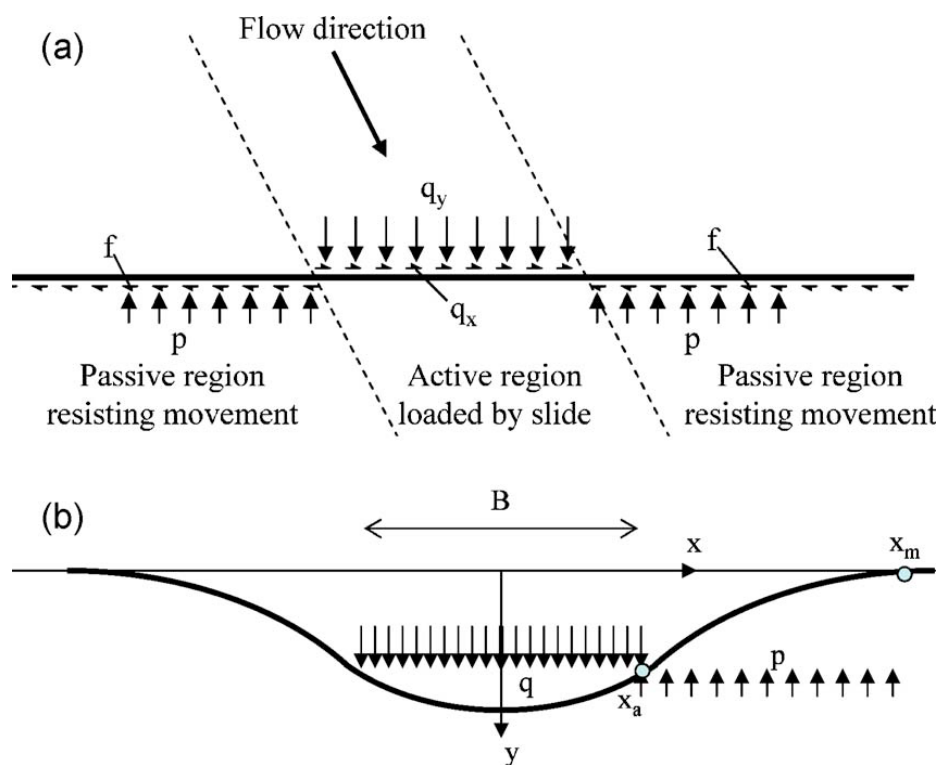


**Figure 6.1.1** Idealization of pipeline loading and deformation (Randolph et al, 2010)

An approach for performing an analysis of pipeline response to permanent ground displacement that requires representing the condition of continuous pipeline embedment by discrete axial, vertical, and horizontal soil springs is recommended in Honegger et al. (2009) and illustrated in Figure 6.1.2. Movement of the surrounding soil with respect to the buried

pipeline may force the pipeline to move with the soil or result in differential movement between the pipe and the soil. A key characteristic of soil loading is that it increases only to the point at which gross failure of the soil occurs. Capturing this characteristic requires a non-linear representation of the soil springs. The expressions for maximum soil spring force are based upon laboratory and field experimental investigations on pipeline response, as well as general geotechnical approaches for related structures such as piles, embedded anchor plates, and strip footings. Recommendations for defining soil springs for analysis of pipeline response to landslides can be found in C-CORE (2003), Honegger & Nyman (2004), O'Rourke et al. (2008), Honegger et al. (2009) and Randolph et al. (2010).

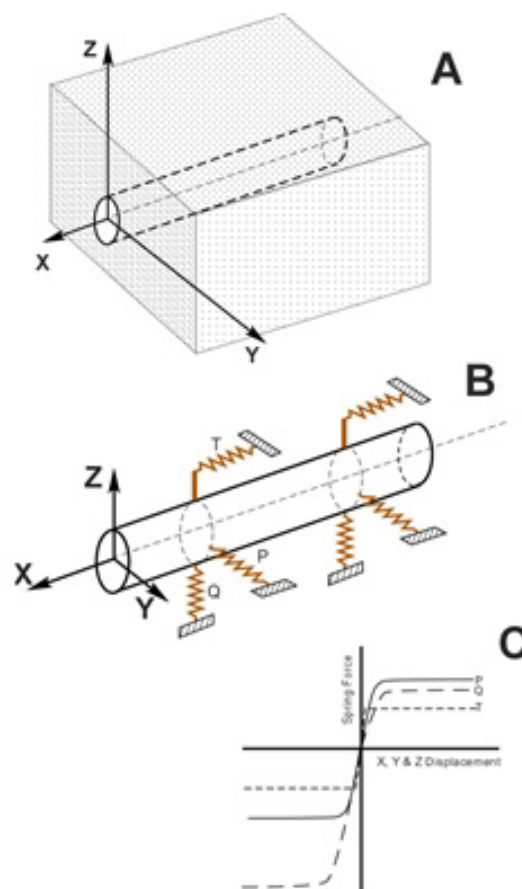


**Figure 6.1.2** Spring Analog for Analyzing Pipeline-Soil Interaction (Honegger et al., 2009)

### 6.1.2 Empirical relationships

The most commonly used empirical relations to estimate pipeline performance caused by permanent deformation are depicted in Table 6.1.1 and Figures 6.1.3 and 6.1.4.

**Table 6.1.1** Empirical relations for pipelines related to PGDs.

Empirical relation	Influence factors	Reference
Bi-linear relation	PGD (inches) Material	Porter et al. (1991))
$R.R/km. = K(7.821 * PGD^{0.56})$	PGD (m) K: indicator connected with pipe material	Honegger & Eguchi (1992)
$R.R/km = 100 * (1 - \exp(-0.283 * PGD^{1.33}))$ $R.R/km = 100 * (1 - \exp(-0.899 * PGD^{1.11}))$ $R.R/km = 100 * (1 - \exp(-0.578 * PGD^{1.55}))$ $R.R/km = 100 * (1 - \exp(-1.120 * PGD^{1.69}))$ $R.R/km = 100 * (1 - \exp(-0.743 * PGD^{0.71}))$ $R.R/km = 100 * (1 - \exp(-1.120 * PGD^{0.761}))$ $R.R/km = 100 * (1 - \exp(-0.644 * PGD^{1.37}))$ $R.R/km = 100 * (1 - \exp(-1.530 * PGD^{1.62}))$ $R.R/km = 100 * (1 - \exp(-0.961 * PGD^{1.64}))$ $R.R/km = 100 * (1 - \exp(-1.830 * PGD^{1.83}))$	PGD (m) Material Joint type	Heubach (1995)
$R.R/km. = K2 * 23.674 * (PGD)^{0.53}$	PGD (m) K2: indicator connected with pipe material and joint type	Eidinger & Avila (1999)
$R.R/km. = K2 * 11.223 * PGD^{0.319}$	PGD (m) K2: indicator connected with pipe material and joint type	ALA (2001a,b)

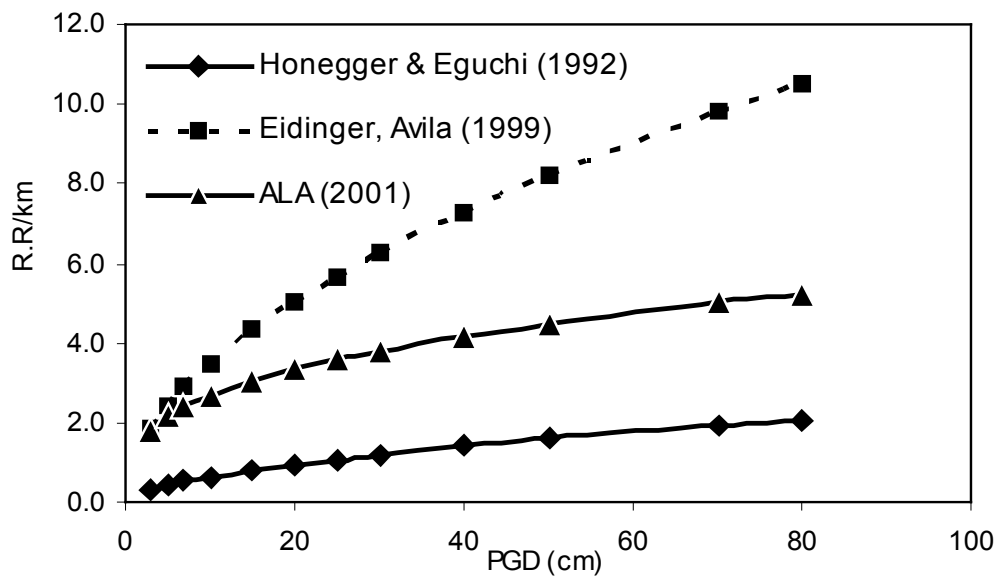


**Figure 6.1.3** Comparison between different empirical relations for pipeline failures for the case of PGDs (brittle pipes)

The above relations were validated with the observed damage (pipeline failures) of Lefkas 2003 and of Düzce 1999 earthquake. The relation of Honegger & Eguchi (1992) was found to give the best estimated results compared with the real records. The other two relations

Eidinger & Avila (1999) and ALA (2001) overestimate the damage. O'Rourke & Deyoe (2004) proposed a fragility curve that correlates the RR with ground strains (fig. 6.1.4). The ground strains used by Sano et al. (1999) were back-calculated from pre-and post- event photogrammetric analysis. Moreover, O'Rourke & Deyoe E (2004) proposed a fragility relation that accumulate both the wave propagation and the PGD repairs rates R.R. to ground strains:

$$R.R. = k_1 * 513 * \epsilon^{0.89} \quad [6.1]$$

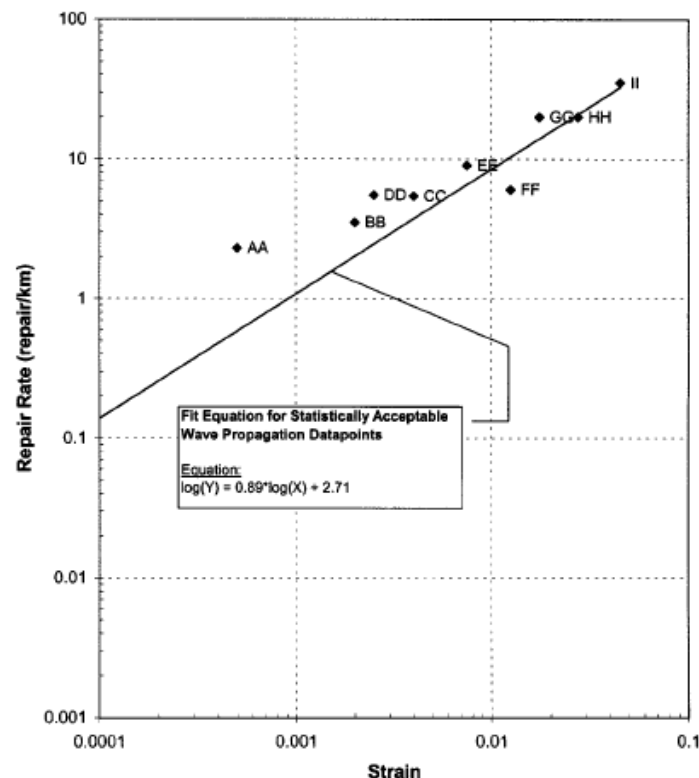


Figure 6.1.4 Pipe repair ratio R.R. vs ground strains (O'Rourke & Deyoe, 2004).

### 6.1.3 Damage states

The definition of damage state is an important factor in order to estimate the pipeline performance. ALA (2002) defines the occurrence and number of repairs using the Monte-Carlo technique. A Poisson process can be used to estimate whether or not a specific pipeline has suffered one or more breaks. According to HAZUS, for areas prone to ground failure, 80% of pipeline failure is assumed to be breaks and 20% is assumed to be leaks. Heubach (1995) considers "break" as the failure which results in the complete interruption of liquid/ solid/ gas transfer through the pipeline, while "failure" is considered to be any malfunction leading to a pipe leakage without complete interruption of liquid/ solid/ gas transfer. Rashidov et al. (2000) provide 4 damage states for pipelines subjected to the seismic loads. ATC 13 (1985) defines 7 damage states according to Repair Rate R.R. (see Table 6.1.2).

**Table 6.1.2** Pipeline damage states (ATC-13).

Description of damage state	Pipes	
	Breaks/ km	% Failures
None	0	0
Slight	0.25	0.6
Light	0.75	2
Moderate	5.5	14
Heavy	15	38
Major	30	75
Destroyed	40	100

Ballantyne & Heubach (1996) propose a different categorization of damage state (see Table 6.1.3).

**Table 6.1.3** Damage state according to Repair Rate.

Description of damage state	Repair Rate (RR/km)
No-damage	$0 \leq R.R \leq 0.001$
Low	$0.001 < R.R \leq 0.01$
Low- Moderate	$0.01 < R.R \leq 0.1$
Moderate	$0.1 < R.R \leq 0.7$
Moderate- High	$0.7 < R.R \leq 1.4$
High	$1.4 < R.R$

## **6.2 PHYSICAL VULNERABILITY OF PERSONS TO LANDSLIDES (AUTH)**

### **6.2.1 Introduction**

A literature review on physical vulnerability of persons to different landslide hazards is presented. The aim is to identify the most important factors concerning the different aspects of physical vulnerability of persons to landslides and review relative models that could be incorporated in a risk assessment framework. The critical review by Dr A. Kaynia is very much appreciated and acknowledged.

Physical vulnerability of persons to landslides comprises a complex and somewhat subjective task within a landslide risk assessment study (Dai et al. 2002). It is referred to the probability that a particular life (the element at risk) will be lost, given the person(s) is affected by the landslide hazard (AGSO, 2001; 2007). It depends on many factors such as the landslide type, size and intensity, the resistance ability of the individual persons affected by the landslide hazard and their relative position to the exposed area. For instance, it may be quite important for a fast moving landslide (debris flow, rock fall) while it is generally negligible for slow moving landslides. The resistance of the person to landslides is believed to be a function of the intellectual maturity (e.g. perception about risk) and physical ability (e.g. age) (Uzielli et al. 2008) and it is different for persons in open space, vehicles and inside buildings. Early warning system can also affect (reduce) the vulnerability of persons. Due to the complex, dynamic nature of the population, vulnerability changes over time resulting to increased variability on its estimation. Considering the large uncertainties and complexities associated with the physical vulnerability of persons to landslides, all existing methodologies (either quantitative or qualitative) are based on expert judgment and empirical data.

### **6.2.2 Review of quantitative methodologies**

Leone (1996) introduced damage matrices to assess the vulnerability of person that correlate the injury or loss of life with vulnerability values. Their effective applicability requires statistical analysis of detailed records on landslides and their consequences on the population. Michael-Leiba et al. (2000) proposed fixed vulnerability values for persons that range between 0 (none destroyed) and 1 (all destroyed) for different landslide types (hill slopes, debris flows) and considering the proximity of the person to the affected area (Table 6.2.1). Data on slope failures and associated injuries and casualties were derived from the Australian Landslide database.

**Table 6.2.1** *Vulnerability to destruction of people*

Unit	Vulnerability of resident people
Hill slopes	0.05
Units susceptible to proximal debris flow	0.9
Units susceptible to distal debris flow	0.05

Bell and Glade (2004) proposed fixed judgmentally- based vulnerability values for persons in open space and inside buildings for different landslide types (rockfalls, debris flows, snow avalanches) and for three levels of hazard/magnitude (low, medium, high). These vulnerability values were applied to a village of 300 inhabitants in NW Iceland impacted by different landslide hazards. However, their use in other risk assessment studies should be made with caution as they are basically based on local information. Wong et al. (1997), Finlay et al. (1999) and AGSO (2001,2007) suggested vulnerability values for persons based on historic records of Hong Kong for injuries and fatalities arising from landslide debris for rockfalls and debris flows, depending on where they are geographically located at the moment of the event (open space, vehicle, building). They also correlated the loss (injury or death) with these vulnerability values (Table 6.2.2).

**Table 6.2.2** *Vulnerability of a person being affected by a landslide in open space, in a vehicle and in a building (after Wong et al., 1997)*

Location	Description	Vulnerability of a person		
		Data range	Recommended value	Comment
Open space	Struck by rockfall	0.1–0.7	0.5	May be injured but death unlikely
	Buried by debris	0.8–1	1	Death by asphyxia
	Not buried, but hit by debris	0.1–0.5	0.1	High chance of survival
Vehicle	Vehicle is buried/crushed	0.9–1	1	Death almost certain
	Vehicle is damaged only	0–0.3	0.3	High chance of survival
Building	Building collapse	0.9–1	1	Death almost certain
	Building inundated with debris and person is buried	0.8–1	1	Death highly likely
	Building inundated with debris, but person is not buried	0–0.5	0.2	High chance of survival
	Debris strikes the building only	0–0.1	0.05	Virtually no danger

Uzielli et al. (2008) developed a conceptual framework for scenario-based, quantitative estimation of physical vulnerability of persons to landslides based on expert judgment and empirical data. Vulnerability was defined quantitatively as a function of landslide intensity

and the susceptibility of the population. The susceptibility of person in open space and vehicles was modeled considering three different factors depending on the population density ( $\xi_{\text{PDN}}$ ), the annual income represented as the Gross Domestic Product per capita ( $\xi_{\text{GDP}}$ ) (reference intervals adopted from World Bank's World Development Report, 2005) and the age of the population at risk ( $\xi_{\text{AGE}}$ ). Figures 6.2.1 and 6.2.2 present graphically the proposed models for population density and income factors, first discussed in the United Nations Environment Program (UNEP, 2000). It is seen that lower GDP per capita and higher population density tend to increase susceptibility and, hence, vulnerability. The susceptibility factor for population age expresses the reduced resilience (and therefore the increased vulnerability) of age categories in comparison with a reference age range (20–50 yrs) in which maximum resilience can be expected.

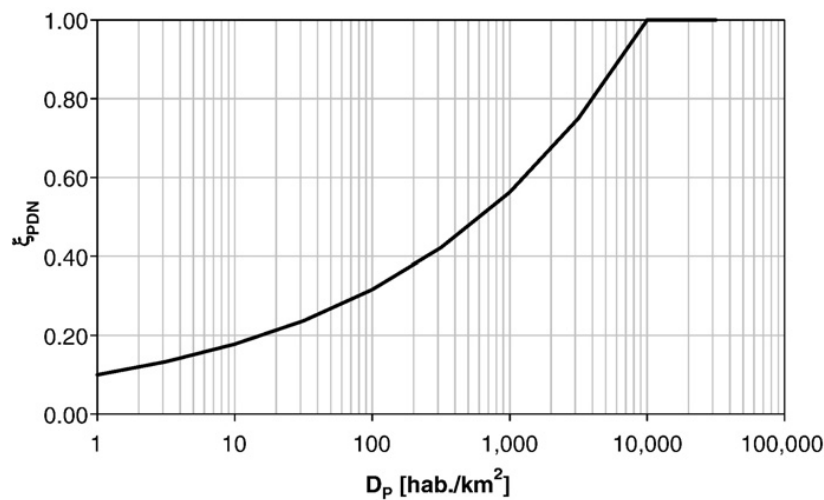


**Figure 6.2.1** Model for population density susceptibility factor (Uzielli et al., 2008)

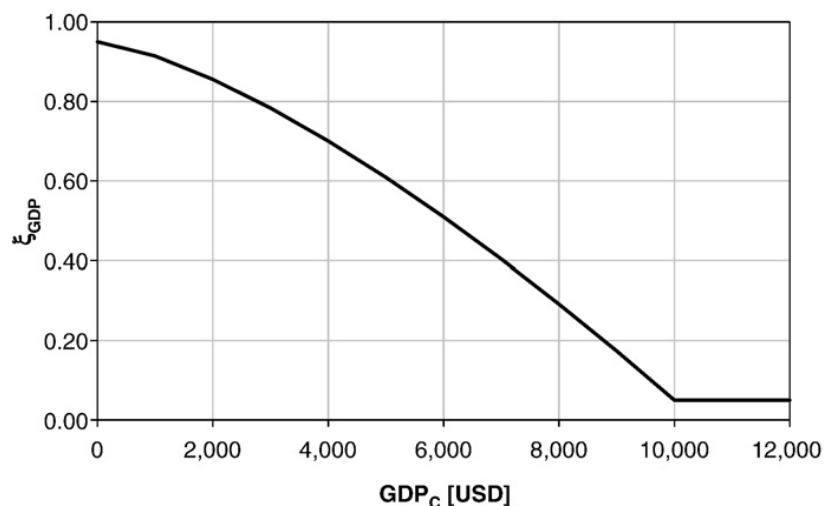


**Figure 6.2.2** Model for income susceptibility factor. (Uzielli et al., 2008)

The susceptibility of persons in structures was modeled to account for the possibility for evacuation conditioned on the post-landslide stability and serviceability of the structures

based on the work of Ragozin and Tikhvinsky, (2000). Pertinent susceptibility analytical models were proposed for all the considered factors. The method allows explicit consideration of the uncertainties in the parameters and models. Kaynia et al. (2008) explored the applicability of this methodology based on the First-Order Second-Moment (FOSM) approach to estimate landslide risks in regional scale. Li et al. (2010) based on the work of Uzielli et al. (2008) and Kaynia et al. (2008) proposed a new quantitative model to assess vulnerability of persons to landslides based on the landslide intensity and the resistance ability of the affected person. Different analytical functions have been proposed for persons in open space, vehicles and inside buildings. The vulnerability of non-stationary elements (persons in open space and vehicles) is recommended to be calculated using the sliding velocity as a measure of landslide intensity. Hence, it is considered negligible for slow moving landslides (sliding velocity  $<5 \times 10^{-1}$  mm/s) as the escape evacuation is very likely. Figure 3 shows the relation between the velocity and the dynamic intensity for persons in open space. The resistance factor for persons in open space and vehicles was given as a function of the physical factor  $\xi_{phy}$  (reflecting the physical ability to withstand a given intensity landslide) and the knowledge factor  $\xi_{kng}$  (e.g. the intellectual maturity of escaping the hazard). The vulnerability of persons in structures was associated to the vulnerability of the damaged structures using an analytical relationship. Table 6.2.3 presents the recommended average vulnerability values of persons in buildings whereas Figure 6.2.4 shows the exponential fit between the average vulnerability value of persons in structures ( $V_{p-s}$ ) and the corresponding vulnerability of structures.

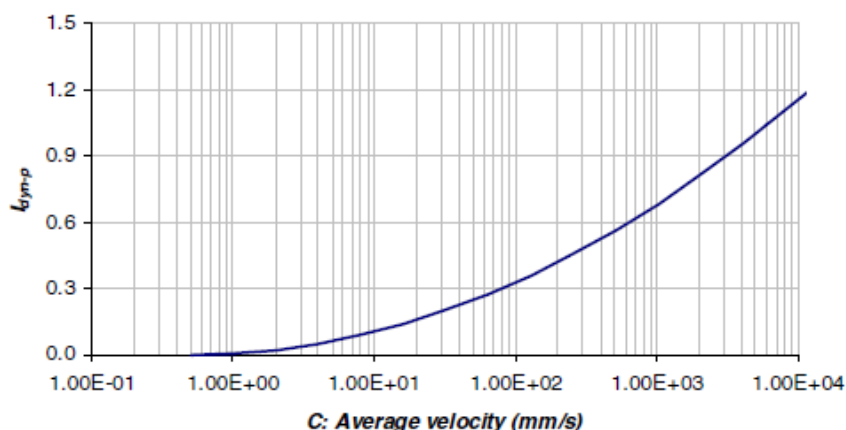


**Figure 6.2.3** Model for dynamic intensity factor for persons in open space (Li et al, 2010)

**Table 6.2.3** Vulnerability of structures and population in buildings (Li et al. 2010)

Vulnerability of structures	Population damages						Sum of PoPs
	Light injuries		Serious injuries		Fatalities		
	PoP <sup>a</sup>	PoP <sup>b</sup> (%)	PoP	Pol (%)	PoP	Pol (%)	
0.1	0.0012	85.7	0.00016	11.4	0.00004	2.9	0.0014
0.3	0.0138	85.7	0.00184	11.4	0.00046	2.9	0.0161
0.5	0.0686	85.7	0.00914	11.4	0.00229	2.9	0.08
0.7	0.2229	85.7	0.02971	11.4	0.00743	2.9	0.26
0.9	0.39	54.5	0.22	30.8	0.105	14.7	0.715
1	0.4	40	0.4	40	0.2	20	1

PoP probability of one person in structures being injured in different degrees, Pol percentage or proportion of different injury degrees to all injuries

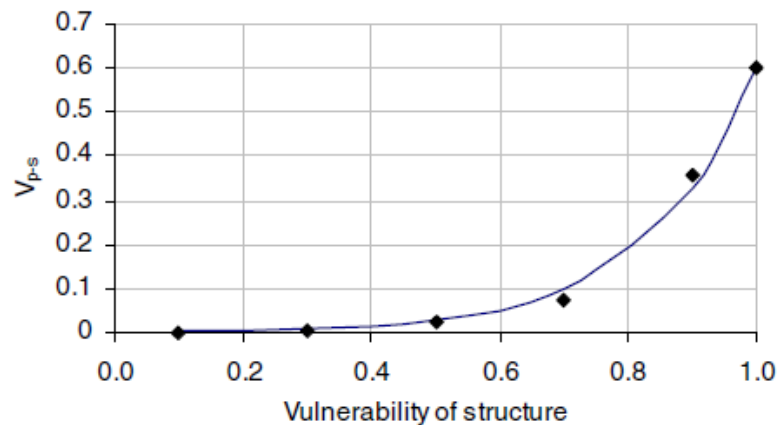


**Figure 6.2.4** Fitting curve of vulnerability of persons in structures (Li et al, 2010)

Jaisway et al. (2010) proposed a quantitative approach for landslide risk assessment along transportation lines that was applied to a road and a railway alignment in the Nilgiri hills in southern India. They proposed vulnerability values (defined as the probability of loss of life) for people in different types of moving vehicles hit by landslides of different magnitude classes (M-I, M-II, M-III) (Table 6.2.4). These were determined as a function of the landslide volume as: M-I <math>10^2 \text{ m}^3</math>,

**Table 6.2.4** Estimated vulnerability for persons in moving vehicles impacted by landslides (Jaisway et al. 2010).

Person in a moving vehicle	Landslide magnitude		
	M-I	M-II	M-III
Bus	0.001	0.1	0.8
Lorry	0.001	0.1	0.8
Car	0.01	0.1	1
Motorbike	0.5	1	1
Train	0.5	0.5	0.5

Jaisway et al (2011) proposed a quantitative procedure for estimating landslide vulnerability and risk to life and property. Ranges of possible vulnerability values (minimum, maximum and average) for persons occupying different types of buildings affected by a landslide of a given magnitude class were assigned (Table 4) based on expert opinion and historic events. Magnitude classes M-I, M-II, and M-III in the table refer to landslides with minimum to maximum landslide volumes ranging from 100 to  $1000 \text{ m}^3$  (average =  $550 \text{ m}^3$ ), from 1000 to  $10000 \text{ m}^3$  (average =  $5500 \text{ m}^3$ ), and from 10 000 to  $100000 \text{ m}^3$  (average =  $55000 \text{ m}^3$ ) respectively. Four building types were considered based on the material strength of building structure: Type-1 (tin shed), Type-2 (brick in mud without column structure), Type-3 (brick in cement with column structure), and Type-4 (reinforced concrete).

**Table 6.2.5** Vulnerability of people in buildings impacted by a landslide (Jaisway et al,2011).

Building types	Landslide magnitude class								
	M-I			M-II			M-III		
	min	avg	max	min	avg	max	min	avg	max
Type-1	0.4	0.8	1	1	1	1	1	1	1
Type-2	0.2	0.6	0.8	0.8	1	1	1	1	1
Type-3	0.1	0.4	0.6	0.6	0.8	1	1	1	1
Type-4	0	0	0.2	0.2	0.6	0.8	0.8	1	1

Das et al (2011) proposed a stochastic framework for quantifying spatio-temporal vulnerability of elements at risk to landslides. For the calculation of population vulnerability, the maximum number of persons occupying a building is considered as a Poisson equation.

$$\Pr [V_{b(i)p(j)}(s, t)] = 1 - \exp(-\gamma E_{b(i)p(j)}(s, t))$$

where the coefficient  $\gamma$  is obtained from the damage data in the study area.  $E_{b(i)p(j)}(s, t)$  is the number of persons within a building.  $V_{b(i)p(j)}(s, t)$  values were quantified using a maximum threshold of 70 people on the basis of local information.

The aforementioned model was applied in a part of the northern Himalayas in India to calculate the vulnerability values of persons occupying three different types of buildings (residential, schools, and office) at different times of the day. Figure 6.2.5 presents the temporal and spatial distribution of population vulnerability in the study area.

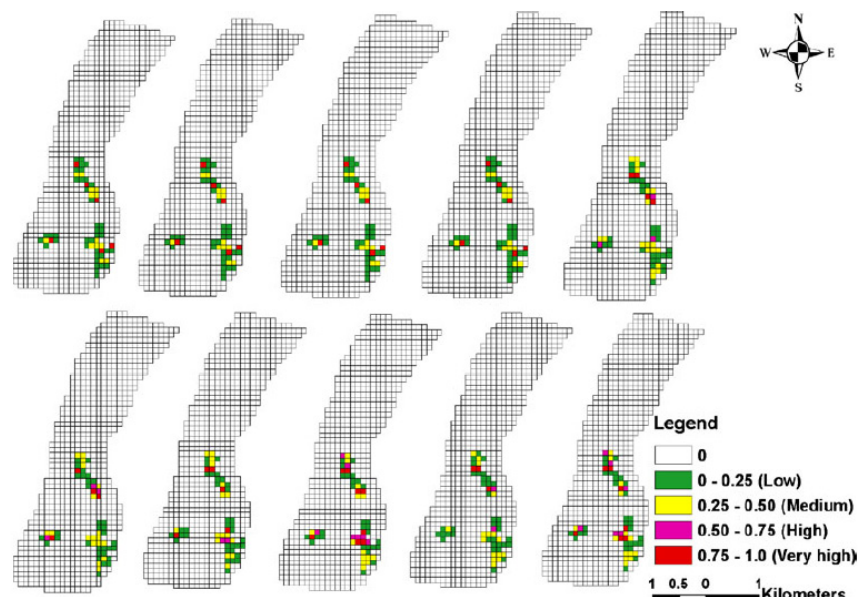


**Figure 6.2.5** Population vulnerability at different locations at different time zones of the day (clockwise from top left) (1) 0600–0800, (2) 0800–0900, (3) 0900–1000, (4) 1000–1200, (5) 1200–1400, (6) 1400–1600, (7) 1600–1700, (8) 1700–1800, (9) 1800–2000, (10) 2000–0600 hours (Das et al, 2011)

### **6.2.3 Conclusive remarks**

A review of existing methodologies to assess physical vulnerability of population to landslides has been presented. It is seen that all methods use empirical data and expert judgment to estimate vulnerability due to the large uncertainties and complexities involved. However, recently developed approaches (e.g. Uzielli et al., 2008; Li et al., 2010; Das et al., 2011) allow for the incorporation of (at least some of) these uncertainties in the models by proposing analytical functions to assess vulnerability rather than fixed vulnerability values. The use of such approaches and the development of new more advanced ones may significantly benefit from their calibration with real event data.

---

## 7 REFERENCES

- Agliardi, F., Crosta, G.B. and Frattini, P. (2006). "Integrating rockfall risk assessment and countermeasure design by 3D modelling techniques", *Natural Hazards and Earth System Sciences*, Vol. 9, pp. 1059-1073.
- AGS (2007). "Practice Note Guidelines for Landslide Risk Management 2007", *Australian Geomechanics*, Volume 42, No. 1, March, pp. 63-114.
- AGSO (2001). "Natural hazards and the risk they pose to South-East Queensland". AGSO-Geoscience Australia. Digital report on CD-ROM. 389 Pages.
- Amatruda, G., Bonnard, Ch., Castelli, M., Forlati, F., Giacomelli, L., Morelli, M., Paro, L., Piana, F., Pirulli, M., Polino, R., Prat, P., Ramasco, M., Scavia, C., Bellardone, G., Campus, S., Durville, J.-L., Poisel, R., Preh, A., Roth, W., Tentschert, E.H. (2004). A key approach: the IMIRILAND project method. In: Identification and mitigation of large landslide risks in Europe. Ch. Bonnard, F. Forlati, C. Scavia (Ed.), 13-43.
- American Lifelines Alliance (2001a). "Seismic fragility formulations for water systems" Part 1 – Guideline. ASCE-FEMA, 104 pp.
- American Lifelines Alliance (2001b). "Seismic fragility formulations for water systems" Part 2 – Appendices. ASCE-FEMA, 239 pp.
- American Lifelines Alliance (2002). "Development of Guidelines to Define Natural Hazards Performance. Objectives for Water Systems". Volume I. September, 104 pp.
- Applied Technology Council (1985). "Earthquake Damage Evaluation Data for California", Palo Alto.
- Armanini, A. (1993). "On the dynamic impact of debris flows". Proc. International workshop on debris flow. Kagoshima, Japan, pp. 89-99.
- Aubry, D., Chouvet, D., Modaressi, A., Modaressi H. (1986). GEFDYN : Logiciel d'Analyse de Comportement Mécanique des Sols par Eléments Finis avec Prise en Compte du Couplage Sol-Eau-Air, Manuel scientifique, Ecole Centrale Paris, LMSS-Mat.
- Azevedo, J., Guerreiro L., Bento R., Lopes M., Proença J., (2010). "Seismic vulnerability of lifelines in the greater Lisbon area." *Bulletin of Earthquake Engineering*, Vol. 8, pp. 157–180.
- Ballantyne, D.B, Heubach, W. (1996). "Earthquake Loss Estimation for the City of Everett Washington Lifelines", K/J/C 906014.00, Federal Way, Washington: Kennedy/ Jenks/ Chilton.
- Baoping Wen, B., Wang, S., Wang, E., Zhang, J. (2004). Characteristics of rapid giant landslides in China", *Landslides*, vol 1, pp. 247–261.
- Baxter, P. J., Boyle, R., Cole, P., Neri, A., Spence, R.J.S., Zuccaro, G., (2005). "The impacts of pyroclastic surges on buildings at the eruption of the Soufrière Hills volcano, Montserrat" *Bulletin of Volcanology* Publisher: Springer-Verlag GmbH ISSN: 0258-8900 (Paper) 1432-0819 (Online) DOI: 10.1007/s00445-004-0365-7 Issue: Volume Vol. 67, Number No. 4 Date: April 2005 Ppages.: 292 - 313
- Bell, R. and Glade, T. (2004). "Quantitative risk analysis for landslides - Examples from Bvldudalur, NW-Iceland". *Natural Hazards and Earth System Sciences*, Vol. 4, No. 1, pp. 117-131, 2004.
- Bird, J.F., Bommer, J.J., Crowley, H., Pinho, R. (2006a). "Modelling liquefaction-induced building damage in earthquake loss estimation". *Soil Dynamics and Earthquake Engineering* Vol. 26, No. 1, pp. 15-30.

- Bird, J.F., Crowley, H., Pinho, R., Bommer, J.J. (2006b). "Assessment of building response to liquefaction induced differential ground deformation". *Bulletin of the New Zealand Society for Earthquake Engineering*, Vol. 38, No. 4, pp. 215-234.
- Bouckovalas, G.D. and Papadimitriou, A.G. (2005). "Numerical evaluation of slope topography effects on seismic ground motion". *Soil Dynamics and Earthquake Engineering*, Vol. 25, No 7-10, pp. 547-558.
- Bourdeau, C. Havenith H.B. , Fleurisson J.A., Grandjean, A.G. (2004). "Numerical Modelling of Seismic Slope Stability". *Engineering Geology for Infrastructure Planning in Europe*, Springer Berlin / Heidelberg, Vol. 104, pp. 671-684.
- Bray, J.D. and Travasarou, F., (2007). "Simplified Procedure for Estimating Earthquake-Induced Deviatoric Slope Displacements". *Journal of Geotechnical and Geoenvironmental Engineering*, Vol. 133, No. 4, pp. 381-392.
- Bray, J.D., (2007). *Simplified seismic slope displacement procedures*. *Earthquake Geotechnical Engineering*, Ed. K. D. Pitilakis, 2007 Springer.
- Bucher, K., (1997). *Dynamische Berechnung von Steinschlag-einwirkungen*, *Proceedings, Schweizerische Gesellschaft für Boden und Felsmechanik*, Conference Paper Montreux.
- Burland J.B. (1995). "Assessment of risk of damage to buildings due to tunnelling and excavations". Invited special lecture. *Proc. 1<sup>st</sup> International Conference on Earthquake Geotechnical Engineering*. IS-Tokyo '95, pp. 1189-1201.
- Cascini, L., Fornaro, G., Peduto, D. (2010). "Advanced low- and full-resolution DInSAR map generation for slow-moving landslide analysis at different scales". *Engineering Geology*, 112 (1-4), 29-42, doi:10.1016/j.enggeo.2010.01.003.
- C-CORE, (2003). *Extended model for pipe soil interaction*, final report prepared for Pipeline Research Council International, C-CORE Report R-02-044-113.
- CEB, Comité Euro-International du Béton (1990). *CEB-FIP Model Code 1990*. Redwood Books. Trowbridge. Wiltshire. U.K.
- Chau, K.T., Wong, R.H.C., Wu, J.J. (2002). "Coefficient of restitution and rotational motions of rockfall impacts", *International Journal of Rock Mechanics & Mining Sciences*, Vol. 39, pp. 69-77.
- Coe, J.A., Godt, J.W., Tachker, P. (2004). *Map showing recent (1997-98 El Nino) and historical landslides, Crow Creek and vicinity, Alameda and Contra Costa Counties, California*. U.S. Geological Survey Scientific Investigations Map, SIM-2859, 16 p.
- Corominas, J., Copons, R., Moya, J., Vilaplana, J.M., Altimir, J., Amigó, J. (2005). "Quantitative assessment of the residual risk in a rock fall protected area", *Landslides*, Vol. 2, pp. 343-357.
- Crowley, H., Pinho, R., Bommer, J.J. (2004). "A probabilistic displacement-based vulnerability assessment procedure for earthquake loss estimation". *Bulletin of Earthquake Engineering*, Vol. 2, No. 2, pp. 173-219.
- Cruden, D.M., Varnes, D.J., (1996). "Landslide types and process. In "Landslides – Investigation and Mitigation", *Transportation Research Board Special Report n° 247* (A.T. Turner & R.L. Shuster Ed.), National Academy Press, Washington DC, pp. 36-75.
- Dai, F.C., Lee, C.F., Ngai, Y.Y. (2002). "Landslide risk assessment and management: an overview". *Engineering Geology*, Vol. 64, No 1, pp 65-87.
-

- Das, I., Kumar, G., Stein, A., Bagchi, A., Dadhwal, V.K. (2011). "Stochastic landslide vulnerability modeling in space and time in a part of the northern Himalayas, India". *Environmental Monitoring and Assessment*, Vol. 178, pp. 25–37.
- Du, R., Kang, Z., Chen, X., Zhu, P. (1987). "A comprehensive Investigation and Control Planning for Debris Flow in the Xiaojiang River Basin of Yunnan Province". Science Press, 287 pp.
- Duncan, J. M. and Wright, S. G., Soil strength and slope stability. JohnWiley & Sons, New-York, 2005, 312 pp.
- Dussauge-Peisser, C., Helmstetter, A., Grasso, J.-R., Hantz, D., Desvarreux, P., Jeannin, M., and Giraud, A., (2002). Probabilistic approach to rock fall hazard assessment: potential of historical data analysis, *Natural Hazards and Earth System Sciences*, Vol. 2, pp. 15-26.
- EC8, Part 5 (2002). European Standard.
- Eidinger, J., Avila, E. (1999). "Guidelines for the seismic upgrade of Water Transmission Facilities" ASCE, TCLEE, Monograph No. 15.
- Evans, S.G. and Hungr, O. (1993). "The assessment of rockfall hazard at the base of talus slopes", *Canadian Geotechnical Journal*, Vol. 30, pp. 620-636.
- Faber, M. H., (2009). Lecture Notes on Risk and Safety in Engineering, ETH Zurich.
- Faella, C. (2005). Flowslide effects on constructions. Panel Report. Proceedings of the International Conference on "Fast Slope Movements – Prediction and Prevention for Risk Mitigation", Naples (Italy). Pàtron Editore, Vol. 2, 53-61.
- Faella, C., Nigro, E., (2003). "Dynamic impact of the debris flows on the constructions during the hydrogeological disaster in Campania-1998: failure mechanical models and evaluation of the impact velocity". Proc. of the Int. Conf. on "Fast Slope Movements – Prediction and Prevention for Risk Mitigation", Napoli. Vol. 1: 179-186. Pàtron Editore.
- Federal Emergency Management Agency and National Institute of Building Sciences (2009a) Multi-hazard loss estimation methodology, HAZUS-MH MR4 user manual, prepared for the Federal Emergency Management Agency, Washington DC, United States.
- Federal Emergency Management Agency and National Institute of Building Sciences (2009b) Multi-hazard loss estimation methodology, HAZUS-MH MR4 technical manual, prepared for the Federal Emergency Management Agency, Washington DC, United States.
- Fell, R., Corominas, J., Bonnard, C., Cascini, L., Leroi, E., Savage, W.Z. (2008). "Guidelines for landslide susceptibility, hazard and risk zoning for land-use planning", *Engineering Geology*, Vol. 102, pp. 99–111.
- Ferlisi S., Pisciotta G. (2007). "A preliminary study of landslide induced property damages towards consequence analysis". Proceedings of the First North American Landslide Conference. Vail (Colorado), 3-9 June. Editors: V.R. Schuster, R.L. Schuster, A.K. Turner. AEG Publication n. 23. ISBN 978-0-975-4295-3-2. (on CD-ROM).
- Finlay, J., Mostyn, G. R., Fell, R. (1999). "Landslides: Prediction of Travel Distance and Guidelines for Vulnerability of Persons". Proc 8th. Australia New Zealand Conference on Geomechanics, Hobart. Australian Geomechanics Society, ISBN 1 86445 0029, Vol 1, pp.105-113.
- Fotopoulou, S., Pitilakis K., Anagnostopoulos, C. (2011). "Vulnerability Assessment of RC buildings due to earthquake induced slow moving slides". 5<sup>th</sup> international Conference on Earthquake Geotechnical Engineering, Santiago, Chile.
-

- 
- Fotopoulou, S., Pitilakis, K., “An analytical approach for the vulnerability assessment of RC buildings subjected to earthquake induced ground displacements”, COMPDYN 2011, III ECCOMAS Thematic Conference on Computational Methods in Structural Dynamics and Earthquake Engineering, M. Papadrakakis, M. Fragiadakis, V. Plevris (eds.) Corfu, Greece, 26–28 May.
- Fuchs, S., Heiss, K., Hübl, J. (2007). “Towards an empirical vulnerability function for use in debris flow risk assessment”. *Natural Hazards and Earth System Sciences*, Vol. 7, pp. 495-506.
- Galli, M., Guzzetti, F. (2007). “Landslide Vulnerability Criteria: A Case Study from Umbria, Central Italy”. *Environ Manage*, 40:6, 49–664 DOI 10.1007/s00267-006-0325-4.
- Giani, G. P., Giacomini, A., Migliazza, M., and Segalini, A., (2004). “Experimental and Theoretical Studies to Improve Rock Fall Analysis Protection Work Design”, *Rock Mechanics and Rock Engineering*, Vol 37, No. 5, pp. 369-389.
- Giovinazzi S. and King A. (2009). “Estimating seismic impacts on lifelines: an international review for RiskScape”, *Proc. of 2009 NZSEE Conference*, New Zealand, April 2009.
- Glade, T. (2003). “Vulnerability assessment in landslide risk analysis”. *Die Erde*, Vol. 134 , No. 2, pp. 123-146.
- Glade, T., Crozier, M.J. (2005). The nature of landslide hazard and impact. In: Glade T, Anderson MG, Crozier MJ (eds) *Landslide hazard and risk*. Wiley, Chichester, pp 43–74.
- Gutenberg, B., and Richter, F., (1949). *Seismicity of the earth and associated phenomena*, Princeton University Press, Princeton, New Jersey.
- Heidenreich, B., (2004). Small- and half scale experimental studies of rockfall impacts on sandy slopes, No. 3059, Ecole Polytechnique Fédérale de Lausanne.
- Heubach, W. (1995). “Seismic Damage Estimation for Buried Pipeline Systems”, *Proceedings of the Fourth US Conference on Lifeline Earthquake Engineering*, TCLEE, Monograph No.6, ASCE, pp. 312-319.
- Heubach, W. (1995). “Seismic Damage Estimation for Buried Pipeline Systems” *Proceedings of the Fourth US Conference on Lifeline Earthquake Engineering*, TCLEE, Monograph No.6, ASCE, pp312-319.
- Honegger, D. G, Eguchi, R.T. (1992). Determination of the Relative Vulnerabilities to Seismic Damage for Dan Diego Country Water Authority [SDCWA] Water Transmission Pipelines.
- Honegger, D., Gailing, R., Hart, J., Phillips, R., Popelar C. (2009). “Guidelines for managing risks to pipelines through landslide and subsidence hazard areas”, 17th JTM, 11/15 May 2009, Milan
- Honegger, D.G., Nyman, D.J., (2004). Seismic design and assessment of natural gas and liquid hydrocarbon pipelines, Pipeline Research Council International, Inc., No. L51927.
- Hovius, N., Stark, C. P., and Allen, P. A., (1999). Sediment flux from a mountain belt derived by landslide mapping, *Geology*, **25**(, 33), pp. 231-238.
- Hungr, O. Evans, S. G., and Hazzard, J., (1999). Magnitude and frequency of rock falls and rock slides along the main transportation corridors of southwestern British Columbia, *Canadian Geotechnical Journal*, **36**, pp. 224-238.
- Hungr, O., Morgan, G.C., Kallerhals, R. (1984). “Quantitative analysis of debris torrent hazard for design of remedial measures”, *Canadian Geotechnical Journal*, Vol. 21, pp. 663-677.
- Itasca Consulting Group (2004). Particle Flow Code in 2 Dimensions (PFC- 2D), version 3.10. User’s manual.
-

- Itasca Consulting Group, Inc. (2005). *FLAC (Fast Lagrangian Analysis of Continua)*, ver. 5.0. Itasca Consulting Group, Inc., Minneapolis.
- Jaiswal, P., Westen, C.J. van., Jetten, V. (2010). "Quantitative assessment of direct and indirect landslide risk along transportation lines in southern India." *Nat. Hazards Earth Syst. Sci.*, Vol. 10, pp. 1253–1267.
- Jaiswal, P., Westen, C. J. van., Jetten, V. (2011). "Quantitative estimation of landslide risk from rapid debris slides on natural slopes in the Nilgiri hills, India." *Nat. Hazards Earth Syst. Sci.*, Vol. 11, pp. 1723–1743.
- JCSS (2001). Probabilistic Model Code, Joint Committee on Structural Safety. Available online: [www.jcss.ethz.ch](http://www.jcss.ethz.ch).
- JCSS (2008). Risk Assessment in Engineering, Joint Committee on Structural Safety. Available online: [http://www.jcss.ethz.ch/publications/JCSS\\_RiskAssessment.pdf](http://www.jcss.ethz.ch/publications/JCSS_RiskAssessment.pdf)
- Jibson, R.W. and Jibson, M.W. (2003). Java programs for using Newmark's method and simplified decoupled analysis to model slope performance during earthquakes. US Geological Survey Open File Report: 03-005.
- Kappos, A. J., Panagopoulos, G. (2010). "Fragility curves for reinforced concrete buildings in Greece." *Structure and Infrastructure Engineering*, Vol. 6, No.1, pp. 39-53.
- Kappos, A. J., Panagopoulos, G., Panagiotopoulos, Ch., Penelis, Gr. (2006). "A hybrid method for the vulnerability assessment of R/C and URM buildings", *Bull. of Earthquake Engineering*, Vol. 4, No. 4, pp. 391-413.
- Kaynia, A., Papatoma-Köhle, M., Neuhaeuser, B., Ratzinger, K., Wenzel, H., Medina-Cetina, Z. (2008). "Probabilistic Assessment of Vulnerability to Landslide: Application to the village of Lichtenstein, Baden-Württemberg, Germany." *Engineering Geology*. Vol. 101, pp. 33-48.
- Kramer S.L., Stewart J.P. (2004). Geotechnical Aspects of Seismic Hazards. In: *Earthquake Engineering: from Engineering Seismology to Performance-Based Engineering*, Y. Bozorgnia, V. Bertero (Eds.), CRC Press, 4, 85 pp.
- Ktenidou, O.-J. (2010). Theoretical and instrumental study of site and topographic effects on strong ground motion in Aegion. Ph.D. thesis, Aristotle University Thessaloniki, Greece.
- Lee, S.-G., Winter, M. G. (2010). "The effects of debris flow in the Republic of Korea and some issues for successful management and mitigation", *Geologically Active: Proceedings, 11th IAEG Congress* (Eds: Williams, A. L., Pinches, G. M., Chin, C. Y., McMorran, T. M., Massey, C. I.), 1243-1250. London: CRC Press.
- Leone, F., Asté, J.P., Leroi, E., (1996). Vulnerability assessment of elements exposed to mass-movement: working toward a better risk perception. In: Senneset, K. (Ed.), *Landslides-Glissements de Terrain*, vol. 1. Balkema, Rotterdam, pp. 263–269.
- Leroueil S., Vaunat J., Picarelli L., Locat J., Lee H.J., Faure, R. (1996). Geotechnical characterization of slope movements. *Proc. 7th Int. Symp. on Landslides, Trondheim*, v.1, 53-74.
- Li, Z., F. Nadim, Huang H., Uzielli, M., Lacasse, S. (2010). "Quantitative vulnerability estimation for scenario-based landslide hazards." *Landslides*, pp. 1-10.
- Lichtenan, C. (1973). Die Berechnung von sperren in beton und eisenbeton, *Kolloquium on torrent dams ODC 384.3*, Mitteilungen der forstlichen bundes versuchsanstalt, Wien.
- Lindley, D.V., (1965). *Introduction to Probability and Statistics from a Bayesian Viewpoint*. Vol. 1 & 2. Cambridge University Press.
-

- 
- Liu, X. (2006). "Site-specific Vulnerability Assessment for Debris Flows: Two Case Studies" *Journal of Mountain Science*, Vol. 3, No. 1, pp. 20~27.
- Cardinali, M., Galli M., Guzzetti F., Ardizzone F., Reichenbach P., Bartoccini P. (2006). "Rainfall induced landslides in December 2004 in south-western Umbria, central Italy: types, extent, damage and risk assessment". *Natural Hazards and Earth System Sciences*, Vol 6, pp. 237–260.
- Mander, J.B., Priestley, M.J.N., Park, R. (1988). "Theoretical stress-strain model for confined concrete", *Journal of Structural Engineering*, Vol. 114, No. 8, pp. 1804-1826.
- Maquaire, O., Thiery, Y., Malet, J.-P., Weber, C., Puisant, A., Wania, A. (2004). Current practices and assessment tools of landslides vulnerability in mountains basins – identification of exposed elements with a semi-automatic procedure. In: Proc. of the IX International Symposium on Landslides, Lacerda, Ehrlich, Fontoura & Sayão (eds), 1, A.A. Balkema Publishers, pp. 171-176.
- Matsushita, T., Ikeya, H. (1992). Methods for evaluation of debris flow counter measure. Proceedings of the International Symposium INTERPAEVENT 1992, Bern, pp. 337-348.
- Mavrouli, O. and Corominas, J. (2010a). "Vulnerability of simple reinforced concrete buildings in front of the rockfall impact", *Landslides*, Vol. 7, No. 2, pp. 169-180.
- Mavrouli, O. and Corominas, J. (2010b). "Rockfall vulnerability assessment for reinforced concrete buildings, *Natural Hazards and Earth System Sciences*", Vol. 10, No. 10, pp. 2055-2066.
- Mejia, L.H., Dawson, E.M. (2006). Earthquake Deconvolution for FLAC. Proc. 4th International FLAC Symposium, Madrid, Spain, 211-219.
- Melchers, R.E. (2002). *Structural Reliability Analysis and Prediction*. John Wiley & Sons.
- Michael-Leiba, M., Baynes, F., Scott, G. (2000). "Quantitative landslide risk assessment of Cairns, Australia", in E. Bromhead, N. Dixon and M-L. Ibsen (eds.), *Landslides in Research, Theory and Practice*, 3 volumes, Proceedings of VIII International Symposium on Landslides, Cardiff, Wales, 26–30 June 2000, Thomas Telford, London 2, pp. 1059–1064.
- Milne, F. D., Werritty, A., Davies, M. C. R., Browne, M. J. (2009). "A recent debris flow event and implications for hazard management", *Quarterly Journal of Engineering Geology and Hydrogeology*, 42(1), 51-60.
- Milutinovic, Z.V., Trendafiloski, G.S. (2003). WP4: Vulnerability of current buildings. Risk-UE Project: An advanced approach to earthquake risk scenarios with applications, <http://www.risk-ue.net>.
- Montani, S., Descoeurdes, F., (1996). Etude expérimentale de la chute de blocs impactant une dalle en béton armé recouverte par des matériaux amortissants, Mandat 98/92 Publ. OFR No.524, Swiss Federal Institute of Technology, EPF Lausanne.
- Mouroux. P., Le Brun, B. (2006). Presentation of RISK-UE Project, *Bull. of Earthquake Engineering*, V. 4, No. 4, 323-339.
- Muttoni, A., (2003). Einführung in die Norm SIA 262, Dokumentation D 0182, Swiss Society of Engineers and Architects (SIA), pp. 47-65.
- National Institute of Building Sciences (NIBS), (2004). "HAZUS-MH: Users's Manual and Technical Manuals". Report prepared for the Federal Emergency Management Agency, Washington, D.C.
- Negulescu, C. Foerster, E. (2010), "Parametric studies and quantitative assessment of the vulnerability of a RC frame building exposed to differential settlements", *Natural Hazards and Earth System Sciences*, Vol. 10, 1781-1792, doi: 10.5194/nhess-10-1781-2010.
-

- Newmark, N.M., (1965). "Effects of earthquakes on dams and embankments". *Geotechnique*, Vol. 15, pp. 139–160.
- O'Rourke, M., Deyoe, E. (2004). "Seismic Damage to segmented buried pipe", *Earthquake Spectra*, Vol.20, No.4, pp. 1167-1187.
- O'Rourke, T.D., Jezerski, J. M., Olson, N. A., Bonneau, A.L., Palmer, M.C., Stewart, H.E., O'Rourke, M. J., and Abdoun, T., (2008). "Geotechnics of pipeline system response to earthquakes," *Proceedings of Geotechnical Earthquake Engineering and Soil Dynamics IV*.
- O'Rourke, T.D., Toprak, S., Sano, Y. (1998) "Factors affecting water supply damage caused by the Northridge earthquake.", *Proceedings of the Sixth US National Conference on Earthquake Engineering*. [CD-ROM].
- O'Rourke, T.D., Toprak, S., Sano, Y. (1998). "Factors affecting water supply damage caused by the Northridge earthquake.", *Proceedings of the Sixth US National Conference on Earthquake Engineering*. [CD-ROM].
- Peng, W.F., Wang, C.L., Chen, S.T., Lee S.T. (2009). "Incorporating the effects of topographic amplification and sliding areas in the modeling of earthquake-induced landslide hazards, using the cumulative displacement method". *Computers and Geosciences*, Vol. 35, No. 5, pp. 946-966.
- Picarelli, L. (2010). "Discussion on "A rapid loess flowslide triggered by irrigation in China" by D. Zhang, G. Wang, C. Luo, J. Chen, and Y. Zhou", *Landslides*, Vol. 7, pp. 203-205.
- Pisciotta, G. (2008). Physical vulnerability of elements at risk in landslide prone areas. PhD Thesis, University of Salerno.
- Pitilakis K. et al. (2011). "Case studies of environmental and societal impact of landslides –Part A: Case studies for environmental (physical) vulnerability". Deliverable 2.7 in EU FP7 research project No 226479 SafeLand – living with landslide risk in Europe: Assessment, effects of global change, and risk management strategies.
- Pitilakis, K., Alexoudi, M., Argyroudis S., Monge O., Martin C. (2006a). "Vulnerability and Risk Assessment of Lifelines." *Assessing and Managing Earthquake Risk*, Vol. 2, pp. 185-211.
- Pitilakis, K., Alexoudi, M., Argyroudis, S., Monge, O., Martin, C. (2006b). "Earthquake risk assessment of lifelines." *Bulletin of Earthquake Engineering*, Vol. 4, No 4, pp. 365-390.
- Pitilakis, K.D. ,*Geotechnical Earthquake Engineering*. Ziti Publications, 2010. (in Greek)
- Polese, M., Verderame, G. M., Mariniello, C., Iervolino, I., and Manfredi, G. (2007). "Vulnerability curves for gravity load designed RC buildings in Naples – Italy", *Journal of Earthquake Engineering*, Vol. 12, No. 2, pp. 234–245.
- Porter, K.A., Scawthorn, C., Honegger, D.G, O'Rourke, T.D, Blackburn, F. (1991). "Performance of Water Supply Pipelines in Liquefied Soil", *Proceedings 4th US – Japan Workshop on Earthquake Disaster Prevention for Lifeline Systems*, NIST Special Publication 840.
- Ragozin A.L., Tikhvinsky I.O. (2000). "Landslide hazard, vulnerability and risk assessment." In: Bromhead, E., Dixon, N., Ibsen, M.-L. (Eds.), *Landslides. In: Research, Theory and Practice. Proceedings of the 8th International Symposium on Landslides*, Cardiff, 26–30 June 2000, pp. 1257–1262.
- Randolph, M.F., Seo, D., White, D.J. (2010). "Parametric Solutions for Slide Impact on Pipelines" *Journal of Geotechnical and Geoenvironmental Engineering*, Vol. 136, pp. 940-949.
-

- Rashidov, T. E., Kuzmina, A., Mirjalilov, I., Rashidov (2000). "Vulnerability of Lifeline Systems in Tashkent, Uzbekistan", Proceedings of 6th Conference on Seismic Zonation, Palm Springs (CA), Balkema.
- Remennikov, A.M., Kaewunruen, S. (2006). "Impact resistance of reinforced concrete columns: experimental studies and design considerations". Proc. of 19th Australasian Conference on the Mechanics of Structures and Materials. 29 November – 1 December 2006. Christchurch. New Zealand. 817-824.
- Remondo, J., Bonachea, J., Cendrero, A. (2005). "A statistical approach to landslide risk modelling at basin scale: from landslide susceptibility to quantitative risk assessment". Landslides, Vol. 2, pp. 321-328.
- Sano, Y., O'Rourke, T., Hamada, M. (1999). "GIS evaluation of Northridge earthquake ground deformation and water supply damage" Proceedings of the 5th US Conference on Lifeline Earthquake Engineering, TCLEE Monograph #16, ASCE, pp.832-839
- Schellenberg, K. (2008). On the design of rockfall protection galleries. Ph. D. Thesis, ETH Zurich.
- Schubert, M. (2009). Konzepte zur informierten Entscheidungsfindung im Bauwesen. Ph. D. Thesis, ETH Zurich.
- Schubert, M. and Straub, D. (2008). Modeling and managing uncertainties in rock-fall hazards. Georisk, Vol. 2, No. 1, pp. 1-15.
- Schubert, M., Faber, M.H., Jacquemoud, J. and Straub, D. (2010). RiskNow - Falling Rocks Excel®-basiertes Werkzeug zur Risikoermittlung bei Steinschlagschutzgalerien. Report prepared for the Swiss Federal Road Authority (ASTRA).
- Schubert, M., Straub, D. and Faber, M.H. (2005). Reliability of rock-fall protection galleries - A case study with a special focus on the uncertainty modelling. Proceedings ICOSSAR'05, 9th International Conference on Structural Safety and Reliability, Rome, Italy.
- Scotton, P., Deganutti, A. M. (1997). "Phreatic line and dynamic impact in laboratory debris flow experiments". Proceedings of the First International Conference on Debris-Flow. Hazard Mitigation: Mechanics, Prediction and Assessment, San Francisco, pp. 777-786.
- SeismoSoft, (2007). SeismoStruct – A computer program for static and dynamic nonlinear analysis of framed structures, (online): Available from URL: [www.seismosoft.com](http://www.seismosoft.com)
- Sezen, H. (2008). "Shear deformation model for reinforced concrete columns. Structural Engineering and Mechanics". Vol. 28, No. 1, pp. 39-52.
- Sheidegger, A.E.(1975). Physical aspects of natural catastrophes. New York: John Wiley & Sons.
- Shinozuka, M. Statistical analysis of bridge fragility curves. In Proceedings of the US-Italy Workshop on protective systems for bridges, New-York, 1998.
- Shinozuka, M., Feng, M. Q., Lee, J. and Naganuma, T. (2000). "Statistical analysis of fragility curves. Journal of Engineering Mechanics", ASCE, Vol. 126, No. 12, pp.1224–1231.
- Skempton, A.W., Mac Donald, D.H. (1956). "Allowable Settlement of Structures". Proc. Institute of Civil Engineers, Part III, Vol. 5, pp. 727-768.
- Soeters, R., van Westen, C.J. (1996). "Slope instability recognition, analysis and zonation". In A.K. Turner and R.L. Schuster (eds.). Landslides Investigation and Mitigation. TRB Special Report 247, National Academy Press, Washington D.C., pp. 129-177.
-

- Spence, R.J.S., Baxter, P.J., Zuccaro, G. (2004a). "Building vulnerability and human casualty estimation for a pyroclastic flow: a model and its application to Vesuvius". *J Volcanol Geotherm Res*, Vol. 133, pp. 321–343.
- Spence, R.J.S., Zuccaro, G., Petrazzuoli, S., Baxter, P.J. (2004b). "The resistance of buildings to pyroclastic flows: analytical and experimental studies and their application to Vesuvius". *Natural Hazards Review*, Vol 5, pp. 48–59
- Swanson, R., Jones, W. (1982). "Mudslide effects on offshore pipelines." *Transp. Engrg. J.*, 108\_6\_, 585–600.
- Sweeney, M., Gasca, A., Garcia Lopez, M., Palmer, A. (2004). "Pipelines and landslides in rugged terrain: A database, historic risks and pipeline vulnerability." *Proc., Int. Conf. on Terrain and Geohazard Challenges Facing Onshore Oil and Gas Pipelines*, Thomas Telford, London, 641–659.
- Terzi, B., Alexoudi, M., Chatzigogos, T., (2008). "Fragility curves for ductile pipelines due to permanent ground deformation. Sensitivity analyses", 3o Greek Conference on Antiseismic Engineering & Technical Seismology, 5-7 November 2008, Athens, p. 1812 (in Greek).
- Toyos G., Oppenheimer C., Pareschi M.T., Sulpizio R., Zanchetta G., Zuccaro G. (2003) "Building damage by debris flows in the Sarno area, southern Italy – in Debris Flow Hazards Mitigation: Mechanics, Prediction, and Assessment. pp.1209-1220 Edited by Dieter Rickenmann & Cheng-Lung Chen - 2003 Millpress, Rotterdam, ISBN 90 77017 78 X.
- Tsang H, Lam N. (2008). "Collapse of Reinforced Concrete Column by Vehicle Impact". *Computer-Aided Civil and Infrastructure Engineering*. Vol. 23, No. 6, pp. 427-436.
- United Nations Environment Programme — UNEP, 2000. *Insight on common/key indicators for global vulnerability mapping*. Expert Meeting on Vulnerability and Risk Analysis and Indexing, Geneva, September 11–12, 2000.
- Uzielli, M., Nadim, F., Lacasse, S., Kaynia, A.M. (2008). "A conceptual framework for quantitative estimation of physical vulnerability to landslides", *Eng. Geol.* Vol. 102, pp. 251–256.
- Van Westen, C.J. (2004). "Geo-Information tools for landslide risk assessment: an overview of recent developments". *Proceedings of the IX International Symposium on Landslides*, Lacerda, Ehrlich, Fontoura & Sayão (eds.), 1, A.A. Balkema Publishers, pp. 39-56.
- Varnes, D.J., (1984). "Landslides hazard zonation: A review of principles and practice". UNESCO, Paris.
- Viscardi, A. (2010). *Gli effetti indotti sul costruito da frane a cinematica lenta*. PhD Thesis, University of Salerno.
- Vitolo, E. (2009). *Analisi degli effetti indotti dai fenomeni di flusso rapido*. PhD Thesis, University of Salerno.
- Voellmy, A. (1955). *Über die Zerstörungskraft von Lawinen Schweiz*. *Bauzeitung*, Vol. 73, pp. 212-285
- Whitman, R. V., Reed, J. W., Hong, S. T. (1973). *Earthquake damage probability matrices*, Proc. of the Fifth World Conference on Earthquake Engineering, Roma.
- Wieczorek, G.F. and Snyder, J.B. (2010). "Historical rock falls in Yosemite National Park", *US Geol. Surv. Open-File Report 03-491*, 2004. [pubc.usgs.gov](http://pubc.usgs.gov) (last accessed on august 2010).
-

- Winter, M. G., Macgregor, F., Shackman, L. (2005). "Scottish Road Network Landslides Study", 119p. Trunk Roads: Network Management Division Published Report Series. Edinburgh: The Scottish Executive.
- Winter, M. G., Heald, A. P., Parsons, J. A., Macgregor, F., Shackman, L. (2006). "Scottish debris flow events of August 2004", *Quarterly Journal of Engineering Geology and Hydrogeology*, 39(1), 73-78.
- Winter, M. G., F Macgregor, F. Shackman, L. (2008). "Scottish road network landslides study: implementation", 278p. Transport Scotland Published Report Series. Edinburgh: Transport Scotland.
- Winter, M. G., Dent, J., Macgregor, F. Dempsey, P., Motion, A., Shackman, L. (2010). "Debris flow, rainfall and climate change in Scotland", *Quarterly Journal of Engineering Geology & Hydrogeology*, 43(4), 429-446.
- Wong, H.N., Ho, K.K.S., Chan, Y.C. (1997). Assessment of consequence of landslides. Proceedings of the International Workshop on Landslide Risk Assessment, Honolulu, Hawaii (USA), A.A. Balkema Publishers, pp.111-147.
- Zuccaro, G, Petrazzuoli, S.M. (2004). "Structural Resistance of RC Buildings under Pyroclastic Flows: A Study on the Vesuvian Area", *Jour. of Volcanological and Geoth. Research*.
- Zuccaro, G. et al., (2000). Final Report European Project ENV4-CT98 0699: "Human and Structural Vulnerability Assessment for Emergency Planning in Future Eruptions of Vesuvius using Volcanic Simulations and Casualty Modeling". Directorate XII Commission. EU. June, 2000.
- Zuccaro, G., Cacace, F., Spence, R.J.S., Baxter, P.J., (2008). "Impact of explosive eruption scenarios at Vesuvius", *Journal of Volcanology and Geothermal Research*, Vol. 178, pp. 416–453.
- Zuccaro, G., Petrazzuoli, S.M. (2003). "Structural Vulnerability to Pyroclastic and Debris Flows", Proceedings of the International Conference on: Fast Slope Movements-Prediction and Prevention for Risk Mitigation, Sorrento, May 11 – 13.

## 8 APPENDICES

### 8.1 APPENDIX I: QUESTIONNAIRE AND RESPONSES FOR ROADS AND DEBRIS FLOW

#### 8.1.1 Questionnaire

##### *8.1.1.1 Introduction*

The EU FP 7 project SafeLand includes some fundamental work to develop quantitative risk assessment methods for landslides. One innovative facet of this work is the development of fragility curves to assess the vulnerability of elements, including roads, due to landslides. Fragility curves are developed by assessing the probability of certain damage states being met or exceeded as a consequence of some event i.e. a landslide of a particular magnitude/intensity/volume or other measurable character. The fragility curves which will be produced will be similar to those used for different assets in earthquake engineering.

The purpose of this questionnaire is to establish the views of practitioners on this subject. That is, for a given volume of material deposited on a road following a debris flow, what is the probability of certain damage states being exceeded?

We would be much obliged if you could take the time to complete the Probability Tables using your expert judgement. Information is provided on the following explanation sheet to allow the tables to be completed.

We also ask that you rate your personal experience of debris flow and road vulnerability, based on a scale of 0 to 10 where 0 represents no experience and 10 represents extensive experience. In order that we understand the uncertainties associated with increased landslide volumes we ask that you provide an indication of your confidence in assigning probabilities to each landslide volume.

For each landslide volume we also ask that you give some indication of the frequency of events in your geographic area.

Furthermore, it would be much appreciated if you could take the time to respond to the three questions which follow the tables.

By working with practitioners we hope to produce the foundations of a valuable tool for assessing the vulnerability of roads to landslides.

### *8.1.1.2 Explanation Sheet*

#### **1. Landslide Volume**

For the purposes of this assessment five landslide volume categories have been proposed in order to give as broad a view of landslide hazard as possible. The landslide volumes used are:

- <math> < 10 \text{ m}^3 </math>
- <math> 10 \text{ m}^3 </math>
- <math> 100 \text{ m}^3 </math>
- <math> 1,000 \text{ m}^3 </math>
- <math> 10,000 \text{ m}^3 </math>
- <math> 100,000 \text{ m}^3 </math>

It has been assumed that the volume of landslide debris refers to the volume of landslide deposited at the level of the road. Factors including the initial slope geometry, soil characteristics, and triggering mechanisms will be considered in a preliminary stage. In order to simplify the analysis a segment of road 500m long will be considered.

#### **2. Road Characterisation**

The roads under consideration are:

- High speed
  - 80-110km/h speed limit
  - At least one lane running in each direction, most likely in conjunction with a hard strip
- Local
  - Speed limit typically <math> < 50 \text{ km/h} </math>
  - One lane running in each direction or single-track
  - May be paved (bituminous, unreinforced or reinforced concrete) or unpaved

### 3. Damage States and Definitions

The damage states to be considered are:

**Table 1.** Damage state definition

Damage State	High Speed Roads	Local Roads
P1 (Limited damage)	Encroachment limited to verge/hardstrip	Partial blockage of carriageway
P2 (Serious damage)	Blockage of hardstrip and one running lane	Complete blockage of carriageway and/or damage to ancillaries
P3 (Destroyed)	Complete blockage of carriageway and/or repairable damage to surfacing	Complete blockage of carriageway and/or damage to surfacing. For unpaved roads the surfacing may remain damaged but passable at reduced speeds post clean-up

### 4. Description of Probabilities

Using expert judgement, the probability of each damage state being exceeded should be assigned using the qualitative descriptors given below. The descriptors have been coded A-G in order to assist with completion of the Probability Tables, and correspond to values which will be used to construct the fragility curves.

The qualitative descriptors “Highly Improbable” and “Extremely Unlikely” should be used with caution, and only where an extensive, high quality dataset supports the classification.

**Table 2.** Description of probabilities

Qualitative Descriptor	Description	Qualitative Descriptor Code	Values for Analysis
Highly improbable	Damage state almost certainly not exceeded, but cannot be ruled out	A	0.000001
Improbable (remote)	Damage state only exceeded in exceptional circumstances	B	0.00001
Very unlikely	Damage state will only be exceeded in very unusual circumstances	C	0.0001
Unlikely	Damage state may be exceeded, but would not be expected to occur under normal circumstances	D	0.001
Likely	A good chance the damage state may be exceeded under normal circumstances	E	0.01
Very likely	Damage state expected to be exceeded	F	0.1
Extremely likely	Damage state almost certainly exceeded	G	1.0

*8.1.1.3 Questionnaire*

**First Name:**

**Family Name:**

**Organization/Institute:**

**I. Probability Tables**

Please complete the following tables and designate qualitative probability descriptors to each category using the **codes A-G** (Table 2 in Explanation sheet). Feel free to add comments as you feel necessary.

**Table I.1** High Speed Roads

Landslide Volume (m <sup>3</sup> )	Probability of Exceeding Damage State		
	Limited Damage	Serious Damage	Destroyed
<10			
10			
100			
1,000			
10,000			
100,000			

**Table I.2** Local Roads

Landslide Volume (m <sup>3</sup> )	Probability of Exceeding Damage State		
	Limited Damage	Serious Damage	Destroyed
<10			
10			
100			
1,000			
10,000			
100,000			

## II. Experience Rating

Please rate your experience on a scale from 0 to 10.

**Table II** Experience Rating

No experience										Extensive experience
0	1	2	3	4	5	6	7	8	9	10

## III. Confidence Rating

Rate your degree of confidence on a scale from 0 to 10 on the estimates for each landslide volume.

**Table III** Confidence Rating

Landslide Volume (m <sup>3</sup> )	Degree of Confidence (0: none, 10: absolute)
<10	
10	
100	
1,000	
10,000	
100,000	

## IV. Frequency of Events

For each landslide volume please place a mark in the box which best describes the frequency of occurrence in your geographic region.

**Table IV** Frequency of Events

Landslide Volume (m <sup>3</sup> )	Every year	1 in 10 years	Every 10s of years	Every 100s of years
<10				
10				
100				
1,000				
10,000				
100,000				

## V. OPTIONAL QUESTIONS

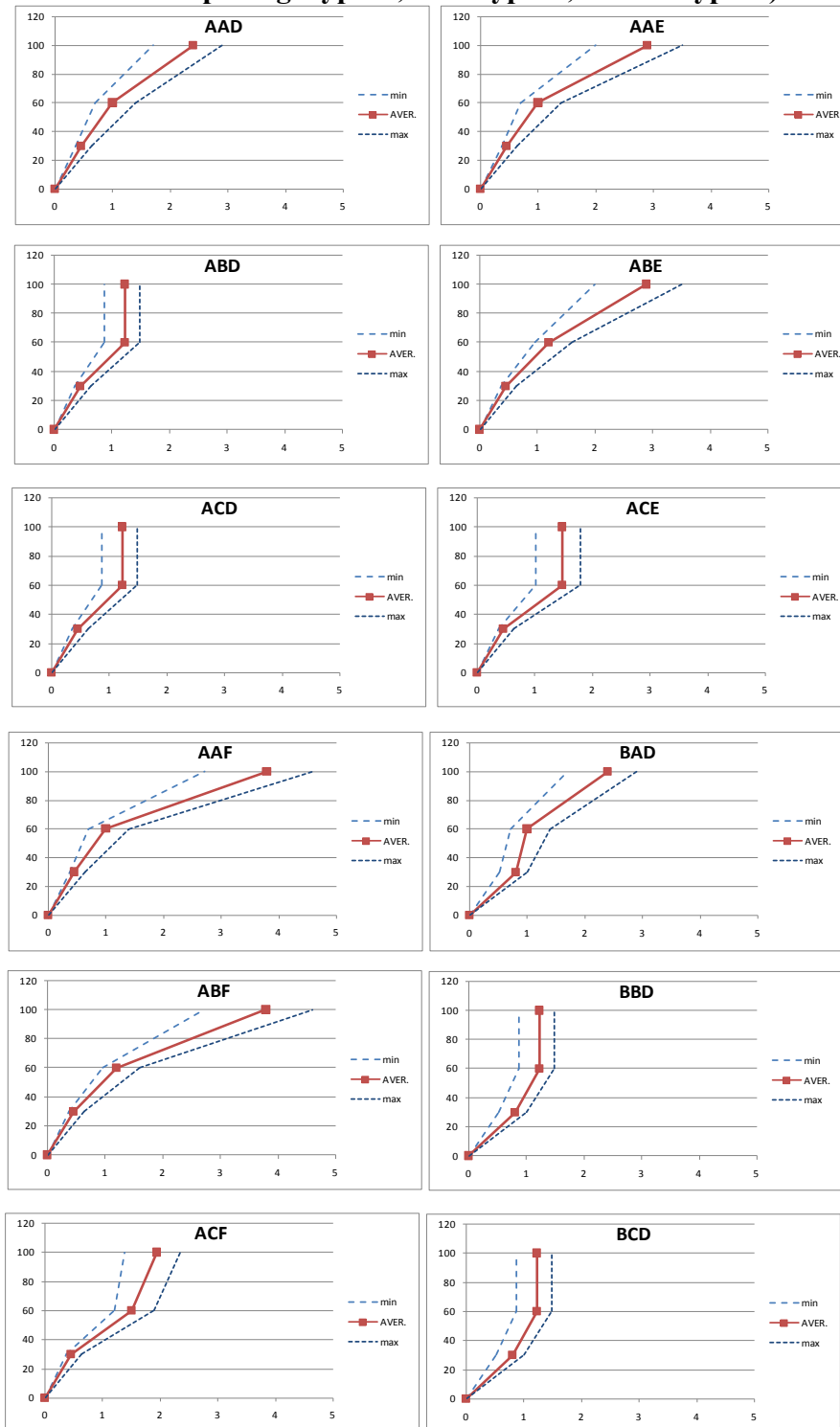
Additionally, we would be grateful if you could offer us your views on the following issues as set-out below:

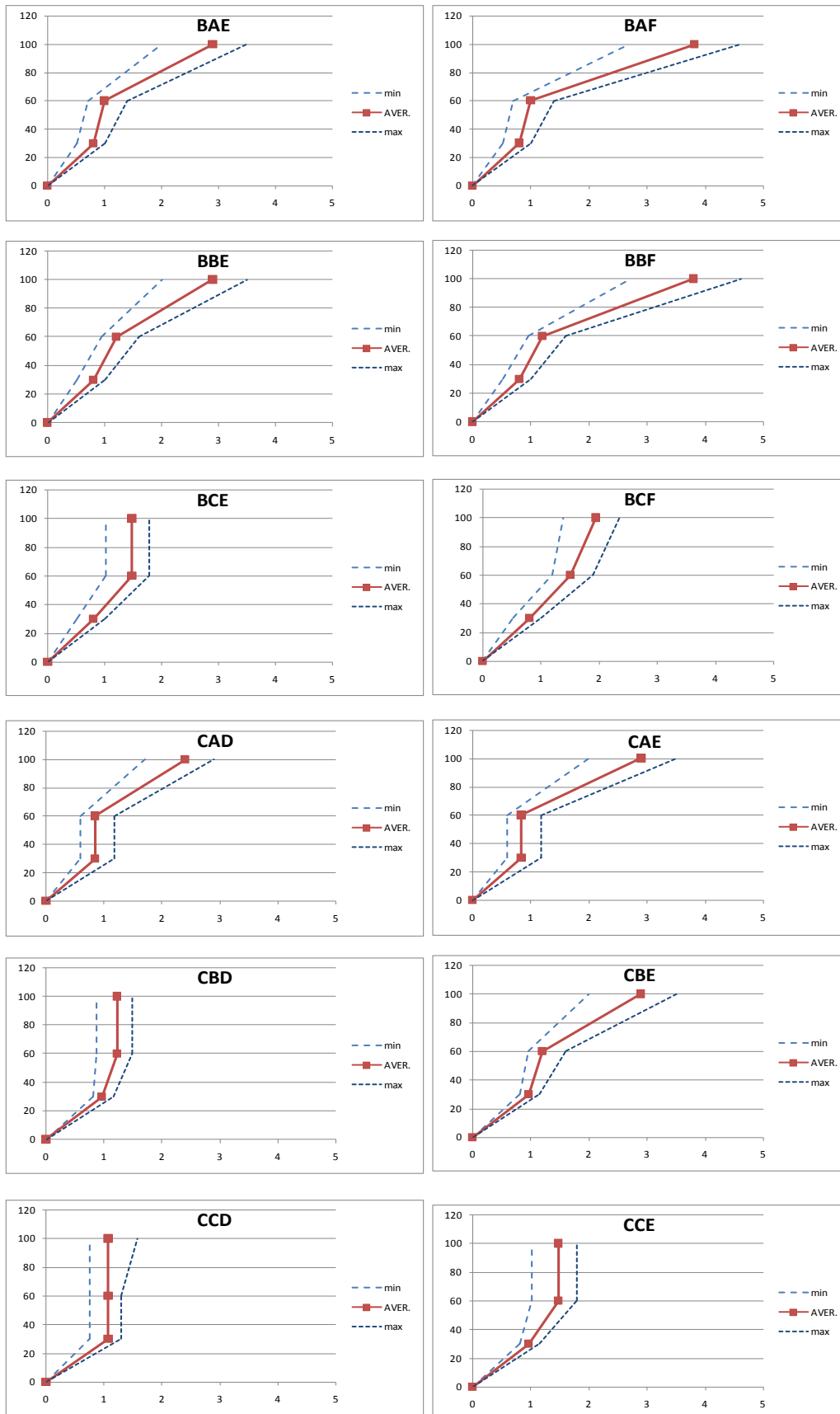
1. For the purposes of the development of fragility curves do you consider the proposed landslide volumes appropriate? Do the proposed volumes cover most scenarios?
2. Roads have been divided into two categories: high speed and local. Initially this was driven by road speed limits that are in operation; however, they correspond well to road construction. That is, high speed roads are typically designed, constructed, and maintained to a higher quality than local roads, due to a need for improved safety and performance. In your opinion, is this two-tier classification sufficient or does it represent an over-generalisation?
3. Do the damage state definitions given adequately describe the damage state levels? i.e. Does blockage of the hardstrip and one running lane on a high speed road constitute "moderate damage"?

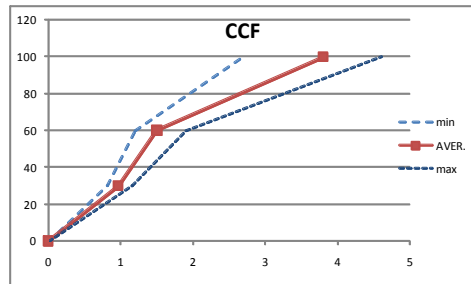
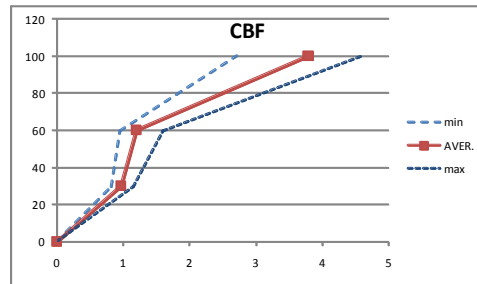
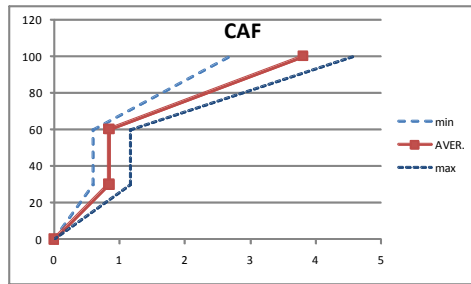
## 8.2 APPENDIX II

### 8.2.1 R.C. Buildings – vulnerability curves for each combination

(e.g. ACB means Openings type A, infill type C, Frame type B)







### 8.2.2 Masonry buildings – vulnerability curves for each combination

(e.g. AC means Openings type A, Walls type C)

